Dissertation zur Erlangung des Doktorgrades
der Fakultät für Chemie und Pharmazie
der Ludwig-Maximilians-Universität München

Structural and Biochemical Characterisation of the Bacterial Mre11-Rad50 DNA Repair Complex

Lisa Christine Käshammer
aus
Karlsruhe, Deutschland

2020

Erklärung

Diese Dissertation wurde im Sinne von § 7 der Promotionsordnung vom 28. November 2011 von Herrn Prof. Dr. Karl-Peter Hopfner betreut.

Eidesstattliche Versicherung

Diese Dissertation wurde eigenständig und ohne unerlaubte Hilfe erarbeitet.

München, 22.02.2020

.....
Lisa Käshammer

Dissertation eingereicht am 27.02.2020

1. Gutachter: Prof. Dr. Karl-Peter Hopfner
2. Gutachter: Prof. Dr. Roland Beckmann

Mündliche Prüfung am 20.05.2020

This thesis has been prepared from October 2016 to February 2020 in the laboratory of Professor Dr. Karl-Peter Hopfner at the Gene Center of the Ludwig-Maximilians-Universität München.

This is a cumulative thesis based on the following publications:

Jan-Hinnerk Saathoff, Lisa Käshammer, Katja Lammens, Robert Thomas Byrne, Karl-Peter Hopfner, The bacterial Mre11–Rad50 homolog SbcCD cleaves opposing strands of DNA by two chemically distinct nuclease reactions, *Nucleic Acids Research*, Volume 46, Issue 21, 30 November 2018, Pages 11303-11314, https://doi.org/10.1093/nar/gky878

Lisa Käshammer*, Jan-Hinnerk Saathoff*, Katja Lammens, Fabian Gut, Joseph Bartho, Aaron Alt, Brigitte Kessler, Karl-Peter Hopfner, Mechanism of DNA End Sensing and Processing by the Mre11-Rad50 Complex, *Molecular Cell*, Volume 76, 07 November 2019, Pages 382-394, https://doi.org/10.1016/j.molcel.2019.07.035

* These authors contributed equally.

Contents

Abstract

The DNA in all organisms is constantly exposed to a variety of different substances and processes that can lead to a plethora of different DNA damages. DNA double strand breaks (DSBs) are one of the most deleterious types of DNA damage since they can cause severe chromosomal rearrangements. Two basic mechanisms emerged for the repair of DSBs: Non-homologous end joining (NHEJ) and homologous recombination (HR). NHEJ allows the direct ligation of two DNA ends. This pathway can be employed throughout the cell cycle, however it can also lead to insertions or deletions. HR is a more complex pathway that uses the sister chromatid as a template and thus allows error free DSB repair after the DNA has been replicated.

One of the first protein complexes recognising a DSB is the Mre11-Rad50-Nbs1 (MRN) complex. The heterotetrameric Mre11-Rad50 core complex (M_2R_2) is conserved in eukaryotes, prokaryotes, archaea and phages and consists of the manganese dependent nuclease Mre11 and the SMC-like ATPase Rad50. Rad50 is composed of a bipartite nucleotide binding domain (NBD) and up to 500 Å long coiled coils that end in a zinc hook. The MRN complex is implicated in DNA tethering as well as DNA damage signalling and telomere maintenance. One of MRN's main function is the initial processing of the DNA to prepare it for long range resection required for HR. For this purpose, the complex has exonuclease and endonuclease activity to cleave protein blocked DNA ends e.g. from abortive topoisomerases.
Despite many years of research, several questions about the MRN complex remain unanswered. The ATP-bound Rad50 NBDs block the Mre11 nuclease active site and it is not clear how the DNA can access the Mre11 nuclease for cleavage. Furthermore, the coiled coils play an important role for the MRN complex, however their function is still not understood.

The first part of this thesis describes the biochemical characterisation of the *Escherichia coli* Mre11-Rad50 (*Ec*MR) complex. It was shown that *Ec*MR dependent DNA binding and ATPase activity increase with DNA length. The ATPase activity is also influenced by the DNA topology, with linear DNA having the highest stimulatory effect. In addition, DNA distortion or melting could be involved during endonucleolytic incision and this was shown by the use of various DNA substrates. Interestingly, two different cleavage chemistries were observed for *Ec*MR depending on the nuclease activity. Thus, *Ec*MR generates different DNA ends, leaving either $3'$ or $5'$ phosphorylated DNA ends, respectively.

In the second part of the thesis the structural data of the *Ec*MR is described. The pivotal coiled coil domain induces a high level of complexity and make the MR complex a challenging

substrate for structural analysis. Due to the recent advances in cryo-EM, the full-length *Ec*MR complex was used for structural studies. Two structures of the head complex, consisting of the Mre11 dimer and the Rad50^{NBD} were determined to near atomic resolution. In the ATPγS bound resting state, the *Ec*MR head complex resembles previously observed MR structures from other organisms. The Mre11 dimer is located in an autoinhibitory state below the Rad50^{NBD} and the coiled coils point outwards. The second structure captures the *Ec*MR in an active, DNA-bound cutting state in complex with ADP. In this conformation, the coiled coils clamp around the DNA and form a rod that could be resolved up to a distance of 200 Å from the head. Additionally, the Mre11 dimer dislocates from the bottom to the side of the Rad50^{NBD}, which allows access of the DNA to the nuclease active site, something that could not be observed in previous Mre11:DNA structures.
The structural as well as biochemical data will be discussed and integrated into possible models.

1 Introduction

1.1 DNA Damage

All cellular organisms, known today use deoxyribonucleic acid (DNA) to store their genetic information[1]. DNA itself is a reactive molecule constantly exposed to endogenous and exogenous factors that cause DNA modifications and DNA damage[2]. DNA damage is a double-edged sword for an organism. On the one hand, mutations resulting from DNA damage drive evolution and help organisms to adapt to an ever changing environment. On the other hand, too much DNA damage has severe consequences for an organism including death and disease[1,2]. Therefore, it is important for the organism to repair DNA damage fast and effectively.
DNA damage can be caused by a plethora of endo- and exogenous factors (see Section 1.1.1 and 1.1.2). Thus, the organism has to deal with many different types of DNA damage, ranging from simple base deamination and DNA adducts to severe DNA lesions, like highly toxic DNA double strand breaks (DSBs)[2].
Several DNA repair pathways have evolved and are used to repair different DNA lesions (see Figure 1). This includes mismatch repair (MMR)[3], base excision repair (BER)[4] and nucleotide excision repair (NER)[5] which are required for the repair of mismatched nucleotides, abasic sites and small to bulky adducts, respectively[2]. The repair of strand breaks in the DNA backbone is mediated by pathways of single strand break repair (SSBR)[6] or double strand break repair (DSBR). In DSBR two major pathways exist: Non-homologous end joining (NHEJ) and homologous recombination (HR, see Section 1.2.1 and 1.2.2)[7,8]. Interstrand crosslinks (ICLs) require the Faconia anemia complex for repair[9]. A small subset of DNA lesions can be repaired by direct reversal, often involving only a single enzyme e.g. photolyase, which reverses cyclobutane pyrimidine dimers[10].
In addition to DNA damage repair, cells also posses mechanisms to allow DNA damage tolerance, one of which are the translesion synthesis (TLS) polymerases that are less stringent in their base-pairing requirements and can replicate damaged DNA[2,11]. The DNA damage response (DDR) of a cell does not only involve DNA damage repair, but also processes for detection and signalling of the damage[11].
The response of a cell to DNA damage can have several outcomes and depends on different factors, e.g. the cell type, cell cycle state and the type and amount of DNA damage. Generally, a low dose of DNA damage results in the activation of pro-survival pathways, like DNA repair, cell-cycle checkpoints and senescence. However, if the DNA damage persists or cannot be repaired, the balance between pro-survival and pro-death pathways shifts towards the pro-death

pathways, including apoptosis, necrosis and high levels of autophagy[12].
The importance of DNA damage repair is highlighted by various diseases resulting from defects in these repair pathways. This includes cancer, which is the second leading cause for death in the United States[13] and the European Union[14] and results from mutations in the DNA. Accumulation of DNA mutations are also associated with neurodegenerative diseases like Alzheimer's and Parkinson's as well as ageing. In meiosis and different processes involving the immune system, DNA damage and its subsequent repair are needed (see Section 1.1.3.1 and 1.1.3.2) and therefore defects in DNA damage repair are also implicated in immune deficiencies and infertility[11].

DNA damaging proteins are of interest for drug targets especially for the treatment of cancer. Cancer cells often lost many of the cell-cycle checkpoints which allows an uncontrolled DNA replication and proliferation of the cell[1]. However, it also makes these cells susceptible to DNA damage since sites of damage will accumulate in these cells and eventually trigger cell death[15]. Therefore, DNA damaging substances are already used to treat cancers (e.g. radiotherapy or topoisomerase inhibitors)[11].
In addition, many cancer inactivate certain genes that are involved in DDR (e.g. breast cancer 1 and 2 (BRCA1 and BRCA2) in ovarian cancer)[16,17]. As a result, these cells often have DNA damage repair defects, which increases their susceptibility to DNA damaging substances. Furthermore, these cells are often sensitive to agents that inhibit a second DNA repair pathway that is used as a replacement of the inactivated repair pathway[16]. For instance, it was found that BRCA deficient cells are much more susceptible to inhibition of PARP than cells with wildtype BRCA[18]. Cell death resulting from the combined inhibition of two genes, while the inhibition of each gene on its own has little effect is known as synthetic lethality[19].
Detailed knowledge about DDR processes will therefore help us to understand basic cellular mechanisms and find treatment for various diseases.

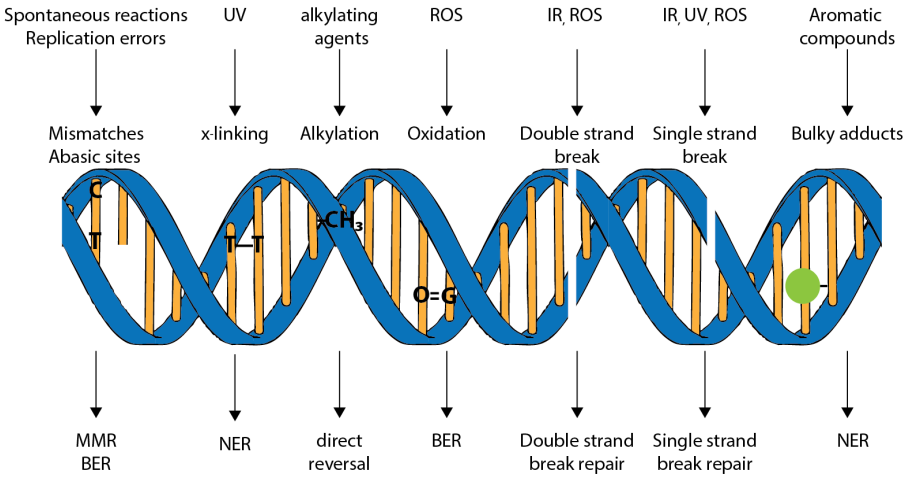

Figure 1: Different types of DNA damage introduced by endo- and exogenous factors. The upper part of the Figure shows different DNA damaging agents and the DNA damage these agents can generate in the DNA. Below the DNA are the different repair pathways used to repair these DNA lesions shown. Figure modified from[2].

1.1.1 Exogeneous Sources for DNA Damage

Ionizing radiation (IR) encloses different types of energetic radiation, like ultraviolet (UV) light (A, B and C) as well as α-, β- and γ-radiation from radioactive decay and X-rays[2]. UV light is one of the leading causes of skin cancer[20] and IR can damage the DNA either directly (∼35%) or indirectly by the generation of radicals, mostly from water, in proximity to the DNA[21]. Exposure to IR leads to a variety of different DNA lesions, including SSBs, DSBs and pyrimidine dimers, with the latter being a characteristic DNA damage generated upon exposure to UV radiation[21].

The DNA bases contain nucleophilic centres which react preferably with electrophiles and several chemicals have been identified that attack these vulnerable positions in the DNA and cause a variety of different DNA lesions[21]. Alkylating agents are highly abundant in the environment, e.g. in tobacco smoke or fuel combustion products and can transfer an alkyl group on biomolecules. While having cancerogenic effects themselves, members of this class of chemicals are also used as chemotherapeutic drugs[22].

Another example of carcinogenic environmental chemicals are polycyclic aromatic hydrocarbons (PAH), which are present in tobacco smoke, charred food and when organic material is not combusted completely[2]. Interestingly, PAHs are not cancerogenic themselves, but their metabolic intermediates are and these intermediates are mainly generated by the P450 monooxygenase system in the liver[21]. The class of PAHs includes the very well studied and highly cancerogenic benzo*(a)*pyrene[21].

Naturally produced toxins produced from microorganisms and fungi can also result in DNA damage[2]. The most cancerogenic natural product known to date is Aflatoxin B1 which is produced by *Aspergillus flavus* and *Aspergillus parasiticus* and especially toxic for the liver[23].
The compounds listed above only represents a very small portion of the known exogeneous DNA damaging substances.

1.1.2 Endogenous Sources for DNA Damage

DNA replication is a major factor in the generation of endogenous DNA damage. First, DNA replication of incorrectly paired nucleotides leads to the fixation of a mutation[2,24]. Second, DNA replication itself leads to misincorporated nucleotides, insertions and deletions.
Several DNA polymerases are known in human cells, and the two main DNA polymerases δ and ϵ required for DNA replication have a very low error rate of $10^{-5} - 10^{-7}$, due to their proof-reading activity[25]. Together with the MMR machinery that checks the replicated DNA for mismatches, an error rate of $10^{-9} - 10^{-10}$ is achieved for DNA replication in human cells[25,26]. For the human genome with $3 * 10^9$ bases this means that there are fewer than three mutations per cell and cell cycle generated due to DNA replication.
Mistakes by the DNA replication machinery may stem from repetitive sequences that cause

slippage of the polymerase and lead to insertions or deletions[27]. Additionally, the use of NTPs instead of dNTPs can lead to mutations[28].

Topoisomerases are another class of enzymes that can lead to DNA damage. Topoisomerases are required to relax the superhelical tension in the DNA generated during replication and transcription[29]. During the reaction mechanism, a SSB or DSB is introduced in the DNA backbone and a transient covalent bond between the DNA and a tyrosine residue of the topoisomerase is formed[30]. In some instances, this complex stays covalently bound to the DNA, e.g. after the encounter of aberrant DNA structures or adducts or the application of certain drugs, e.g. camptothecin.[31–33].

The DNA bases have certain chemical properties making them prone to alteration and two major processes are base deamination and the generation of abasic sites.
Base deamination occurs most frequently on Cytosine and 5-methyl Cytosine and deamination of a base results in a wrong base pairing[24,34]. 5-methyl Cytosine is often found in promotor regions in mammalian cells[35] and deamination causes GC $\rightarrow$ AT transitions[2]. The resulting point mutations are a major cause of inherited diseases in humans[24].
An abasic site is generated when the bond between sugar and base is cleaved, which leaves only the sugar-phosphate backbone[24]. These lesions occur spontaneously or as intermediates in the BER pathway[4,34].

Reactive oxygen species (ROS) are by-products of the respiratory chain and other metabolic processes[36,37]. Furthermore, ROS can be caused by radiolysis caused by the exposure to IR[21]. This is the reason why DNA damage induced by ROS and IR is similar[2]. However, ROS are also used by organisms e.g. as defence against pathogens[38].
Several species of ROS are known e.g. superoxide anion ($O_2^{\cdot -}$), hydrogen peroxide (H_2O_2) and the hydroxyl radical ($HO^{\cdot}$)[39]. The hydroxyl radical is the most reactive ROS and can be produced by Fentons reaction[36,39]. About 100 different DNA lesions caused by ROS are known[2], including oxidation of bases, ring opening of Guanine and Adenine and strand breaks[36,40]. Additionally, ROS can also attack other biomolecules like lipids, which results in the generation of various reactive species, like aldehydes or peroxyl radicals able to modify DNA[39].
Organisms have developed several mechanism to avoid damage by ROS including spatial separation of the respiratory chain from the DNA and antioxidant enzymes, e.g. superoxide dismutase, catalase and peroxiredoxin[2,36]. Elevated ROS levels are implicated in several diseases like cancer and neurodegenerative diseases like Alzheimer's and Parkinson's[39,41].

1.1.3 DNA Double Strand Breaks

Compared to other DNA lesions, DSBs are relatively rare events. For a replicating cell, it was estimated that roughly 50 endogenous DSBs occur per cell and cell cycle[42]. The rate of DSB generation in non replicative cells is much lower and estimated to be 0.05 DSBs per cell in diploid fibroblasts[42]. DSBs belong to the most dangerous DNA lesions, despite their rare occurrance.

If left unrepaired they can lead to gross chromosomal aberrations, including translocation and aneuploidy[43]. Exogenous DSB causing agents are for example IR or chemicals, including chemotherapeutics. IR can cause a DSB by generating two SSBs located in one helical turn[21]. Topoisomerase poisoning results in the trapping of a covalent topoisomerase-DNA complex and the generation of either SSBs (administration of camptothecin) or DSBs (administration of etoposide)[44]. Recently, it was also suggested that transcription is involved in the generation of DSBs[45].

Replication forks can be stalled by several factors e.g. the encounter of Thymidine dimers or unusual secondary structures in the DNA[44]. DSBs can be formed in this process due to several mechanisms, e.g. cleavage of the DNA backbone in stretches of ssDNA, or the generation of DSBs in an attempt to restore a collapsed replication fork, using pathways that involve endonucleases or fragile DNA structures[46]. An example of such a structure is the "chicken foot" structure that can be cleaved by nucleases, producing a one ended DSB (Figure 2)[44].

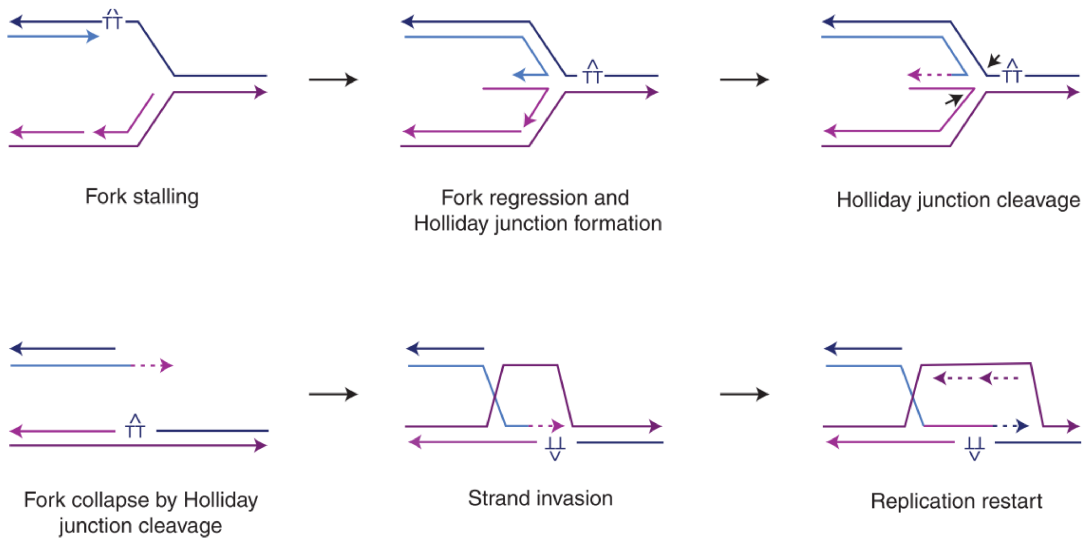

Figure 2: Generation of a one sided DSB during replication by endonucleases. A replication fork stalls on a DNA lesion and regresses, which leads to the formation of a Holliday junction. This structure is recognised by specific enzymes and subsequently cleaved which leads to the generation of a one sided DSB. For faithful replication, steps from HR are required to allow replication restart at a one sided DSB. Figure modified from[44].

Despite the deleterious effects DSBs can have for the cell, the deliberate introduction of DSBs is used in several cellular processes, especially during meiosis and the development of the immune system (see below).

1.1.3.1 V(D)J Recombination

In the human body about 10^{11} different antibody molecules are found, which allows the organism to react to a plethora of different exogenous and endogenous threats, like pathogens or toxins.

The antibody contains a variable region that binds to its antigen and a constant region that is required for binding and signalling in the host organism[47]. The diversity of the antibody variable region can partly be attributed to V(D)J recombination[48].
V(D)J recombination takes place in B-cells for Immunoglobulin (Ig) generation and in T-cells for T cell receptor (TCR) generation[49]. It is a recombination process in which the variable (V), diversity (D) and joining (J) segments are ligated[49]. Recombination occurs at the recombination signal (RS) sequences[48]. Recombination-activating gene-1 and -2 (Rag-1 and Rag-2) bind to two RS sequences and introduce a DSB in each DNA strand[50,51]. As a result one hairpin end (coding end) and one blunt dsDNA (signal end) end is generated per DSB[51]. Two blunt ends are ligated precisely back together, while two coding segments are joined in an imprecise manner. This requires opening of the hairpins and subsequently enzymes may delete or add nucleotides, which increases the variability of the V region even further[51]. Repair of the DSBs is mediated by NHEJ (see Section 1.2.1)[48].

1.1.3.2 Immunoglobulin Class Switching

Five classes of antibodies (IgM, IgD, IgG, IgA and IgE) can be produced by B-cells, however, naive B cells only express IgM and IgD antibodies[52]. The switch of an IgM producing B cell to a B cell producing IgG, IgE or IgA is called Immunoglobulin class switching and improves the response to different pathogens. For instance, IgG1 and IgG2 respond to viruses, while large extracellular parasites are most effectively attacked by IgG4 and IgE[52]. In contrast to V(D)J recombination, the constant region of the antibody is changed. This is achieved by deletion of DNA between two switch regions[53]. For this purpose Cytosines in two switch regions are deaminated and thereby converted to Uracil[54]. Enzymes of the BER or MMR pathways convert the Uracils to DSBs which are then repaired by end joining pathways (see Section 1.2.1), thereby deleting the DNA between both switch regions[52].

1.1.3.3 Spo11-dependent Introduction of DSBs in Meiosis

Meiosis is a special type of cell division found in eukaryotic cells for the generation of cells capable of sexual reproduction. It requires the generation of haploid cells from a diploid mother cell and involves one round of DNA replication followed by two steps of cell division. In meiosis I homologs of each chromosome and in meiosis II the sister chromatids are separated[1].
DSBs in the DNA are generated in prophase of meiosis I[55]. The central protein that creates double strand breaks is Spo11, which belongs to the family of IVA topoisomerase[56–58]. Like other topoisomerases, Spo11 contains an active site tyrosine and a transesterification reaction results in Spo11 covalently bound to the 5′ DNA end[58]. The DSBs are repaired by HR (see Section 1.2.2). It should be noted that while in mitosis the sister chromatid is preferably used as a template in HR, in meiosis the cell preferes to use the homologous chromosome thereby creating genetic exchange between the paternal and maternal allels[8,55].

1.2 DNA Repair

To circumvent the potentially deleterious effects DNA damage can have on an organism, several pathways exist that can repair a variety of different DNA modifications.
Some base modifications can be directly reversed. For instance, the O^6-alkylguanine DNA alkyltransferase can transfer an alkyl group from a Guanine to a Cysteine in its active site, being inactivated itself in the process[59].
Small base modifications, that do not cause significant distortion of the DNA helix, e.g. oxidation, deamination or abasic sites, are removed by the BER pathway. In this pathway an abasic site is generated by a glycosylase and is subsequently excised. The generated single nucleotide gap is either filled with Polymerase β and ligated (short patch repair) or a longer complementary stretch of DNA is synthesised in a strand displacement manner (long patch repair). The generated flap is removed and the remaining nick in the DNA is ligated[4].
For bulky DNA adducts, which distort the DNA helix, including pyrimidine dimers and benzo*(a)*pyrene adducts, the NER pathway is used[2,5]. After initial recognition of the DNA lesion, a long stretch of DNA including the lesion is excised, leaving a ssDNA gap behind. The ssDNA gap is filled and subsequently ligated. NER can occur as global-genome NER or transcription-coupled NER[5].
MMR is an important pathway to decrease the error rate after DNA replication by about 100x and in this pathway mismatched bases as well as insertion-deletion loops resulting from strand slippage at repetitive sequences are recognised[60,61]. In *E.coli*, MutS recognises the DNA damage and MutL is recruited once a DNA damage site has been found[60]. The damaged strand is incised and subsequently removed by an exonuclease. Next, the excised DNA strand is resynthesized by a DNA polymerase and the nick is repaired by a ligase[3,26].
For the repair of ICLs, where bases from complementary strands are covalently linked, the Fanconi anemia proteins mediate repair in a poorly understood mechanism. This pathway seems to involve NER, TLS polymerases and HR[62].
The two main pathways for the repair of DNA double strand breaks are non-homologous end-joining (NHEJ) and homologous recombination (HR) and these two pathways will be discussed below.

1.2.1 Non-Homologous End Joining

In the end-joining pathways, DSBs are repaired by direct ligation. This often involves processing of the ends to remove chemical modifications or to generate microhomology. Therefore, the end-joining pathways are more error-prone than HR. NHEJ can be divided into two pathways; classical NHEJ (c-NHEJ) and alternative NHEJ (alt-NHEJ, also microhomology mediated end-joining (MMEJ) or ϑ-mediated end joining). While c-NHEJ needs no or only little microhomology, alt-NHEJ requires 2-20 nucleotides microhomology and therefore more extensive processing of the DNA ends[7]. Due to its high mutagenic potential, alt-NHEJ is regarded as

the backup pathway of c-NHEJ[63].
Generally, NHEJ consists of three steps: Recognition of the DSB, processing by nucleases or polymerases and subsequent ligation (see Figure 3). In c-NHEJ, the DSB is bound by the Ku70/80 heterodimer, which is highly abundant in the cell[7] and forms a tight complex with DNA[64,65]. Together with the DNA-dependent protein kinase catalytic subunit (DNA-PKcs), the DNA-PK complex is formed, which serves as an interaction platform for other proteins involved in c-NHEJ[66,67]. If the DSB consists of blunt ends and no processing of DNA ends is necessary, the c-NHEJ specific DNA ligase IV in complex with X-ray repair cross-complementing protein 4 (XRCC4) can repair the DSB[68]. Indeed, for human proteins, the complex of Ku70/80, XRCC4 and DNA Ligase IV is sufficient to reconstitute c-NHEJ[69].
However, DSBs often contain ends that are unsuitable for direct ligation, e.g. with chemical modifications or overhangs. Therefore, several other proteins are involved in c-NHEJ. This includes the nuclease Artemis, which degrades 3′ or 5′ overhangs and hairpins that are incompatible for ligation[70]. In addition, resection can also result in the generation of microhomologous regions.
The two polymerases λ and μ (members of the Polymerase X family) are able to add nucleotides in a template-dependent and template-independent manner[71,72]. Since Polymerase μ preferentially adds nucleotides in a template-free manner, it generates microhomologous regions and thereby helps in ligating incompatible 3′ overhangs[73]. Polymerase λ works in a template-based manner and therefore is required at overhangs, where nucleotides have to be filled-in[74].
Several other proteins are involved in processing the ends and making them ligatable (e.g. polynucleotide kinase or Aprataxin) or stabilising the complex and promote the ligation reaction (e.g. XRCC4-like factor (XLF) or paralogue of XRCC4 and XLF (PAXX))[7].

The alt-NHEJ pathway seems to be used as a backup for the c-NHEJ pathway[76]. It requires microhomology of 2-20 nucleotides[7] and therefore 3′ overhangs, possibly generated by Mre11-Rad50-Nbs1 (MRN) in complex with CtBP-interacting protein (CtIP, see Figure 3)[77–80]. In addition, alt-NHEJ involves PARP1 which senses DSBs and promotes alt-NHEJ[81,82]. The polymerase ϑ then uses microhomologies between two 3′ overhangs to extend the DNA, using the other strand as a template[83]. Finally, ligation is performed by DNA ligase I or III[84]. Interestingly, Ku70/80 binding to DSBs inhibits alt-NHEJ, possibly by mechanisms, like competing with PARP1 and suppressing resection[85,86].
Alt-NHEJ and HR (see Section 1.2.2) seem to share the initial resection steps[87], however, while HR leads to an error-free repair of the DSB, alt-NHEJ is a mutagenic pathway that leads to chromosomal translocations, deletions and duplications[63].

The NHEJ pathway described above is found in mammalian cells, however, many bacteria are also able to religate DSBs using NHEJ[88]. One study found that roughly 25% of the sequenced prokaryotes contain one or more bacterial Ku homologues[89]. Additionally, bacterial ligases that sometimes also include a polymerase and nuclease domain, have been identified. NHEJ in bacteria seems to be important if DSBs are introduced during the stationary phase (e.g. by IR)[88].

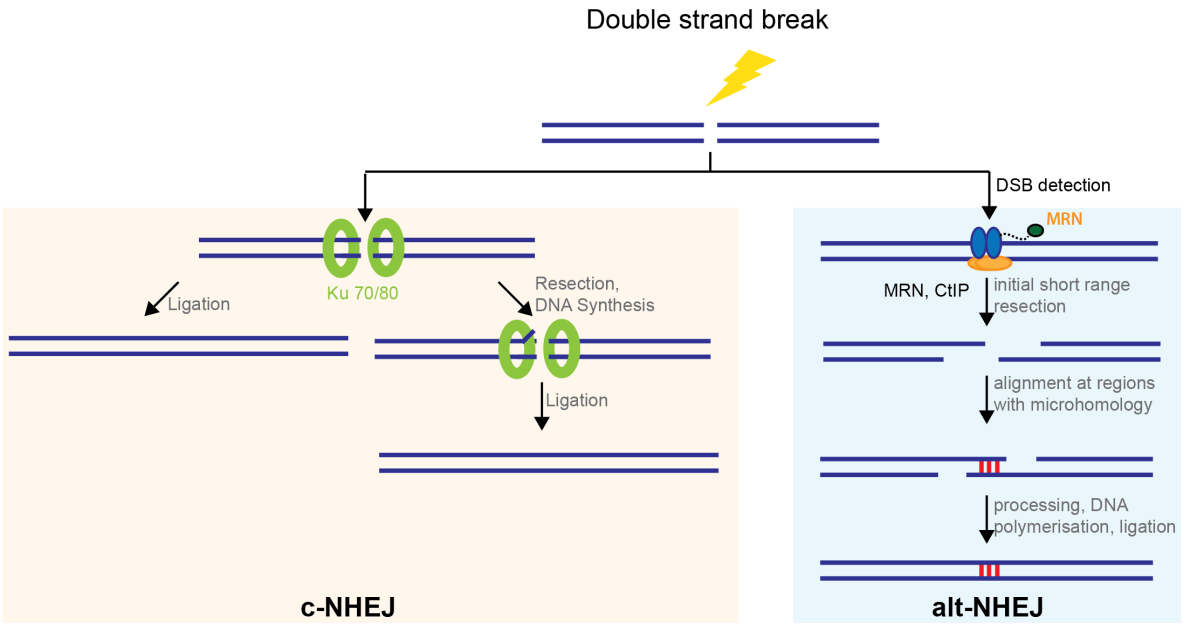

Figure 3: Basic steps in the repair pathways c-NHEJ and alt-NHEJ. On the left hand site the basic steps of NHEJ are shown (orange background). Ku70/80 is one of the first proteins that detects and protects the DSB. Clean DSBs can be ligated directly. Dirty DSBs have to be processed first before they can be ligated. On the right hand steps of the alt-NHEJ pathway are shown (blue background). In this pathway the MRN-CtIP complex recognises the break and is responsible for initial short range resection and the generation of short 3′ overhangs. This can reveal regions of microhomology. Alignment at regions of microhomology and subsequent DNA polymerisation and ligation repairs the break. Figure modified from [7,75].

1.2.2 Homologous Recombination

HR is used in meiosis and mitosis to repair DSBs. In meiosis, HR is important for the exchange of genetic information between both chromosomes (see Section 1.1.3.3), while in mitosis HR enables an error-free repair of DSBs once the DNA has been replicated, which is the case in late S and G2 phase[90]. The basic steps of HR are: (1) detection of the break, (2) long range resection to generate 3′ ssDNA overhangs, (3) strand invasion of the ssDNA into the homologous duplex DNA and formation of the synaptic complex, (4) DNA synthesis, displacement loop (D-loop) and Holliday junction (HJ) migration (5) resolving the generated structure and ligation if nicks were formed.
Proteins involved in HR are essential in all domains of life and can even be found in the T4 bacteriophage[8].

HR is well studied in *Escherichia coli*, where two overlapping pathways exist for DSB repair, the RecBCD pathway for the repair of DSBs and the RecF pathway for the repair of ssDNA gaps[91]. The RecBCD pathway is responsible for more than 95% of DSB repair events in *E.coli*[91].
RecBCD is the nuclease generating 3′ ssDNA overhangs. RecBCD possesses several enzymatic activities including 3′-5′ DNA helicase activity and nuclease activity (RecB)[92–94], recognition of

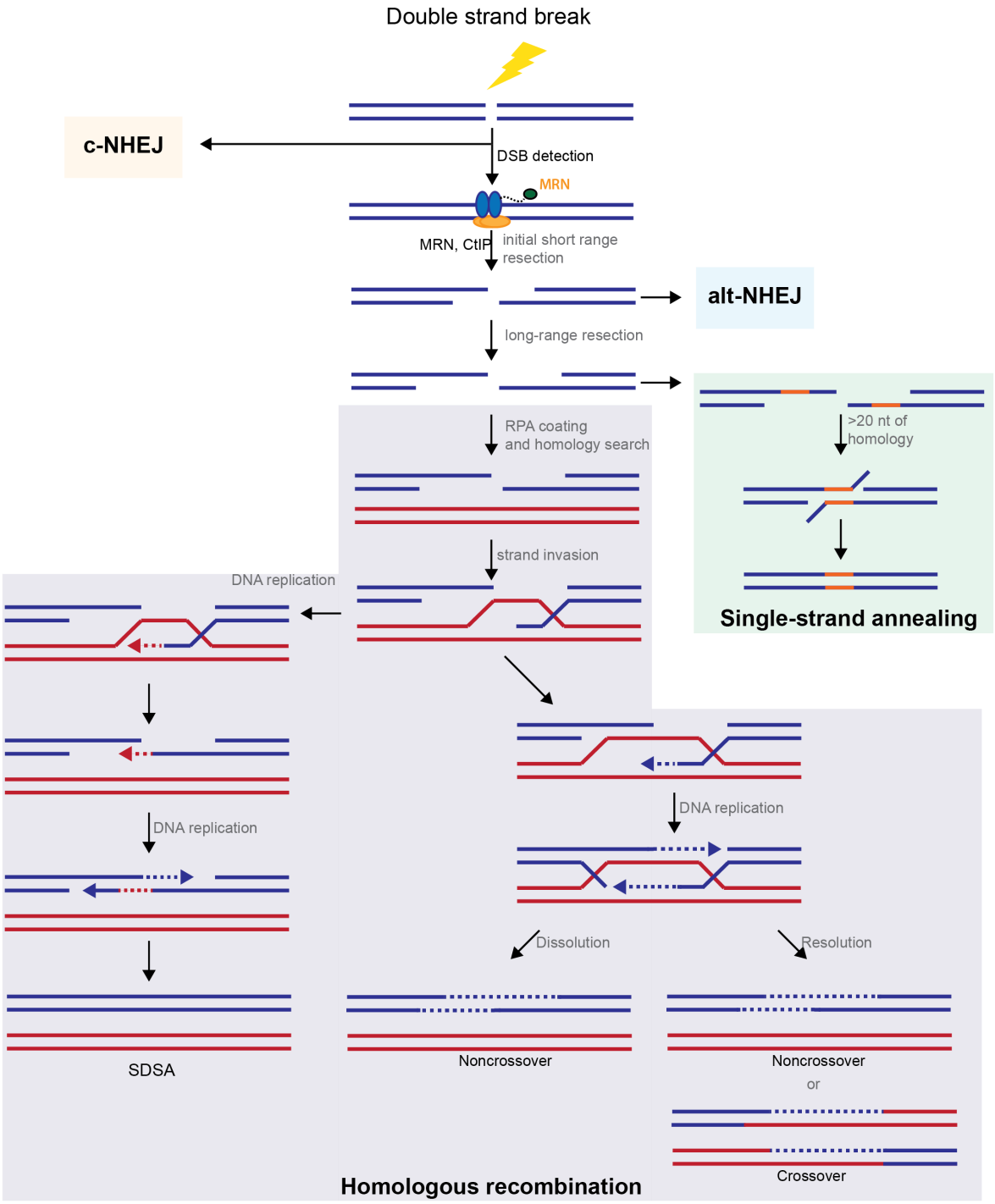

Figure 4: Basic steps in the repair pathways HR and SSA. In HR and SSA, the double strand break is detected by MRN, which works together with CtIP to generate the initial 3′ overhangs by short range resection. Subsequently, long-range resection over several thousands of bases takes place and leaves long 3′ overhangs. For SSA (right hand site, green background), stretches with more than 20 nucleotides are aligned after processing of the DNA and ligation repairs the break. For HR (middle, grey background), RPA coates the single stranded DNA and after homology search the homolog dsDNA stretch is

Figure 4: invaded by the 3′ single strand. For SDSA (left hand site), the generated D-loop is disrupted shortly after DNA replication, which allows annealing of the elongated single strand to DNA of the original molecule. After DNA replication and ligation the break is repaired as NCO products. Alternatively, a Holliday junction can be formed. This structure is either resolved by dissolution (NCO products) or resolution (CO products). Figure modified from [7,75].

a specific DNA sequence [95] (RecC), 5′-3′ DNA helicase activity (RecD) [96] and ATPase activity (RecB and RecD) [97,98]. RecBCD unwinds the DNA and degrades both strands rapidly until a Chi (crossover hotspot instigator, also χ, 5′-GCTGGTGG-3′) sequence is encountered [99,100], a DNA sequence highly overrepresented in the *E.coli* genome [101]. Upon encountering a Chi sequence RecBCD pauses and then continues degradation with a changed processivity, in which the cleavage of the 3′ strand is reduced and the cleavage of the 5′ strand is upregulated [99,102]. RecBCD also helps to coat the emerging 3′ ssDNA strand with RecA monomers, [103] which form a filament on ssDNA, called the presynaptic complex [91]. The RecA filament carries out the search for the homologous sequence [104]. Only recently, data shed light on how the RecA filament can locate the homologous sequence in millions of bases present in a bacterial cell. Single molecule analysis showed that for homology search the coiled structure of the dsDNA and the length of the RecA filament are important. Both factors enhance the probability of finding a homologous sequence. Consequently, the intersegmental contact sampling model was proposed, in which the RecA filament samples the dsDNA and forms weak contact with the DNA. Stable contacts are formed with homologous DNA and subsequently other parts of the filament will bind to this stretch of dsDNA [105,106]. Once the homologous sequence has been found, the 3′ ssDNA pairs with the complementary strand of the duplex DNA (strand invasion) and a heteroduplex is formed [91], also called D-loop [107].
To restore replication on an one sided DSB, the invading strand serves as a primer for DNA synthesis which is followed by DNA replication, as well as disruption of the generated D-loop structure [107]. Alternatively, the second resected strand can invade the template strand and two Holliday junctions are formed [104]. Branch migration is then catalysed by RuvAB, in which RuvA recognises the Holliday junction and RuvB is the motor protein that pushes the HJ forward [108–110]. Additionally, RecG can migrate HJs and is likely involved in fork reversal to enable replication restart at a stalled replication fork [111–113]. Migration of HJs or double HJs (dHJs) results in DNA structures that require endonucleases to be resolved. This is either achieved by RuvC, which cleaves HJs symmetrically, so that the resulting products can be ligated directly [75,114]. This process is called resolution and either non crossover (NCO) or crossover (CO) products can be produced [91]. The second option for resolving HJs is dissolution which results strictly in NCO products and is catalysed by RecQ (helicase) and Topo III (type IA topoisomerase), which passes one strand of DNA through the other [91,115].

In eukaryotic cells the MRN (Mre11-Nbs1-Mrx2 (MRX) in *S. cerevisiae*) complex together with CtIP (Sae2 in *S. cerevisiae*, Ctp1 in *S.pombe*) is required for the initial resection at DSBs (see

Section 1.3 and Figure 4)[116]. MRN/MRX has a 3′-5′ exonuclease activity that would not produce the required 3′ overhangs[117,118]. However, recent data indicate, that MRN incises the 5′ DNA strand next to a DSB and resects towards the DNA end[119,120]. Likely, this incision creates an entry site for the exonuclease 1 (EXO1) or the helicase-topoisomerase BLM-TopIIIα-RMI1 in complex with the nuclease DNA2[121,122]. Both are involved in the long-range resection of the 5′ strand and the generation of the 3′ overhang[116], equivalent to RecBCD in *E.coli*. EXO1 has 5′-3′ exonuclease activity[123] and is also involved in MMR[124]. Independent of EXO1, the DNA2-Sgs1 complex is also able to resect the 5′ DNA strand[125]. Additionally, this long range resection requires the remodelling of chromatin which is executed by human SMARCAD1 (Fun30 in *S.cerevisiae*)[126,127].
Single-stranded DNA in the cell is coated by RPA (single-stranded DNA binding protein (SSB) in *E.coli*) and later replaced by the RecA homologue Rad51 which formes nucleofilaments with ssDNA[8]. While *E.coli* only possesses one Rad51 homologue (RecA), humans have five Rad51 paralogues that assemble into two different complexes[106]. Rad52 in yeast mediates the replacement of RPA with Rad51[106,128,129]. In human cells the exchange of RPA with Rad51 is catalysed by BRCA2, which is absent in *S.cerevisiae*[106,130]. Stabilisation of the presynaptic filament is conveyed by Rad54[131].
Protein members of the RecA family have a highly conserved catalytic domain[106] and homology search likely occurs similar to the bacterial RecA protein, however, this process is still enigmatic. It has been found that a microhomology of only eight nucleotides is sufficient to extended the lifetime of a Rad51-ssDNA-dsDNA complex[132].
Subsequently, the D-loop has to be formed, which means the ssDNA has to replace the analogous strand in the dsDNA[8]. Recently it was shown, that yeast Rad54 promotes the formation of D-loops from synaptic complexes with its ATP-dependent motor activity[133,134].

Once the D-loop is formed, three outcomes are possible: Synthesis-dependent strand annealing (SDSA), dHJs and break-induced replication (BIR)[44].
SDSA seems to be the preferred pathway for HR in mitosis, since it produces mainly NCO products and thereby prevents the loss of heterozygosity (LOH)[8,106,135]. The severity of LOH is highlighted by the development of tumours in hereditary retinoblastoma, which stem in an estimated 40% of the cases from LOH by inter homologue HR[136]. Thus, LOH is prevented in mitotic cells by (1) using the sister chromatid instead of the homologous chromosome at a ratio of 100 to 1 and (2) preferring NCO products[137].
For SDSA the D-loop migrates during the DNA synthesis along the sister strand that serves as template for DNA replication[106]. Reconstitution of DNA synthesis of a D-loop *in vitro* requires PCNA, RFC and Polymerase δ for the yeast and human system[138,139]. The D-loop seems to be a highly dynamic structure[8] and its disruption allows the extended 3′ DNA end to anneal with its original DNA strand counter part[106]. Subsequent DNA synthesis and ligation repairs the break[106].
Alternatively, a dHJ can be formed resulting from D-loop extension and a subsequent second annealing step mediated by Rad52 in yeast[106,140]. The dHJ structure is migrated in both direc-

tions during DNA synthesis[106]. Ligation results in a four-way branched DNA molecule that is resolved by two different mechanisms.[8]. Dissolution is catalysed by the BLM-TopIIIα-RMI 1/2 complex in humans and leads to NCO products[141]. Resolution can either occur symmetrically by GEN1 or asymmetrically by MUS81-EME1 or SLX1-SLX4[75,142–144]. Symmetric resolution leads to CO products, while asymmetric resolution generates NCO products[75].

Single-strand annealing (SSA) is a mutagenic repair pathway of DSBs and requires extensive resection of the DNA duplex and generation of 3′ ssDNA overhangs[145]. In contrast to HR, however, the resulting 3′ overhangs are annealed at homologous regions by Rad52 in an Rad51-independent fashion[7,145,146]. The non-homologous 3′ ssDNA overhangs are then removed by XPF-ERCC1 or by the MSH2-MSH3 complex, which are members of the NER and MMR repair pathways, respectively[7,147,148]. In SSA genetic information is always lost and the extensive resection can lead to deletions of more than 25 kb[145,149]. Furthermore, SSA between different chromosomes results in translocations[145]. This is also a result of the mammalian chromosome structure that includes many repetitive DNA sequences, e.g. Alu elements, providing the more than 20 bp of homology needed for SSA[7,150].

1.2.3 Regulation of NHEJ and HR

Tight regulation of NHEJ and HR are necessary during the cell cycle. HR can only take place once DNA has been replicated, so in late S and G2 phase[90].

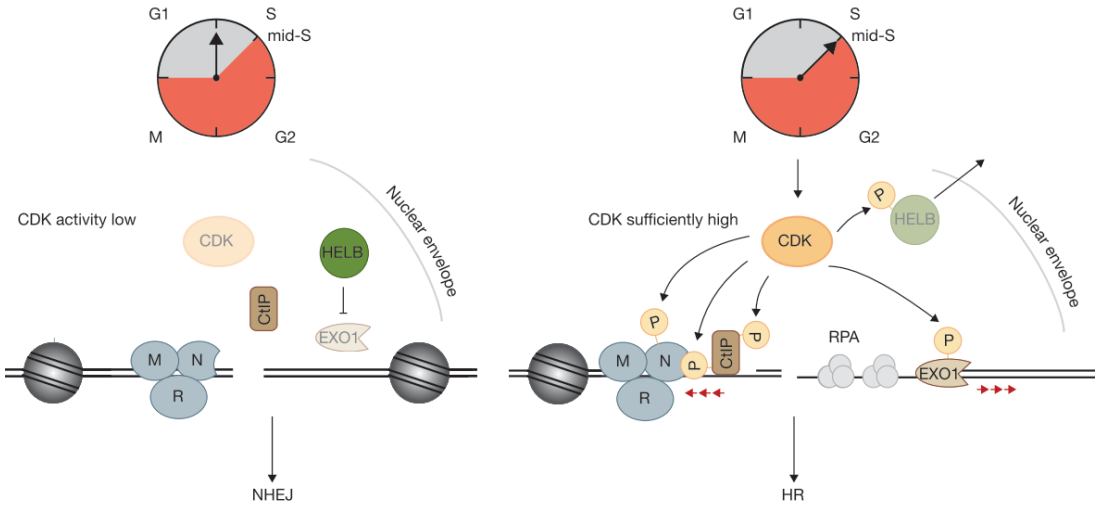

Figure 5: Regulation of HR and NHEJ dependent on the cell cycle. CDK activity is low at the beginning of the cell cycle which results in unphosphorylated and inactive MRN and CtIP. Progression of the cell cycle to S-phase when replicated DNA is available, results in CDK-dependent phosphorylation of proteins that are required for resection during HR. Figure modified from[90].

NHEJ can be active throughout the cell cycle, however, both HR and NHEJ are largely inhibited during mitosis and only very limited DNA repair is done from late prophase onwards, even though

sensing and signalling of DSBs in mitotic cells is similar to interphase[90,151,152]. Regulation of HR and NHEJ pathways depends on cyclin-dependent kinases (CDKs) and the activity of CDKs rises continuously from G1 to the start of mitosis[90]. The central point that commits DSB repair to either HR or NHEJ is the long range resection to generate the $3'$ overhangs needed for HR[153]. Therefore, CDKs are involved in phosphorylating and thereby activating end resection enzymes like EXO1[154], NBS1[155] or CtIP[156] (see Figure 5). Additionally, BRCA1 and 53BP1 work antagonistically and either promote resection or inhibite it, respectively[90]. Thus, 53BP1 moves the repair pathway towards NHEJ and BRCA1 promotes DNA end resection and thereby HR[90].

As a result of cell cycle regulation, NHEJ occurs 50 times more in G1, while the ratio of NHEJ:HR changes to 4:1 in mammalian somatic cells in S and G2 phase[7].

It should be noted, however, that NHEJ and HR do not necessarily compete with each other. One ended DSBs that arise from collapsed replication forks can not be repaired by c-NHEJ[63] and do need HR to resume replication. On the other hand, clean DNA ends without any adducts or damaged nucleotides are likely repaired by NHEJ[157].

1.3 The MRN complex

The MRN complex consists of the three proteins meiotic recombination 11 (Mre11), Radiation sensitivity 50 (Rad50) and Nijmegen breakage syndrome 1 (Nbs1, also nibrin, X-ray sensitive 2 (Xrs2) in yeast). While Mre11 and Rad50 are widely distributed in the phylogenetic tree and can be found in bacteria, archaea, eukaryotes and phages [158], Nbs1 is only present in eukaryotes [157]. The structure of the core complex is highly conserved and consists of a Mre11 dimer and a Rad50 dimer (M_2R_2, see Figure 6). Nbs1 is less conserved and the stoichiometry of M:R:N either 2:2:1 or 2:2:2 [116].

The MRN complex has a plethora of different functions. It is one of the first protein complexes that detects a DSB in the cell and processes the DNA end to prepare it for subsequent repair pathways like HR and alt-NHEJ [116]. Additionally, the complex is also involved in signalling to the cell that a DSB occurred via the kinase ataxia telangiectasia mutated (ATM) [157], which in turn phosphorylates hundreds of proteins that are involved in cell cycle, DDR and apoptosis [159,160] (see Section 1.3.5.1). In the next sections, the individual components of the complex and their function will be described.

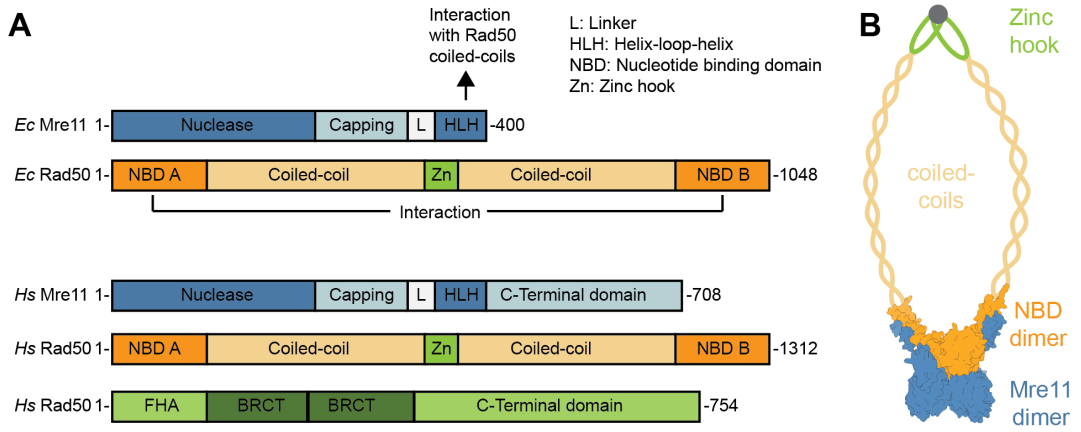

Figure 6: The MRN complex (A) Depiction of the different domains in *Ec*MR (top) and *hs*MRN (bottom). (B) Model for the MR core complex. Mre11 (blue), Rad50 with its long coiled coils (orange) and the zinc hook (gree) are indicated. Figure modified from [157].

1.3.1 Mre11

Mre11 was first identified in 1993 in a screen for proteins involved in meiotic recombination in yeast [161] and is the nuclease of the complex. It consists of a N-terminal nuclease domain, followed by the capping domain, a flexible linker and the Rad50-binding helix-loop-helix (HLH) motif [162,163]. In eukaryotes, the HLH motif is followed by a C-terminal domain, which is required for DNA binding (see Figure 6 A) [164]. A conserved glycine-arginine-rich (GAR) motif was identified in multicellular eukaryotic organisms, which is important for DNA binding, regulation of Mre11 nuclease activity and localisation of Mre11 to DNA damage foci [165].

Eukaryotic Mre11 has 3′-5′ exonuclease activity on dsDNA[117,164] and endonuclease activity on ssDNA[166]. The same basic nucleolytic activities have been observed for the MR and the MRN complex[117,118]. Nuclease activity of Mre11 is strictly Mn^{2+} dependent[117,118,164] and the exonuclease of eukaryotic Mre11 is ATP independent and further stimulated by the presence of Rad50[117]. Binding of Mre11 to DNA has been observed for circular (supercoiled or nicked) dsDNA, however no nuclease activity could be observed on these substrates[164]. Mre11 is also able to cleave hairpin substrates on its own, albeit with a reduced efficiency over the exonuclease activity[117].
Nbs1 has been shown to stimulate the *hs*MR complex to cleave a blocked DNA end endonucleolytically. Simultaneously, Nbs1 restricts the 3′-5′ exonuclease activity of *hs*MR on a free DNA end[167]. On a nicked and blocked substrate, the complex first digests the DNA from the nick towards the blocked DNA end and then endonucleolytically cuts the strand opposite of the nick[167]. Additionally, in yeast the MRN interacting protein Sae2 specifically stimulates the endonuclease activity of the yeast MRX complex. This results in the preferred cleavage of the 5′ terminated DNA strand about 10-15 nucleotides distant to the blocked DNA end[122].

Enzymatic activities on a blocked DNA end are required in different biological settings. The exonucleases Exo1 and Sgs1-Dna2, involved in 5′-3′ long range resection in HR[8], cannot resect a DNA end blocked by Ku 70/80, but need a nick in close proximity to this end[121]. This results in a bidirectional resection model with EXO1 or Sgs-DNA2 resecting away from the DSB, while MRN resects the DNA towards the DSB[168]. The preference of MRN to cleave a blocked DSB on the 5′ strand possibly stems from its involvement in cleaving the meiotic topoisomerase II-like protein Spo11 (Rec12 in fission yeast), which binds covalently to the 5′ end of DNA (see Section 1.1.3.3)[56]. Indeed, Spo11 removal has been found to be dependent on MRN and Ctp1 in yeast[169]. Interestingly, a nuclease dead mutant of Mre11 (H134S in yeast, H85S in *Pyrococcus furiosus*) mimics the ΔMre11 phenotype in *S.pombe* in response to genotoxic chemicals[166]. On the other hand, a mutation that does only affect the 3′-5′ exonuclease (H68S in yeast, H52S in *P. furiosus*) only shows mild effects in response to genotoxic substances, indicating that the endonuclease is required for the repair of DSBs in *S.pombe*[166].

Structures of different Mre11 constructs have been solved from various organisms and high structure conservation was found at the N-terminus of Mre11 from different species and domains of life[162,163,170–174]. The nuclease domain resembles the catalytic domain found in calcineurin like Ser/Thr phosphatases[162]. In the nuclease active site seven conserved residues coordinate two Mn^{2+} ions[162]. The capping domain is located adjacent to the nuclease domain and might have an influence on the DNA substrate specificity[162]. The HLH motif is composed of two helices connected by a short linker and binds to the Rad50 coiled coils about six helical turns distal to the NBD. This binding site provides the main interactions between Rad50 and Mre11[163]. In the eukaryotic *Ct*MR complex this interaction site is more extensive and consists of at least five helices that bind to the Rad50 coiled coils[175]. Mre11 forms a dimer in all structures solved so far[116,162,163,170–174] and the dimer interface is formed by a four helix bundle[166]. Hydrophobic residues with a high sequence identity among different species are responsible for the interactions

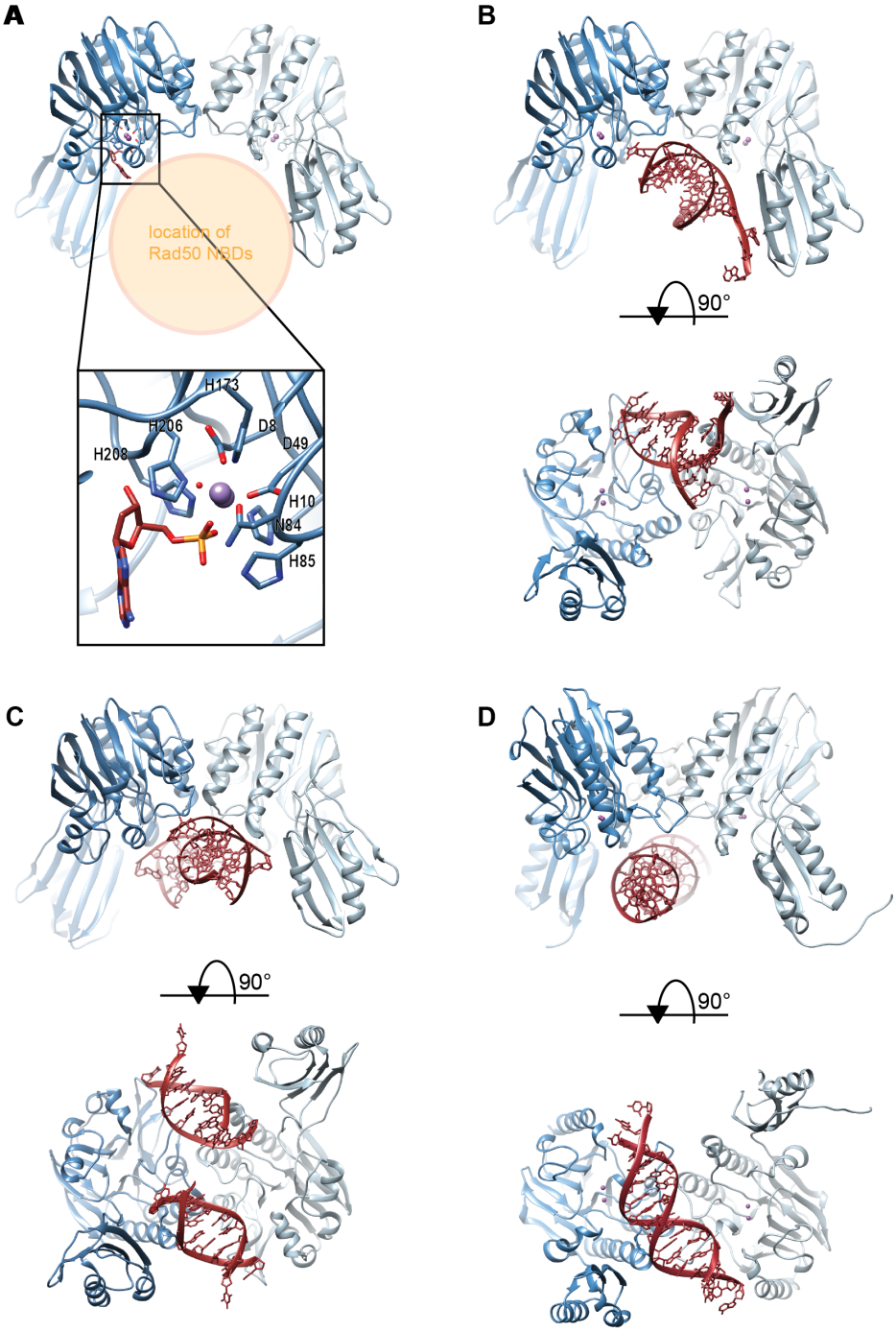

Figure 7: Crystal structure of the Mre11 dimer in complex with different DNA substrates. (A) Structure of the *P. furiosus* Mre11 nuclease and capping domain in complex with AMP. The binding site of the nucleotide binding domain is hinted with an orange circle. An enlargement of the active site with the two bound manganese ions is shown (pdb: 1ii7). (B) Structure of a *Pf*Mre11 dimer in complex with DNA in the synaptic conformation shown in front and bottom view (pdb: 3dsd). (C) Structure of a *Pf*Mre11 dimer in complex with DNA in the branched conformation shown in front and bottom view (pdb: 3dsc). (D) Structure of a *Methanococcus janaschii* Mre11 dimer in complex with DNA shown in front and bottom view (pdb: 4tug).

between these helices[166]. The dimer interface is present in all structures solved so far, apart from the human Mre11 dimer, in which a disulphide bridge between two Cysteines (C146) is formed[173]. This Cysteine bridge would restrict the movement between Mre11 dimers and reduce the flexibility that is observed in structures of yeast Mre11[116]. Interestingly, while the structure of the nuclease domain is conserved among different species, the orientation between two Mre11 monomers in a dimer is not strictly conserved, resulting in different angles of Mre11 monomers towards each other[116].

One question that could not be solved so far is, how DNA is bound and processed by Mre11. Crystal structures of *Pf*Mre11 dimers in complex with two different DNA substrates revealed how two DNA molecules might be bridged by the Mre11 complex or how a collapsed replication fork might be bound by Mre11. However, since the DNA did not access the active site directly, these structures could not explain how the DNA is processed by Mre11[166]. Additionally, if Rad50 is present and bound to ATP, it blocks the Mre11 active site (see Figure 8) as well as the DNA binding sites found in Mre11 (see Figure 7)[166,171,176]. However, ATP hydrolysis is indispensable for the endonuclease activity of Mre11[122,177] and this conundrum could not be solved so far.
Separation of function mutations have been found for Mre11 and Rad50. These mutations cause the loss of some, but not all functions of the complex. Mouse models showed that nuclease activity of Mre11 is required for DSB repair by HR and genomic stability following IR or replicative stress, but not for signalling of DNA damage[178]. Similarly, $Mre11^{D16A}$ cannot process DNA and causes MMS sensitivity and shortened telomeres, even though the DNA binding activity is still intact[164].

1.3.2 Rad50

Rad50 belongs to the family of structural maintenance of chromosomes (SMC) proteins and has a similar structure (see below). A hallmark of SMC proteins is the N- and C-terminal nucleotide binding domain (NBD A and NBD B, respectively) separated by long coiled coils[157,179]. In Rad50 these coiled coils can extend between 15 nm in the T4 bacteriophage and 50 nm in eukaryotic Rad50 and the N- and C-terminal parts of the coiled coils are connected by a conserved zinc hook domain[116]. NBD A and B interact with each other and thus the whole Rad50 monomer folds back onto itself, generating a Zn hook on one end and a NBD on the other end, separated by antiparallel coiled coils (see Figure 6)[157]. The structure of the NBD is related to ATP-binding cassette (ABC) transporters[180] and upon ATP binding, the NBD A and B of two Rad50 monomers dimerise and sandwich two ATP molecules between them[180,181] (see Figure 8).

Five highly conserved motifs are present in the Rad50 NBD, that are required for ATP binding and hydrolysis. In the N-terminal domain the Walker A motif and the Q-loop are present. In the C-terminal domain of Rad50, the signature motif, Walker B and the D-loop can be found[180](Figure 9).

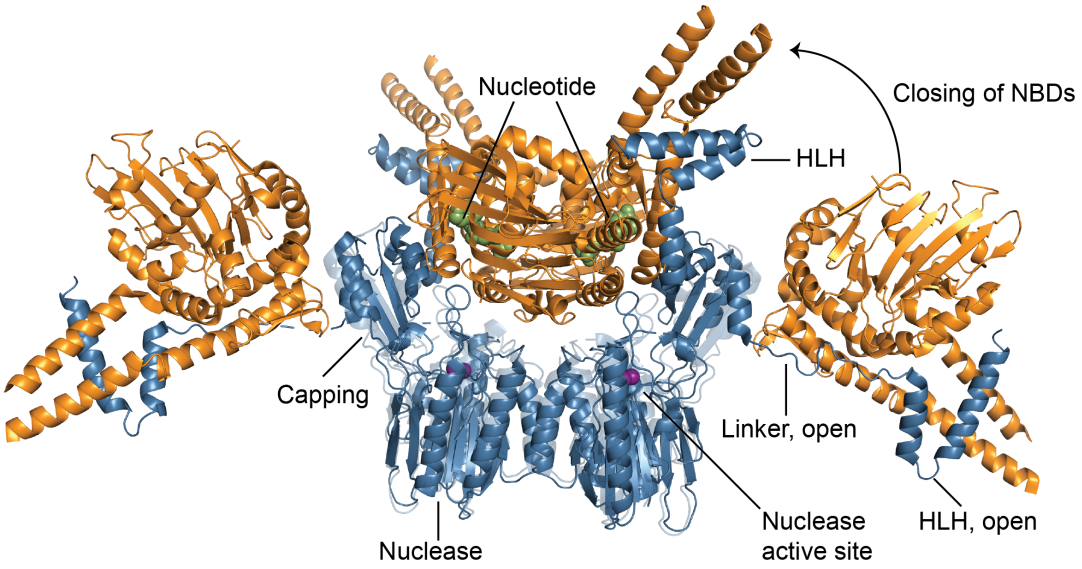

Figure 8: Open and closed conformations of the MR head complex in response to ATP binding. Crystal structure of the *Thermotoga maritima* MR head complex in its open nucleotide free state (pdb: 3QG5) and in its closed nucleotide bound state (pdb: 3QF7).

Rad50 is a very weak ATPase and *hs*MR hydrolyses ATP only with a rate of 0.05 ATP per molecule and minute[182]. Similar low rates have been measured for the MR complex from other species[182,183]. ATP hydrolysis of MR is stimulated by the addition of dsDNA by 10 to 20 fold, in yeast and human, respectively. Additionally, the ATPase rate could be enhanced 2 fold by the addition of Nbs1[182]. The characteristic of a low ATPase rate is shared by the SMC proteins, that hydrolyse 0.1-2 ATP/sec per SMC dimer[184]. The hydrolysis rate is far slower than for other proteins involved in DNA metabolism, e.g. about 740 ATP molecules for RecBCD per s^{-1} and RecBCD molecule are hydolysed[185]. This might indicate that ATP hydrolysis in the MRN complex serves as a switch rather than an energy source that allows translocation along the DNA like helicases[180]. However, how ATP binding and the hydrolysis cycle is coupled to the function of the MR complex is not known to date[184]. For the NBDs several separation of function mutations have been found. These Rad50S mutations are located on the β-sheets and have a much more severe defect in meiosis than in DNA repair (highlighted in Figure 9 A)[186].

Three structures have been solved of Rad50 NBDs in complex with double stranded DNA[175,187,188]. For *Thermotoga maritima*, dsDNA is bound to residues in the coiled coils and the tip of the NBD, while for *Methanococcus janaschii* and *Chaetomium thermophilum*, dsDNA is bound across the NBD[175,187]. These structures explain the requirement of ATP for DNA binding, however, in these conformations the dsDNA cannot access the active site of Mre11 (see Figure 9). The hydrolysis of ATP might lead to disengaged NBDs, which was proposed to result in the opening of the NBDs and the subsequent accommodation of DNA in the Mre11 active site (Figure 8)[181].

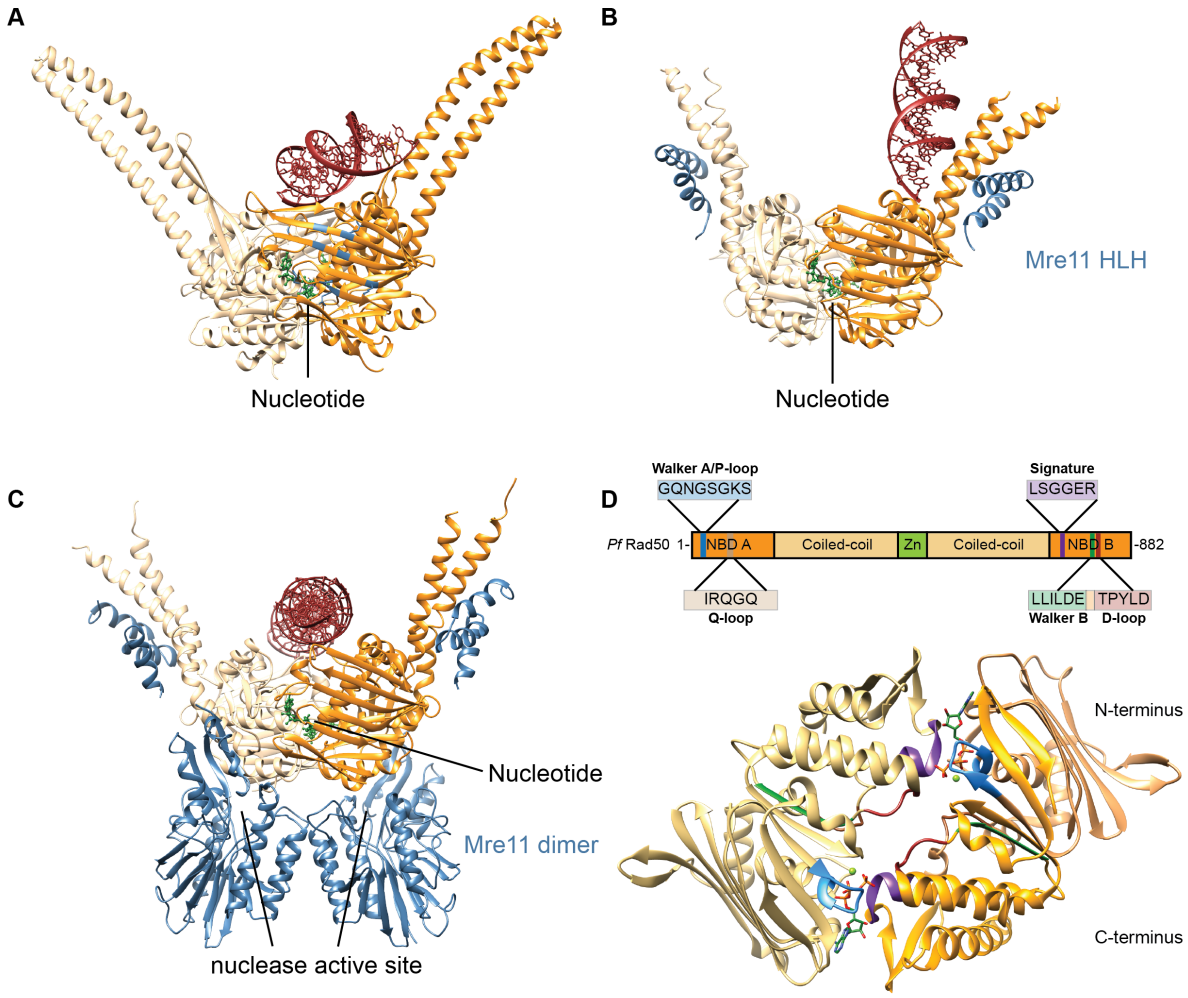

Figure 9: Structures of the Rad50 NBDs in complex with DNA. (A) Structure of the *Chaetomium thermophilum* Rad50 NBDs (pdb: 5dac) in complex with nucleotides (green) and DNA (red). Rad50S mutants are located on the β-sheets and indicated in blue. (B) Structure of the *Thermotoga maritima* Rad50 NBDs (pdb: 4w9m) in complex with nucleotides (green) and DNA (red). The Mre11 HLH motifs are shown in blue. (C) Structure of the *Methanococcus janaschii* Rad50 NBDs (pdb: 5dny) in complex with nucleotides (green) and DNA (red). The Mre11 dimer is shown in blue. (D) Domain organisation of Rad50 with the important motifs involved in ATP binding and hydrolysis indicated in the domain overview and the crystal structure of the *Pyrococcus furiosus* Rad50 NBDs (pdb: 1f2u). The C- and N-terminus of the right monomer is coloured in different shades of orange. Conserved motifs in the ATPase are highlighted: Walker A motif/P-loop (blue), Q-loop (brown), signature motif (violet), Walker B motif (green) and D-loop (red).

In the folded structure a conserved zinc hook is located opposite to the ATPase head domain. The zinc hook is present in homologs of Rad50 in all species[189]. It consists of a CX_1X_2C motif[189], with X_1 being Proline (85%) or Tyrosine (10%) and X_2 mostly being Leucine (80%) or Valine[190]. Zinc induces dimerization in the zinc hook domain, resulting in a zinc ion that is coordinated tetrahedrally by four Cysteines (two from each Rad50 polypeptide chain)[189]. X-ray crystallography has shown that the zinc hook can exist in two different conformations[189,191] (see Figure 10 A and B). The zinc hook of *P. furiosus* adopts a conformation in which the two

coiled coils extend in opposite direction, allowing bridging of DNA molecules as far a 1200 Å apart [189]. More recently, the structure of the human zinc hook was solved, which adopted a rod like conformation, in which both coiled coils extend into the same direction. In this study an additional dimerization interface and a break in the coiled coils in close proximity to the zinc hook was discovered. This break might be required to enable structural changes that occur upon ATP hydrolysis [191].
Mutations in the zinc hook region of the protein have severe consequences for the protein function. Deletion of the zinc hook results in a ΔRad50 like phenotype [192,193]. Interestingly, separation of function mutations do not only exist for the ATPase domain of Rad50 but also for the zinc hook domain. Disturbing the coiled coil dimerization interface close to the zinc hook or destabilising residues in the zinc hook region causes a phenotype in which the ability to repair DNA is still intact, but signalling of DNA damage is impaired [191,194]. Interestingly, the zinc hook domain can be substituted by other dimerization domains which partly restores MRN functions [116]. Replacing the zinc hook with the inducible FKBP dimerization cassette, partially rescues the phenotype, however, only if homodimerization is induced [192]. This indicates that dimerization of the zinc hook is one important function of this domain.

The connecting feature between the globular ATPase head and the zinc hook are the antiparallel coiled coils. The exact function of the coiled coils has not been determined, yet, and also the question why the coiled coils have to be so long could not be answered. Intriguingly, the coiled coil length is conserved between related species but differs between different domains of life [116]. This might indicate that chromosome organisation in different organisms requires a certain length of the Rad50 coiled coils. Truncation of the coiled coils has effects on several functions of the MRN complex and leads to reduced telomere length and spore viability in yeast [193]. However, studies with truncated coiled coils are difficult to perform since shortening of the coiled coils might alter the structure and thereby the functionality of the coiled coils. The coiled coils also seem to be involved in DNA binding and are required for efficient binding of MRN to DNA [196].
The coiled coils are a highly flexible structure that can adopt a variety of different conformations and do not only contain α-helices but also certain breaks with increased flexibility. For human Rad50, two of such flexible regions have been described, allowing the coiled coils to adopt a range of different conformations [197] and analysis of the human MRN complex with atomic force microscopy (AFM) revealed that the coiled coils change their conformation from an open structure to a parallel orientation upon DNA binding (Figure 10 C) [195]. This highlights the high flexibility of the coiled coils and might explain the two different conformation of the zinc hook found in X-ray crystallography [189,191].

The class of SMC proteins is composed of three different complexes in eukaryotes: Cohesin (SMC1/3), Condensin (SMC2/4) and SMC5/6 [184]. SMC proteins are highly conserved and are present in all three domains of life and almost all species [198]. In eukaryotes, the SMC proteins are heterodimers, while in prokaryotes homodimers are formed [184]. The closest relative of the SMC proteins are members of the Rad50 superfamily and both have a similar overall architecture (see Figure 11) [179,198]. Like in Rad50 their N- and C-terminus consists of an ABC ATPase domain.

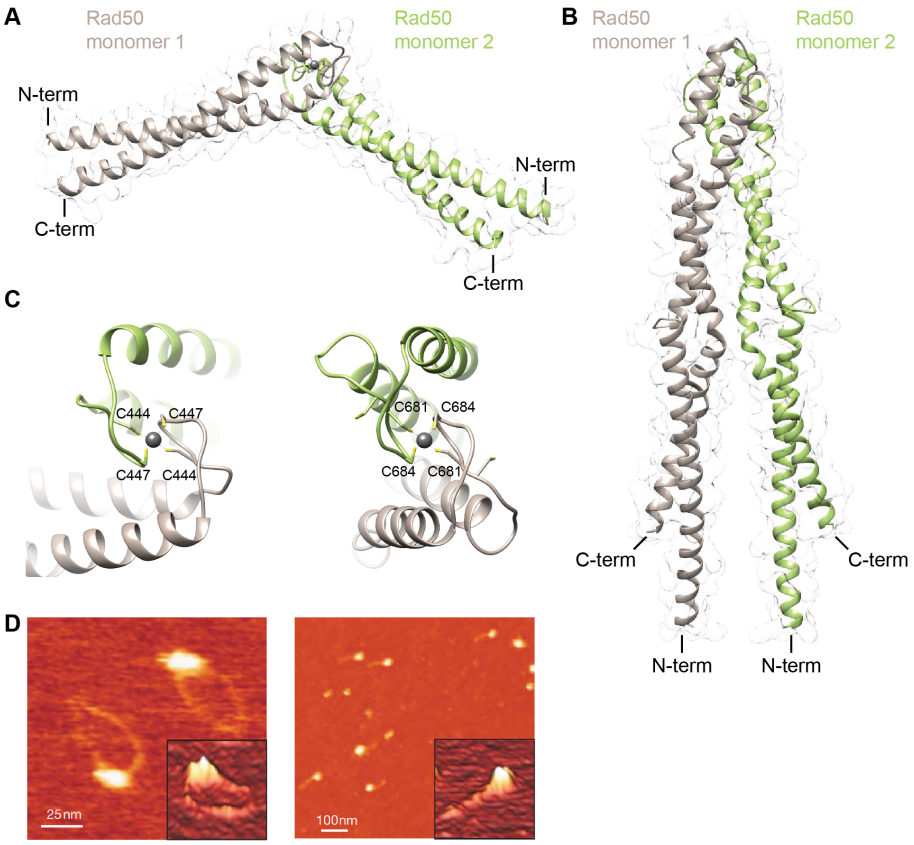

Figure 10: The zinc hook of *Pf*Rad50 and *hs*Rad50. (A) Crystal structure of the *P.furiosus* zinc hook in an open conformation that could tether two DNA molecules via intermolecular interactions between two Rad50 molecules (PDB: 1l8d). (B) Crystal structure of the human zinc hook in a closed conformation that shows a rod like conformation of the Rad50 coiled coils and intramolecular interactions between two Rad50 molecules (PDB: 5gox). (C) AFM images of *hs*MRN without (left) and with (right) DNA. Figure in C adopted from [195].

Instead of a zinc hook, the SMC proteins contain a hinge domain, which is connected to the head by flexible coiled coils [179]. Interestingly, substitution of the hinge domain with the Rad50 zinc hook in *Bacillus subtilis* does not affect the funtion of the SMC protein [199].

In complex with additional factors, SMC proteins fulfil several important functions in the cell. Cohesin holds sister chromatids together and condensin is required for the condensation of the chromosomes during cell division. SMC5/6 is the least well researched complex and involved in DNA repair [200].

Recently, parts of the *E. coli* SMC protein MukBEF coiled coil structure was solved. A flexible elbow region in the coiled coils was identified which allows bending of the coiled coils and brings head and hinge domain in close contact. This shows that the coiled coils do not only serve as a linker between head and hinge/zinc hook but are also involved in the molecular function of the proteins [201]. However, to date folding of the coiled coils has not been reported for Rad50.

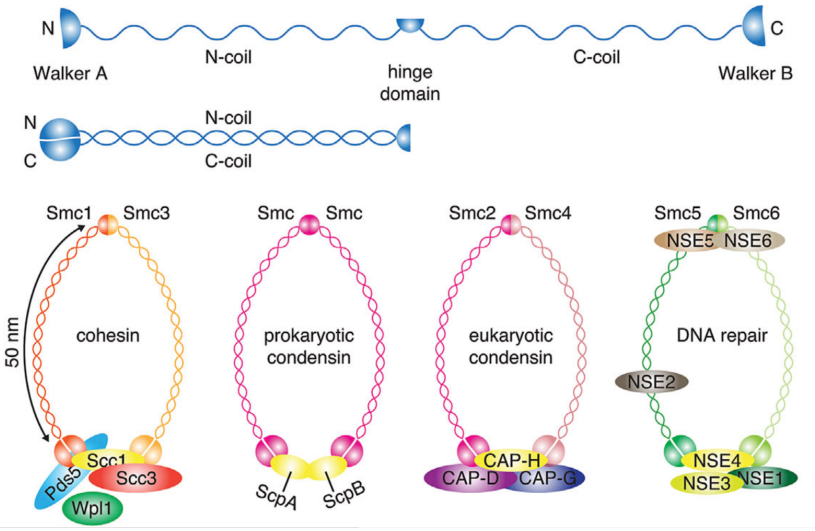

Figure 11: The prokaryotic and eukaryotic SMC proteins. The SMC proteins are related to Rad50 and have a similar domain organisation. ABC ATPase domains are located at the C- and N-terminus and in the middle of the sequence the hinge domain is located, analogous to the Rad50 zinc hook. The hinge and the ABC ATPase domains are separated by coiled coils (top). The two halves of the sequence fold back onto themselves in the tertiary structure (middle). In prokaryotes one homodimeric SMC protein exists (second from left) while eukaryotic organisms contain three different SMC proteins, Cohesin (Smc1/3), Condensin (Smc2/4) and Smc5/6. Figure adopted from [179].

1.3.3 Nbs1

Nbs1 is only present in eukaryotes and less conserved than Mre11 and Rad50 [190]. In fission yeast Nbs1 is denoted Xrs2. No enzymatic activity could be attributed to Nbs1 to date and it seems to serve as a protein interaction platform and scaffolding protein. Nbs1 consists of a N-terminal fork head associated (FHA) domain followed by two breast cancer associated 1 C terminus (BRCT) domains [202] (see Figure 12 A). FHA domains are present in several proteins and involved in different cellular processes, like DNA repair or transcription [203]. These domains recognise phosphothreonine residues and indeed, *S.pombe* Nbs1 has been shown to bind a phosphorylated Ctp1 peptide with its FHA domain (Figure 12 B) [202,203]. BRCT domains are found in proteins involved in DDR and can occur as single or multicopy domain [204]. BRCT domains are important interaction domains, e.g. for proteins or phosphorylated peptides [204]. Interaction of the Nbs1 FHA-BRCT-BRCT domain is best studied for mediator of the DNA-damage checkpoint 1 (MDC1), which binds to Nbs1 after phosphorylation of its SDT motifs [205,206]. The result of this interaction is a prolonged retention time of MRN on the site of a DSB [206,207].
The C-terminus of Nbs1 does not seem to harbour any known folds, however conserved motifs involved in DSB signalling have been associated with this region of the protein [116]. Crystal structures of *S. pombe* Mre11 nuclease and capping domain together with the Mre11 binding peptide from Nbs1 (residues 474 to 531) revealed that two Nbs1 peptides bind to one nuclease domain each. In addition, one Nbs1 molecule engages a loop on top of Mre11. This loop in Mre11 is specific to eukaryotes and binds to the highly conserved NFKxFxK motif. Interestingly, this

interaction results in an asymmetric complex, despite the 2:2 stoichiometry of Mre11 and Nbs1 (Figure 12 C)[170].

At the very C-terminus of Nbs1 an acidic patch, as well as a FxY/F motif are located that are important for interaction with HEAT repeats of the ATM kinase[208]. The acidic patch is a conserved motif that is also present in ATRIP (interacts with the kinase ATM- and Rad3 related (ATR)) and Ku80 (interacts with the kinase DNA-PKcs, see Figure 13)[209]. Additionally, NBS1 contains nuclear localisation signals and without Nbs1, Mre11 and Rad50 do not translocate to the nucleus[210,211].

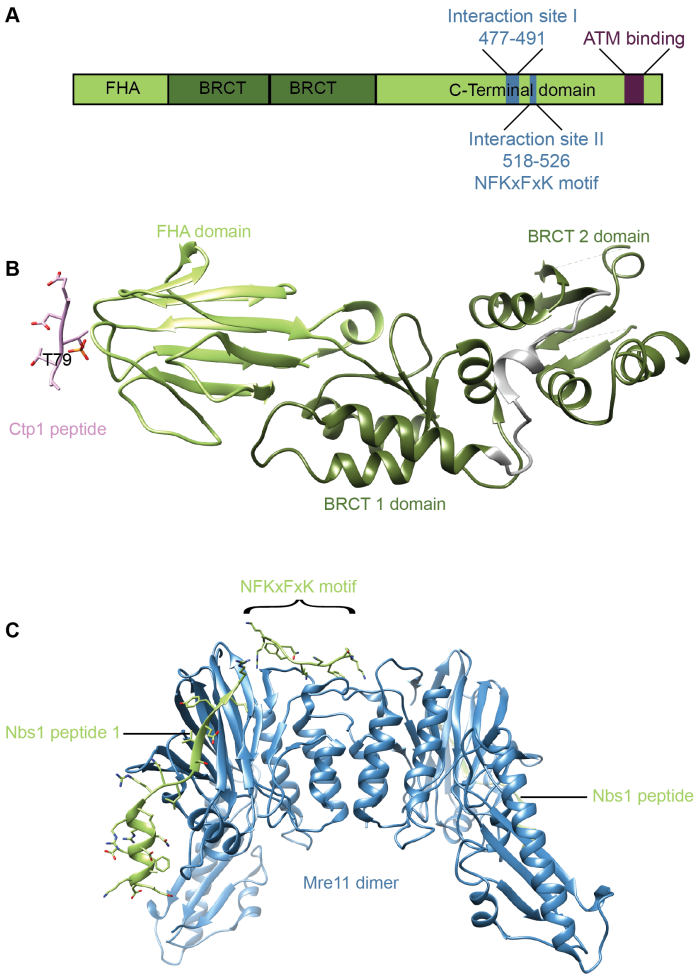

Figure 12: Structures of Nbs1 and the Mre11 dimer in complex with a Nbs1 peptide. (A) Domain organisation of Nbs1. (B) Structure of the FHA, BRCT1 and BRCT2 domains of Nbs1 (green) in complex with a phosphorylated Ct1p peptide (rose) from *S. pombe* (pdb: 3huf). (C) Mre11 dimer (blue) in complex with two Nbs1 peptide molecules (green) *S. pombe* (pdb: 4fbq).

1.3.4 CtIP

One of the most important interaction partners of MRN is CtBP1 interacting protein (CtIP, Ctp1 in fission yeast and Sae2 in budding yeast)[212] which is a largely unstructured protein with a N-terminal coiled coil tetramerization domain[213,214]. Highly conserved parts in CtIP/Sae2/Ctp1 are only the oligomerisation domain at the N-terminus and two motifs at the C-terminus (RHR/RNR in CtIP/Ctp1 and Sae2, CXXC in CtIP/Ctp1),[215]. Between these domains resides an intrinsically disordered region, which facilitates interaction with several proteins[215], like Nbs1[202] or BRCA1[216,217].
The enzymatic functions of CtIP and its homologues are still not fully understood. CtIP/Ctp1/Sae2 have been shown to bind DNA[213,214,218,219]. In addition, some studies report a nuclease activity for CtIP[218,219], however, others fail to find any nuclease activity[122,177,214]. The DNA binding activity might be important to bridge DNA ends[214,220]. It is known that CtIP/Ctp1/Sae2 is a cofactor for MRN/X and stimulates its nuclease activity[122,221,222]. *In vitro* this has been described for the budding yeast MRX complex which was stimulated in the presence of Sae2 to endonucleolytically cleave a dsDNA 10-15 bp away from a streptavidin block. This cleavage occurred preferably on the 5′ terminated strand[122] and a similar behaviour could also be observed for phosphorylated CtIP and MRN from human[177].
CtIP/Ctp1/Sae2 contains several motifs for phosphorylations[212]. Phosphorylation by CDK on Sae2 S267 is important for DNA resection, as is the analogue phosphorylation site T847 in CtIP[156,223]. Thus, the phosphorylation by CDK allows the cell to control DNA resection and restrict it to S and G2 phase.

1.3.5 MRN in a Cellular Context

1.3.5.1 DNA Damage Signalling

Aside from its enzymatic activities and DNA resection function, the MRN complex is also involved in DNA damage signalling, which occurs through ATM and possibly also ATR[224]. Together with ATR and DNA-PKcs, ATM belongs to the PI3K-like protein kinases (PIKK) and all three proteins phosphorylate a plethora of substrates on Ser or Thr[225]. Every kinase is activated by a different DNA structure; DNA-PKcs recognises DSBs bound by Ku[226] while ATR binds to RPA coated ssDNA[227], which results from processing during repair via HR or stalled replication forks. ATM is recruited to DSBs via Nbs1 (see Figure 13)[209,228]. Interestingly, the C-terminal interaction motif for their respective kinase is shared by Nbs1, Ku80 and ATRIP[209]. Activation of the kinases results in many cellular changes, like checkpoint activation and DNA repair or apoptosis and senescence[224].

ATM is a catalytic inactive dimer and upon DNA damage this homodimer transitions to its active monomer form[225]. The exact mode of interaction between MRN and ATM is not known,

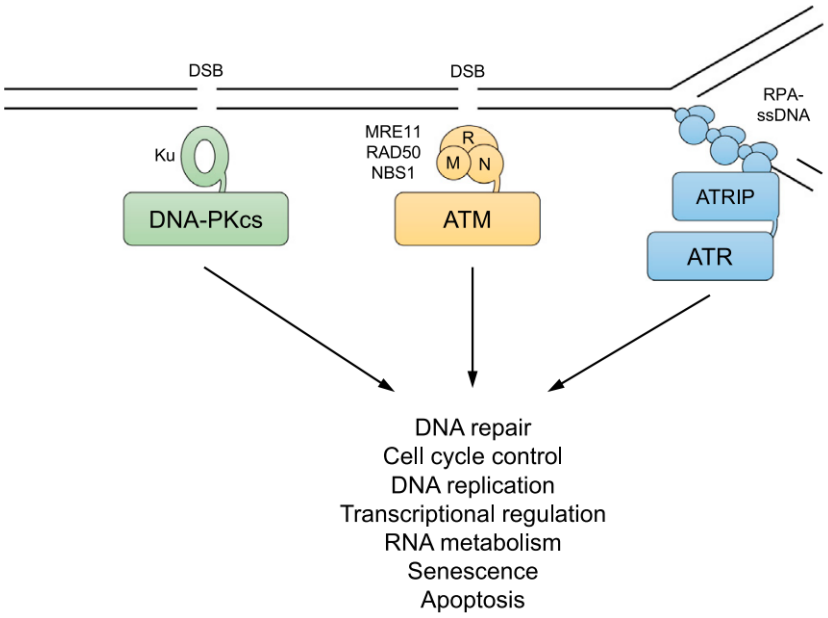

Figure 13: Signalling of DNA-PK, ATR and ATM. Three main kinases are involved in DNA damage signalling. DNA-PKcs is activated by Ku70/80 and DSBs (green), ATM is activated by MRN and DSBs (yellow) and ATR is activated by ATRIP and single stranded RPA-coated DNA. Activation of the kinases has an effet on several cellular processes, like cell cycle and cell death. Figure from [224].

yet. The ATM interaction site maps to the C-terminal residues of Nbs1 (see Figure 12) [209], however, the corresponding region on ATM has not been found, yet.

MRN promotes ATM activation, as seen by *in vitro* experiments monitoring the phosphorylation status of known ATM substrates [229,230]. In addition, the presence of DNA ends together with MRN increases ATM activation even further [230]. Additionally, ATM activation by MRN seems to require ATP binding to Rad50, but not ATP hydrolysis [196] and Mre11 nuclease activity seems to be dispensable for ATM activation and signalling [178,196].

Interestingly, MRN does not only recruit and activate ATM in response to DSBs [228,231] but all three proteins are also amongst its phosphorylation targets [232–234]. ATM-dependent phosphorylation of MRN has different effects. For instance, Nbs1 phosphorylation is important for induction of the S-phase checkpoint [232,235] and preventing Mre11 phosphorylation leads to defects in HR, possibly by limiting resection by EXO1 [234]. In addition to MRN, ATM activation results in the phosphorylation of more than 700 proteins on more than 900 sites [159,160]. This also includes other kinases meaning that ATM-dependent signalling is not only restricted to ATM substrates [224]. It should be noted, that the structure of the DSB changes in the course of its repair. In the beginning it is a blunt ended DSB that is transformed to a $3'$ ssDNA RPA coated overhang when repaired through HR. This change also shifts signalling by ATM to signalling by ATR, which recognises ssDNA [225].

1.3.5.2 Telomere Maintenance

The linear chromosomes of eukaryotes pose a challenge to cells, due to their similarity to DSBs and the shortening of the chromosome that occurs in each round of replication. This shortening of the chromosome is a side effect of the replication occuring in 5′-3′ direction and removal of the RNA primer from the lagging strands leaves a shorter 5′ strand. To avoid any loss of genetic information from the chromosome end and to protect the ends from recognition as DSBs, telomeres are present in eukaryotic cells to protect the chromosome end [43].
In vertebrates, telomeres consist of duplex DNA repeats (5′-TTAGGG-3′ in humans) of thousands of base pairs and a 3′ overhang of several hundred bases which is associated with six proteins that form the shelterin complex [157]. In humans and other higher eukaryotes, a t-loop is formed, in which the single stranded DNA overhang invades the DNA duplex and base pairs with the complementary strand, similar to the strand invasion intermediate present in HR (see Figure 14) [43]. The telomeres are shortened in every cell cycle, which limits the number of replication cycles [157] and thereby exhibits a tumour suppressor function [43].
Dysfunctional telomeres are generated when protection of the chromosome ends is abolished, e.g. by losing parts of the shelterin complex. Telomeres can then be recognised by DNA repair proteins and consequently are processed by NHEJ or HR factors to attempt repair. For a cell this has severe consequences, including cell cycle arrest, apoptosis and chromosomal aberrations [43,236].

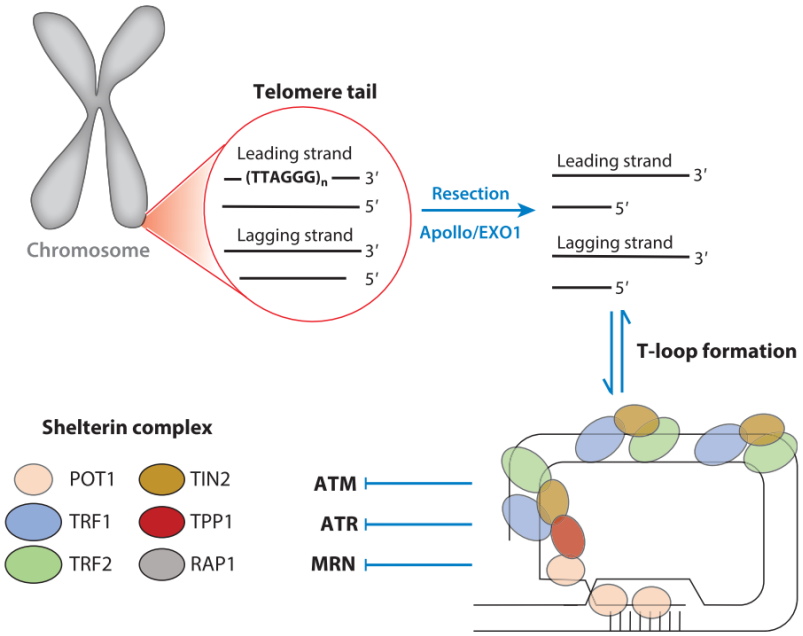

Figure 14: The structure of telomeres. The end structures of chromosomes are made up of telomeres, consisting of thousands of base pair long repeats and a 3′ overhang of several hundred base pairs. Together with the six proteins of the shelterin complex the telomere is formed. Figure from [157].

Initially, studies in yeast suggested a connection between telomeres and MRX, since the disruption of any of the MRN complex components led to shortened telomeres [237,238]. Later it

was shown, that recruitment of telomerase regulators was facilitated by telomere associated MRX in late S-phase[239]. Analogous to the yeast MRX complex, Nbs1 and Mre11 were found to localise to telomeres in human fibroblasts[240] and the interaction of all three members of the MRN complex with the shelterin protein TRF2 has been shown by immunoprecipitation[241]. A crystal structure of human Telomeric repeat-binding Factors 2 (TRF2) TRF homology domain in complex with a Nbs1 peptide (aa 419-449), indicated one interaction that might recruit MRN to the telomeres. Interestingly, this interaction is dependent on phosphorylation of S432 of Nbs1, which is dependent on CDK2 and thus couples this interaction to the cell cycle. As a result, Nbs1-TRF2 interaction is present in G1 and decreases in S and G2[242].
Dysfunctional telomeres lead to the accumulation of DNA damage response factors in human diploid fibroblasts (e.g. γ-H2AX, 53BP1 and Nbs1)[243] and the generation of telomere dysfunction-induced loci[236]. Similar to DSBs, MRN is required to activate ATM at dysfunctional telomeres[79,178].
Cells do possess a reverse transcriptase, called telomerase, which is able to maintain telomere length. This protein is usually inactivated in somatic cells, however, most cancers use the telomerase to keep dividing. An alternative pathway is the Mre11-dependent and recombination-based alternative lengthening of telomeres (ALT)[157], thus MRN is implicated in the continuous division of a subset of cancer cells.

1.3.5.3 Virus defence

Several viruses have been found to interact with DNA damage repair proteins, either to enhance their own replication or to circumvent detection[244]. Recognition of viral DNA can lead to repair attempts, rendering the viral DNA unusable for further viral reproduction or causing DNA damage signalling that might result in apoptosis[244].
Thus some viruses exist that contain proteins able to interact with MRN and alter its behaviour[157]. For instance, Adenovirus 5 contains oncoproteins, that are required during viral replication to avoid the formation of concatemers[245]. The Adenovirus 5 proteins target MRN for degradation and mislocalise MRN[245,246]. Consequently, if these viral proteins are not present concatemer formation depending on MRN and its nuclease activity is observed[245]. Additionally, a local DNA damage response is elicited by ATM in response to Adenovirus infection, which allows host DNA replication and inhibits viral DNA replication[246].
In addition to Adenoviruses, human papillomavirus 16 and Kaposi sarcoma herpesvirus also seem to employ strategies to circumvent MRN antiviral effects[157,247,248].
The inhibition of MRN and other DNA repair factors might be a reason for the tumorigenic potential that is exhibited by some of these viruses[157].

1.3.6 Involvement of the MRN Complex in Disease

Several germline mutations in the MRN complex are known, causing different syndromes, albeit with similar characteristics. Only hypomorphic mutations in humans were described, possibly because a complete loss of gene function is lethal, as seen in mice[116,178] and all disorders are autosomal recessiv[249].
Mutations in Mre11 cause ataxia-telangiectasia-like disease (ATLD), which is similar to the phenotype seen in patients with ataxia-telangiectasia (AT) caused by mutations in ATM. Nijmegen breakage syndrome (NBS) is caused by mutations in NBS1, while NBS-like disorder (NBSLD) patients carry mutations in Rad50. A hallmark of all syndromes is the increased genome instability, which causes a cancer predisposition in NBS and AT patients. Since only very few cases of ATLD and NBSLD have been reported, a predisposition for cancer can neither be excluded nor included[190].
Additionally, patients with ATLD and AT exhibit neurodegeneration, cerebellar ataxia and immunodeficiency[116,249]. Patients with NBS and NBSLD show microcephaly, mental retardation and in the case of NBS also immunodeficiency[116,249]. However, it was also reported that mutations in Mre11 can cause a NBSLD phenotype[249]. The clinical presentation varies with the type of mutation any of the three proteins carry. For instance, about 30 cases of ATLD are reported in the literature but only two presented with early onset of malignancies[250,251]. This shows that MRN is a highly intricate complex and that the functions of Mre11, Rad50 and Nbs1 are intertwined and cannot be separated from each other.

Data from structural studies and patient screens can be used to understand the effect of mutations in these complexes. N117S in human Mre11 (N122 in *S.pombe*), interacts with a conserved phenylalanine of the NFKxFxK motif and causes ATLD3 and 4[116,252]. Several other mutations can be mapped to the interaction sites between Mre11 and Nbs1. This includes the $Mre11^{W210C}$ mutation (causing ATLD7/8)[253] , $Mre11^{W243R}$ (ATLD 17/18)[254] and $Mre11^{D113G}$ (NBSLD)[249 116]. These mutations do not only affect complex stability and function but can also have an effect on the protein levels of Rad50 or Nbs1[250,255]. Furthermore, some of the known mutations lead to decreased Mre11 protein levels due to degradation e.g. nonsense-mediated mRNA decay[251] or alternative splicing events[250].
Premature degradation of Rad50 was observed in a patient with two different mutations in Rad50, reducing protein levels to only 5% compared to wild type cells[256].
For NBS patients, slightly more cases (over 150) have been reported in the literature. The most prominent mutation found in NBS patients is the 657del5 mutation, which leads to a premature stop codon. Due to the reinitiation of translation at an other start codon, two protein fragments of NBS1 are generated with amino acids 1-221 and 218-745[257,258].

DDR proteins are often mutated in cancers and mutations in MRN have been found in more than 50 cancers[157] however, less than 1% of cancer patients carry MRN gene variations[259]. Several studies have connected alterations in all three components of MRN to different types of cancer including breast cancer[260], acute myeloid leukemia (Rad50)[261] and prostate cancer (Nbs1)[262].

MRN is also an interesting target in cancer therapy. Targeting Rad50 in different cells leads to an increased sensitivity for other DNA damaging substances[259]. Furthermore, administration of the Mre11 exonuclease inhibitor mirin sensitizes different cancer cell lines to genotoxic substances, e.g. glioblastoma cells to alkylating agents[263]. This indicates, that MRN might not only be involved in the formation and progression of cancer but also serves as a promising cancer target.

1.4 The Bacterial MR Complex

In prokaryotes and archaea the MRN complex consists only of the Mre11 dimer and the Rad50 dimer[157]. Despite little sequence conservation, the structure of the Mre11 N-terminus, and the general complex assembly is quite conserved amongst species[116]. However, in contrast to the eukaryotic complex, *E. coli* cells do not require MR to be viable[264]. In *E. coli* the homologs of Mre11 and Rad50 are called SbcD and SbcC, respectively. For clarity reasons, the *E.coli* complex will be named *Ec*MR throughout the text.

*Ec*MR has similar enzymatic activities to eukaryotic MRN. 3′-5′ exonuclease activity on dsDNA ends and endonuclease activity on closed ssDNA was observed for *Ec*MR [265,266]. In contrast to the eukaryotic complex, the *Ec*MR dsDNA exonuclease activity is ATP-dependent. Cleavage of ssDNA only requires Mre11 and is ATP and Rad50 independent[265]. *Ec*MR is also able to cleave hairpins, preferably at the 5′ end of the bubble near the transition site from loop to double-strand[266,267]. This cleavage is dependent on the binding of ATP but not its hydrolysis. The resulting products carry a 5′ phosphate group and a 3′ OH group[267]. Interestingly, one study found that *Ec*MR cleaves hairpins, dsDNA and also cruciforms in a plasmid in steps of ∼10 bp[268].
Similar to the eukaryotic MRN complex, *Ec*MR was shown to incise blocked DNA ends with 20-28 nucleotides distance to the block[269]. Cleavage of a blocked DNA end is a relevant *in vivo* activity and helps to clear abortive topoisomerases and one study reported elevated gyrase-DNA levels in *E.coli* cells lacking the MR complex (see Figure 15)[264].
DSB repair in *E.coli* relies mainly on the RecBCD pathway and to a lesser extend on the RecFOR pathway (see Section 1.2.2). However, one study found, that *E.coli* cells are less viable when *Ec*MR is deleted in a strain in which DSBs are introduced by a DNA-methylation dependent endonuclease, which might point to a role in DSB repair depending on the type of DSB[270]. It should be noted, that the role of MR possibly differs in different bacterial cells. For instance, in *Bacillus subtilis*, MR deficient cells show slightly increased MMC sensitivity and[271] and in *Deinococcus radiodurans* deletion of MR causes increased susceptibility to γ-radiation[272].
In *E.coli*, Rad50 seems to localise to replication forks, while Mre11 was distributed throughout the cell[273]. *Ec*MR is partly regulated by RpoS, a factor that responds to different types of cellular stress, e.g. starvation, high/low pH or DNA damage[274]. *Ec*MR expression increases RpoS dependent during the post exponential phase in rich medium or was constitutively upregulated during growth on minimal medium[273].

What is the function of *Ec*MR if it is not required for the viability of cells? Several studies find a connection between genetic stability and *Ec*MR. Early experiments indicated that Rad50 is involved in the processing of palindromic DNA structures and interferes with the replication of a palindrome containing Phage λ [275]. Later it was shown, that *Ec*MR activity on a palindrome is replication dependent and that a two-ended DSB is created after the replication fork passed. The repair of this DSB requires proteins from the RecBCD pathway, the replication restart protein PriA and the Holliday junction processing enzymes RuvABC and RecG[276]. Palindromes and

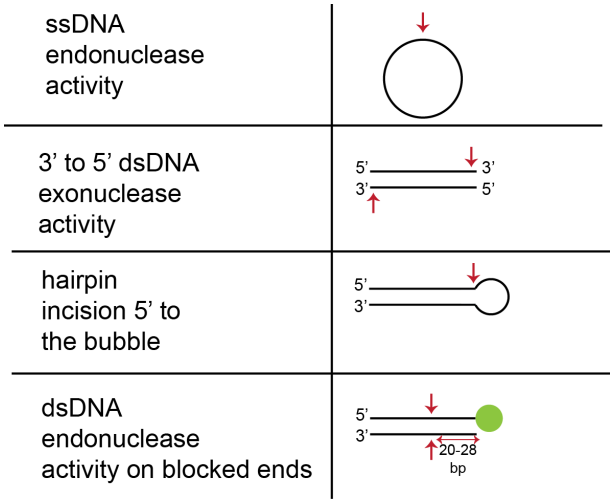

Figure 15: Main enzymatic activities of *Ec*MR. The four main nucleolytic activities of *Ec*MR include ssDNA endonuclease activity, 3′-5′ exonuclease activity, hairpin opening activity and dsDNA endonuclease activity on blocked DNA ends.

interrupted palindromes (also spaced inverted repeats) in DNA are places of increased genomic instability and their ability to form hairpin and cruciform structures can result in the alteration in DNA sequence e.g. deletions[277]. *Ec*MR seems to play an important role in maintaining the genome integrity, since inverted chromosomal duplications were found in *Ec*MR RecA mutant strains of *E.coli*[278].

Similar to palindromes, triplet repeats are a cause of DNA instability and different human diseases[279]. Triplet repeats are able to form pseudo-hairpins and *Ec*MR is able to cleave the pseudo-hairpin in a similar fashion as a regular hairpin on the loop/duplex-DNA transition region. The ability to cleave these pseudo-hairpins prevents *E.coli* from amplification of triplet repeats and thus a higher degree of DNA instability[266]. This has also been shown on a cellular level, where deletion of *Ec*MR was necessary to generate triplet repeat expansion[280]. Similarly, propagation of a plasmid with $(TGG)_{24}$ present on the leading strand is severely impaired, however, deletion of *Ec*MR restores propagation in *E.coli*[281].

Additionally, *Ec*MR might be involved in the final steps of DNA replication. To complete DNA replication in bacteria, the two generated DNA strands have to be merged at the *ter* region. This process seems to dependend on *Ec*MR and ExoI. Mutations of *Ec*MR and ExoI gives viable cells, however, close inspections of the ter region shows DNA amplifications. Joining of the DNA ends is also dependent on RecA and RecBCD and *Ec*MR is possibly required to cleave an over replicated intermediate[282].

Analysis of *Ec*MR with scanning force microscopy (SFM) indicated a mainly heterotetrameric form (M_2R_2, 73%) in which the coiled coil apexes present the main interaction interface[283]. Heterodimers have been observed to a lesser extend (21%) as well as multimers (4%). The overall contour length from apex to head domain was 39 nm, albeit heterogeneity in the length distribution was observed in *Ec*MR (24-57 nm). The conformations found for *Ec*MR and also the archaeal MR complex were quite different from the conformations observed for the eukaryotic

complexes of human and yeast protein (heterotetramers mainly joined at the heads with or without zinc hook engagement and a higher amount of multimers). However, it should be noted, that no ATP or ATPγS was used in this study[283]. Since ATP leads to the engagement of the head complex[181] this might be the reason for the observed dimeric head structures of *Ec*MR.

The only structural information available on *Ec*MR before this thesis came from a crystal structure of the Mre11 dimer with the residues 1-340 (nuclease and capping domain)[174]. This crystal structure shows that the active site is very similar to the structures of *Pf*Mre11 and *Tm*Mre11. Differences between the structures could be found in other parts e.g. the angle between the two nuclease domains. However, since Rad50 is not present in these structures the differences might be attributed to the missing ATPase. The mutation of any of the active site residues (D8, H10, D48, N83, H84, H184, H222, H224) results in a nuclease dead protein. Like the eukaryotic Mre11, the nuclease is clearly dependent on Mn^{2+} ions, since only the addition of manganese results in DNA degradation by Mre11[174].

1.5 Objectives

The MR(N) complex is a key player in HR in eukaryotes and the MR core complex is conserved across all domains of life. MR(N) has been studied extensively over the last decades from different organisms, however, several questions remain unanswered. The crystal structures solved so far cannot explain how the DNA accesses the Mre11 nuclease active site. In addition, the coiled coils were always shortened for X-ray crystallography despite being vital for the complex function. Many studies used thermophilic organisms for biochemical and structural studies. Proteins from these organisms often require higher temperatures to function properly, however, at these temperatures the increased autohydrolysis rate of ATP and melting of dsDNA pose problems for biochemical analyses.
Thus, the aim of this work was to elucidate the mechanism that underlies the DNA binding and processing properties of the MR complex by structural and biochemical means. The *Ec*MR complex is used as a model protein and has the advantage of being a simpler system than the MRN complex from eukaryotic organisms, since it has no additional post-translational modifications or cofactors. In addition, it comes from a mesophilic organism, which allows thorough biochemical characterisation. Furthermore, the full-length complex can be purified in sufficient amounts from *E. coli* cells.

In the first part of this thesis, biochemical assays were used to characterise *Ec*MR. Mainly, nuclease and ATPase activity as well as DNA binding were analysed. DNA substrates of different length and composition (e.g. AT- and GC-rich DNA) elucidated the DNA binding and cleavage properties of *Ec*MR.

The main goal of this work was solving the structure of the full-length *Ec*MR:DNA complex with cryo-electron microscopy (cryo-EM). Cryo-EM allows the use of full-length proteins and the presence of flexible domains in the protein structure. In order to elucidate if the full-length coiled coil domain has an effect on the head domain, *Ec*MR in complex with ATPγS was solved. Additionally, this DNA-free structure served as a good reference to understand DNA induced structural changes.
In a second step, the cryo-EM structure of full-length *Ec*MR in complex with a 60bp dsDNA and ADP was solved. Biochemical assays were used to validate the solved structures and support the proposed model.

2 Publications

2.1 The bacterial Mre11–Rad50 homolog SbcCD cleaves opposing strands of DNA by two chemically distinct nuclease reactions

Jan-Hinnerk Saathoff, Lisa Käshammer, Katja Lammens, Robert Thomas Byrne, Karl-Peter Hopfner, The bacterial Mre11–Rad50 homolog SbcCD cleaves opposing strands of DNA by two chemically distinct nuclease reactions, *Nucleic Acids Research*, Volume 46, Issue 21, 30 November 2018, Pages 11303-11314, https://doi.org/10.1093/nar/gky878

Summary

In this publication the biochemical properties of *Ec*MR are characterised. We found, that DNA binding and DNA-dependent ATPase stimulation was dependent on the length of the dsDNA substrate. Furthermore, ATPase stimulation was DNA topology dependent and maximal *Ec*MR ATPase stimulation was observed with linear DNA, while supercoiled DNA showed the lowest stimulation. In accordance with previously published data on *Ec*MR, we observed exonuclease activity on free and endonuclease activity on protein blocked DNA ends. The endonucleolytic incision was located 20-25 bp away from the protein block and was sensitive to the stability of the DNA duplex, since AT/GC-content and the presence of a DNA bubble influenced the endonuclease activity. The Mre11 dimer interface was investigated using the destabilising V68D mutant and the $M^{V68D}R$ complex incised the DNA endonucleolytically only in the presence of a DNA bubble. To investigate the chemistry of the cleavage reaction, DNA products of the *Ec*MR cleavage reaction were treated with either phosphatase or kinase. Two different cleavage chemistries were observed and 5′ clipping and 3′ endonuclease activity were chemically similar as well as 3′ exonuclease and 5′ endonuclease. As a result, a DNA strand that was exonucleolytically cleaved contains 3′ and 5′ OH groups, while a DNA strand after endonucleolytic incision contains 3′ and 5′ phosphate groups.
Taken together, we propose a mechanism in which the DNA is melted by *Ec*MR in the course of the cleavage process. In our model, the differences in cleavage chemistry between the exonuclease and the endonuclease reaction could be explained by opposite positioning of *Ec*MR on the DNA.

Author Contribution

I performed biochemical assays, especially nuclease assays and DNA binding assays together with Jan-Hinnerk Saathoff to analyse the biochemical properties of *Ec*MR. I was involved in analysing and discussing the results together with Jan-Hinnerk Saathoff and Karl-Peter Hopfner.

Published online 2 October 2018

Nucleic Acids Research, 2018, Vol. 46, No. 21 ***11303–11314***
doi: 10.1093/nar/gky878

The bacterial Mre11–Rad50 homolog SbcCD cleaves opposing strands of DNA by two chemically distinct nuclease reactions

Jan-Hinnerk Saathoff[1,2], Lisa Käshammer[1,2], Katja Lammens[1,2], Robert Thomas Byrne[1,2] and Karl-Peter Hopfner[1,2,3,*]

[1]Department of Biochemistry, Ludwig-Maximilians-Universität München, Feodor Lynen Straße 25, 81377 Munich, Germany, [2]Gene Center, Ludwig-Maximilians-Universität München, Feodor Lynen Straße 25, 81377 Munich, Germany and [3]Center for Integrated Protein Science, Munich, Germany

Received June 06, 2018; Revised September 14, 2018; Editorial Decision September 17, 2018; Accepted September 19, 2018

ABSTRACT

The Mre11–Rad50 complex is a DNA double-strand break sensor that cleaves blocked DNA ends and hairpins by an ATP-dependent endo/exonuclease activity for subsequent repair. For that, Mre11–Rad50 complexes, including the *Escherichia coli* homolog SbcCD, can endonucleolytically cleave one or both strands near a protein block and process free DNA ends via a 3′-5′ exonuclease, but a unified basis for these distinct activities is lacking. Here we analyzed DNA binding, ATPase and nuclease reactions on different DNA substrates. SbcCD clips terminal bases of both strands of the DNA end in the presence of ATPγS. It introduces a DNA double-strand break around 20–25 bp from a blocked end after multiple rounds of ATP hydrolysis in a reaction that correlates with local DNA meltability. Interestingly, we find that nuclease reactions on opposing strands are chemically distinct, leaving a 5′ phosphate on one strand, but a 3′ phosphate on the other strand. Collectively, our results identify an unexpected chemical variability of the nuclease, indicating that the complex is oriented at a free DNA end and facing a block with opposite polarity. This suggests a unified model for ATP-dependent endo- and exonuclease reactions at internal DNA near a block and at free DNA ends.

INTRODUCTION

The maintenance and accurate replication of genomes are fundamental processes in all kingdoms of life. Genome integrity is challenged by DNA damage caused by a large variety of physical, chemical and biochemical activities. DNA damage and complications in DNA replication can cause genomic alterations ranging from point mutations to gross chromosomal aberrations and aneupleuidy, which in humans is associated with the development of cancer and other diseases. In all phylogenetic kingdoms the propagation and maintenance of the genome critically depends on various pathways that detect, signal and repair DNA damage and deal with replicative stress (1).

The nuclease Mre11 and the ATPase Rad50 form an evolutionary highly conserved complex, which is involved in genome maintenance and replication by detecting and processing DNA double-strand breaks, hairpins and other abnormal terminal DNA structures (2). The bacterial homologs are known as SbcC (ATPase) and SbcD (nuclease) and form the SbcCD complex (3). The eukaryotic complexes contain a third subunit, Nbs1 in mammals and Xrs2 in yeast, and are denoted MRN or MRX (2). MRN/X and SbcCD detect DNA end structures and can process blocked or obstructed DNA ends and hairpins to make them accessible for DSB repair (4–8). The main DSB repair pathways following DNA end processing by MRN/X are various end joining reactions and homologous recombination (HR) (9,10).

MRN has a variety of biochemical activities. It displays 3′-5′ dsDNA exonuclease and ssDNA endonuclease activities, and opens hairpins in the presence of ATP (4,11–13). However, the physiologically most critical activity appears to be an ATP hydrolysis-dependent 5′ endonuclease activity at a 15–25 bp distance from blocked DNA ends, followed by limited 3′-5′ resection towards the DNA end (14–18). The endonucleolytic incision is essential to remove covalent DNA–protein crosslinks (DPCs), such as those formed by abortive topoisomerases in cycling cells or by the topoisomerase-like Spo11 during meiosis (8,19). MRN/X is also capable of removing the DSB binding factor Ku from DNA ends prior to HR (20–23). The mechanism of sensing of blocked ends by MRN/X or SbcCD is unclear, but recent

*To whom correspondence should be addressed. Tel: +49 89 2180 76953; Email: hopfner@genzentrum.lmu.de
Present address: Robert Thomas Byrne, Crelux GmbH, Am Klopferspitz 19a, 82152 Martinsried, Germany.

11304 *Nucleic Acids Research, 2018, Vol. 46, No. 21*

studies show that MRN can bind internal sites of DNA and slide towards blocked DNA ends (24).

Like MRN/X, SbcCD has 3′-5′ exonuclease activity, cuts the DNA near protein-bound DNA ends and cleaves hairpin structures 5′ of the loop (7,25). *In vivo* studies revealed that SbcCD cleaves covalently bound topoisomerases from DNA and removes specific DNA-secondary structures, including hairpins and cruciform structures (3,26,27). This role is conserved in budding yeast, where the Mre11 nuclease activity is essential to open hairpin structures and prevent the formation of palindromic duplications (6,28). More recent studies showed that SbcCD is critical in enabling proper replication termination by processing DNA bridges between the duplicated chromosomes that arise after the two convergent replication forks have passed each other (29).

Whereas the uncapping of hairpins and de-blocking of protein-bound DNA ends appears to be an evolutionarily conserved biochemical activity, pro- and eukaryotic complexes also show some differences. MRN/X is much more regulated through Nbs1/Xrs2 and requires the additional factor CtIP/Sae2/Ctp1 for end resection (30,31). In contrast, SbcCD possesses intrinsic, robust endonuclease activity by itself and can shorten the DNA ends further through an ATP-dependent binary endonuclease activity that cleaves both DNA strands, introducing serial DNA double-strand breaks in ∼10 bp intervals (32). This endonucleolytic cleavage of both strands has been recently reported for MRN, suggesting that even the complete clipping of blocked DNA termini is an evolutionarily conserved, inherent activity of the complexes (33).

Mre11/SbcD forms a dimer *via* two protein phosphatase 2 family phosphodiesterase/nuclease domains (34), and additionally contains a DNA-binding 'capping' domain (35,36), a linker, and a Rad50 binding domain (RBD) (37). SbcC/Rad50 contains an ATP-binding cassette (ABC) type nucleotide binding domain (NBD) with a 15–50 nm long antiparallel coiled-coil insertion that is capped by a zinc-hook dimerization motif (38). Two Mre11 and two Rad50 monomers assemble with a globular DNA binding and processing head module, containing the Mre11 dimer and two Rad50 NBDs, and a rod or ring-like protrusion that is formed by the two coiled-coils (34,39,40). Structural studies revealed that the ATP-dependent dimerization of the Rad50 NBD is coupled to the binding of ∼20 bp of DNA (41,42). However, previous studies have failed to provide a mechanism for how MRN/SbcCD detects DNA ends, let alone how it processes them in an ATP-dependent manner. In the crystal structure of the ATP bound and ATP/DNA bound conformations of Rad50, Mre11's DNA binding cleft and nuclease active site are blocked by the Rad50 dimer, although ATP is required for nuclease activities of the complex (42–44).

Here, we further investigate the ATP-dependent nuclease activities of the SbcCD complex. We characterize the influence of topology and length of DNA on stimulating SbcCD's ATPase, showing that relaxed DNA more efficiently triggers ATP turnover than supercoiled DNA. The presence of DNA ends primarily increases affinity, whereby SbcCD binds ∼25–30 bp. Whereas exonuclease activity requires ATP binding but not hydrolysis, endonuclease activity is robustly stimulated by blocked ends, ATP hydrolysis and an increased AT-content. Together with quantitative estimation of ATP turnover per cleavage and the requirement of SbcD dimer formation and dynamics, the data suggest a model in which repeated ATP hydrolysis by SbcCD near a blocked end generates a melted DNA amenable for cleavage. Most importantly, we find that DNA cleavage on opposing 3′ and 5′ strands, both at the DNA end and at internal sites, are chemically distinct and the phosphodiester is hydrolysed either at the 3' or at the 5' side. The chemical signature suggests a different binding polarity of SbcCD at a DNA end compared to facing a protein block and helps sterically unify endo- and exonuclease reactions.

MATERIALS AND METHODS

Cloning, protein expression and purification of SbcCD

The genes encoding SbcD and SbcC were cloned into the plasmids pET21b and pET28 (with a modified multiple cloning site), respectively. The gene encoding SbcD was cloned such that the recombinant protein had a C-terminal hexahistidine tag.

Recombinant SbcCD was produced by co-transforming SbcC and SbcD plasmids into *Escherichia coli* BL-21 (DE3) cells. A single colony was picked and grown in LB media to an OD_{600} of 0.6 at 37°C under aerobic conditions. Recombinant protein expression was induced by addition of 0.5 mM IPTG and the cultures were grown overnight at 18°C. Cells were harvested by centrifugation, resuspended in lysis buffer (25 mM Tris pH 7.5, 150 mM NaCl, 10 mM Imidazole and 5 mM β-mercaptoethanol) and disrupted by sonication. The lysate was cleared by centrifugation and applied onto Ni-NTA resin (Qiagen), followed by 2 wash steps with Lysis buffer and subsequent elution (25 mM Tris pH 7.5, 100 mM NaCl, 200 mM Imidazole and 5 mM β-Mercaptoethanol). The elution fractions were applied onto a 1 ml Q HiTrap column (GE Healthcare) and eluted with a linear gradient from 0–100% Buffer A (25 mM Tris pH 7.5, 100 mM NaCl) and Buffer B (25 mM Tris pH 7.5, 1000 mM NaCl). SbcCD eluted as one peak at 30% Buffer B and the peak fractions were pooled, concentrated and further purified by size-exclusion chromatography using a Superose 6 10/30 GL column (GE Healthcare) equilibrated with Buffer C (50 mM Tris pH 7.5, 150 mM NaCl, 10% glycerol). SbcCD eluted as a single peak and the fractions of interest were pooled, concentrated and flash frozen in 10 μl aliquots.

DNA substrates

For ATPase activation, ΦX174 RFI, RFII or Virion DNA (New England BioLabs®) was used. Linear plasmid DNA was produced by treating ΦX174 RFI with PsiI (New England BioLabs®) followed by heat inactivation.

All oligonucleotides were purchased from Metabion (Planegg, Germany) and purified *via* polyacrylamid gels. RB22 (CGGGTAGTAGATGAGCGCAGGGACACCG AGGTCAAGTACATTACCCTCTCATAGGAGGTG) and RB27 (CACCTCCTATGAGAGGGTAATGTACT TGACCTCGGTGTCCCTGCGCTCATCTACTACC CG) were annealed in annealing buffer (50 mM NaCl, 25 mM Tris pH 7.5, 10 mM $MgCl_2$) with a molar excess of 1.1

Nucleic Acids Research, 2018, Vol. 46, No. 21 **11305**

of unlabeled oligo over the labeled oligo. Oligonucleotides for ATPase and DNA binding assays had a different sequence and were annealed in a 1:1 molar ratio. HS 21 (CGCTTTATCAGAAGCCAGACATTAACGCTTCT GGAGAAACTCAACGAGCTGGACGCGGAT) was annealed to the complement HS37 (ATCCGCGTCCAG CTCGTTGAGTTTCTCCAGAAGCGTTAATGTCT GGCTTCTGATAAAGCG). If shorter double-stranded DNA was used, the HS21 sequence was trimmed on the 3′ end and annealed to the oligonucleotide with the respective complement sequence. For the fluoresecence anisotropy binding experiments, the dsDNA was 6-FAM labeled on the 5′ terminus.

Nuclease assay

Nuclease assays were carried out in assay buffer (25 mM Tris pH 7.5, 50 mM KCl, 5 mM $MgCl_2$, 1 mM $MnCl_2$, 0.1 mg/ml BSA, 1 mM DTT) with 1000 nM SbcCD (heterotetramer) and 200 nM of DNA substrate. Where indicated, reactions were supplemented with a 15-fold excess of a single-chain variable fragment against fluorescein (FAM-scFv) (45) or Streptavidin (IBA) over DNA concentration. Unless specified otherwise, reactions were started by DNA addition. Reactions containing DNA with free ends were incubated at 37°C for 15 min, reactions containing end-blocked DNA were incubated for 5 min. Reactions were terminated by mixing 10 μl of the reaction with an equal volume of 2× loading buffer (8 M urea, 20 mM EDTA, 6% Ficoll® 400).

For kinase and phosphatase treatment, the nuclease reactions were terminated by heating to 80°C for 15 min. 10 μl of the nuclease reaction were treated with either T4 Polynucleotide Kinase or Antarctic Phosphatase (New England BioLabs®) in the enzyme-specific 1× reaction buffer in a final volume of 20 μl. The reactions were terminated by adding equal volume of 2× loading buffer. To generate short cleavage products, the 60 bp substrate was treated with ExoIII, DnaseI (both New England BioLabs®) and Benzonase® (Merck Millipore) according to manufacturer's specifications.

Reaction products were resolved on 12% denaturing polyacrylamide gels (Rotiphorese® DNA sequencing system) in 1× TBE buffer. Gels were run for 90 min at a constant power of 32 W and scanned by a Typhoon fluorescence imager (GE healthcare). 6-FAM-labeled substrates were imaged with a 473 nm laser and 510 nm filter. The images were analyzed and integrated with the ImageJ software.

ATP Hydrolysis assays to measure steady-state kinetics

To monitor the hydrolysis rate of ATP, the hydrolysis of ATP was coupled to oxidation of NADH, which can be monitored spectrophotometrically. The reaction buffer contained NADH (0.35 mM), pyruvate kinase/lactate dehydrogenase (20 U/ml PK, 30 U/ml LDH), phosphoenol pyruvate (2 mM) and ATP (1 mM). The assays were conducted at 37°C in assay buffer (25 mM Tris pH 7.5, 50 mM KCl, 5 mM $MgCl_2$, 1 mM $MnCl_2$, 1 mM ATP, 0.1 mg/ml BSA, 1 mM DTT) and the reaction was started by the addition of SbcCD. The rate of NADH decay/oxidation was monitored fluorometrically by measuring the absorbance at 340 nm on an Infinite M1000 microplate reader (Tecan) at 37°C over a period of 20 min. (46). Estimates of kinetic data (k_{cat}, K_M, K_{act}) were determined by fitting reaction data to the Michaelis-Menten equation with Prism (GraphPad).

Fluorescence anisotropy DNA binding assays

SbcCD dilutions were prepared in assay buffer (25 mM Tris pH 7.5, 50 mM KCl, 5 mM $MgCl_2$, 1 mM $MnCl_2$, 1 mM DTT) and mixed with the DNA substrate (5 nM final assay concentration, in assay buffer) in a 1:1 (v/v) ratio. After incubation for 20 min at 25°C, the fluorescence anisotropy was measured at an excitation wavelength of 470 nM and emission wavelength of 520 nM. Data were analyzed with Prism (GraphPad) and K_D values determined by fitting the anisotropy data to a bimolecular equilibrium model: $Y = Af - (Af - Ab)\frac{x}{Kd - x}$

RESULTS

DNA ends and DNA topology differentially stimulate SbcCD's ATPase

Human and yeast MRN/X have ATPase rates <0.1 ATP/min, which is stimulated 20-fold for human MRN and 10-fold for yeast MRX by linear double-stranded DNA (dsDNA) (47,48). In the absence of DNA, we obtained a similarly low ATPase activity with a k_{cat} of 0.008 s^{-1} for SbcCD. 60 base pair (bp) dsDNA stimulated the ATPase hydrolysis 26-fold, while single-stranded DNA (ssDNA) had no effect. SbcCD has a K_M for ATP hydrolysis of 46 ± 6 μM in the presence of dsDNA (Supplementary Figure S1A), in the same range as human MR(N) and phage T4 gp46/47 (48,49). Altogether, SbcCD displays similar basal ATPase characteristics as its orthologs in other domains of life.

To test to the role of DNA topology on ATP hydrolysis we measured the stimulatory effect of a 5.4 kb plasmid in (i) supercoiled (ii) relaxed (iii) linearized and (iv) single-stranded state. SbcCD and ATP were kept at constant concentrations and the DNA was added in increasing amounts. Circular single-stranded DNA did not stimulate ATP hydrolysis of SbcCD. The supercoiled plasmid activated the ATPase up to 9-fold ($k_{cat} = 0.072 \pm 0.006\ s^{-1}$), whereas the nicked plasmid activated the ATPase 26-fold ($k_{cat} = 0.21 \pm 0.02\ s^{-1}$). The increased activation of relaxed DNA is clearly direct and not attributable to higher affinity binding, since the K_{act} (concentration at half maximal activation) is 2-fold lower for the supercoiled plasmid than for the nicked plasmid. It should be noted that even though nicked and supercoiled DNA can stimulate SbcCDs ATPase activity, we did not observe any DNA cleavage activity. In contrast, linearized plasmid DNA is readily degraded (Figure 1A, Supplementary Figure S2). Comparing the ATPase stimulation of a 60 bp dsDNA and a linearized plasmid revealed that 60 bp dsDNA is able to stimulate the ATPase activity stronger than the linearized Plasmid at the same molarity (Supplementary Figure S3).

Linearizing the plasmid with PsiI, which generates blunt ends, stimulated k_{cat} of ATP hydrolysis ($0.200 \pm 0.007\ s^{-1}$) similar to a nicked plasmid, however K_{act} is lowered 4-fold, showing an increased affinity at lower DNA concentrations. One DNA break/hairpin in an *E. coli* cell would

11306 *Nucleic Acids Research, 2018, Vol. 46, No. 21*

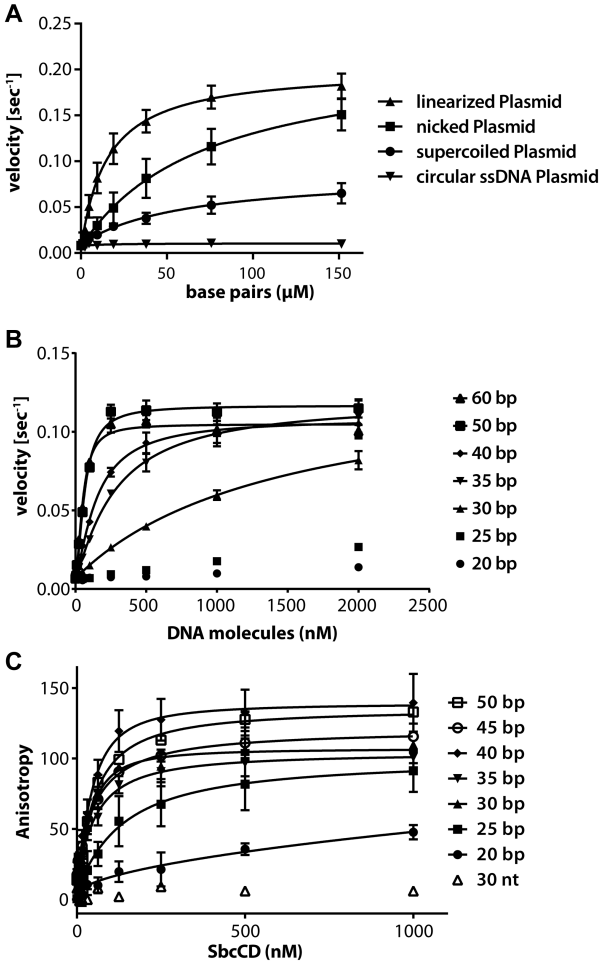

Figure 1. ATP hydrolysis stimulation and DNA binding of the SbcCD^{wt} complex. (**A**) The ATP hydrolysis rate of SbcCD^{wt} was measured in dependence to increasing plasmid DNA concentrations. Bacteriophage ΦX174 Plasmid DNA (5386 bp in length) was added as single-stranded, supercoiled, nicked or linear DNA. The data were fit to a Michaelis–Menten equation, error bars indicate the deviation from three replicates. (**B**) DNA stimulation of ATP hydrolysis by the nuclease-deficient SbcCD^{H84Q} complex. The steady-state ATPase rates were measured at 37°C in the presence of 1 mM ATP, 5 mM $MgCl_2$ and 1 mM $MnCl_2$. DNA with 20–60 bp in length was added as an activator. The data was fit to a Michaelis-Menten equation, error bars represent the standard deviation of three measurements. (**C**) DNA binding of SbcCD^{H84Q} to 20–50 bp DNA was assayed in the presence of 1 mM ATP, 5 mM $MgCl_2$ and 1 mM $MnCl_2$. DNA concentration was kept at 5 nM; the SbcCD^{H84Q} concentration ranged from 2 to 1000 nM. Data points represent the change in fluorescence anisotropy and the data were fit to a 1 to 1 binding equation. Error bars represent the deviation from three independent experiments.

correspond to an approximately nanomolar concentration of DNA breaks, not taking into account molecular crowding effects (50). At this concentration, the ATPase was activated 7-fold by linear DNA, but only 2-fold by nicked DNA (Figure 1A, Supplementary Table S1C).

Our data show that both topological features of the DNA and the presence of DNA ends affect the ATPase rate of SbcCD. k_{cat} is higher with relaxed DNA than with supercoiled DNA, but it is not further enhanced by the presence of DNA ends. DNA ends appear to primarily increase the affinity of the complex but not its intrinsic ATP turnover rate.

DNA length requirements for DNA binding and ATPase activity

To determine the minimal length that is required for robust ATPase activation we tested dsDNA from 20 to 60 bp in length. A nuclease-deficient mutant (SbcCD^{H84Q}) of SbcCD was used in the assays to prevent DNA degradation during the course of the study. H84Q decreased the ATPase activity of SbcCD by ∼15% (Supplementary Figure S1A). 20 and 25 bp DNA did not substantially stimulate ATP hydrolysis of SbcCD. A moderate activation was obtained with 30 bp DNA. Increasing the length of DNA to 35 bp and longer robustly stimulated the ATPase rate (Figure 1B). Since we used concentrations of the SbcCD heterotetramer of 500 nM to also probe for effects of shorter DNAs, binding affinities well <500 nM of DNA >40 bp (see below) did not allow us to derive affinities in these studies. Rather, we titrated DNA end binding by SbcCD. In the case of 50 and 60 bp DNA, the near maximal ATPase activation was already obtained at a concentration of 250 nM DNA, where the concentration of DNA ends is the same as the concentration of SbcCD. With shorter DNA, steric competition might prevent productive (ATPase) binding of two complexes to both DNA ends. In any case, the 20–25 bp minimal requirement for the DNA stimulation of ATPase activity coincides well with the footprint of ATP bound NBD dimers of Rad50, which is ∼20 bp.

To see how the DNA length dependent activation of the ATPase coincides with DNA binding affinity, we measured DNA interaction through changes in the fluorescence anisotropy of labeled DNA of different lengths. We first tested DNA binding in the presence and absence of ATP. SbcCD did not bind single stranded DNA (ssDNA) in either the presence or absence of ATP. In addition, we could not detect binding to dsDNA in the absence of ATP, indicating that the formation of engaged NBDs is critical for DNA binding by SbcCD (Figure 1B, Supplementary Figure S1C). Next, we evaluated the affinity of SbcCD in the presence of 1 mM ATP for dsDNA oligonucleotides, ranging from 20 to 50 bp in 5 bp increments. SbcCD shows low affinity to 20 bp DNA and moderate affinity to 25 bp DNA (K_D = 146 ± 46 nM). However, lengthening the DNA to 30 bp DNA resulted in a notable increase in binding affinity (K_D = 43 ± 7 nM). Further lengthening of the DNA did not affect the K_D, which remained in the range of 50 to 60 nM (Figure 1C, Supplementary Figure S4). Therefore, maximal DNA end binding has a 'footprint' of ∼25–30 bp, whereby affinity is not enhanced by longer DNA.

Characterizing the nuclease activities of SbcCD on 60 bp DNA

MRN/X and SbcCD comprise nuclease activities that are conserved amongst bacteria, yeast and human, but also show unexplained differences. Conserved functions are the (i) 3′-5′ exonuclease on dsDNA, (ii) cleavage of dsDNA ad-

Nucleic Acids Research, 2018, Vol. 46, No. 21 **11307**

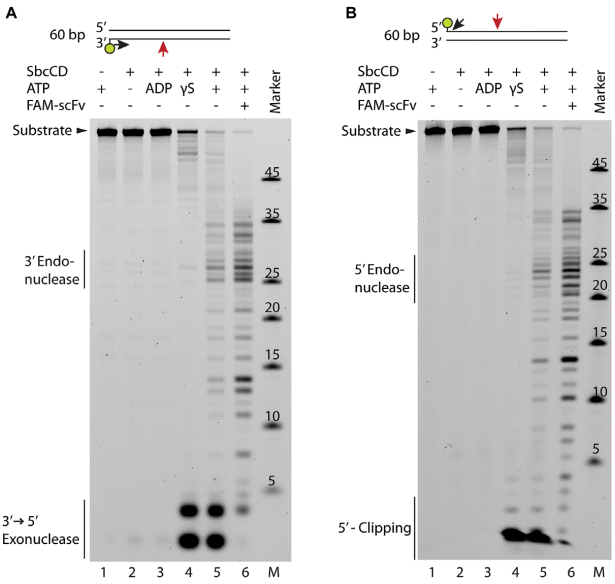

Figure 2. Nuclease activity of SbcCD^{wt} towards 60 bp DNA. (**A**) SbcCD^{wt} was assayed in the presence of 1 mM ADP or ATP(γS), 5 mM $MgCl_2$ and 1 mM $MnCl_2$ at 37°C. The 60 bp DNA substrate was labeled on the 3′ end with 6-FAM. FAM-scFv is a single chain fragment that binds to Fluorescein dyes with a K_D of 4 nM. Reactions with unblocked DNA substrates were quenched after 15 min, reactions containing FAM-scFv were quenched after 5 min. The cleavage products were separated by Urea-PAGE and visualized on a Typhoon scanner. Major cleavage products of SbcCD are depicted above. (**B**) Nuclease assay as in (A), but with 5′ labeled 60 bp DNA.

jacent to a protein-blocked DNA end, (iii) cleavage of hairpin structures on the 5′ side of a hairpin, and (iv) cleavage of 3′ and 5′ overhangs (7,11,12,25). On a long hairpin substrate, SbcCD displayed a progressive 'binary' endonuclease that nicks both DNA strands and introduces DNA double-strand breaks in 10 bp intervals (32), an activity that has not been reported so far for enzymes from other species.

To further characterize the nuclease activities of SbcCD, we tested the degradation of a 60 bp DNA labeled with a fluorescent dye at the 5′ or 3′ terminus. In the absence of ATP and presence of ADP, faint low molecular weight products appear which may point to a residual 3′ exonuclease activity independent of ATP. The presence of non-hydrolysable ATPγS induces robust 3′-5′ exonuclease activity of SbcCD (Figure 2A, lanes 2–4). Of note, we also observed a clipping activity near the 5′ end of DNA (Figure 2B, lanes 4 and 5). This is likely due to prior degradation of the 3′ terminus, as phosphorothioate protection of the complementary 3′ end led to a high reduction of this activity (Supplementary Figure S5, lanes 5–8). In the presence of ATP, internal DNA cleavage products could be detected. They appear most prominently at 27 bp from the 3′ end and 23 bp from the 5′ end (Figure 2A and B, lane 5). We then tested the cutting efficiency in the presence of a protein block, formed by an anti-fluorescein antibody derived single-chain fragment variable (FAM-scFv) (45). The block is similar in size to the streptavidin–biotin conjugate used in previous experiments (7) and mimics a blocked DNA end or a DNA–protein crosslink (DPC), structures that often occur at DNA double-strand breaks (DSBs). The presence of a protein block stimulated the endonucleolytic cleavage, as predominantly endonuclease products appeared (Figure 2A and B, lane 6). In contrast to the exonuclease that is fully active in the presence of ATPγS, the block-stimulated endonucleolytic incision is highly decreased in presence of ATPγS and therefore promoted by ATP hydrolysis (Supplementary Figures S6 and S7A, lanes 4 and 5). An 80 bp duplex DNA was also incised 27 bp from the DNA end, therefore the 27 bp distance was determined by the labeled DNA end (Supplementary Figure S5, lanes 1–4).

SbcCD's endonuclease activity is sensitive to the melting stability of DNA

The mechanism how Mre11 family proteins such as SbcD incise double-stranded DNA is not known yet. Structures of Mre11 with dsDNA reveal that the manganese ions of Mre11 are concealed in the active site and the bound B-DNA is at least 5 Å away from a position that could be productive for cleavage. At least endonucleolytic activity would require, from sterical considerations on the basis of available structures, DNA duplex unwinding in order to reach the active site metals. Indeed unwinding activity was reported for the human MRN. This process was Nbs1- and ATP-dependent and enhanced by a 44 nucleotide overhang (11,51). Processive DNA unwinding of a 50 bp duplex was also reported for MR from *Thermotoga maritima* (42).

To relate putative melting of duplex DNA to nucleolytic incision, we designed DNA substrates with different local AT and GC contents, since the local stability of B-DNA can be tuned via the GC/AT content (52). 60 bp DNA was modified from position 15 to 29 (relative to the 6-FAM dye) with, (i) mixed AT/GC-content, (ii) 100% AT-content or (iii) 100% GC-content. The endonuclease activity was tested in both the presence and absence of a protein-bound DNA end. The unlabelled DNA end was protected from degradation by phosphorothioates on the 3′ terminus.

As observed in previous assays, SbcCD cleaved 60 bp DNA with mixed AT/GC content 27 bp from the 3′ end with moderate activity (Figure 3A lane 5). Endonuclease became more efficient with AT-rich DNA and almost vanished with GC-rich DNA (Figure 3A lanes 6–7). Therefore, SbcCD's endonuclease is sensitive to local stability of the dsDNA and, as judged from AT/GC content, performs better when the DNA can be melted more easily. Of note, the cutting preference at AT-rich regions was overridden by a protein block and the three duplex DNAs were incised with apparently similar efficiencies (Figure 3A, lanes 8–10).

We next interrogated whether DNA stability affects ATPase rates or DNA affinity. Indeed, SbcCD bound AT-rich DNA with a higher affinity than GC-rich DNA. The affinity increased 3-fold from a K_D of 132 nM to 45 nM. In contrast, the AT/GC content did not affect the ATPase activation under the nuclease assay conditions (Figure 3B and C). Thus, the increase in endonucleolytic efficiency or increase in binding affinity to AT-rich DNA cannot be attributed to higher ATPase rates. It rather appears that continuous ATPase activity generates perhaps melted or otherwise confor-

11308 *Nucleic Acids Research, 2018, Vol. 46, No. 21*

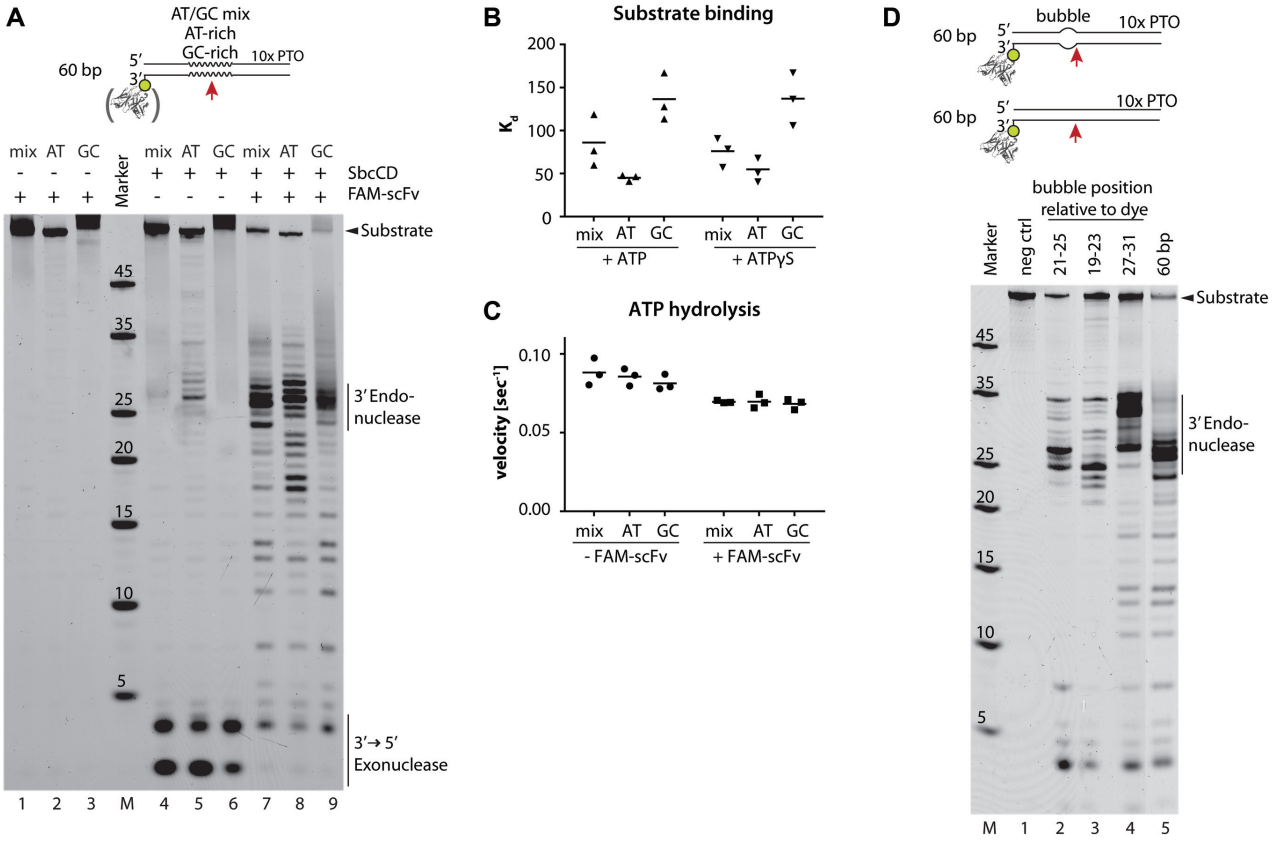

Figure 3. SbcCD cleaves double-stranded DNA dependent on the local AT/GC concentration and pre-melted DNA stretches. (**A**) Nuclease activity of SbcCD^{wt} was assayed in the presence 1 mM ATP, 5 mM $MgCl_2$ and 1 mM $MnCl_2$ at 37°C. The DNA was labeled on the 3′ end with 6-FAM and contained different AT/GC concentrations from position 15 - 29 (relative to the dye). FAM-scFv - single chain fragment that binds to the 6-FAM dye. (**B**) Dissociation constants (K_D) of SbcCD^{H84Q} were obtained by fitting fluorescence anisotropy data to a 1 to 1 binding equation. Bar represents the mean of three values. (**C**) The steady-state ATP hydrolysis rates of SbcCD^{wt} were measured during the nuclease reactions in (A). Bar represents the mean of three values. (**D**) The nuclease activity of SbcCD^{wt} towards 60 bp DNA with pre-melted DNA regions (bubble) was tested. SbcCD^{wt} cleaves the DNA substrates 5′ to the pre-melted region

mationally altered DNA that is more efficiently bound and cleaved by the nuclease.

To see how efficiently ATP hydrolysis and endonuclease are coupled, we monitored the rate of ATP hydrolysis under conditions identical to the nuclease assay (Figure 3C). In the course of 60 bp DNA degradation, SbcCD hydrolyzed approximately 800 molecules ATP to degrade one molecule of DNA in the absence of a protein block. Protein-blocked DNA used up 200 ATP molecules per DNA cleavage. Since exonuclease activity is observed in the presence of the non- or slowly hydrolysable analog ATPγS, it appears that cleavage of terminal nucleotides does not strictly require rounds of ATP hydrolysis. However, the lack of endonuclease activity observed in the presence of ATPγS, and consistently the high numbers of ATP hydrolysis events per endonucleolytic cleavage suggest that rounds of ATP hydrolysis catalyze an inefficient or reversible step prior or during cleavage.

Encouraged by these novel findings, we designed DNAs with unpaired stretches of five nucleotides (bubbles) mimicking melted DNA at various distances from the DNA ends. A protein-blocked 60 bp fully base paired duplex was digested in the previously characterized pattern, having a major incision species at 27 bp. Introduction of the bubble from position 27 to 31 leads to incision events at position 31–35, another prominent cleavage product appeared at 27 bp. Locating the bubble at position 19–23 leads to a major cleavage site at 25 nucleotides, position 21–25 guides the incision to 27 bp (Figure 3D, lanes 2–5). Therefore, SbcCD cleavage occurs at the 5′ side of unpaired DNA. Increasing the length of the bubble to seven nucleotides reduced cutting efficiency, so it is unlikely that SbcCD unwinds DNA very extensively at this site. In the presence of non-hydrolysable ATPγS we could not detect endonucleolytic degradation with any of the substrates (Supplementary Figures S7 and S8). These experiments suggest that the endonucleolytic incision of duplex DNA by SbcCD is sensitive to the thermodynamic stability of B-DNA and that some local changes in DNA structure occur prior to endonuclease activity as a result of ATP hydrolysis cycles. However, preformed bubbles do not relieve the necessity of ATP hydrolysis and are also poorer endonuclease substrates than base-paired DNA. For instance, ATP hydrolysis could also help load the complex

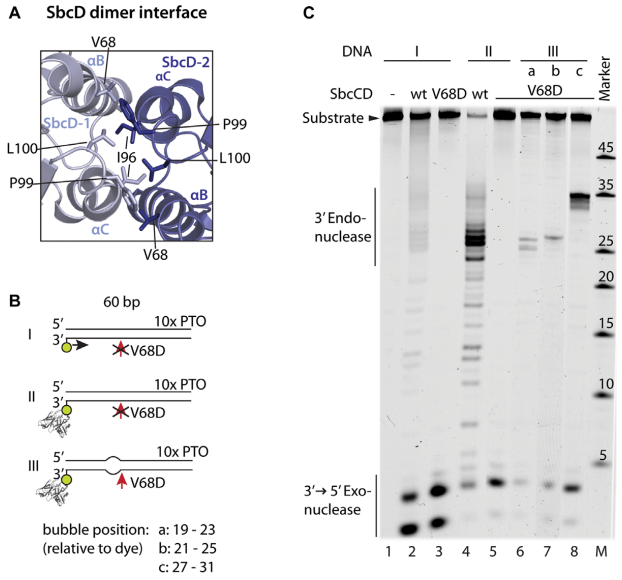

Figure 4. SbcD dimer disruption affects endo- but not exonuclease activity. (**A**) SbcD homodimeric interface (PDB: 4M0V). The view shows the SbcD-SbcD four-helix bundle interaction. The interaction is mainly mediated by a hydrophobic cluster consisting of Val68, Iso96, Phe99, and Leu100 on the top of the four-helix bundle. (**B**) DNA substrates are schematized that were used in (C). (**C**) Nuclease activities of SbcCD^{V68D} was assayed in the presence 1 mM ATP, 5 mM $MgCl_2$ and 1 mM $MnCl_2$ at 37°C. SbcCD^{V68D} retains exonuclease activity, but looses endonuclease activity on duplex DNA. The presence of bubbles re-establishes the endonuclease activity of SbcCD^{V68D}.

onto internal DNA in the presence of a block, but other scenarios are also possible.

SbcD dimer interface dynamics during endonucleolytic degradation of SbcCD

To investigate the impact of the SbcD dimer state during nucleolytic processing, we compared the nuclease activities of SbcCD^{wt} to a SbcCD complex with a destabilized SbcD interface. The dimeric assembly of two SbcD protomers is mediated by a conserved four-helix bundle interaction which bears a hydrophobic cluster consisting of Val68, Ile96, Phe99 and Leu100 (Figure 4A) (53). The interface was weakened by mutating Val68 to a negatively-charged aspartate (SbcD^{V68D}).

Right-Angle Light Scattering (RALS) analysis of the SbcD nuclease and capping domain showed that SbcD mainly forms a monomer during size-exclusion chromatography in the absence of SbcC, with a very slight residual fraction of 4% dimeric SbcD. This residual dimer is absent in SbcD^{V68D}. Therefore, SbcD itself appears to be an at least transient homodimer whereas the addition of a second interface by SbcC in the presence of ATP induces stable complex formation of the SbcCD – head domain and the full length complex (Supplementary Figures S9A and B and S10). Mutations at similar sites in yeast and bacteriophage Mre11 have been analyzed before and found to impact on the viability *in vivo* or nuclease characteristics *in vitro* (35,54).

SbcCD^{V68D} degrades dsDNA exonucleolytically in an ATP-dependent fashion similar to SbcCD^{wt}. Therefore, the three-dimensional fold of SbcD and the catalytic site is functional and the association between DNA and SbcCD^{V68D} is intact. Furthermore, a fully functional SbcD dimer interface is apparently not required for exonuclease activity, similar to the dispensability of ATP hydrolysis (but not ATP binding) for the exonuclease. However, SbcCD^{V68D} did not show significant endonucleolytic activity and we could not detect any dsDNA degradation in the presence of ATPγS (Supplementary Figure S8). Introduction of a bubble structure re-established the endonuclease activity. The positions of the incision were identical to SbcCD^{wt}, however, the cutting efficiency reduced by approximately 5-fold, depending on the position of the bubble (Figure 4C). Therefore, destabilization of the dimerization interface of SbcD correlated with the loss of endonuclease activity of SbcCD. The presence of unpaired DNA re-established the ATP dependent endonuclease activity to some extent.

The nuclease and capping domain of SbcD^{V68D} display similar ssDNA endonuclease activity towards a covalently closed single-stranded plasmid DNA as SbcD^{wt}. Full-length SbcCD^{wt} and SbcCD^{V68D} required ATP for ssDNA cleavage. Both proteins cleaved ssDNA with a similar efficiency in the presence of ATP. SbcCD^{wt} also cleaved in the presence of ATPγS, whereas the endonuclease of SbcCD^{V68D} was strongly reduced (Supplementary Figure S11A and B).

These data suggest that a destabilized SbcD interface induces a defect in SbcCD that affects the endo- but not the exonuclease activity. SbcCD^{V68D} also cleaves single-stranded plasmid DNA and bubble structures in the presence of ATP. Therefore, the defect could be a dysfunction of SbcCD^{V68D} to generate a DNA substrate which is competent for endonucleolytic cleavage. Introduction of a pre-melted stretch compensates this defect and SbcCD^{V68D} regains endonuclease activity. The most likely explanation is that SbcD dimers with a fully functional interface are needed to generate melted DNA.

SbcCD cleaves opposing strands of dsDNA with different chemistries, leaving 3′ and 5′ phosphates respectively

To further investigate and characterize the mode of cleavage catalysis, we treated the cleavage products with Antarctic Phosphatase and T4 Polynucleotide Kinase enzymes and compared them to the untreated cleavage products. The addition or removal of the negatively-charged phosphate changed the mobility of the oligonucleotides during electrophoresis and allowed us to detect the presence or absence of a phosphate group at the unlabeled termini.

Analysis of a 60mer DNA duplex with a 3′ label revealed that the 3’ exonuclease products were not shifted by kinase treatment but by phosphatase treatment, indicating the presence of a 5′ phosphate and cleavage of the P–$O^{5'}$ phosphoester bond (Figure 5A, lanes 6–8). The resulting cleavage products were validated using well characterized nucleases ExoIII, DNase I and Benzoase (Supplementary Figure S12, 55–58). Comparison of the cleavage products produced by the different nucleases suggests that SbcCD can direcly cleave the phosphodiester linkage of the 6-FAM at the 3′

11310 Nucleic Acids Research, 2018, Vol. 46, No. 21

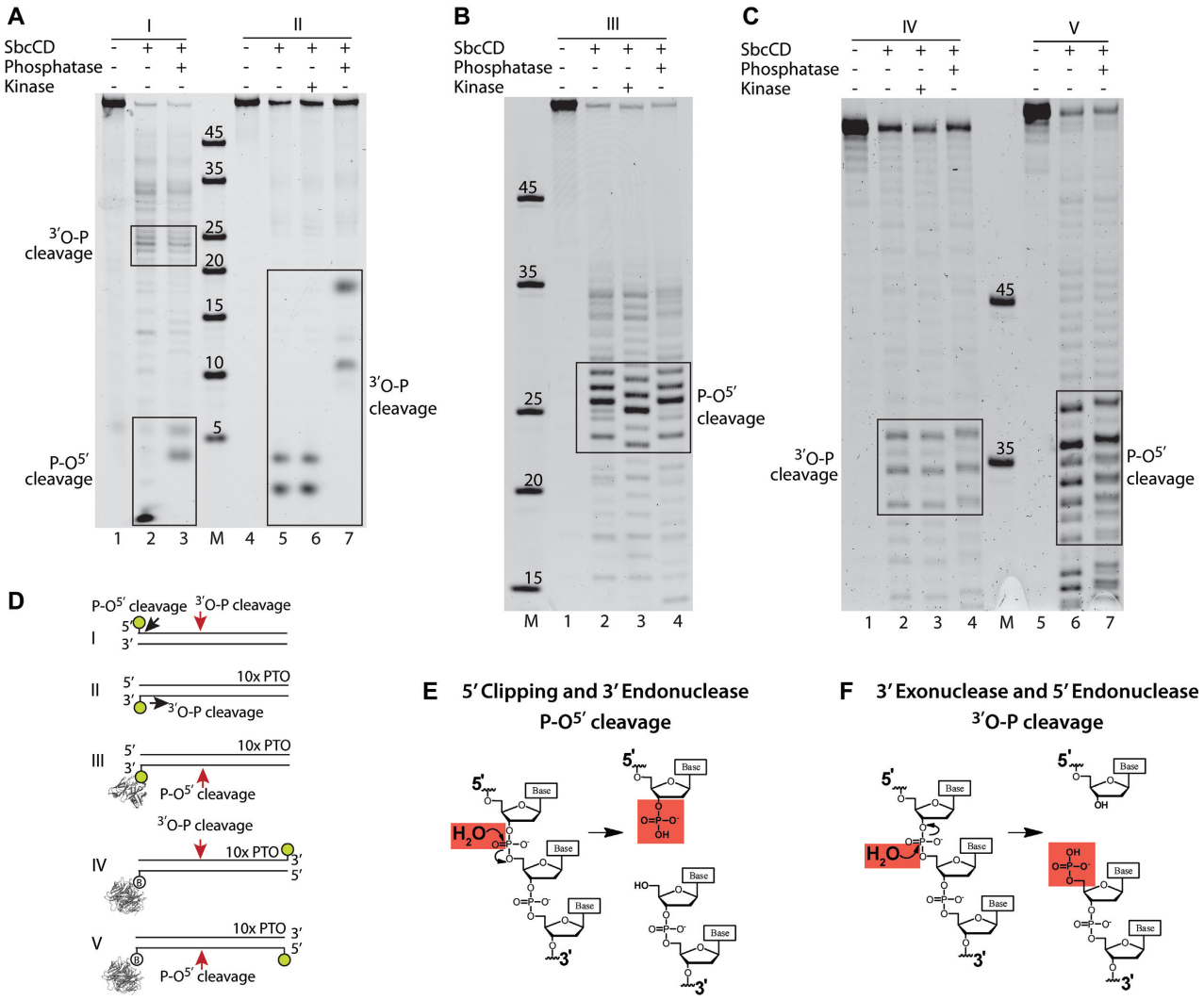

Figure 5. The position of SbcCD's DNA backbone cleavage is cleavage- and strand-specific. (**A**) SbcCD^{wt} was assayed in the presence of 1 mM ATP, 1 mM $MnCl_2$ and 5 mM $MgCl_2$ at 37°C. The cleavage products of the quenched nuclease reactions were treated with T4 Polynucleotide Kinase or Antarctic Phosphatase to remove or add a phosphate to the DNA ends. The altered electrophoretic migration indicates the absence or presence of a phosphate of the cleavage products. (**B**) Nuclease assay as in (A), but with 60 bp DNA which was protein bound DNA end inducing endonuclease activity. (**C**) Nuclease assay as in (A), but oligos were labeled at the unblocked DNA end. (**D**) DNA substrates and respective cleavage products in (A–C) are schematized. (**E** and **F**) The chemical drawing shows the S_N2 reaction during exo- and endonucleolytic cleavage of the phosphate backbone.

end. The major cleavage at the DNA end was observed to be between base 3 and 4 (from the 3′ end), liberating a trinucleotide (Supplementary Figure S12A). We also see to a smaller amount cleavage between bases 1–2, 2–3, 4–5 and 5–6, so there is apparently some structural flexibility in recognition of 3′ 6-FAM bound DNA ends by SbcCD. This is consistent with the ability of SbcCD to recognize and cleave hairpins (33). Comparison of the exonuclease cleavage polarity of SbcCD^{wt} and SbcCD^{V68D} did not indicate any differences (Supplementary Figure S13).

Analysis of the same 60mer DNA duplex, but with a 5′ label revealed two sets of products; endonuclease products between 20 and 25 bp from the 5′ end, and short 5′ clipping products. The endonuclease cleavage products were not shifted by phosphatase treatment and therefore contain a free 3′-OH, similar to the exonuclease cleavage products on the complementary DNA strand. Interestingly, the 5' clipping products were shifted by phosphatase treatment, indicating the presence of a 3′-phosphate and cleavage of the $^{3'}$O–P bond. Therefore, the 5′ clipping apparently has a different chemistry to the 3′-5′ exonuclease and 5′ endonuclease activities (Figure 5A, lanes 1–3).

Next, we assessed the cleavage chemistry of the 3′ endonuclease activity, using a protein block at the 3′ label. Endonuclease products between 23–27 bp in length were not affected by phosphatase treatment, but migrated faster after kinase treatment. Thus, these products contained a 5′-OH, indicating cleavage of the $^{3'}$O–P bond (Figure 5B). This is

Nucleic Acids Research, 2018, Vol. 46, No. 21 **11311**

similar to the 5′ clipping reaction, but apparently different to the endonucleolytic cleavage of the 5′ strand. However, the 5′ endonuclease produced cleavage fragments harbour a 3′-OH, similar to the 3′-5′ exonuclease.

The observed 3′-OH could either be directly produced from the endonuclease, or alternatively result from a 3′-5′ exonuclease reaction of the nicked DNA. To clearly attribute the observed cleavage chemistries to endonuclease reactions, we analyzed DNA substrates that were fluorescently labeled on the DNA termini opposite to the protein-blocked DNA end. Looking at the endonucleolytic products around 35 bp from the labeled end (∼25 bp from the blocked end), we observed that the kinase treatment did not result in a different mobility, whereas phosphatase treatment led to slower migration of both 3′ and 5′ labeled DNA (Figure 5C). These data suggest that—looking from the blocked DNA-end—the 3′ strand is cleaved at the P-$O^{5'}$-bond, leaving a 3′-phosphate, whereas the 5′ strand is cleaved at the $^{3'}$O-P-bond, leaving a 5′-phosphate (Figure 5E and F). It is likely that some cleavage products that do not shift upon kinase treatment originate from a consecutive endo–exo activity as has been observed for the human MRN complex (33).

In summary, we unexpectedly observe that SbcCD cleaves opposing strands with a chemically different nuclease reaction. The exonuclease and clipping activities at the DNA end operate in such a way that the phosphate groups stay on the short nuclease products, leaving an unphosphorylated DNA end with free 3′-OH and 5′-OH. The DNA end proximal endonuclease activities show the reverse polarity, as if the SbcCD complex is geometrically flipped and just operates in the other direction. Here, both phosphate groups stay at the newly formed (unblocked) DNA end, while the dsDNA portion that contains the block contains a 3′-OH and 5′-OH.

DISCUSSION

Orthologs of the Mre11–Rad50 complex function in the processing of terminal DNA structures in all kingdoms of life. While the primary substrates and targets for the ATP-regulated nuclease activity, i.e. arrested topoisomerase–DNA complexes, hairpins, abnormal replication intermediates and blocked DNA ends differ in different species, Mre11–Rad50 complexes share similar nuclease activities: they possess hairpin opening and 3′-5′ dsDNA exonuclease activities and can cleave blocked DNA ends *via* an endonuclease activity ∼15–25 bp inward from the block (4,5,12,25,33). Collectively, these activities have been suggested to clear diverse types of blocked ends and prepare them for recombinational repair. A common mechanistic basis for these nuclease activities by Mre11/SbcD and their regulation or activation by ATP binding and hydrolysis by Rad50/SbcC remains to be established.

In SbcCD, DNA binding, nuclease activation and ATP binding or turnover are strongly coupled. In the absence of ATP, we neither observe DNA binding nor detectable nuclease activity. Robust activation of SbcCD's ATPase by DNA, or DNA binding to SbcCD requires 25–30 bp, by and large consistent with a structural footprint of ∼20 bp DNA on the ATP-bound NBD dimer of Rad50/SbcC proteins (41,42). The slightly longer DNA needed for full affinity binding and especially for full stimulation of ATP hydrolysis by SbcCD could indicate either a different conformation of the complex when bound to a DNA end, or reflect some cooperative effects when more than one complex is bound, as for instance indicated by recent studies (32).

Interestingly, we find that the ATPase is most robustly activated by relaxed DNA, either in circular or in linear form, but much less by supercoiled DNA. The presence of DNA ends does not increase the maximum ATP turnover rates, but rather increases the affinity of the DNA for SbcCD and thus activates the ATPase at much lower DNA concentrations. Structural results showing that Rad50/SbcC's NBDs do not directly recognize DNA ends is consistent with circular DNA being able to fully activate SbcC's ATPase (42,43,59). Recent single-molecule studies showed that the Mre11 subunit of the MRN complex is necessary for DNA end recognition but not binding to internal DNA (24). It is therefore plausible that high-affinity end-recognition proceeds *via* the SbcD subunit, whereas SbcC's ATPase is activated by the flanking DNA. However, it is yet unclear how Mre11/SbcD and Rad50/SbcC would cooperate in DNA binding and processing, since current structural studies have not shown that or how both subunits can simultaneously bind to DNA. Of note, the activation of SbcC's ATPase by relaxed DNA could be a medium-range signal to sense the presence of DNA breaks or palindromes. While former readily leads to loss of superhelical tension, latter can fold into cruciforms and can also lead to local relaxation of DNA in otherwise supercoiled chromosomal DNA.

Even under conditions of full ATP turnover, we do not observe cleavage of circular supercoiled or circular nicked DNA. In contrast, linear DNA is readily degraded. Clearly, the activation of ATP hydrolysis by DNA is not sufficient to trigger endonuclease activity and requires the presence of DNA ends. In the presence of DNA ends, however, ATPγS is sufficient to activate the exonuclease. Equivalent results have been observed previously for SbcCD and the homologous bacteriophage T4 gp46/47 complex, where it was found that cleavage of the terminal 3′ base does not need ATP hydrolysis, but further processive 3′-5′ exonuclease activity does (49). On the contrary, the endonuclease of SbcCD, which is robustly activated by DNA end blocks, requires ATP hydrolysis in our hands, similar to observations made for eukaryotic homologs (5,33,60). Quantification yields a relation of ATP turnover to endonuclease cuts of around 100:1. Likely, a transient, reversible step is necessary for a more infrequent endonucleolytic cleavage. A putative mechanism is that ATP binding by SbcC leads to the transient, but reversible local melting of DNA, which could then be cleaved by SbcD. In support of this hypothesis are our observations with DNA substrates containing base bias (AT-rich and GC-rich), showing an inverse correlation between thermodynamic stability and efficiency of endonucleolytic cleavage. Of note, in other investigations of SbcCD's nuclease, ATPγS is sufficient to trigger endonucleolytic cleavage (7,32). Perhaps on different DNA substrates or under different experimental conditions, the efficiency of the complex is substantially increased that binding of ATPγS alone is sufficient to prepare DNA for cleav-

11312 Nucleic Acids Research, 2018, Vol. 46, No. 21

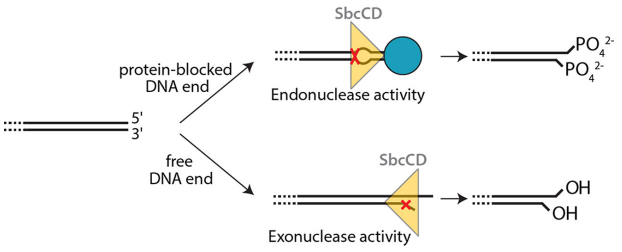

Figure 6. Proposed model for the SbcCD Endo- and Exonuclease mechanism. The SbcCD dimer is shown schematically as a yellow triangle and the cleavage site on DNA is indicated by a red cross. A protein block at the DNA end (blue sphere) stimulates SbcCD's endonuclease activity. Internal cleavage of the DNA requires ATP hydrolysis, the DNA is melted and a transient bubble is formed. The DNA end is phosphorylated at the 5′ and the 3′ termini (upper panel). For exonuclease activity the SbcD dimer is in a reversed orientation, cleavage could involve fraying at free DNA ends. The DNA end is hydroxylated at the 3′ and the 5′ termini (lower panel).

age, relaxing the requirement for the turnover of multiple molecules of ATP. Nevertheless, our findings on the requirement of ATP *vs* ATPγS are generally consistent with what has been observed for the activity of homologs (5,33).

The putative DNA melting required for endonucleolytic cleavage requires a properly formed SbcD dimer, since mutation of the dimer interface reduced endonuclease, but did not reduce exonuclease or endonuclease on a substrate containing a DNA bubble. Structural studies on Mre11 dimers bound to DNA are so far consistent with endonucleolytic cleavage requiring some DNA melting in order for the phosphoesters to reach the active site metals. In addition, the unwinding or melting of short dsDNA has been observed for eukaryotic and bacterial homologs in the presence of ATP (11,42,51). At the DNA end, fraying or other sterical features might already be sufficient for exonuclease activity, requiring only ATPγS-mediated binding of SbcCD to DNA. In the case of internal DNA, however, multiple ATP turnover cycles might be required to open and maintain the DNA in a melted state until it is cleaved by SbcD.

For the endonuclease activity, it was first shown for the *E. coli* homolog SbcCD and subsequently for the eukaryotic MRN and MRX complexes, that Mre11–Rad50 complexes can indeed cleave both strands of the DNA, introducing a DNA double-strand break near the block. To better understand a common or distinct mechanistic nature of these inherent endo- and exonuclease activities of Mre11–Rad50 complex proteins, we analyzed SbcCD's ATP-dependent nuclease activity in the processing of accessible and inaccessible (protein blocked) DNA ends. We unexpectedly found that the endonucleolytic cleavage reactions at opposing DNA strands are chemically distinct. One strand is cleaved such that the phosphate remains at the 5′O, while the opposing strand retains the phosphate at the 3′O. Using the conventional 5′-3′ directionality of DNA, we refer to former activity as $^{3'}$O–P cleavage (phosphate remains at 5′O) and to latter as P–$O^{5'}$ cleavage (phosphate remains at 3′O). It was found before that SbcCD cleaves a hairpin at the 5′ side with an $^{3'}$O–P cleavage (61).

Interestingly, we also observed these two chemically distinct mechanisms at the cleavage reactions at the DNA end, but with a reversed polarity: in addition to the well-characterized 5′-3′ exonuclease activity (O–P cleavage), we found that SbcCD possesses a 5′ clipping activity with P–O cleavage. The observed pattern of $^{3'}$O–P versus P–$O^{5'}$ is therefore not determined by the type of reaction (endo- or exonuclease), but sterically determined by the DNA end. In our opinion the most rational explanation is that SbcCD complexes are situated at an accessible DNA end, and at an internal site next to a blocked end with a reversed polarity. A plausible scenario is shown in Figure 6. Here, a SbcD dimer is situated in such a way that the 3′ strand is exonucleolytically clipped with an $^{3'}$O–P cleavage reaction. If the complex encounters a block through e.g. internal diffusion or scanning, the SbcD dimer could have a different orientation, thus the observed endonucleolytic cleavage at the 5′ strand has the $^{3'}$O–P cleavage chemistry. Consistent with such a model are recent observations on the basis of the bipolar nuclease reaction: here it was proposed that the hairpin/DNA end-bound terminal SbcCD complex and subsequent SbcCD complexes are biochemically distinct (32). For instance, the terminal complex can perform the hairpin opening reaction but may also temporarily act as a block to stimulate endonuclease reactions by further SbcCD complexes at internal sites. The nature of the 10 bp periodicity of the subsequent endonuclease reactions compared to the 20–25 bp of the initial cleavage from the end is not clear yet and requires further investigation.

How can SbcD catalyze both $^{3'}$O–P and P–$O^{5'}$ cleavage events? On the basis of its homology to other phosphodiesterases, the di-metal center of Mre11/SbcD is suggested to coordinate and activate the phosphate and attacking hydroxyl ion. Mre11's nucleolytic cleavage is proposed to be an S_N2-reaction, which requires the in-line nucleophilic attack of a water molecule or hydroxyl ion (34). To produce cleavage products with different cleavage chemistries, either the positions of the water molecule and the phosphate on the di-metal cluster are reversed or, perhaps more likely, water and phosphate occupy the same position, but the strand polarity is reversed. The currently available crystal structures of archaeal Mre11 homologs bound to DNA have not revealed how DNA coordinates the active site metals, since both strands are equally 10–15 Å away from the two metal ions (35,36). While these structures support the sterical need for DNA melting or deformation of DNA to allow the backbones to reach the active site metals for endonucleolytic cleavage, it is possible that either strand could reach the active site while maintaining the overall direction of the DNA. In such a model, the different strand polarity, together with a maintained water and phosphate coordination at the di-metal center, would result in the observed P–$O^{5'}$ and $^{3'}$O–P cleavage reactions on opposing strands.

In summary, we deconvolute and unify key aspects of endo- and exonuclease type reactions in SbcCD. We reveal an unexpected chemical asymmetry in the mode of cleavage reactions that is apparently not determined by endo- versus exonuclease reactions, but best explained by a different orientation of SbcCD during exonuclease and endonuclease reactions with respect to the DNA end. It will be interesting to also analyze eukaryotic homologs for similar activities. What governs such a polarity change in SbcCD is unclear and must await future studies. A possible scenario is

that SbcCD can directionally and actively scan DNA, similar to the recently described DNA transport activities of the related SMC proteins (62), until encounter of a blocked end leads to activation of the endonuclease. At an accessible DNA end, the directionality could be reversed through preferential binding to the DNA end, resulting in processive exonuclease. Our comprehensive study sheds light on the cleavage mechanism of the bacterial MR complex and may help to understand the intricate action of its eukaryotic counterpart.

SUPPLEMENTARY DATA

Supplementary Data are available at NAR Online.

ACKNOWLEDGEMENTS

We thank members of the Hopfner lab for helpful discussion and Prof. Andreas Plückthun for providing the fluorescein scFv. We thank Tobias Becker for generating the DNA binding data of Supplementary Figure S1C.
Author contributions: J.-H.S. designed and conducted biochemical experiments and analyzed the results. L.K. helped with biochemical experiments and analyzed and discussed the results. K.L. and R.B. helped with the analysis and interpretation of the results. K.-P.H. designed the overall study and analyzed the results. K.-P.H. and J.-H.S. wrote the manuscript with contribution from the other authors.

FUNDING

European Research Council (ATMMACHINE), Deutsche Forschungsgemeinschaft [RTG1721, Gottfried Wilhelm Leibniz-Prize] and German Excellence Initiative (Center for Integrated Proteins Science) to K.-P.H.; L.K. acknowledges support from the International Max-Planck Research School Molecular Life Sciences. Funding for open access charge: LMU Munich.
Conflict of interest statement. None declared.

REFERENCES

1. Hoeijmakers,J.H. (2009) DNA damage, aging, and cancer. *N. Engl. J. Med.*, **361**, 1475–1485.
2. Stracker,T.H. and Petrini,J.H.J. (2011) The MRE11 complex: starting from the ends. *Nat. Rev. Mol. Cell. Biol.*, **12**, 90–103.
3. Connelly,J.C. and Leach,D.R. (1996) The sbcC and sbcD genes of Escherichia coli encode a nuclease involved in palindrome inviability and genetic recombination. *Genes Cells*, **1**, 285–291.
4. Paull,T.T. and Gellert,M. (1998) The 3′ to 5′ exonuclease activity of Mre 11 facilitates repair of DNA double-strand breaks. *Mol. Cell*, **1**, 969–979.
5. Cannavo,E. and Cejka,P. (2014) Sae2 promotes dsDNA endonuclease activity within Mre11–Rad50-Xrs2 to resect DNA breaks. *Nature*, **514**, 122–125.
6. Lobachev,K.S., Gordenin,D.A. and Resnick,M.A. (2002) The Mre11 complex is required for repair of hairpin-capped double-strand breaks and prevention of chromosome rearrangements. *Cell*, **108**, 183–193.
7. Connelly,J.C., de Leau,E.S. and Leach,D.R. (2003) Nucleolytic processing of a protein-bound DNA end by the E. coli SbcCD (MR) complex. *DNA Repair (Amst.)*, **2**, 795–807.
8. Neale,M.J., Pan,J. and Keeney,S. (2005) Endonucleolytic processing of covalent protein-linked DNA double-strand breaks. *Nature*, **436**, 1053–1057.
9. Symington,L.S. and Gautier,J. (2011) Double-Strand break end resection and repair pathway choice. *Annu. Rev. Genet.*, **45**, 247–271.
10. Sallmyr,A. and Tomkinson,A.E. (2018) Repair of DNA double-strand breaks by mammalian alternative end-joining pathways. *J. Biol. Chem.*, **293**, 10536–10546.
11. Paull,T.T. and Gellert,M. (1999) Nbs1 potentiates ATP-driven DNA unwinding and endonuclease cleavage by the Mre11/Rad50 complex. *Genes Dev.*, **13**, 1276–1288.
12. Trujillo,K.M. and Sung,P. (2001) DNA structure-specific nuclease activities in the Saccharomyces cerevisiae Rad50*Mre11 complex. *J. Biol. Chem.*, **276**, 35458–35464.
13. Trujillo,K.M., Yuan,S.S., Lee,E.Y. and Sung,P. (1998) Nuclease activities in a complex of human recombination and DNA repair factors Rad50, Mre11, and p95. *J. Biol. Chem.*, **273**, 21447–21450.
14. Nicolette,M.L., Lee,K., Guo,Z., Rani,M., Chow,J.M., Lee,S.E. and Paull,T.T. (2010) Mre11–Rad50-Xrs2 and Sae2 promote 5′ strand resection of DNA double-strand breaks. *Nat. Struct. Mol. Biol.*, **17**, 1478–1485.
15. Garcia,V., Phelps,S.E.L., Gray,S. and Neale,M.J. (2011) Bidirectional resection of DNA double-strand breaks by Mre11 and Exo1. *Nature*, **479**, 241–244.
16. Mimitou,E.P. and Symington,L.S. (2008) Sae2, Exo1 and Sgs1 collaborate in DNA double-strand break processing. *Nature*, **455**, 770–774.
17. Zhu,Z., Chung,W.H., Shim,E.Y., Lee,S.E. and Ira,G. (2008) Sgs1 helicase and two nucleases Dna2 and Exo1 resect DNA double-strand break ends. *Cell*, **134**, 981–994.
18. Cannavo,E. and Cejka,P. (2014) Sae2 promotes dsDNA endonuclease activity within Mre11–Rad50-Xrs2 to resect DNA breaks. *Nature*, **514**, 122–125.
19. Hoa,N.N., Shimizu,T., Zhou,Z.W., Wang,Z.Q., Deshpande,R.A., Paull,T.T., Akter,S., Tsuda,M., Furuta,R., Tsutsui,K. *et al.* (2016) Mre11 is essential for the removal of lethal topoisomerase 2 covalent cleavage complexes. *Mol. Cell*, **64**, 1010.
20. Langerak,P., Mejia-Ramirez,E., Limbo,O. and Russell,P. (2011) Release of Ku and MRN from DNA ends by Mre11 nuclease activity and Ctp1 is required for homologous recombination repair of double-strand breaks. *PLos Genet.*, **7**, e1002271.
21. Mimitou,E.P. and Symington,L.S. (2010) Ku prevents Exo1 and Sgs1-dependent resection of DNA ends in the absence of a functional MRX complex or Sae2. *EMBO J.*, **29**, 3358–3369.
22. Reginato,G., Cannavo,E. and Cejka,P. (2017) Physiological protein blocks direct the Mre11–Rad50-Xrs2 and Sae2 nuclease complex to initiate DNA end resection. *Genes Dev.*, **31**, 2325–2330.
23. Wang,W., Daley,J.M., Kwon,Y., Krasner,D.S. and Sung,P. (2017) Plasticity of the Mre11–Rad50-Xrs2-Sae2 nuclease ensemble in the processing of DNA-bound obstacles. *Genes Dev.*, **31**, 2331–2336.
24. Myler,L.R., Gallardo,I.F., Soniat,M.M., Deshpande,R.A., Gonzalez,X.B., Kim,Y., Paull,T.T. and Finkelstein,I.J. (2017) Single-Molecule imaging reveals how Mre11–Rad50-Nbs1 initiates DNA break repair. *Mol. Cell*, **67**, 891–898.
25. Connelly,J.C., de Leau,E.S. and Leach,D.R. (1999) DNA cleavage and degradation by the SbcCD protein complex from Escherichia coli. *Nucleic Acids Res.*, **27**, 1039–1046.
26. Eykelenboom,J.K., Blackwood,J.K., Okely,E. and Leach,D.R. (2008) SbcCD causes a double-strand break at a DNA palindrome in the Escherichia coli chromosome. *Mol. Cell*, **29**, 644–651.
27. Aedo,S. and Tse-Dinh,Y.C. (2013) SbcCD-mediated processing of covalent gyrase-DNA complex in Escherichia coli. *Antimicrob. Agents Chemother.*, **57**, 5116–5119.
28. Deng,Sarah K., Yin,Y., Petes,Thomas D. and Symington,Lorraine S. (2015) Mre11-Sae2 and RPA collaborate to prevent palindromic gene amplification. *Mol. Cell*, **60**, 500–508.
29. Wendel,B.M., Cole,J.M., Courcelle,C.T. and Courcelle,J. (2018) SbcC-SbcD and ExoI process convergent forks to complete chromosome replication. *PNAS*, **115**, 349–354.
30. Limbo,O., Chahwan,C., Yamada,Y., de Bruin,R.A.M., Wittenberg,C. and Russell,P. (2007) Ctp1 is a Cell-Cycle-Regulated protein that functions with Mre11 complex to control Double-Strand break repair by homologous recombination. *Mol. Cell*, **28**, 134–146.
31. Sartori,A.A., Lukas,C., Coates,J., Mistrik,M., Fu,S., Bartek,J., Baer,R., Lukas,J. and Jackson,S.P. (2007) Human CtIP promotes DNA end resection. *Nature*, **450**, 509–514.
32. Lim,C.T., Lai,P.J., Leach,D.R., Maki,H. and Furukohri,A. (2015) A novel mode of nuclease action is revealed by the bacterial Mre11/Rad50 complex. *Nucleic Acids Res.*, **43**, 9804–9816.

33. Deshpande,R.A., Lee,J.H., Arora,S. and Paull,T.T. (2016) Nbs1 converts the human Mre11/Rad50 nuclease complex into an Endo/Exonuclease machine specific for Protein-DNA adducts. *Mol. Cell*, **64**, 593–606.
34. Hopfner,K.P., Karcher,A., Craig,L., Woo,T.T., Carney,J.P. and Tainer,J.A. (2001) Structural biochemistry and interaction architecture of the DNA double-strand break repair Mre11 nuclease and Rad50-ATPase. *Cell*, **105**, 473–485.
35. Williams,R.S., Moncalian,G., Williams,J.S., Yamada,Y., Limbo,O., Shin,D.S., Groocock,L.M., Cahill,D., Hitomi,C., Guenther,G. *et al.* (2008) Mre11 dimers coordinate DNA end bridging and nuclease processing in double-strand-break repair. *Cell*, **135**, 97–109.
36. Sung,S., Li,F., Park,Y.B., Kim,J.S., Kim,A.K., Song,O.K., Kim,J., Che,J., Lee,S.E., Cho,Y. *et al.* (2014) DNA end recognition by the Mre11 nuclease dimer: insights into resection and repair of damaged DNA. *EMBO J.*, **33**, 2422–2435.
37. Lammens,K., Bemeleit,D.J., Mockel,C., Clausing,E., Schele,A., Hartung,S., Schiller,C.B., Lucas,M., Angermuller,C., Soding,J. *et al.* (2011) The Mre11:Rad50 structure shows an ATP-dependent molecular clamp in DNA double-strand break repair. *Cell*, **145**, 54–66.
38. Schiller,C.B., Seifert,F.U., Linke-Winnebeck,C. and Hopfner,K.P. (2014) Structural studies of DNA end detection and resection in homologous recombination. *Cold Spring Harbor Perspect. Biol.*, **6**, a017962.
39. Hopfner,K.P., Craig,L., Moncalian,G., Zinkel,R.A., Usui,T., Owen,B.A., Karcher,A., Henderson,B., Bodmer,J.L., McMurray,C.T. *et al.* (2002) The Rad50 zinc-hook is a structure joining Mre11 complexes in DNA recombination and repair. *Nature*, **418**, 562–566.
40. de Jager,M., Trujillo,K.M., Sung,P., Hopfner,K.-P., Carney,J.P., Tainer,J.A., Connelly,J.C., Leach,D.R.F., Kanaar,R. and Wyman,C. (2004) Differential arrangements of conserved building blocks among homologs of the Rad50/Mre11 DNA repair protein complex. *J. Mol. Biol.*, **339**, 937–949.
41. Seifert,F.U., Lammens,K., Stoehr,G., Kessler,B. and Hopfner,K.P. (2016) Structural mechanism of ATP-dependent DNA binding and DNA end bridging by eukaryotic Rad50. *EMBO J.*, **35**, 759–772.
42. Liu,Y., Sung,S., Kim,Y., Li,F., Gwon,G., Jo,A., Kim,A.K., Kim,T., Song,O.K., Lee,S.E. *et al.* (2016) ATP-dependent DNA binding, unwinding, and resection by the Mre11/Rad50 complex. *EMBO J.*, **35**, 743–758.
43. Rojowska,A., Lammens,K., Seifert,F.U., Direnberger,C., Feldmann,H. and Hopfner,K.P. (2014) Structure of the Rad50 DNA double-strand break repair protein in complex with DNA. *EMBO J.*, **33**, 2847–2859.
44. Lim,H.S., Kim,J.S., Park,Y.B., Gwon,G.H. and Cho,Y. (2011) Crystal structure of the Mre11–Rad50-ATPgammaS complex: understanding the interplay between Mre11 and Rad50. *Genes Dev.*, **25**, 1091–1104.
45. Pedrazzi,G., Schwesinger,F., Honegger,A., Krebber,C. and Pluckthun,A. (1997) Affinity and folding properties both influence the selection of antibodies with the selectively infective phage (SIP) methodology. *FEBS Lett.*, **415**, 289–293.
46. Norby,J.G. (1988) Coupled assay of Na+,K+-ATPase activity. *Methods Enzymol.*, **156**, 116–119.
47. Trujillo,K.M., Roh,D.H., Chen,L., Van Komen,S., Tomkinson,A. and Sung,P. (2003) Yeast xrs2 binds DNA and helps target rad50 and mre11 to DNA ends. *J. Biol. Chem.*, **278**, 48957–48964.
48. Deshpande,R.A., Lee,J.H. and Paull,T.T. (2017) Rad50 ATPase activity is regulated by DNA ends and requires coordination of both active sites. *Nucleic Acids Res.*, **45**, 5255–5268.
49. Herdendorf,T.J., Albrecht,D.W., Benkovic,S.J. and Nelson,S.W. (2011) Biochemical characterization of bacteriophage T4 Mre11–Rad50 complex. *J. Biol. Chem.*, **286**, 2382–2392.
50. Milo,R., Jorgensen,P., Moran,U., Weber,G. and Springer,M. (2010) BioNumbers–the database of key numbers in molecular and cell biology. *Nucleic Acids Res.*, **38**, D750–D753.
51. Cannon,B., Kuhnlein,J., Yang,S.H., Cheng,A., Schindler,D., Stark,J.M., Russell,R. and Paull,T.T. (2013) Visualization of local DNA unwinding by Mre11/Rad50/Nbs1 using single-molecule FRET. *PNAS*, **110**, 18868–18873.
52. Yakovchuk,P., Protozanova,E. and Frank-Kamenetskii,M.D. (2006) Base-stacking and base-pairing contributions into thermal stability of the DNA double helix. *Nucleic Acids Res.*, **34**, 564–574.
53. Liu,S., Tian,L.F., Liu,Y.P., An,X.M., Tang,Q., Yan,X.X. and Liang,D.C. (2014) Structural basis for DNA recognition and nuclease processing by the Mre11 homologue SbcD in double-strand breaks repair. *Acta Crystallogr. D, Biol. Crystallogr.*, **70**, 299–309.
54. Albrecht,D.W., Herdendorf,T.J. and Nelson,S.W. (2012) Disruption of the bacteriophage T4 Mre11 dimer interface reveals a two-state mechanism for exonuclease activity. *J. Biol. Chem.*, **287**, 31371–31381.
55. Rogers,S.G. and Weiss,B. (1980) Exonuclease III of Escherichia coli K-12, an AP endonuclease. *Methods Enzymol.*, **65**, 201–211.
56. Vanecko,S. and Laskowski,M. Sr (1961) Studies of the specificity of deoxyribonuclease I. II. Hydrolysis of oligonucleotides carrying a monoesterified phosphate on carbon 3′. *J. Biol. Chem.*, **236**, 1135–1140.
57. Kunitz,M. (1950) Crystalline desoxyribonuclease; isolation and general properties; spectrophotometric method for the measurement of desoxyribonuclease activity. *J. Gen. Physiol.*, **33**, 349–362.
58. Liao,Q., Chiu,N.H., Shen,C., Chen,Y. and Vouros,P. (2007) Investigation of enzymatic behavior of benzonase/alkaline phosphatase in the digestion of oligonucleotides and DNA by ESI-LC/MS. *Anal. Chem.*, **79**, 1907–1917.
59. Seifert,F.U., Lammens,K. and Hopfner,K.P. (2015) Structure of the catalytic domain of Mre11 from Chaetomium thermophilum. *Acta Crystallogr. F, Struct. Biol. Commun.*, **71**, 752–757.
60. Anand,R., Ranjha,L., Cannavo,E. and Cejka,P. (2016) Phosphorylated CtIP functions as a Co-factor of the MRE11-RAD50-NBS1 endonuclease in DNA end resection. *Mol. Cell*, **64**, 940–950.
61. Connelly,J.C., Kirkham,L.A. and Leach,D.R. (1998) The SbcCD nuclease of Escherichia coli is a structural maintenance of chromosomes (SMC) family protein that cleaves hairpin DNA. *PNAS*, **95**, 7969–7974.
62. Terakawa,T., Bisht,S., Eeftens,J.M., Dekker,C., Haering,C.H. and Greene,E.C. (2017) The condensin complex is a mechanochemical motor that translocates along DNA. *Science*, **358**, 672–676.

2.2 Mechanism of DNA End Sensing and Processing by the Mre11-Rad50 Complex

Lisa Käshammer*, Jan-Hinnerk Saathoff*, Katja Lammens, Fabian Gut, Joseph Bartho, Aaron Alt, Brigitte Kessler, Karl-Peter Hopfner, Mechanism of DNA End Sensing and Processing by the Mre11-Rad50 Complex, *Molecular Cell*, Volume 76, 07 November 2019, Pages 382-394, https://doi.org/10.1016/j.molcel.2019.07.035

* These authors contributed equally.

Summary

In this publication we report the first cryo-EM structures that were solved using the full-length *Ec*MR complex. The resting state *Ec*MR head complex bound to the ATP analogue ATPγS resembled previously published structures of the head complex. The coiled coils were only visible in close proximity to the $Rad50^{NBDs}$ since they were too flexible to be resolved. The *Ec*MR cutting state was solved in complex with ADP and a 60bp dsDNA. In the cutting state, the Mre11 dimer moved to the side and formed a DNA binding channel together with Rad50. This channel allowed the DNA to reach the active site of Mre11, which has not been observed in previous MR crystal structures. Thus, our structure explains for the first time how *Ec*MR recognises a free DNA end and how the DNA is accommodated in the active site. The DNA was mainly bound by residues located in the $Rad50^{NBDs}$ and the coiled coils. Mutations in these DNA binding residues abolished DNA binding. Surprisingly, the coiled coils of both Rad50 monomers interacted with each other in the cutting state and formed a rod that clamps one dsDNA duplex between them. This rod was solved to a length of about 200 Å. A new interaction site was formed between the Rad50 β-sheets of the NBD and the Mre11 nuclease domain (denoted fastener). Mutations in the fastener strongly decreased exo- and endonuclease activity of *Ec*MR and a charge reversal mutant partially restored the nuclease activities.
Based on these results we propose a model in which the *Ec*MR complex is present in an autoinhibited state with open coiled coils, in which it scans the DNA for DSBs. Once a DSB is found, the coiled coils can close and the movement of the nuclease dimer to the side allows formation of a nuclease proficient complex.

Author Contribution

I generated the grids for the cryo-EM data. I processed the obtained cryo-EM data and built the resulting structures with help of Katja Lammens and Karl-Peter Hopfner. Together with Jan-Hinnerk Saathoff I purified the *Ec*MR mutants to analyse interesting residues, identified in the structure. To analyse these mutants I performed nuclease, DNA binding, and ATPase assays together with Jan-Hinnerk Saathoff and Fabian Gut. I wrote the manuscript together with Karl-Peter Hopfner.

Article

Molecular Cell

Mechanism of DNA End Sensing and Processing by the Mre11-Rad50 Complex

Graphical Abstract

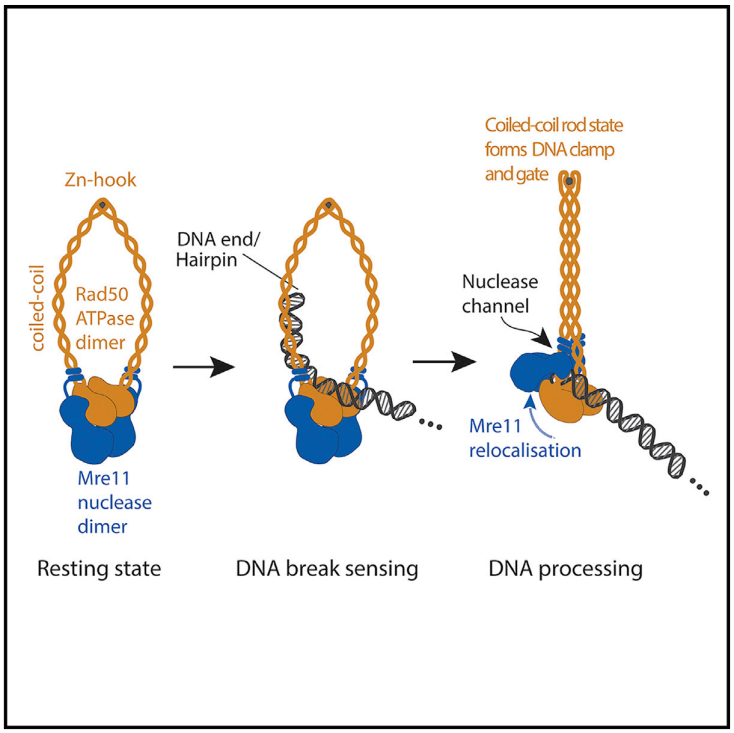

Authors

Lisa Käshammer, Jan-Hinnerk Saathoff, Katja Lammens, ..., Aaron Alt, Brigitte Kessler, Karl-Peter Hopfner

Correspondence

hopfner@genzentrum.lmu.de

In Brief

Käshammer et al. use cryoelectron microscopy and biochemical studies to reveal, at near-atomic resolution, how the ATP-dependent nuclease Mre11-Rad50 can sense and process a wide range of DNA termini to enable repair and recombination of breaks and hairpins in chromosomal DNA.

Highlights

- cryo-EM structure of *Ec*Mre11-Rad50 bound to a DNA break
- Mre11 dimer binds the DNA end at the side of Rad50
- Mre11 and Rad50 assemble a transient DNA cutting channel
- The coiled coils form a rod-shaped DNA gate and clamp

Käshammer et al., 2019, Molecular Cell *76*, 382–394
November 7, 2019
https://doi.org/10.1016/j.molcel.2019.07.035

CellPress

CellPress

Molecular Cell
Article

Mechanism of DNA End Sensing and Processing by the Mre11-Rad50 Complex

Lisa Käshammer,[1,2,4] Jan-Hinnerk Saathoff,[1,2,4] Katja Lammens,[1,2] Fabian Gut,[1,2] Joseph Bartho,[1,2] Aaron Alt,[1,2] Brigitte Kessler,[1,2] and Karl-Peter Hopfner[1,2,3,5,*]

[1]Department of Biochemistry, Ludwig-Maximilians-Universität, 81377 Munich, Germany
[2]Gene Center, Ludwig-Maximilians-Universität, 81377 Munich, Germany
[3]Center for Integrated Protein Science, 81377 Munich, Germany
[4]These authors contributed equally
[5]Lead Contact
*Correspondence: hopfner@genzentrum.lmu.de
https://doi.org/10.1016/j.molcel.2019.07.035

SUMMARY

DNA double-strand breaks (DSBs) threaten genome stability throughout life and are linked to tumorigenesis in humans. To initiate DSB repair by end joining or homologous recombination, the Mre11-nuclease Rad50-ATPase complex detects and processes diverse and obstructed DNA ends, but a structural mechanism is still lacking. Here we report cryo-EM structures of the *E. coli* Mre11-Rad50 homolog SbcCD in resting and DNA-bound cutting states. In the resting state, Mre11's nuclease is blocked by ATP-Rad50, and the Rad50 coiled coils appear flexible. Upon DNA binding, the two coiled coils zip up into a rod and, together with the Rad50 nucleotide-binding domains, form a clamp around dsDNA. Mre11 moves to the side of Rad50, binds the DNA end, and assembles a DNA cutting channel for the nuclease reactions. The structures reveal how Mre11-Rad50 can detect and process diverse DNA ends and uncover a clamping and gating function for the coiled coils.

INTRODUCTION

DNA double-strand breaks (DSBs) are a frequent cause of gross chromosomal aberrations and genome instability in all kingdoms of life (Myung et al., 2001). They are produced by ionizing radiation and genotoxic chemicals, arise at stalled and collapsed replication forks, and are products of abortive topoisomerases. Sensitive detection, signaling, and repair of DSBs is a critical process throughout life to maintain the integrity of genetic information (Blackford and Jackson, 2017; Ciccia and Elledge, 2010).

Repair of DSBs proceeds through homologous recombination (HR) or end joining pathways, typically in a cell cycle-regulated manner in eukaryotes (Chang et al., 2017; Hustedt and Durocher, 2016; Kowalczykowski, 2015; Wright et al., 2018). DNA resection and synthesis in HR and ligation in end joining require chemically "clean" DNA termini, but DSBs can be chemically very heterogeneous, including covalent protein adducts. These "dirty" DNA ends require nucleolytic processing by homologs of the Mre11-Rad50 protein family to enable subsequent repair or DNA damage signaling (Cejka, 2015; Hoa et al., 2016; Mimitou and Symington, 2008; Oh et al., 2016; Paull, 2018; Rahal et al., 2010).

Homologs of Rad50 and Mre11 are found in all kingdoms of life. They form $Mre11_2$-$Rad50_2$ heterotetramers, where two Rad50 ATP-binding cassette (ABC)-type nucleotide binding domains (NBDs) and a Mre11 nuclease dimer assemble as a catalytic head module that binds and cleaves DNA in a reaction regulated by ATP-induced conformational changes between the two NBDs (Hopfner et al., 2001). Rad50 homologs also possess intriguing 15- to 60-nm-long coiled coils (CCs) that can form large proteinaceous rings or rods, joined by an apical Zn-hook dimerization motif (Hopfner et al., 2002; Moreno-Herrero et al., 2005; Park et al., 2017). The CCs are functionally important (Hohl et al., 2011), but their mechanistic role is not understood. Eukaryotic Mre11-Rad50 interacts with Nijmegen breakage syndrome protein 1 (NBS1, known as Xrs2 in yeast), a protein that, among other functions, recruits the DNA damage checkpoint kinase ataxia telangiectasia mutated (ATM) (Carney et al., 1998; Falck et al., 2005).

Prokaryotic Mre11-Rad50 (MR) and eukaryotic Mre11-Rad50-Nbs1/Mre11-Rad50-Xrs2 (MRN/MRX) complexes have the intriguing function to sense both, clean and blocked DNA ends (Paull, 2018). The capability to clear blocked DNA ends is critical in eukaryotes to maintain genome integrity and ensure proper replication. Related functions exist in *E. coli*, where *E. coli* Mre11-Rad50 (*Ec*MR, also called SbcC-SbcD) processes palindromic hairpins, cleaves near protein blocks, and is implicated in the resolution of DNA replication termination structures (Connelly et al., 2003; Eykelenboom et al., 2008; Wendel et al., 2018).

The nature of the block appears to be of no importance and can be, for instance, streptavidin bound to biotinylated DNA termini (Cannavo and Cejka, 2014), the eukaryotic DNA end binding factor Ku (Reginato et al., 2017; Wang et al., 2017), or an abortive topoisomerase (Neale et al., 2005). The hydrolysis of ATP enables MR to cleave DNA 15–25 bp away from diverse blocks through endonuclease activity (Cannavo and Cejka, 2014; Connelly et al., 2003; Deshpande et al., 2016; Neale et al., 2005; Wang et al., 2017). MR(N) complexes also cleave

hairpins and possess 3′→5′ exonuclease activity, either inward from a clean DNA end or toward the DNA end following the internal endonucleolytic 5′ incision (Garcia et al., 2011; Paull and Gellert, 1998). It is mechanistically unclear how MR complexes can detect and process these chemically diverse terminal DNA structures without also cleaving internal DNA containing stable proteins (e.g., nucleosomes). The mechanism of end recognition and cleavage is even more puzzling because human MRN can internally bind to and diffuse along DNA until a DNA block is reached (Myler et al., 2017).

The structural mechanism of how MR(N) complexes sense and process clean and blocked DNA ends is not understood. A number of crystallographic studies with truncated proteins ($Rad50^{\Delta CC}$) revealed the basic architecture of interactions at the catalytic head domain and binding of DNA to Rad50 and Mre11 (Lammens et al., 2011; Lim et al., 2011; Möckel et al., 2012; Williams et al., 2008, 2011). ATP binding to Rad50 leads to a tightly engaged Rad50 NBD dimer, forming a DNA binding platform along the two NBDs (Hopfner et al., 2000; Liu et al., 2016; Seifert et al., 2016). Strangely, the current crystallographic studies suggest that Rad50 blocks Mre11's nuclease active sites in this ATP state (Liu et al., 2016, Möckel et al., 2012; Lim et al., 2011), although ATP is critical for nucleolytic processing by MR/MRN (Cannavo and Cejka, 2014; Herdendorf et al., 2011; Paull and Gellert, 1999; Saathoff et al., 2018). This incompatibility between structural and biochemical data in the processing of DNA ends and a general lack of understanding of DNA end recognition by MR/MRN currently hampers conceptual advances in the mechanism and biology of DSB repair (Paull, 2018).

Here we employed cryoelectron microscopy (cryo-EM) to study the full-length *E. coli* Mre11-Rad50 homolog in resting state (bound to adenosine-5′-o-(3-thio-triphosphate) [ATPγS]) as well as in a DNA end recognition and the cutting state (bound to DNA and ADP after ATP hydrolysis). The structures reveal an unanticipated structural state that resolves the above-mentioned mechanistic discrepancy. Rad50 forms the main DNA binding element through both NBDs and CCs. Upon DNA binding, the two Rad50 CC domains zip up and form a narrow clamp around a single DNA duplex. This structural change allows the Mre11 dimer to move from the bottom to the side of the complex and bind the DNA end. We biochemically show that this state is also involved in the endonucleolytic DNA end processing at blocked DNA ends. Rather than being mere linkers, the CCs act as clamps and gates for the recognition and processing of diverse DNA end structures. Our structures provide a new structural concept and framework for Mre11-Rad50 complex proteins that clarify key aspects of DNA end recognition and processing.

RESULTS

The Cryo-EM Structure of *Ec*MR in the "Resting" State

To reveal the mechanism of ATP-dependent DNA end sensing and processing by MR complexes, we used cryo-electron microscopy and single-particle reconstruction on *Ec*MR. We first addressed the structure of *Ec*MR in the absence of DNA, vitrified the protein in the presence and absence of ATPγS, and recorded transmission electron micrographs. Without nucleotides, we did not obtain homogeneous particles. Addition of ATPγS led to visibly more homogeneous particles and enabled us to obtain a 3.5 Å reconstruction and atomic structure of its DNA binding and processing head module (Figures 1A–1C; Figure S1; Table 1). The catalytic head of *Ec*MR consists of two *Ec*Rad50 NBDs and the *Ec*Mre11 dimer. Both *Ec*Mre11s match the high-resolution crystal structure of the *Ec*Mre11 nuclease extremely well ($EcMre11^{NUC}$, composed of phosphodiesterase and capping domains) (Figure S2A) and are anchored to the *Ec*Rad50 CCs via their C-terminal helix-loop-helix (HLH) domains. The $EcRad50^{NBD}$s are engaged by jointly binding two Mg^{2+}-ATPγS molecules in their interface and are situated in the DNA binding cleft of the $EcMre11^{NUC}$ dimer (Figure S4A). The structure recapitulates previous crystal structures of Mre11 bound to the truncated (ΔCCs) $Rad50^{NBD}$ (Lim et al., 2011; Möckel et al., 2012; Figure S2B). Although the head module is well resolved, the ~40-nm-long CCs are apparently flexible and only defined in the reconstruction up to the binding site of $EcMre11^{HLH}$. The angle of protrusion of the two CCs from the head suggests that they form wide, presumably flexible proteinaceous rings. The precise shape needs to be determined in future studies. We observed a homogeneous complex of approximately $(Mre11)_2$-$(Rad50)_2$ (M_2R_2) stoichiometry in gel filtration and did not see formation of higher-order complexes through addition of ATP and DNA, supporting a model where the CCs are joined within an M_2R_2 complex (Figure S2C).

In atomic force microscopy (AFM) studies, *Ec*MR forms predominantly V-shaped M_2R_2 complexes, joined at the Zn-hook (de Jager et al., 2004). In the absence of ATP, the *Ec*Mre11 nuclease domains were separated and attached each as monomers to the disengaged *Ec*Rad50 NBDs. Thus, ATP promotes stable head complexes with dimeric Mre11 by joining the two Rad50 NBDs, and we consistently observed slight compaction of the complex by ATP in solution (Figure S2C). Because *Ec*MR is constantly exposed to ATP in the cell but hydrolyzes it only with 0.008 ATP/s/active site (Saathoff et al., 2018), the obtained ATPγS-bound state likely represents a major autoinhibited resting state of the complex with blocked Mre11 nuclease sites.

The Cryo-EM Structure of *Ec*MR in the "Cutting" State

To understand how *Ec*MR recognizes DNA ends, we reconstituted a complex of the nuclease-deficient *Ec*MR mutant H84S ($EcM^{H84S}R$) with 60-bp double-stranded DNA (dsDNA) in the presence of ATP and recorded transmission electron micrographs. Three-dimensional reconstruction led to a cryo-EM map at a nominal resolution of 4.2 Å that enabled us to derive a near-atomic model of the *Ec*MR catalytic head module and parts of the CCs bound to DNA (Figure 1D–1F; Figure S3; Table 1). The structure captures how *Ec*MR senses and processes DNA ends, and we denoted this condition the cutting state. Inspection of the map at the nucleotide binding sites of the NBDs reveals the presence of Mg^{2+}-ADP. Because ATP binding is critical for DNA binding by *Ec*MR, the structure represents a post-ATP-hydrolysis state, which appears to be quite long-living before ADP → ATP exchange or DNA release (Figures S4B and S4C).

DNA end sensing induces two large conformational changes in the cutting state compared with the resting state (Figures 1D–1F; Figures S1 and S3; Video S1). The CCs move inward,

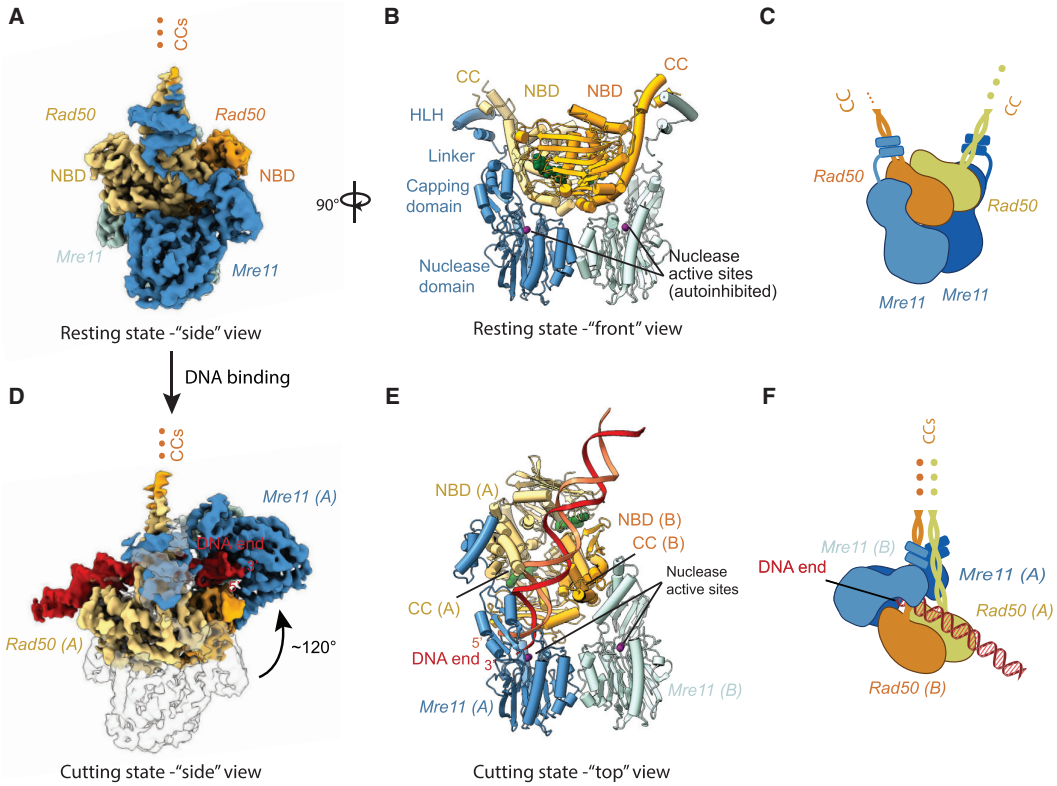

Figure 1. Structure of *Ec*Mre11-Rad50 in the Resting and Cutting States

(A) Density map of the dimeric *Ec*Rad50 ABC ATPase (orange/yellow) bound to the *Ec*Mre11 nuclease dimer (light/dark blue) in the resting state in side view. Subunits as well as the nucleotide binding domain (NBD) and coiled-coils (CC) are annotated. The CCs extend further (dots) but are not visualized in the map.

(B) Atomic model of the resting state catalytic head in front view, using the color code of (A).

(C) Scheme of the resting state catalytic head, using the color code of (A).

(D) Density map model of the cutting state in side view. DNA end binding leads to a large change in the architecture. The *Ec*Mre11 nuclease moves from its autoinhibited location (gray and transparent) with blocked active sites to bind the DNA end in the cutting state. The NBDs and CCs generate a DNA binding clamp and assemble with *Ec*Mre11, forming an active-site channel that harbors the DNA end. Only *Ec*Mre11 protomer A binds DNA (red), whereas *Ec*Mre11 protomer B plays an architectural role. Color code as in (A) with DNA colored in red.

(E) Atomic model of the cutting state in top view using the same color code as in (D).

(F) Scheme of the cutting state catalytic head using the same color code as in (D).

See also Figures S1–S4, Table 1, and Video S1.

zip up, and fold into an apparently rod-like geometry. Intriguingly, in this rod state, the CCs tightly clamp around a single dsDNA duplex, whereas the *Ec*Mre11 dimer relocates from its auto-inhibited position at the "bottom" of the Rad50 NBD dimer to the side of the NBD dimer. Here it forms, together with *Ec*Rad50^{NBD}, an active-site channel that harbors the DNA end. Compared with the resting state, the cutting state can be depicted as an almost rigid body rearrangement of *Ec*Mre11^{NUC} and *Ec*Rad50^{NBD} dimers, enabled by the flexible linker between *Ec*Mre11^{NUC} and *Ec*Mre11^{HLH} (Figure S4D). *Ec*Rad50^{NBD} also undergoes some internal subdomain rotations and changes in loop regions in response to DNA binding and ATP hydrolysis. Repositioning of the *Ec*Mre11^{NUC} dimer at the side of the *Ec*Rad50^{NBD}s sterically requires the inward movement of the CCs; thus, the rod formation of Rad50's CCs presumably precedes or coincides with Mre11 dimer relocalization.

The two *Ec*Rad50^{NBD}s generate a composite dsDNA binding platform that spans 22 bp of a DNA duplex, with dsDNA protruding on both sides (Figures 1D–1F). One dsDNA arm extends from the opposite side of the *Ec*Mre11 dimer location, whereas the other arm is bound by *Ec*Mre11 in the channel. The latter is positioned for nucleolytic cleavage and likely represents the "free DNA end" in the 3′→5′ exonuclease state. The pivotal role of Mre11 in binding the DNA end is consistent with the critical role of human Mre11 in DNA end sensing of MRN (Myler et al., 2017). Interestingly, only one of the two *Ec*Mre11 subunits contacts the DNA end (referred to as subunit "A"), whereas *Ec*Mre11 (subunit "B") helps to position the actively cutting subunit.

In sum, the structures uncover an intriguingly asymmetric and unanticipated structural state as the basis for DNA binding by *Ec*MR that clarifies the prevailing mystery of ATP-dependent detection and processing of DNA ends by MR.

Table 1. Cryo-EM Data Collection, 3D Reconstruction, and Model Refinement Statistics

	*Ec*MR Resting State (EMDB-10107) PDB: 6S6V	*Ec*MR Cutting State (EMDB-10116) PDB: 6S85
Data Collection and Processing		
Magnification	130,000	165,000
Voltage (kV)	300	300
Electron exposure (e–/Å^2)	68	73.6
Defocus range (μm)	–1.0 (–3.5)	–1.0 (–3.5)
Pixel size (Å)	1.06	0.82
Symmetry imposed	C2	C1
Initial particle images (no.)	2,809,916	1,130,635
Final particle images (no.)	142,229	151,271
Map resolution (Å)	3.5	4.2
FSC threshold	0.143	0.143
Refinement		
Initial model used (PDB code)	PDB: 4M0V, homology model of PDB: 3QF7	PDB: 4M0V, Rad50 from resting state
Model resolution (Å)	3.66	4.34
FSC threshold	0.5	0.5
Map sharpening *B* factor (Å^2)	–131	–194
Model Composition		
Non-hydrogen atoms	11,820	12,977
Protein residues	1,498	1,488
Ligands		
Mn^{2+}	4	4
Mg^{2+}	2	2
ATPγS	2	–
ADP	–	2
dsDNA	–	63 nt
B factors (Å^2)		
Protein	83.3	66.03
Ligand		
ATPγS	52.91	–
ADP	–	73.63
dsDNA	–	152.36
RMSDs		
Bond lengths (Å)	0.009	0.007
Bond angles (°)	0.897	0.918
Validation		
MolProbity score	1.82	2.27
Clashscore	6.21	18.66
Poor rotamers (%)	0.24	1.03
Ramachandran Plot		
Favored (%)	92.22	91.87
Allowed (%)	7.78	8.47
Disallowed (%)	0.0	0.34

A Fastener Loop Connects *Ec*Mre11^{NUC} with *Ec*Rad50^{NBD}

To form the cutting state, the phosphodiesterase domain of *Ec*Mre11 (A) is locked onto *Ec*Rad50^{NBD} (B) by a loop in *Ec*Mre11^{NUC}, which we denote "fastener" (amino acids [aa] 137–149) (Figure 2A). The fastener binds the outer β sheet of *Ec*Rad50^{NBD} (B) and holds both domains in place by mainly polar and ionic interactions. To validate this new interface, we mutated the central K149^{EcMre11}-E115^{EcRad50} salt bridge connecting the fastener and Rad50^{NBD}. *Ec*Mre11Rad50^{E115K} and *Ec*Mre11^{K149E}Rad50 display reduced endo/exonuclease and altered DNA binding activity, although the ATPase activity is increased (Figures S4E and S4F). Remarkably, the charge-reverting double mutant *Ec*Mre11^{K149E}Rad50^{E115K} rescues the endonuclease on blocked DNA ends as well as the exonuclease on free ends (Figures 2B and 2C). These data not only validate the cutting state structure but also indicate that the observed conformation is implicated in the endonucleolytic cutting of blocked ends. The increased ATPase rate could be a result of a weaker fastener-NBD interaction causing faster ADP-to-ATP exchange within Rad50's ATP cycle.

The Nuclease Active Site Is Located in a Transient Channel between Mre11 and Rad50

In the active-site channel between *Ec*Mre11^{NUC} and *Ec*Rad50^{NBD}, one DNA strand directly contacts the di-manganese cluster and is properly positioned for nucleolytic cleavage (the actual reaction is prevented by the H84S^{EcMre11} mutation) (Figure 2D; Figure S5A). Difference density analysis is consistent with the presence of two manganese ions, which are added to the buffer prior to plunge freezing (Figures S5B and S5C). The overall recognition is consistent with biochemically prevailing 3′→5′ exonuclease on free DNA ends and shows how DNA binds to Mre11 in the active cutting state. The binding mode is notably different from that obtained in crystallographic studies of prokaryotic Mre11-DNA complexes in the absence of Rad50. There, DNA was bound across the Mre11^{NUC} dimer, suggesting that Mre11 has different DNA binding modes (Figure S5C; Sung et al., 2014; Williams et al., 2008). Some density extends from the di-metal binding site toward the exit of the channel but has a poor quality that does not allow interpretation (Figure 2E). Biochemical data show that *Ec*MR preferentially cleaves the 3′ strand between terminal bases 3 and 4 (Saathoff et al., 2018). Thus, the additional density could stem from DNA that extends ~3 bases beyond the di-metal cluster but may also stem from a disordered *Ec*Mre11 loop (aa 188–203) (Figure S5D). This loop is not critical for cutting per se but seems

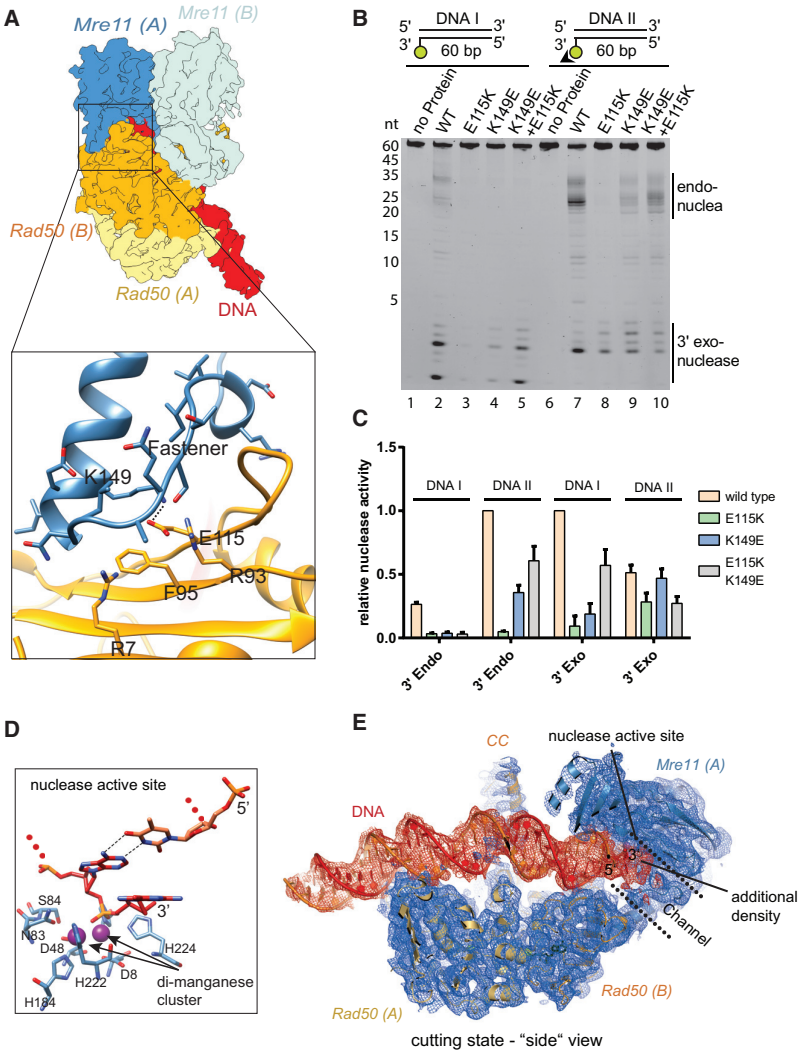

Figure 2. The Fastener Locks a Transient Active-Site Channel between Mre11 and Rad50

(A) The new *Ec*Mre11-EcRad50 interface in the cutting state is stabilized by binding of the *Ec*Mre11 fastener loop (blue) to the *Ec*Rad50 NBD (orange).

(B) Functional analysis of the salt bridge between E115^{EcRad50} and K149^{EcMre11}. Although single mutants reduce nuclease activity, both exonuclease (DNA I with a fluorescein label [green]) and endonuclease (DNA II with a fluorescein label and protein block [triangle]) are substantially rescued by a charge-reverting double mutant, E115^{EcRad50}+K149^{EcMre11}.

(C) Quantification of (B) (n = 3 technical replicates). Error bars indicate the standard deviation.

(D) Details of the interaction of the 3′ strand at or near the DNA end with the di-metal cluster of *Ec*Mre11, showing that the DNA is poised for cleavage in the observed cutting state (prevented by the H84S mutation).

(E) The nuclease active site is located in a channel between *Ec*Rad50 and *Ec*Mre11, which is principally large enough to accommodate hairpins and even extended dsDNA for endonuclease, although bending/melting of DNA or changes in the protein assembly need to occur. Shown is the color-coded density map superimposed with the structural model. Additional density extending into the structure could indicate some promiscuity in DNA end binding.

See also Figures S4 and S5.

to regulate the nuclease specificity (Figure S5E). Importantly, the nuclease channel is wide enough to accommodate longer DNA for endonucleolytic cleavage, as suggested by the biochemistry (Figures 1D and 2B). However, structural alterations in dsDNA (such as melting/unwinding) or changes in the protein are required to accommodate internal DNA and avoid clashes in the current conformation.

In summary, *Ec*Mre11 binds the DNA end through a transiently formed channel, which is consistent with and can explain the broad specificity of MR for diverse types of DNA termini.

The CCs Fold into a Rod Structure upon DNA Binding

To resolve more of the CCs, we employed different classification schemes during the electron microscopy (EM) data evaluation process that enabled us to reconstruct ~1/3 of their macrostructure (Figure 3A). The CCs have a segmented structure and zip up from the more flexible conformations into a closed "rod," clamping around the DNA duplex that is bound at the NBDs (Figure 3B). DNA-induced rod formation matches extremely well the DNA-driven transition of human MRN observed at low resolution by atomic force microscopy (Moreno-Herrero et al., 2005), DNA-bound rods of *Ec*MR in AFM studies (de Jager et al., 2004), and recent analysis of the human Zn-hook (Park et al., 2017; Figure 3A). The Zn-hook dimers joining the apices of the CCs can adopt open V-shaped and closed rod-shaped dimers and, thus, may act as a hinge to allow open, probably ring-like states and closed rod states of the CCs (Hopfner et al., 2002; Park et al., 2017). Although, at this resolution, we cannot assign a sequence at the CCs, a highly conserved sequence region (GEIR motif) in bacterial MR homologs could mark an important site near the first CC-CC "zipper" contact (Figure 3B). We tested several mutations in this motif. Although GEIR→GAIA did not lead to noticeable alteration of the nuclease reactions, GEIR→AEIR robustly reduced endonuclease activity on blocked DNA ends, whereas exonuclease activity on free DNA ends is almost as efficient as in the wild type (WT) (Figure 3C; Figure S5E). Because this mutation still leads to a complex with a stoichiometry and size similar to that of the WT *Ec*MR, the most plausible interpretation is that G→A affects the structure and dynamics of the CCs, which appear

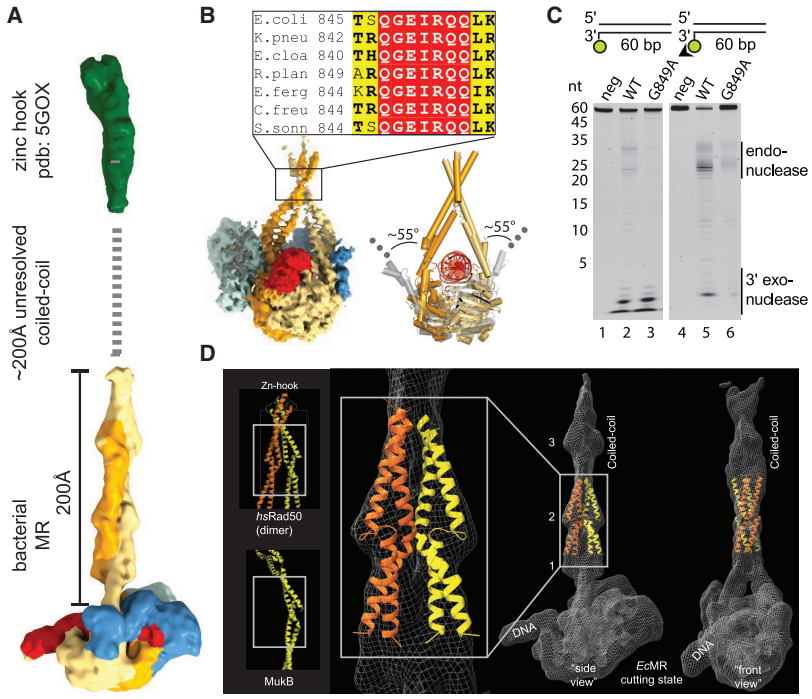

Figure 3. The CCs Form a Long Rod upon DNA Duplex Binding

(A) Low-resolution reconstruction and map showing ~200 Å of the zippered CCs emerging from the DNA binding module (color code of Figure 1). The Zn-hook in rod conformation (PDB: 5GOX) is shown to visualize the approximate site of *Ec*MR.

(B) Left: medium-resolution reconstruction and map showing the CCs up to the first zipper contact. Right: pseudoatomic model visualizing the large ring-to-rod transition of the CCs driven by DNA binding. Top: a conserved sequence motif (GEIR) maps to the region of the first zipper contact.

(C) Mutating the GEIR motif affects endonuclease activity on free and fluorescein-blocked DNA ends (triangle) (see also Figure S5E).

(D) The dimeric CC apex at the human Zn-hook (PDB: 5GOX) and the CC at the MukB elbow region (PDB: 6H2X) harbor a folded CC break element that can be readily docked into the CC zipper contact of *Ec*MR.

See also Figure S5.

to be particularly critical for ATP-dependent endonucleolytic cleavage of blocked DNA.

In our reconstruction, we can visualize two more folded interruptions of the CCs that appear to form CC-CC zipper contacts (Figure 3D). These interaction points match in shape a CC-CC contact of the human hook element in the rod conformation (Park et al., 2017) as well as regions of the "elbow" element of the structural maintenance of chromosome (SMC) ABC-ATPase MukB (Bürmann et al., 2019), indicating wider structural conservation in the Rad50/SMC protein family. Although we cannot assign a sequence motif to these elements yet, secondary structure analysis suggests that *Ec*Rad50 in total has at least five of these folded interruptions in the CCs that could form zipper contacts (Figure S5F).

The CCs Form a Clamp around DNA

The rod conformation is induced and stabilized by joint binding of DNA by the CCs (e.g., K194 and K890) and the NBDs (e.g., R102, K128, and K130) (Figure 4A). Point mutations in DNA binding residues in both NBDs and CCs did not affect basal ATPase rates but nearly abolished DNA binding and DNA-induced ATPase and nuclease activities (Figures 4B–4D). Consistently, *Ec*MR$^{\Delta CC}$ and/or *Ec*MR^{hook} (C506S and C509S mutations in the Zn-hook) lost high-affinity DNA binding (Figure S5G) and linear plasmid degradation activity (Figure S5H). The strong effect of the CC lysines K194 and K890 on DNA binding and ATPase could also be due to the formation of CC-DNA interactions in the pre-hydrolysis ATP state (not visualized here). Alternatively, the cutting state structure could allow more rapid ATP turnover. This is due to the fact, that the NBD dimer is not bound at the Mre11 dimer cleft and, therefore, could more easily open up for ADP→ATP exchange. Together, these data show the CCs, their DNA-clamping activity, and their proper Zn-hook-mediated dimerization are functionally critical for high-affinity DNA binding and ATP-dependent nuclease.

The interaction with the CCs noticeably bends DNA along the NBDs compared with a crystal structure of archaeal MR$^{\Delta CC}$, where DNA is much straighter and is not bound by the CCs (Figures 4E and 4F; Figure S6A; Liu et al., 2016). The observed bent DNA conformation is more difficult to achieve with negatively supercoiled DNA and may add to the sensing of damaged DNA because negatively supercoiled DNA is present in undamaged *E. coli* chromosomes. Consistently, negatively supercoiled DNA stimulates ATP hydrolysis by *Ec*MR much less than relaxed DNA (Saathoff et al., 2018).

Interestingly, the CC-mediated upward bending leads to a single-base-pair registry shift along the NBDs compared with the archaeal MR (ΔCC) ATPγS complex (Figures 4E and 4F). Thus, it is also plausible that ATP-driven conformational changes in the NBDs modulate the way DNA binds in MR and could affect DNA processing. Although the details need to be clarified in future studies, ATP-driven directional registry shifts (like in a DNA translocase to promote directional movement) could help detect the presence of stable protein-DNA adducts through a steric filter by the CCs that allow DNA but not bulky adducts to pass.

Loading onto Linear DNA Is Critical for the Processing of DNA Blocks

Our structural analysis, in conjunction with analysis of the Zn-hook, indicates that, in the cutting state, the CCs form a closed rod all the way from the DNA binding head to the Zn-hooks,

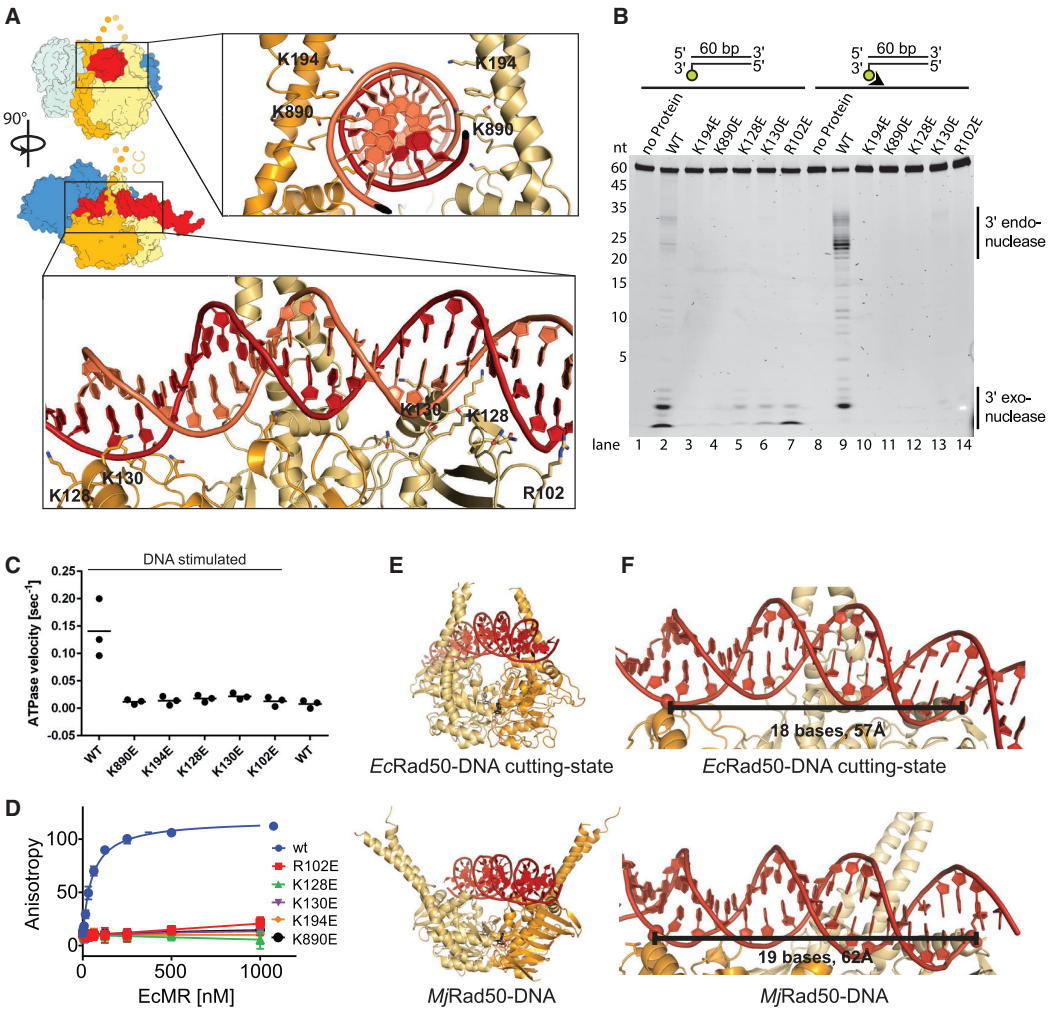

Figure 4. The CCs Form a Chemo-mechanical DNA Clamp

(A) Details of the interaction of DNA with the CCs (top panel) and the NBD (bottom panel) of *Ec*Rad50, showing that the CCs and NBDs form a narrow gate and clamp. Selected DNA binding residues are highlighted.

(B) Nuclease activity of *Ec*MR DNA binding mutants, analyzed with fluorescently labeled 60-bp DNA containing a free DNA end (DNA I) and a DNA end blocked by a single-chain fragment against fluorescein (DNA II). The *Ec*Rad50 DNA-binding lysine and arginine were mutated to glutamate.

(C) Analysis of DNA-stimulated ATPase activity. The DNA binding mutants show no stimulation of ATPase but basal ATPase activity (n = 3 technical replicates). The calculated mean is indicated by a black line. All ATP rates were measured with the nuclease dead Mre11^{H84Q} mutant to avoid DNA degradation.

(D) DNA binding by fluorescence polarization anisotropy reveals that both NBD and CCs DNA binding residues are functionally critical (n = 3 technical repeats). Error bars indicate the standard deviation. All DNA binding measurements were done with the nuclease dead Mre11^{H84Q} mutant to avoid DNA degradation.

(E) Comparison of the DNA interaction of the cryo-EM *Ec*MR cutting-state structure (left) with the X-ray structure of *Methanocaldococcus jannaschii* (Mj) Rad50-DNA (right).

(F) ADP-*Ec*MR cutting state (right) binds DNA with a 1-bp registry shift across the NBDs compared with ATPγS *Mj*Rad50 (left) because of CC-mediated upward bending and distortion of DNA.

See also Figure S6A.

except for a fairly narrow opening near the NBDs that accommodates one DNA duplex (Figure 3A). A second duplex between the CCs (such as through entrapping a loop) would possibly interfere with rod formation by preventing zipper contacts. Because the GEIR motif mutation suggests that CC geometry is very sensitively coupled to functional endonuclease, topological entrapment of a linear DNA end rather than a loop could confer endonuclease specificity toward DNA end structures.

To test this model, we analyzed a DNA fragment that contains biotin moieties on both ends and is either double-blocked in a linear (one streptavidin per end) or circular (both ends bound to one streptavidin) fashion. Addition of *Ec*MR leads to rapid

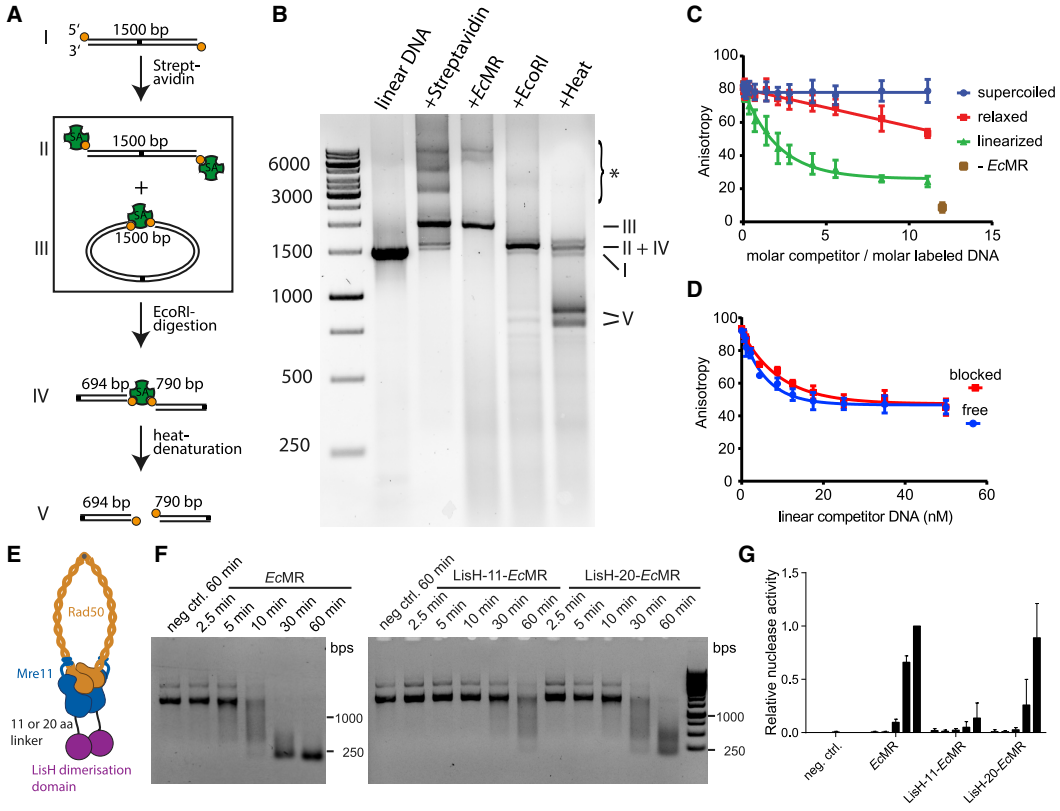

Figure 5. Loading onto Linear DNA Is Critical for the Processing of DNA Blocks

(A) Assay for processing of internal and terminal protein blocks. DNA with 5′ biotin (orange) is incubated with streptavidin (green), forming linear and circular species. After incubation with *Ec*MR, products are analyzed further using EcoRI digestion (black box) and heat denaturation.

(B) Streptavidin addition to linear DNA results in linear (~1,500-bp migration with one or two streptavidin-blocked DNA ends), circular (~2,000-bp migration), and different higher-order linear or circular species (asterisk). *Ec*MR leads to selective digestion of the linear species and some of the higher-order species, presumably the linear ones. In contrast, the circular species is stable. EcoRI addition and heat denaturation confirm the topology of the circular species.

(C) Linear but not relaxed or supercoiled circular DNA efficiently competes for binding to *Ec*MR with linear, 60-bp, fluorescently labeled DNA in fluorescence polarization anisotropy experiments (n = 3 technical replicates). Error bars indicate the standard deviation.

(D) Like (C), but using a linear competitor with free or protein-blocked ends (n = 3 technical replicates). Error bars indicate the standard deviation.

(E) Scheme of the LisH-*Ec*MR fusion approach to conformationally restrict and stabilize the Mre11 dimer.

(F) Time-dependent linear DNA degradation of 1,500-bp linear DNA containing a streptavidin block on both ends. WT *Ec*MR rapidly degrades DNA to short fragments, whereas LisH fusion proteins are severely (11-bp linker) or moderately (20-bp linker) compromised. Error bars indicate the standard deviation.

(G) Quantification of the occurrence of the less than 250-bp product over time in (F) (n = 3 technical replicates).

See also Figure S6.

degradation of the linear but not the circular product in the same reaction mixture, although both contain chemically identical protein-blocked nucleic acid termini (Figures 5A and 5B; Figure S6B). Consistently, *Ec*MR binds to linear plasmid DNA with higher affinity than circular supercoiled and relaxed DNA, regardless of whether the DNA end is free or protein blocked (Figures 5C and 5D). Because the only discriminating feature in these studies is the DNA topology, a plausible role of the CCs and their rod formation is the topological detection of DNA breaks through a gating mechanism; i.e., rods can form when a single duplex, but not a loop, threads through the CCs. In support of topological detection of blocks at linear DNA rather than direct chemical recognition of DNA termini, we also find cleavage of Ku70/80 blocked DNA ends by *Ec*MR with an inward-shifted cut site, as observed for eukaryotic MRN/MRX (Reginato et al., 2017; Wang et al., 2017; Figure S6C). Thus, *Ec*MRs biochemical properties are very similar to the eukaryotic MRN-CtBP-interacting protein (CtIP) in that it, too, cleaves at a defined distance from a stable protein-DNA complex, irrespective of the nature of the protein and the way it is bound to DNA. However, here we show that the block needs to be on linear DNA rather than within a DNA circle for recognition and cleavage, providing a DNA topology/accessibility mechanism for the recognition of broken DNA instead of chemical detection of free DNA termini.

Linking the Mre11 Dimer Slows Down Endonuclease

To load onto blocked DNA, the Mre11 dimer would need to relocate from its autoinhibited conformation over the protein block to

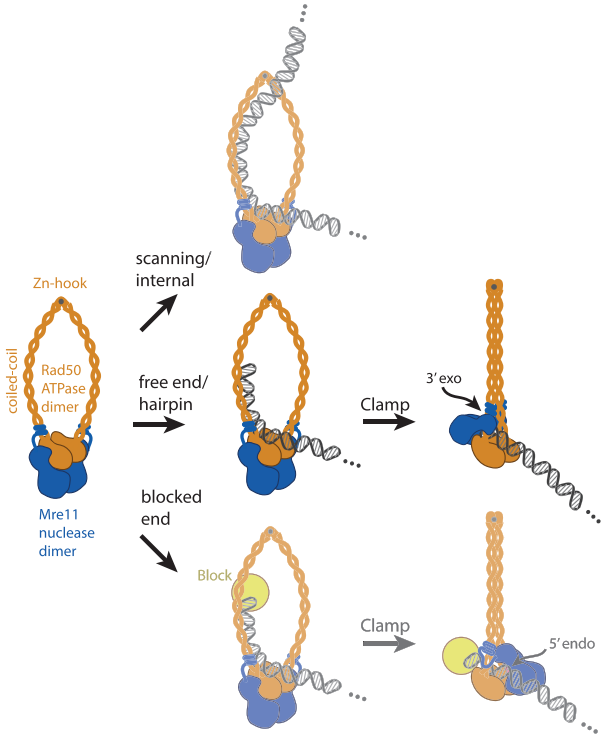

Figure 6. Model of DNA Sensing and Processing by MR

Proposed model of the sensing and cutting of DNA ends by *Ec*MR. Binding of internal DNA could lead to a scanning state (top panel). Encounter of a free (center panels) or blocked (bottom panel) DNA end would allow ring-to-rod transition of the CCs to form the high-affinity cutting state at or near DNA ends. Free DNA ends are bound directly by Mre11, as seen in the cryo-EM structure. Biochemical data suggest that a blocked end is bound in a reversed manner. See also Figure S7.

settle on the other side of DNA. Possibly, the Mre11 dimer transiently opens up for this to occur, which is reasonable because bacterial and archaeal $Mre11^{NUC}$ are monomeric in the absence of Rad50 (Figure S6D; Hopfner et al., 2001; Saathoff et al., 2018). We tested this hypothesis by fusing the Lis1 homology motif (LisH) dimerization domain (Delto et al., 2015) to the N terminus of *Ec*Mre11, which adds an additional tether between the two $Mre11^{NUC}$ domains (Figure 5E). LisH stabilizes the Mre11 dimer without leading to higher-order oligomers in *Ec*MR (Figures S6D and S6E). We assayed DNA degradation for two linker lengths between LisH and Mre11 (11 and 20 residues) using the linear DNA fragment with biotin-streptavidin blocks on both sides (Figure 5F). Degradation of long DNA proceeds by repetitive endonuclease reactions on both strands (Lim et al., 2015), and we consistently observed the appearance of short DNA (<250 bp) fragments. LisH-*Ec*MR degrades plasmids in a delayed manner. LisH-20-*Ec*MR's endonuclease is 3–5 times delayed, although it has normal exonuclease. LisH-11-*Ec*MR hardly shows any endonuclease products (Figure 5G), although its 3′→5′ exonuclease is only ~3 times reduced compared with the WT (Figures S6F and S6G). The lower exonuclease of LisH-11-*Ec*MR could originate from reduced loading on free DNA ends, which might be at least facilitated by dimer dynamics. The residual endonuclease activity of the 20-residue linker could be because it might allow Mre11 dimers to disengage and re-engage on the other side of DNA, with the LisH dimer remaining at the original side of DNA. In any case, our data suggest that the Mre11 dimer interface needs to be dynamic, especially for the endonuclease reaction.

DISCUSSION

Mre11 and Rad50 are phylogenetically conserved DNA end-processing machines (Paull, 2018; Syed and Tainer, 2018), required to clear aberrant or blocked terminal DNA structures and hairpins to enable repair and maintain genome integrity, but the mechanism of end recognition and processing by MR complexes has remained unclear. Using cryo-electron microscopy and biochemical analysis, we visualize resting and DNA cutting states of the *E. coli* MR complex, revealing how MR binds and processes DNA end structures. Our structures show that *Ec*MR adopts a nuclease-autoinhibited resting state in the absence of DNA. DNA binding induces a global conformational change that encompasses both the catalytic head module and the CC region, leading to rod formation of the CCs and repositioning of the Mre11 dimer to the side of the complex, where it assembles a DNA cutting channel and binds the free DNA end.

Combining our cryo-EM structures in the presence of ATPγS with AFM data in the absence of nucleotides (de Jager et al., 2004), a major state in the cellular environment could be M_2R_2, possibly joined into a proteinaceous ring by the Rad50 Zn-hook dimerization domains, although we do not want to rule out other configurations (Figure 6). Linear DNA could then induce the observed rod state in the CCs that enables and perhaps triggers relocalization of the Mre11 protein from an auto-inhibited state beneath the Rad50 NBDs to the active location at the side. The Zn-hooks would act as hinges and remain joined, consistent with crystallographic studies showing open and closed/rod states in the Zn-hooks (Hopfner et al., 2002; Park et al., 2017). Such a model is consistent with *in vivo* studies suggesting that the CCs functionally connect hook and head elements through transmission of structural changes (Hohl et al., 2015). We provide a putative mechanistic basis for this functional coupling *in vivo* because formation of stable zipper contacts along the CCs likely requires properly structured head and hook regions. The previously observed DNA-induced rod formation of human MRN CCs in low-resolution AFM analysis suggests that this global conformational switching is a conserved feature of MR/MRN/MRX complexes (Moreno-Herrero et al., 2005; Park et al., 2017).

The CCs might also act as linkers of distant DNA elements (de Jager et al., 2001; Hopfner et al., 2002; Seeber et al., 2016), in addition to the functions in DNA clamping and gating proposed here. Zn-hook dimerization might switch from intra- to intercomplex configurations, CC rods from different complexes could interact by other means, or additional DNA interactions in the CCs could mediate DNA tethering.

The CCs appear to be a critical structural switch with several functions, including topological gating to DNA ends and assembly of an active clamp for high-affinity DNA binding. The space

between the CCs near the NBDs can accommodate only one DNA duplex. A second duplex within the CCs might prevent, or at least interfere, with formation of a fully engaged rod with multiple zipper contacts, avoiding cutting of internal DNA because the clamp around DNA might not form properly (Figure 6). Evidence of such a global conformational role of CCs is supported by biochemical analysis showing that mutations in the DNA binding residues of the CCs, CC truncation, or mutation of the Zn-hook all have defective nuclease activity and no longer form high-affinity DNA interactions.

Although we do not see degradation of circular DNA, even in the presence of an ''internal streptavidin-biotin'' connecting two DNA ends (Figures 5A and 5B), *Ec*MR can still bind circular DNA. Circular DNA stimulates *Ec*MRs ATPase, so circular DNA likely interacts with Rad50's ATPase domains even though it is not cleaved (Saathoff et al., 2018). Likewise, human MRN can load to internal sites of DNA, followed by one-dimensional diffusion until a DNA end is reached and DNA cleavage occurs (Myler et al., 2017). Scanning is largely a property of the Rad50 protein and does not even require the full CCs in the human MRN setting, whereas end recognition requires Mre11, in agreement with our structure and consistent with the proposed model (Figure 6) (Myler et al., 2017). These peculiar properties could be explained if interactions with circular DNA, still triggering ATP hydrolysis at the NBDs, and with linear DNA are different. A possible explanation is the apparent restriction of a stable rod conformation to a single passage of DNA through the CCs (Figure 6).

Rod like-states could be a universal mechanistic feature of Rad50/SMC proteins because rod formation and structural changes are also proposed for the distantly related SMC protein family, which forms cohesin and condensin complexes (Diebold-Durand et al., 2017; Uhlmann, 2016). Although there are many underlying functional and structural differences, the general architecture of ABC ATPases coupled to CC rings/rods is quite conserved between SMC proteins and MR. For instance, the structural breaks in the CC rods that mediate the CC-CC zipper contacts are similar to structural elements found in Rad50's hook and MukB's elbow region, suggesting related architectural principles (Bürmann et al., 2019; Park et al., 2017). Thus, although the rod state of *Ec*MR appears to be adapted to passage of a single DNA duplex through the proteinaceous ring, a related mechanistic link between a certain number of DNA duplexes within SMC protein rings (or their absence) and the head module could be relevant for the dynamic interaction of SMC proteins with chromosomal DNA, as shown by recent biochemical analyses (Vazquez Nunez et al., 2019).

Our high-resolution structure of the cutting-state catalytic head reveals how MR detects and processes a DNA end through a new, previously unobserved asymmetric conformational state, where Mre11 binds to the side of Rad50 to assemble a DNA-processing channel (Figure 6). The transient formation of this channel and its structural properties offer an explanation of MR's broad nuclease reactions because it can accommodate different DNA structures. The channel readily accommodates a free DNA end, poised to cleave the 3′ strand exonucleolytically, consistent with the prevalence of 3′ exonuclease on free DNA ends. The channel could also accommodate nicked and bent dsDNA and hairpins, explaining why MR readily opens hairpin structures and can resect DNA 3′→5′ from the nick. The channel is also wide enough to accommodate internal dsDNA. However, internal DNA would need to be bent/melted to fit into the channel, and/or the protein adapts structurally. DNA bending/melting for efficient endonuclease is indeed suggested by biochemical studies (Cannon et al., 2013; Liu et al., 2016, ; Saathoff et al., 2018), and the structural effect of the CCs on DNA geometry and ATP-induced registry shifts of DNA along the NBDs are, in principle, well suited to provide chemo-mechanical means for triggering endonuclease activity. However, additional conformational states during the endonuclease reaction are possible as well. For instance, *Ec*MR-induced endonucleolytic cuts at opposing DNA strands occur with a different cleavage chemistry, suggesting an additional mode of DNA approach to the di-metal center (Saathoff et al., 2018). In addition, crystallographic analysis shows alternative DNA binding modes of the Mre11 nuclease dimer in the absence of Rad50 (Sung et al., 2014; Williams et al., 2008). Although DNA was not bound at the di-metal centers in these structures, these DNA contacts could represent states during DNA end tethering or endonucleolytic reactions. Thus, the requirement of the fastener-NBD interaction for endonucleolytic processing suggests that key aspects of the cutting state are also relevant for endonuclease, the precise mechanism of endonucleolytic processing of blocked DNA by MR requires future studies.

Our results provide some insights into the possible orientation of MR relative to the block in such a reaction. It is unlikely that the block is positioned directly at the exit of the active-site channel; i.e., the location of the DNA end in the observed cutting state. In such a scenario, DNA cleavage should occur closer to the end than observed experimentally. Both the distance between the block and the endonucleolytic cut sites and the cleavage chemistries in biochemical assays argue for location of the block at the Mre11 distal side (Saathoff et al., 2018; Figure 6). This model, suggesting that the CCs clamps are a filter for the block, would explain the fairly consistent distance between endonucleolytic cleavage and block (Cannavo and Cejka, 2014; Deshpande et al., 2016; Saathoff et al., 2018) and mechanistically unify 3′ exo- and 5′ endonuclease through a simple flip of the location of the Mre11 dimer relative to Rad50 on DNA. Loading of *Ec*MR in the flipped orientation would require transient dissociation of the Mre11 dimer, followed by reassembly on the other side of the DNA duplex (Figure 6). Our LisH fusion proteins indeed provide evidence that such transient disassembly is critical for endonuclease reactions but that reassembly of a functional Mre11 dimer on DNA is crucial because mutations that weaken the Mre11 dimer interface cripple *Ec*MR's endonuclease *in vitro* and MRN's function in *S. pombe in vivo* (Williams et al., 2008).

Finally, our results have implications for eukaryotic MRN/X, which requires Nbs1/Xrs2 and CtIP/Sae2 constitutive or transient subunits for efficient DNA processing *in vivo* (Hoa et al., 2016; Mimitou and Symington, 2008; Sartori et al., 2007) and *in vitro* (Anand et al., 2016; Cannavo and Cejka, 2014; Deshpande et al., 2016). Comparison of the bacterial MR cutting state with a model of a putative equivalent eukaryotic complex reveals that the fastener loop of *Ec*Mre11 binds precisely to the surface cluster of residues corresponding to *S. cerevisiae* Rad50S

mutations (Figure S7; Alani et al., 1990). Rad50S mutations phenocopy sae2Δ, cluster on a surface patch on the Rad50 NBDs, and have been proposed early on (Hopfner et al., 2000) and recently demonstrated to disrupt an interaction of Sae2 with Rad50 (Anand et al., 2016). Intriguingly, in *Ct*Mre11 (also *Sp*Mre11), this element is much shorter and conspicuously lacks the long loop that locks *Ec*Mre11^{NUC} to *Ec*Rad50^{NBD} at the "Rad50S" site. It is therefore possible that, instead of a Mre11-intrinsic fastener, the interaction of eukaryotic MRN in the cutting state could be mediated by CtIP/Sae2, which interacts at this site.

In summary, although structures of MRN-CtIP cutting states and structures of MR complexes bound to blocked DNA are needed to clarify activation of the eukaryotic system and the endonuclease activity of MR/MRN, we present structural and biochemical data that provide a new comprehensive framework and mechanistic concept for the detection and processing of diverse DNA ends by the Mre11-Rad50 nuclease complex.

STAR★METHODS

Detailed methods are provided in the online version of this paper and include the following:

- KEY RESOURCES TABLE
- LEAD CONTACT AND MATERIALS AVAILABILITY
- EXPERIMENTAL MODEL AND SUBJECT DETAILS
  - Organisms as source for materials used in experiments
- METHOD DETAILS
  - Expression and purification of EcMR
  - Expression and Purification of *Ct*Ku70/80
  - Nuclease assays
  - ATPase assays
  - DNA binding assays
  - Competitive DNA binding assay
  - Blocked dsDNA degradation assay
  - Circularization Assay
  - Size Exclusion Analysis
  - Cryo electron microscopy grid preparation
  - Cryo electron microscopy data collection
  - Data processing and 3D reconstruction
  - Model building
- QUANTIFICATION AND STATISTICAL ANALYSIS
- DATA AND CODE AVAILABILITY

SUPPLEMENTAL INFORMATION

Supplemental Information can be found online at https://doi.org/10.1016/j.molcel.2019.07.035.

ACKNOWLEDGMENTS

We thank the MPI Biochemistry cryo-EM facility and Mike Strauss for data collection and Dirk Kostrewa, Roland Beckmann, and Christophe Jung for technical help and suggestions. We thank Sebastian Eustermann for insightful discussions and help with modeling of the coiled-coil element. We thank Robert Thomas Byrne for help with data processing and Thomas Fröhlich for mass spectrometry. We thank Sandra Schuller for support in the initial grid preparation. K.-P.H. is supported by the Deutsche Forschungsgemeinschaft (CRC1361), the European Research Council (ERC Advanced Grant ATMMACHINE), the Gottfried-Wilhelm-Leibniz Prize, and the Center for Integrated Protein Sciences Munich (CIPSM). K.L. is supported by CRC1054. L.K. acknowledges support from the International Max Planck Research School of Molecular and Cellular Life Sciences. F.G. acknowledges support from Research Training Group 1721.

AUTHOR CONTRIBUTIONS

L.K. prepared cryo-EM grids and performed structure determination and modeling. J.-H.S., L.K., and F.G. performed the biochemical analysis. L.K., J.-H.S., and K.-P.H. analyzed results. L.K., J.-H.S., and B.K. purified the proteins. A.A. provided Ku70/80. K.L. and J.B. helped with data collection, structure determination, analysis, and modeling. K.P-H. and L.K. wrote the paper with contributions from all other authors. K.-P.H. designed the overall study.

DECLARATION OF INTERESTS

The authors declare no competing interests.

Received: March 22, 2019
Revised: June 17, 2019
Accepted: July 25, 2019
Published: September 3, 2019

SUPPORTING CITATIONS

The following references appear in the Supplemental Information: Ludwiczak et al. (2019); Zimmermann et al. (2018).

REFERENCES

Afonine, P.V., Poon, B.K., Read, R.J., Sobolev, O.V., Terwilliger, T.C., Urzhumtsev, A., and Adams, P.D. (2018). Real-space refinement in PHENIX for cryo-EM and crystallography. Acta Crystallogr. D Struct. Biol. *74*, 531–544.

Alani, E., Padmore, R., and Kleckner, N. (1990). Analysis of wild-type and rad50 mutants of yeast suggests an intimate relationship between meiotic chromosome synapsis and recombination. Cell *61*, 419–436.

Anand, R., Ranjha, L., Cannavo, E., and Cejka, P. (2016). Phosphorylated CtIP Functions as a Co-factor of the MRE11-RAD50-NBS1 Endonuclease in DNA End Resection. Mol. Cell *64*, 940–950.

Biasini, M., Bienert, S., Waterhouse, A., Arnold, K., Studer, G., Schmidt, T., Kiefer, F., Gallo Cassarino, T., Bertoni, M., Bordoli, L., et al. (2014). SWISS-MODEL: modelling protein tertiary and quaternary structure using evolutionary information. Nucleic Acids Res. *42*, W252–W258.

Bieniossek, C., Richmond, T.J., and Berger, I. (2008). MultiBac: multigene baculovirus-based eukaryotic protein complex production. Curr. Protoc. Protein Sci. *Chapter 5*, Unit 5.20.

Blackford, A.N., and Jackson, S.P. (2017). ATM, ATR, and DNA-PK: The Trinity at the Heart of the DNA Damage Response. Mol. Cell *66*, 801–817.

Bürmann, F., Lee, B.G., Than, T., Sinn, L., O'Reilly, F.J., Yatskevich, S., Rappsilber, J., Hu, B., Nasmyth, K., and Löwe, J. (2019). A folded conformation of MukBEF and cohesin. Nat. Struct. Mol. Biol. *26*, 227–236.

Cannavo, E., and Cejka, P. (2014). Sae2 promotes dsDNA endonuclease activity within Mre11-Rad50-Xrs2 to resect DNA breaks. Nature *514*, 122–125.

Cannon, B., Kuhnlein, J., Yang, S.H., Cheng, A., Schindler, D., Stark, J.M., Russell, R., and Paull, T.T. (2013). Visualization of local DNA unwinding by Mre11/Rad50/Nbs1 using single-molecule FRET. Proc. Natl. Acad. Sci. USA *110*, 18868–18873.

Carney, J.P., Maser, R.S., Olivares, H., Davis, E.M., Le Beau, M., Yates, J.R., 3rd, Hays, L., Morgan, W.F., and Petrini, J.H.J. (1998). The hMre11/hRad50 protein complex and Nijmegen breakage syndrome: linkage of double-strand break repair to the cellular DNA damage response. Cell *93*, 477–486.

Cejka, P. (2015). DNA End Resection: Nucleases Team Up with the Right Partners to Initiate Homologous Recombination. J. Biol. Chem. *290*, 22931–22938.

Chang, H.H.Y., Pannunzio, N.R., Adachi, N., and Lieber, M.R. (2017). Non-homologous DNA end joining and alternative pathways to double-strand break repair. Nat. Rev. Mol. Cell Biol. *18*, 495–506.

Ciccia, A., and Elledge, S.J. (2010). The DNA damage response: making it safe to play with knives. Mol. Cell *40*, 179–204.

Connelly, J.C., de Leau, E.S., and Leach, D.R. (2003). Nucleolytic processing of a protein-bound DNA end by the E. coli SbcCD (MR) complex. DNA Repair (Amst.) *2*, 795–807.

de Jager, M., van Noort, J., van Gent, D.C., Dekker, C., Kanaar, R., and Wyman, C. (2001). Human Rad50/Mre11 is a flexible complex that can tether DNA ends. Mol. Cell *8*, 1129–1135.

de Jager, M., Trujillo, K.M., Sung, P., Hopfner, K.-P., Carney, J.P., Tainer, J.A., Connelly, J.C., Leach, D.R.F., Kanaar, R., and Wyman, C. (2004). Differential arrangements of conserved building blocks among homologs of the Rad50/Mre11 DNA repair protein complex. J. Mol. Biol. *339*, 937–949.

Delto, C.F., Heisler, F.F., Kuper, J., Sander, B., Kneussel, M., and Schindelin, H. (2015). The LisH motif of muskelin is crucial for oligomerization and governs intracellular localization. Structure *23*, 364–373.

Deshpande, R.A., Lee, J.H., Arora, S., and Paull, T.T. (2016). Nbs1 Converts the Human Mre11/Rad50 Nuclease Complex into an Endo/Exonuclease Machine Specific for Protein-DNA Adducts. Mol. Cell *64*, 593–606.

Diebold-Durand, M.L., Lee, H., Ruiz Avila, L.B., Noh, H., Shin, H.C., Im, H., Bock, F.P., Burmann, F., Durand, A., Basfeld, A., et al. (2017). Structure of Full-Length SMC and Rearrangements Required for Chromosome Organization. Mol. Cell *67*, 334–347.e5.

Emsley, P., and Cowtan, K. (2004). Coot: model-building tools for molecular graphics. Acta Crystallogr. D Biol. Crystallogr. *60*, 2126–2132.

Eykelenboom, J.K., Blackwood, J.K., Okely, E., and Leach, D.R. (2008). SbcCD causes a double-strand break at a DNA palindrome in the Escherichia coli chromosome. Mol. Cell *29*, 644–651.

Falck, J., Coates, J., and Jackson, S.P. (2005). Conserved modes of recruitment of ATM, ATR and DNA-PKcs to sites of DNA damage. Nature *434*, 605–611.

Garcia, V., Phelps, S.E.L., Gray, S., and Neale, M.J. (2011). Bidirectional resection of DNA double-strand breaks by Mre11 and Exo1. Nature *479*, 241–244.

Goddard, T.D., Huang, C.C., Meng, E.C., Pettersen, E.F., Couch, G.S., Morris, J.H., and Ferrin, T.E. (2018). UCSF ChimeraX: Meeting modern challenges in visualization and analysis. Protein Sci. *27*, 14–25.

Herdendorf, T.J., Albrecht, D.W., Benkovic, S.J., and Nelson, S.W. (2011). Biochemical characterization of bacteriophage T4 Mre11-Rad50 complex. J. Biol. Chem. *286*, 2382–2392.

Hoa, N.N., Shimizu, T., Zhou, Z.W., Wang, Z.Q., Deshpande, R.A., Paull, T.T., Akter, S., Tsuda, M., Furuta, R., Tsutsui, K., et al. (2016). Mre11 Is Essential for the Removal of Lethal Topoisomerase 2 Covalent Cleavage Complexes. Mol. Cell *64*, 1010.

Hohl, M., Kwon, Y., Galván, S.M., Xue, X., Tous, C., Aguilera, A., Sung, P., and Petrini, J.H. (2011). The Rad50 coiled-coil domain is indispensable for Mre11 complex functions. Nat. Struct. Mol. Biol. *18*, 1124–1131.

Hohl, M., Kochańczyk, T., Tous, C., Aguilera, A., Krężel, A., and Petrini, J.H. (2015). Interdependence of the rad50 hook and globular domain functions. Mol. Cell *57*, 479–491.

Hopfner, K.P., Karcher, A., Shin, D.S., Craig, L., Arthur, L.M., Carney, J.P., and Tainer, J.A. (2000). Structural biology of Rad50 ATPase: ATP-driven conformational control in DNA double-strand break repair and the ABC-ATPase superfamily. Cell *101*, 789–800.

Hopfner, K.P., Karcher, A., Craig, L., Woo, T.T., Carney, J.P., and Tainer, J.A. (2001). Structural biochemistry and interaction architecture of the DNA double-strand break repair Mre11 nuclease and Rad50-ATPase. Cell *105*, 473–485.

Hopfner, K.-P., Craig, L., Moncalian, G., Zinkel, R.A., Usui, T., Owen, B.A.L., Karcher, A., Henderson, B., Bodmer, J.-L., McMurray, C.T., et al. (2002). The Rad50 zinc-hook is a structure joining Mre11 complexes in DNA recombination and repair. Nature *418*, 562–566.

Hustedt, N., and Durocher, D. (2016). The control of DNA repair by the cell cycle. Nat. Cell Biol. *19*, 1–9.

Jermutus, L., Honegger, A., Schwesinger, F., Hanes, J., and Plückthun, A. (2001). Tailoring in vitro evolution for protein affinity or stability. Proc. Natl. Acad. Sci. USA *98*, 75–80.

Kowalczykowski, S.C. (2015). An Overview of the Molecular Mechanisms of Recombinational DNA Repair. Cold Spring Harb. Perspect. Biol. *7*, a016410.

Lammens, K., Bemeleit, D.J., Möckel, C., Clausing, E., Schele, A., Hartung, S., Schiller, C.B., Lucas, M., Angermüller, C., Söding, J., et al. (2011). The Mre11:Rad50 structure shows an ATP-dependent molecular clamp in DNA double-strand break repair. Cell *145*, 54–66.

Lim, H.S., Kim, J.S., Park, Y.B., Gwon, G.H., and Cho, Y. (2011). Crystal structure of the Mre11-Rad50-ATPγS complex: understanding the interplay between Mre11 and Rad50. Genes Dev. *25*, 1091–1104.

Lim, C.T., Lai, P.J., Leach, D.R., Maki, H., and Furukohri, A. (2015). A novel mode of nuclease action is revealed by the bacterial Mre11/Rad50 complex. Nucleic Acids Res. *43*, 9804–9816.

Liu, Y., Sung, S., Kim, Y., Li, F., Gwon, G., Jo, A., Kim, A.K., Kim, T., Song, O.K., Lee, S.E., and Cho, Y. (2016). ATP-dependent DNA binding, unwinding, and resection by the Mre11/Rad50 complex. EMBO J. *35*, 743–758.

Ludwiczak, J., Winski, A., Szczepaniak, K., Alva, V., and Dunin-Horkawicz, S. (2019). DeepCoil - a fast and accurate prediction of coiled-coil domains in protein sequences. Bioinformatics. Published online January 2, 2019. https://doi.org/10.1093/bioinformatics/bty1062.

Mastronarde, D.N. (2005). Automated electron microscope tomography using robust prediction of specimen movements. J. Struct. Biol. *152*, 36–51.

Mimitou, E.P., and Symington, L.S. (2008). Sae2, Exo1 and Sgs1 collaborate in DNA double-strand break processing. Nature *455*, 770–774.

Möckel, C., Lammens, K., Schele, A., and Hopfner, K.P. (2012). ATP driven structural changes of the bacterial Mre11:Rad50 catalytic head complex. Nucleic Acids Res. *40*, 914–927.

Moreno-Herrero, F., de Jager, M., Dekker, N.H., Kanaar, R., Wyman, C., and Dekker, C. (2005). Mesoscale conformational changes in the DNA-repair complex Rad50/Mre11/Nbs1 upon binding DNA. Nature *437*, 440–443.

Myler, L.R., Gallardo, I.F., Soniat, M.M., Deshpande, R.A., Gonzalez, X.B., Kim, Y., Paull, T.T., and Finkelstein, I.J. (2017). Single-Molecule Imaging Reveals How Mre11-Rad50-Nbs1 Initiates DNA Break Repair. Mol. Cell *67*, 891–898.e4.

Myung, K., Chen, C., and Kolodner, R.D. (2001). Multiple pathways cooperate in the suppression of genome instability in Saccharomyces cerevisiae. Nature *411*, 1073–1076.

Neale, M.J., Pan, J., and Keeney, S. (2005). Endonucleolytic processing of covalent protein-linked DNA double-strand breaks. Nature *436*, 1053–1057.

Oh, J., Al-Zain, A., Cannavo, E., Cejka, P., and Symington, L.S. (2016). Xrs2 Dependent and Independent Functions of the Mre11-Rad50 Complex. Mol. Cell *64*, 405–415.

Park, Y.B., Hohl, M., Padjasek, M., Jeong, E., Jin, K.S., Krężel, A., Petrini, J.H., and Cho, Y. (2017). Eukaryotic Rad50 functions as a rod-shaped dimer. Nat. Struct. Mol. Biol. *24*, 248–257.

Paull, T.T. (2018). 20 Years of Mre11 Biology: No End in Sight. Mol. Cell *71*, 419–427.

Paull, T.T., and Gellert, M. (1998). The 3′ to 5′ exonuclease activity of Mre 11 facilitates repair of DNA double-strand breaks. Mol. Cell *1*, 969–979.

Paull, T.T., and Gellert, M. (1999). Nbs1 potentiates ATP-driven DNA unwinding and endonuclease cleavage by the Mre11/Rad50 complex. Genes Dev. *13*, 1276–1288.

Pedrazzi, G., Schwesinger, F., Honegger, A., Krebber, C., and Plückthun, A. (1997). Affinity and folding properties both influence the selection of antibodies with the selectively infective phage (SIP) methodology. FEBS Lett. *415*, 289–293.

Pettersen, E.F., Goddard, T.D., Huang, C.C., Couch, G.S., Greenblatt, D.M., Meng, E.C., and Ferrin, T.E. (2004). UCSF Chimera–a visualization system for exploratory research and analysis. J. Comput. Chem. *25*, 1605–1612.

Punjani, A., Rubinstein, J.L., Fleet, D.J., and Brubaker, M.A. (2017). cryoSPARC: algorithms for rapid unsupervised cryo-EM structure determination. Nat. Methods *14*, 290–296.

Rahal, E.A., Henricksen, L.A., Li, Y., Williams, R.S., Tainer, J.A., and Dixon, K. (2010). ATM regulates Mre11-dependent DNA end-degradation and microhomology-mediated end joining. Cell Cycle *9*, 2866–2877.

Reginato, G., Cannavo, E., and Cejka, P. (2017). Physiological protein blocks direct the Mre11-Rad50-Xrs2 and Sae2 nuclease complex to initiate DNA end resection. Genes Dev. *31*, 2325–2330.

Rohou, A., and Grigorieff, N. (2015). CTFFIND4: Fast and accurate defocus estimation from electron micrographs. J. Struct. Biol. *192*, 216–221.

Saathoff, J.H., Käshammer, L., Lammens, K., Byrne, R.T., and Hopfner, K.P. (2018). The bacterial Mre11-Rad50 homolog SbcCD cleaves opposing strands of DNA by two chemically distinct nuclease reactions. Nucleic Acids Res. *46*, 11303–11314.

Sartori, A.A., Lukas, C., Coates, J., Mistrik, M., Fu, S., Bartek, J., Baer, R., Lukas, J., and Jackson, S.P. (2007). Human CtIP promotes DNA end resection. Nature *450*, 509–514.

Scheres, S.H. (2012). RELION: implementation of a Bayesian approach to cryo-EM structure determination. J. Struct. Biol. *180*, 519–530.

Seeber, A., Hegnauer, A.M., Hustedt, N., Deshpande, I., Poli, J., Eglinger, J., Pasero, P., Gut, H., Shinohara, M., Hopfner, K.P., et al. (2016). RPA Mediates Recruitment of MRX to Forks and Double-Strand Breaks to Hold Sister Chromatids Together. Mol. Cell *64*, 951–966.

Seifert, F.U., Lammens, K., Stoehr, G., Kessler, B., and Hopfner, K.P. (2016). Structural mechanism of ATP-dependent DNA binding and DNA end bridging by eukaryotic Rad50. EMBO J. *35*, 759–772.

Sung, S., Li, F., Park, Y.B., Kim, J.S., Kim, A.K., Song, O.K., Kim, J., Che, J., Lee, S.E., and Cho, Y. (2014). DNA end recognition by the Mre11 nuclease dimer: insights into resection and repair of damaged DNA. EMBO J. *33*, 2422–2435.

Syed, A., and Tainer, J.A. (2018). The MRE11-RAD50-NBS1 Complex Conducts the Orchestration of Damage Signaling and Outcomes to Stress in DNA Replication and Repair. Annu. Rev. Biochem. *87*, 263–294.

Tang, G., Peng, L., Baldwin, P.R., Mann, D.S., Jiang, W., Rees, I., and Ludtke, S.J. (2007). EMAN2: an extensible image processing suite for electron microscopy. J. Struct. Biol. *157*, 38–46.

Uhlmann, F. (2016). SMC complexes: from DNA to chromosomes. Nat. Rev. Mol. Cell Biol. *17*, 399–412.

van Dijk, M., and Bonvin, A.M. (2009). 3D-DART: a DNA structure modelling server. Nucleic Acids Res. *37*, W235-9.

Vazquez Nunez, R., Ruiz Avila, L.B., and Gruber, S. (2019). Transient DNA Occupancy of the SMC Interarm Space in Prokaryotic Condensin. Mol. Cell *75*, 209–223.e6.

Wang, W., Daley, J.M., Kwon, Y., Krasner, D.S., and Sung, P. (2017). Plasticity of the Mre11-Rad50-Xrs2-Sae2 nuclease ensemble in the processing of DNA-bound obstacles. Genes Dev. *31*, 2331–2336.

Wendel, B.M., Cole, J.M., Courcelle, C.T., and Courcelle, J. (2018). SbcC-SbcD and ExoI process convergent forks to complete chromosome replication. Proc. Natl. Acad. Sci. USA *115*, 349–354.

Williams, R.S., Moncalian, G., Williams, J.S., Yamada, Y., Limbo, O., Shin, D.S., Groocock, L.M., Cahill, D., Hitomi, C., Guenther, G., et al. (2008). Mre11 dimers coordinate DNA end bridging and nuclease processing in double-strand-break repair. Cell *135*, 97–109.

Williams, G.J., Williams, R.S., Williams, J.S., Moncalian, G., Arvai, A.S., Limbo, O., Guenther, G., SilDas, S., Hammel, M., Russell, P., and Tainer, J.A. (2011). ABC ATPase signature helices in Rad50 link nucleotide state to Mre11 interface for DNA repair. Nat. Struct. Mol. Biol. *18*, 423–431.

Wright, W.D., Shah, S.S., and Heyer, W.D. (2018). Homologous recombination and the repair of DNA double-strand breaks. J. Biol. Chem. *293*, 10524–10535.

Zheng, S.Q., Palovcak, E., Armache, J.P., Verba, K.A., Cheng, Y., and Agard, D.A. (2017). MotionCor2: anisotropic correction of beam-induced motion for improved cryo-electron microscopy. Nat. Methods *14*, 331–332.

Zimmermann, L., Stephens, A., Nam, S.Z., Rau, D., Kübler, J., Lozajic, M., Gabler, F., Söding, J., Lupas, A.N., and Alva, V. (2018). A Completely Reimplemented MPI Bioinformatics Toolkit with a New HHpred Server at its Core. J. Mol. Biol. *430*, 2237–2243.

STAR★METHODS

KEY RESOURCES TABLE

REAGENT or RESOURCE	SOURCE	IDENTIFIER
Chemicals, Peptides, and Recombinant Proteins		
ATP	Sigma	A3377
ATPγS	Sigma	A1388
ADP	Sigma	A0752
2-Mercaptoethanol	Carl Roth	4227
DTT	Carl Roth	6908
Imidazole	Carl Roth	3899
b-Octylglycoside	Sigma	O8001
BSA	New England bioLabs	B9000S
FAM-scFv	Prof. Dr. Plückthun, University of Zürich Pedrazzi et al., 1997; Jermutus et al., 2001	N/A
Bradford Roti_Quant	Carl Roth	K015
Urea	Carl Roth	3941
EDTA	VWR International	6381-92-6
Ficoll 400	Carl Roth	CN90.3
Rotiphorese DNA sequencing system	Carl Roth	A431.1
MgCl2	Merck	7791-18-6
$MnCl_2$	Sigma	M3634
Streptavidin	IBA	2-0203-100
Pyruvat kinase/Lactatic dehydrogenase from rabbit muscle	Sigma	P0294
Phosphoenol Pyruvate	ITW Reagents	A2271
NADH	Carl Roth	AE12
TCEP	Sigma	646547
SIGMAFAST Protease Inhibitor Cocktail Tablet, EDTA free	Merck	S8830
GeneRuler 1 kb DNA Ladder	Thermo Fisher Scientific	SM0311
Deposited Data		
*Ec*MR coordinates (resting state)	This Paper	PDB: 6S6V
*Ec*MR head EM map (resting state)	This Paper	EMDB: EMD-10107
*Ec*MR coordinates (cutting state)	This Paper	PDB: 6S85
*Ec*MR head EM map (cutting state)	This Paper	EMDB: EMD-10116
*Ec*MR head with longer coiled coils EM map	This Paper	EMDB: EMD-10114
*Ec*MR head with long coiled coils, low resolution EM map	This Paper	EMDB: EMD-10115
Full Gel Images	This Paper	https://doi.org/10.17632/g5ypj2dyj2.1
Experimental Models: Cell Lines		
E. coli Rosetta	Expression Systems	N/A
E. coli BL21	Expression Systems	N/A
E. coli XL1 Blue	Expression Systems	N/A
Spodoptera frugiperda sf21 cells	Expression Systems	N/A
Trichoplusia ni cells	Expression Systems	N/A

(*Continued on next page*)

Continued

REAGENT or RESOURCE	SOURCE	IDENTIFIER
Oligonucleotides		
Oligonucleotides	Metabion	N/A, See Table S1
Recombinant DNA		
pET21b-*Ec*Mre11	Saathoff et al., 2018	N/A
pET29-*Ec*Rad50	Saathoff et al., 2018	N/A
pACEBac1-pIDK-*Ct*Ku70/80	This Paper	N/A
pBR322	Fermentas	SD0041
Software and Algorithms		
SerialEM	Mastronarde, 2005	http://bio3d.colorado.edu/SerialEM/
MotionCor2	Zheng et al., 2017	https://msg.ucsf.edu/em/software/motioncor2.html
CTFFind4.1	Rohou and Grigorieff, 2015	http://grigoriefflab.janelia.org/ctffind4
Relion 2.1b1	Scheres, 2012	https://www3.mrc-lmb.cam.ac.uk/relion/index.php?title=Main_Page
Phenix	Afonine et al., 2018	https://www.phenix-online.org/
UCSF Chimera	Pettersen et al., 2004	https://www.cgl.ucsf.edu/chimera/
Pymol	Schrödinger	https://pymol.org/2/
Chimera X	Goddard et al., 2018	https://www.rbvi.ucsf.edu/chimerax/
COOT	Emsley and Cowtan, 2004	https://www2.mrc-lmb.cam.ac.uk/Personal/pemsley/coot/
Prism	GraphPad	N/A
EMAN2	Tang et al., 2007	http://blake.bcm.tmc.edu/EMAN2/
CryoSPARC	Punjani et al., 2017	https://cryosparc.com/
SWISS-MODEL server	Biasini et al., 2014	https://swissmodel.expasy.org/
3D-DART	van Dijk and Bonvin, 2009	http://haddock.chem.uu.nl/dna/dna.php
Gautomatch	Dr. Jack Zhang	https://www.mrc-lmb.cam.ac.uk/kzhang/

LEAD CONTACT AND MATERIALS AVAILABILITY

Further information and requests for resources and reagents should be directed to and will be fulfilled by the Lead Contact Karl-Peter Hopfner (hopfner@genzentrum.lmu.de).

EXPERIMENTAL MODEL AND SUBJECT DETAILS

Organisms as source for materials used in experiments

E. coli XL1 Blue cells were used for amplification of plasmid DNA.

E. coli BL21 (DE3) and *E.coli* Rosetta2 were used for recombinant protein expression.

Spodoptera frugiperda sf21 insect cells were used for virus production.

Trichoplusia ni insect cells were used for recombinant protein expression.

METHOD DETAILS

Expression and purification of EcMR

*Ec*Mre11^{fl} (cloned in pET21b, 6xHis-tag) and *Ec*Rad50^{fl} (cloned in pET29) were co-transfected into *E. coli* BL21 or Rosetta cells (Novagen). *E. coli* cultures were grown in LB medium at 37°C to an OD_{600} of 0.6. Protein expression was induced with 0.5 mM IPTG and carried out for 16 h at 18°C. The cells were harvested by centrifugation and the pellet was resuspended in lysis buffer (25 mM Tris pH 7.5, 150 mM NaCl, 10 mM Imidazole and 5 mM β-Mercaptoethanol) before cell disruption by sonication. The cell lysate was cleared by centrifugation and the supernatant was applied onto 2.5 mL of pre-equilibrated Ni-NTA (QIAGEN). The beads were washed with 20 mL lysis buffer and 25 mL wash buffer (25 mM Tris pH 7.5, 125 mM NaCl, 20 mM Imidazole and 5 mM β-Mercaptoethanol). The protein was eluted with 10 mL elution buffer (25 mM Tris pH 7.5, 100 mM NaCl, 200 mM Imidazole and 5 mM

β-Mercaptoethanol). The eluate was applied onto a 1 mL HiTrapQ column (GE) and eluted by a step gradient with increasing salt (Buffer A: 100 mM NaCl, 25 mM Tris pH 7.5, Buffer B: 1 M NaCl, 25 mM Tris pH 7.5). The peak fractions were pooled, concentrated and purified via size-exclusion chromatography using a Superose 6 10/300 (GE Healthcare) column in size-exclusion buffer (125 mM NaCl, 20 mM Tris pH 7.5, 10% Glycerol). The protein fractions of interest were pooled, concentrated, flash frozen and stored at −80°C until further use.

Expression and Purification of *Ct*Ku70/80

Codon-optimized synthetic DNA (Genscript, Piscataway, USA) encoding *ct*Ku70 (N-terminal human rhinovirus 3C-protease cleavable 6xHis-tag) and *ct*Ku80 was PCR amplified and cloned into pACEBac1 and pIDC respectively and expressed using the MultiBac technology (Bieniossek et al., 2008). Recombination steps were carried out in *Escherichia coli* XL1Blue cells (Stratagene) under addition of Cre recombinase (NEB). Baculoviruses were generated in *Spodoptera frugiperda* (SF21) insect cells (IPLB-Sf21AE). *Trichoplusia ni* High Five cells (Invitrogen) were co-infected with 1:5000 of baculovirus. Cells were cultured for 72 h at 27°C and harvested by centrifugation.

For purification, cells from 250 mL cells were disrupted in lysis buffer (50 mM HEPES pH 7.5, 1 M NaCl, 400 mM NH_4OAc, 5% glycerol, 0.5 mM TCEP supplemented with a SIGMAFAST Protease Inhibitor Cocktail Tablet, EDTA free (Merck)) and gently sonified. Raw lysate was incubated for 1 h at 50°C and subsequently cleared by centrifugation at 34500 g and 4°C for 30 min. The supernatant was applied onto 2 mL of pre-equilibrated Ni-NTA (QIAGEN). The beads were washed with 20 mL wash buffer (50 mM HEPES pH 7.5, 250 mM NaCl, 10 mM Imidazole and 0.5 mM TCEP). The protein was eluted with 10 mL elution buffer (50 mM HEPES pH 7.5, 250 mM NaCl, 500 mM Imidazole and 0.5 mM TCEP). The affinity tag was cleaved by overnight incubation with human rhinovirus 3C-protease at 4 °C during dialysis into low salt buffer (50 mM HEPES pH 7.5, 150 mM NaCl and 0.5 mM TCEP). The filtered protein was loaded onto a 5 mL HiTrap Heparin HP column (GE Healthcare), equilibrated in the dialysis buffer and eluted with an increasing salt gradient. The peak fractions were pooled, concentrated and purified via size-exclusion chromatography using a Superose 6 16/60 (GE Healthcare) column in size-exclusion buffer (20 mM HEPES pH 7.5, 200 mM NaCl and 0.5 mM TCEP). The protein fractions of interest were identified by SDS-PAGE, pooled, concentrated, flash-frozen in liquid N_2 and stored at −80 °C until required.

Nuclease assays

The nuclease reaction was carried out in assay buffer (25 mM Tris pH 7.5, 50 mM KCl, 5 mM $MgCl_2$, 1 mM $MnCl_2$, 0.1 mg/ml BSA, 1 mM DTT, 1 mM ATP) with 250 nM *Ec*MR and 50 nM 6-FAM labeled 60 bp dsDNA substrate. Where indicated, reactions were supplemented with a 15-fold excess of a single-chain variable fragment against fluorescein (FAM-scFv) to generate a blocked DNA end (Pedrazzi et al., 1997). Prior to each nuclease reaction, the precise *Ec*MR-concentration was determined according to Bradford using the Roti-Quant solution (Roth). The reaction was started by protein addition and incubated at 37°C for 5 min for a blocked dsDNA end and for 15 min for an unblocked dsDNA. 10 μL of each reaction was terminated by mixing equal volume of loading buffer (8 M Urea, 20 mM EDTA, 6% Ficoll 400). The reaction products were resolved on 12% denaturing polyacrylamide gels (Rotiphorese® DNA sequencing system) in 1x TBE buffer. Gels were run at 90 min at a constant power of 32 W and scanned by a Typhoon fluorescence imager (GE healthcare). FAM-labeled substrates were imaged with a 473 nm Laser and 510 nm filter. The images were analyzed and integrated with the ImageJ software.

ATPase assays

We applied an NADH-coupled assay to monitor the ATP-hydrolysis rate of *Ec*Mre11-Rad50. *Ec*MR (250 nM) was incubated at 37°C in assay buffer (25 mM Tris pH 7.5, 50 mM KCl, 5 mM $MgCl_2$, 1 mM $MnCl_2$, 1 mM ATP, 0.1 mg/ml BSA, 1 mM DTT) in the presence of NADH (0.35 mM), pyruvate kinase/lactate dehydrogenase (20 U/ml PK, 30 U/ml LDH, Sigma) and Phosphoenol Pyruvate (2 mM). To stimulate *Ec*MR's ATPase activity, a 60 bp DNA (1000 nM) was added. The rate of NADH oxidation was monitored fluorometrically by measuring the absorbance at 340 nm on an Infinite M1000 microplate reader (Tecan) over a period of 20 minutes. ATP turnover was calculated using the steady-state rate and corrected for a buffer blank. All ATP rates were measured with the nuclease dead $Mre11^{H84Q}$ mutant to avoid DNA degradation.

DNA binding assays

Fluorescence polarization anisotropy was used to monitor the interaction between *Ec*MR and 35 bp DNA. 2.5 nM of 5′ Fluorescein-labeled DNA was incubated with increasing concentrations of *Ec*MR in assay buffer (25 mM Tris pH 7.5, 50 mM KCl, 1 mM ATP, 5 mM $MgCl_2$, 1 mM $MnCl_2$, 1 mM DTT). After 20 minutes at 25°C, the fluorescence anisotropy was measured at an excitation wavelength of 470 nM and emission wavelength of 520 nM. All DNA binding measurements were measured with the nuclease dead $Mre11^{H84Q}$ mutant to avoid DNA degradation. Data were analyzed with Prism (GraphPad) and K_D values determined by fitting the anisotropy data to a bimolecular equilibrium model:

$$Y = Af - (Af - Ab)\frac{x}{Kd - x}$$

CellPress

Competitive DNA binding assay

For the competition assays, fluorescence polarization anisotropy was used to monitor the interaction between *Ec*MR and long DNA substrates. 2.5 nM of 35 bp 5′ Fluorescein-labeled DNA was incubated with 50 nM *Ec*M^{H84Q}R for 20 minutes at 25°C in assay buffer (25 mM Tris pH 7.5, 50 mM KCl, 1 mM ATP, 5 mM MgCl2, 1 mM MnCl2, 1 mM DTT). For the competition reaction, increasing concentrations of plasmid DNA (pBR322) or 5′ biotinylated 1500 bp were added and incubated for 20 minutes at 25°C. The fluorescence anisotropy was measured at an excitation wavelength of 470 nM and emission wavelength of 520 nM. The anisotropy data were fit with Prism (GraphPad).

Blocked dsDNA degradation assay

To test for degradation of linear and circular DNA with a protein block, a 1500 basepair fragment was amplified by PCR using pET21b vector as template and 5′ biotinylated primers (for: ccgcgcacatttccccgaaaagtgcc, rev: ccagttgatcggcgcgagatttaatcg). DNA ends were blocked in assay buffer (25 mM Tris pH 7.5, 50 mM KCl, 1mM ATP, 5 mM $MgCl_2$, 1 mM $MnCl_2$, 0.1 mg/ml BSA, 1 mM DTT) with 52 nM DNA and 5 μM streptavidin at 20°C. The nuclease reaction was started by adding 50 nM of *Ec*MR and incubated at 37°C. Quenching of the reaction was done after 0, 2.5, 5, 10, 30 and 60 minutes by adding 1.5 μl 200 mM EDTA per 6 μl reaction mix. For agarose gel electrophoresis 6 μl reaction mix were diluted with 14 μl 1.6x loading dye and 8 μl of each sample were then separated by horizontal agarose gel electrophoresis. The DNA and degradation products were separated by horizontal agarose gel electrophoresis and imaged with a Typhoon fluorescence imager (GE healthcare) using 473 nm Laser and 510 nm filter. Degradation products and educts were quantified using ImageJ.

Circularization Assay

Circularization of 5′ biotinylated 1500 bp dsDNA was carried out in assay buffer (25 mM Tris pH 7.5, 50 mM KCl, 1mM ATP, 5 mM $MgCl_2$, 1 mM $MnCl_2$, 0.1 mg/ml BSA, 1 mM DTT) with 20 nM DNA and 10 nM streptavidin at 20°C. The nuclease reaction was started by adding 200 nM of *Ec*MR and incubated 10 minutes at 37°C. The DNA and degradation products were separated by horizontal agarose gel electrophoresis and imaged with a Typhoon fluorescence imager (GE healthcare) using 473 nm Laser and 510 nm filter.

Size Exclusion Analysis

For the size exclusion analysis of *Ec*MR without ATP and DNA, 20 μl of *Ec*MR were mixed with 30 μl SEC buffer I (50 mM KCl, 20 mM Tris pH 7.5). For *Ec*MR in complex with ATP, 20 μl *Ec*MR were mixed with 5 μl 10x buffer (10 mM ATP, 10 mM $MnCl_2$, 50 mM $MgCl_2$) and 25 μl SEC buffer I. For *Ec*MR in complex with ATP and DNA, 20 μl of *Ec*MR were mixed with 5 μl 10x buffer and 25 μl DNA (18 μM, 60 bp). All three samples were incubated at room temperature for 30 min and centrifuged with a table top centrifuge at full speed for 10 min. 50 μl of the mixture were injected onto a S6 5/150 column. For the sample without ATP and DNA SEC buffer I was used. For the samples with ATP and ATP and DNA SEC buffer II was used (50 mM KCl, 20 mM Tris pH 7.5, 5 mM $MgCl_2$, 1 mM $MnCl_2$, 1 mM ATP).

Cryo electron microscopy grid preparation

For the resting state *Ec*MR:ATPγS complex, full length *Ec*MR was purified as described previously with the exception that for the buffers 2 mM DTT instead of 5 mM β-mercaptoethanol were used. After the ion exchange chromatography, the protein was pooled, aliquoted and snap-frozen in liquid nitrogen. Prior to grid preparation the *Ec*MR was thawed and purified via size exclusion chromatography using a S6 5/150 column (buffer: 50 mM KCl, 20 mM HEPES, pH 7.5). The peak fraction was diluted to a final concentration of 0.4 mg/ml and mixed with 10x buffer (10 mM $MnCl_2$, 25 mM $MgCl_2$ and 10 mM ATPγS). Right before grid preparation 5 μL β-octyl glucoside were added to a final concentration of 0.05%. 4.5 μL of the protein solution were applied to Quantifoil R2/1 holey carbon grids and frozen in liquid ethane using a Leica EM GP (Leica, 15°C and 95% humidity).

For the cutting state *Ec*MR:DNA complex, 10x Buffer (10 mM $MnCl_2$, 25 mM $MgCl_2$ and 10 mM ATP) were mixed with 60 bp dsDNA (fwd: 5′-CGCTTTATCAGAAGCCAGACATTAACGCTTC TGGAGAAACTCAACGAGCTGGACGCGGAT-3′) and the peak fraction of *Ec*M^{H84S}R was added. Two datasets were collected on the *Ec*MR:DNA complex with a protein:DNA ratio of 1:5 (dataset I) and 1:3 (dataset II) and protein concentrations of 0.3 mg/ml and 0.5 mg/ml, respectively. For incubation the complex was left on ice for at least 30 min and the protein solution was applied to Quantifoil R2/1 holey carbon grids and frozen in liquid ethane using a Vitrobot IV (FEI, 4°C and 95% humidity).

Cryo electron microscopy data collection

Data was collected with a FEI Titan Krios transmission electron microscope (300 kV) using a Gatan K2 detector and a Gatan GIF Quantum energy filter (slit width 20 eV). SerialEM was used for data acquisition using customized scripts from Mike Strauss (Mastronarde, 2005). For the resting state *Ec*MR:ATPγS complex 8186 micrographs were collected with a pixel size of 1.06 Å and a total electron dose of 68 $e^-/Å^2$. A defocus from −1.0 to −3.5 μM was used and 50 frames were collected in 10 s (0.2 s/frame).

For the cutting state *Ec*M^{H84S}R:DNA complex two datasets were collected with 9336 (dataset I) and 3475 (dataset II) micrographs. Both datasets were collected with a pixel size of 0.82 Å and a total electron dose of 73.6 $e^-/Å^2$ dataset I and II. A defocus from −1.0 to −3.5 μm was used and 25 frames were collected in 5 s (0.2 s/frame).

Data processing and 3D reconstruction

Motioncor2 (Zheng et al., 2017) was used to align the micrographs. Subsequently, the aligned micrographs were used for determining the correlation transfer function with CTFFind 4.1 (Rohou and Grigorieff, 2015). Respectively, 6895 micrographs were selected for the resting state reconstruction. Unless stated otherwise all processing steps were performed with RELION 2.1b1 (Scheres, 2012). The gold standard Fourier shell correlation 0.143 criterion was used to determine the resolutions of the reconstructions. RELION was used for automatic B-factor determination. The exact processing schemes including particle numbers are illustrated in Figure S1 and S3. For the resting state reconstruction, initial manual picking was performed with EMAN2 (Tang et al., 2007) and 1607 particles were picked manually. From the picked particles, 2D classes were calculated using RELION2.1b1. The four best classes were low pass filtered to 20 Å and used for autopicking on a subset of 2935 micrographs (subset I). From these micrographs, 998 166 particles were picked and subjected to 2D classification and classes with clearly defined features were selected. A subset of these particles was used to calculate an initial 3D model using CryoSPARC (Punjani et al., 2017). An initial 3D classification with six classes and C1 symmetry resulted in a reconstruction that was further used as reference. In parallel 2D classes calculated from subset I and low pass filtered to 20 Å were used for autopicking on all 6895 micrographs and in total 2 809 916 particles were picked. After 2D classification 1 187 179 particles were subjected to 3D classification (C2 symmetry) and from these four classes, the best two classes were selected for further processing. Further sorting and 2D classification, yielded a dataset with 472836 particles. 3D Classification into two classes resulted in two reconstructions, one with well-defined *Ec*Mre11 HLH motif and beginning of the *Ec*Rad50 coiled-coils (30%) and one where this part is less well defined (70%). The map with a well defined HLH motif contained 142229 particles and was used for further refinement. The final resolution of this reconstruction after solvent mask post-processing was 3.5 Å.

For the cutting state reconstruction, 7762 micrographs were selected from the initial recorded 9336 micrographs based on manual inspection of the CTF. Gautomatch (developed by K. Zhang, MRC Laboratory of Molecular Biology, Cambridge, UK, https://www.mrc-lmb.cam.ac.uk/kzhang/Gautomatch) was used for initial particle picking. The four best classes with 54 556 particles were low-pass filtered to 20 Å in RELION and used for autopicking in RELION. After several rounds of autopicking and 2D classification 149 098 particles were used to reconstruct an initial model in CryoSPARC. In the initial 3D classification 489 112 particles were classified into four classes using C1 symmetry and one class with 100 194 particles was selected. Further classification yielded a final subset of 58 385 particles. Using the 2D classes generated from dataset I, 696 512 particles were picked in dataset II with RELION from 3178 micrographs (initial 3475). After 2D classification the selected 342 737 particles were subjected to 3D classification with the initial model from a refinement run from dataset I. After particle polishing and movie processing the particles were joined together and solvent masked post-processing resulted in a 4.2 Å reconstruction. After application of a larger mask covering a longer segment of the coiled-coils, the same particles gave a lower overall resolution reconstruction, where the course of the coiled coils could be traced to nine helical turns away from the head complex. To calculate the low resolution (~15 Å) reconstruction with longer coiled-coils, particles from dataset I were subjected to 3D classification and the one class with elongated coiled-coils (24 055 particles) was selected. The box size of these particles was increased to 800 pixel and the particles were further classified with 2D and 3D classification yielding in a reconstruction with 18833 particles.

Model building

UCSF Chimera (Pettersen et al., 2004) was used to dock the existing crystal structure of the *Ec*Mre11 nuclease and capping domain (PDB: 4M0V) into the electron density. For *Ec*Rad50 an initial model calculated from the *Thermotoga maritima* structure (PDB: 3QF7) with the SWISS-MODEL server. The resolution during refinement was restricted to 3.5 Å. The helix-loop-helix (HLH) motif was built from poly-alanine helices generated in COOT (Emsley and Cowtan, 2004) and the linker between the two helices and the linker between capping domain and HLH motif were built manually.

For the cutting state reconstruction, UCSF Chimera was used to dock the crystal structure of the *Ec*Mre11 nuclease and capping domain (PDB: 4M0V) into the electron density. The *Ec*Rad50 model from the resting state cryo-EM structure was used to build *Ec*Rad50 in the processing state structure. Similarly, the HLH motif was fitted into the processing state structure. The linker was built manually into the density of the Mre11 (A) monomer. For the Mre11 (B) monomer the resolution was too low to allow building of the linker. COOT was used for model building alternating with real space refinement in PHENIX 1.14 (Afonine et al., 2018) using the *Ec*Mre11 crystal structure (4m0v) as reference model. Since the directionality and registry of DNA binding could not be determined from the structure dsDNA we used an arbitrary registry from the DNA model generated using the webserver 3D-DART (van Dijk and Bonvin, 2009) on the basis of our experimental sequence. This website was also used to bend the DNA using parameters for bend angle (30), bend zone (9-20) and origin (8). COOT was used to refine the DNA using libg restraints alternating with real-space refinement in PHENIX where base pairs as well as base stacking pairs were defined for refinement.

QUANTIFICATION AND STATISTICAL ANALYSIS

ImageJ was used for quantification of nuclease and plasmid assay products and educts. GraphPad Prism was used for plotting the resulting quantification values (in Figures 2C, 5G, and S6G). Error bars are given as standard deviation of the mean.

GraphPad Prism was used for plotting triplicates of the DNA binding assay (in Figures 4D, 5C, 5D, S4C, S4F, and S5G). Error bars are given as standard deviation of the mean.

GraphPad Prism was used for plotting triplicates of the ATPase assay (Figures 4C and S4E). The calculated mean is indicated by a black line.

DATA AND CODE AVAILABILITY

The coordinate files generated during this study are available at the protein data bank (https://www.rcsb.org/) with the accession codes PDB: 6S6V (resting state) and PDB: 6S85 (cutting state).

The calculated reconstructions generated during this study are available at the Electron Microscopy Data Bank (https://www.ebi.ac.uk/pdbe/emdb/) with the accession codes EMDB: EMD-10107 (resting state), EMDB: EMD-10116 (cutting state head complex at 4.2A), EMDB: EMD-10114 (cutting state head complex at 4.3A) and EMDB: EMD-10115 (cutting state head complex at 15A with long coiled coils). Full gel images are deposited under the following https://doi.org/10.17632/g5ypj2dyj2.1

Molecular Cell, Volume *76*

Supplemental Information

Mechanism of DNA End Sensing and Processing by the Mre11-Rad50 Complex

Lisa Käshammer, Jan-Hinnerk Saathoff, Katja Lammens, Fabian Gut, Joseph Bartho, Aaron Alt, Brigitte Kessler, and Karl-Peter Hopfner

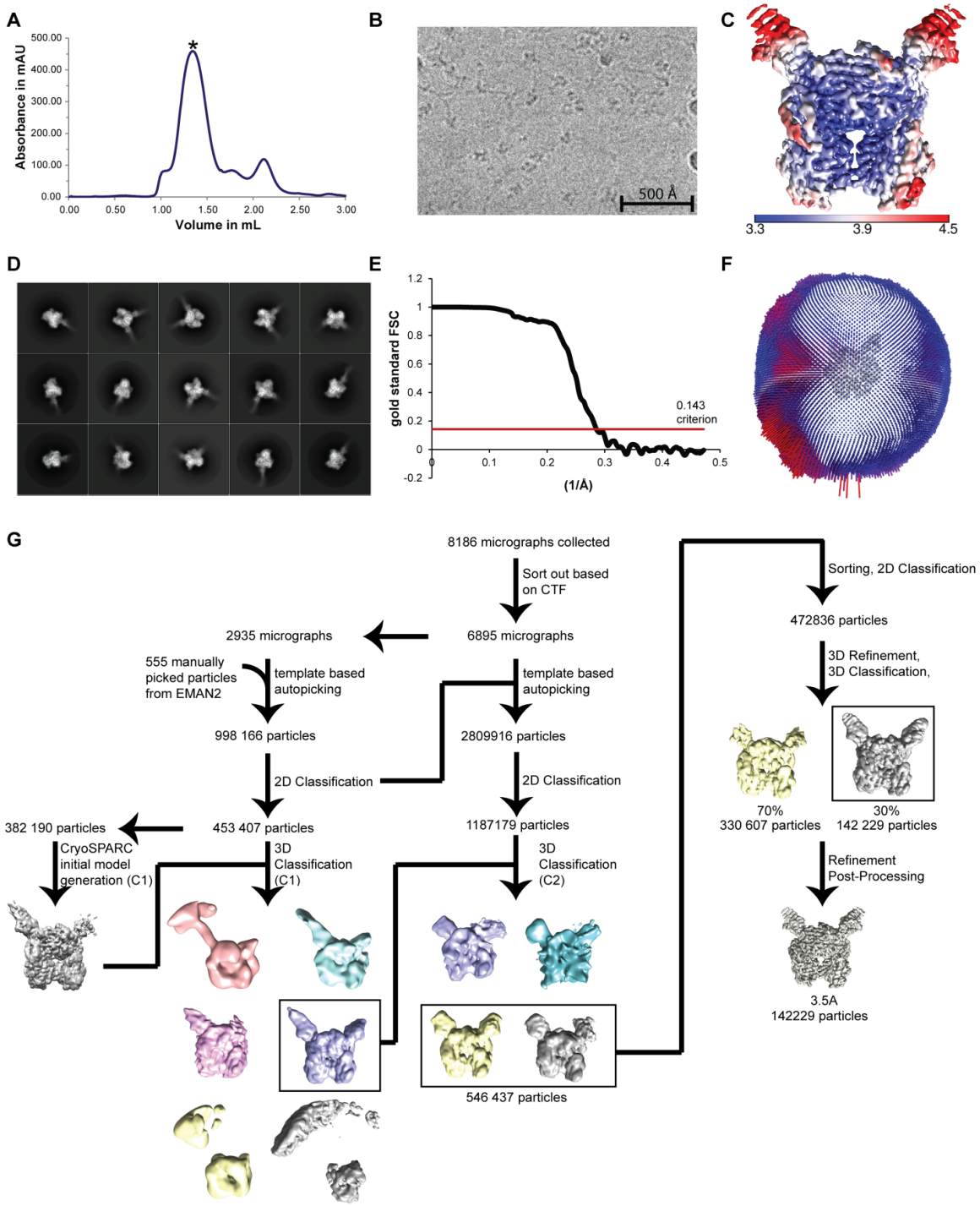
A
Absorbance in mAU
500.00
400.00
300.00
200.00
100.00
0.00
0.00
0.50
1.00
1.50
2.00
2.50
3.00
Volume in mL
B
500 Å
C
3.3
3.9
4.5
D
E
gold standard FSC
1.2
1
0.8
0.6
0.4
0.2
0
-0.2
0
0.1
0.2
0.3
0.4
0.5
(1/Å)
0.143
criterion
F
G
8186 micrographs collected
Sort out based on CTF
6895 micrographs
2935 micrographs
555 manually picked particles from EMAN2
template based autopicking
template based autopicking
998 166 particles
2809916 particles
2D Classification
2D Classification
382 190 particles
453 407 particles
1187179 particles
CryoSPARC initial model generation (C1)
3D Classification (C1)
3D Classification (C2)
546 437 particles
Sorting, 2D Classification
472836 particles
3D Refinement, 3D Classification,
70%
330 607 particles
30%
142 229 particles
Refinement Post-Processing
3.5A
142229 particles

Figure S1 Related to Figure 1| Cryo-EM processing scheme of the resting state

(A) Size exclusion profile of full-length *Ec*MR. The peak used for grid preparation is indicated by an asterisk.

(B) Representative micrograph of the resting state *Ec*MR complex bound to ATPγS.

(C) The local resolution of the resting state reconstruction was calculated using ResMap and is shown as color-coded surface representation.

(D) The fifteen highest populated classes from the 2D classification of the *Ec*MR in resting state are shown.

(E) Gold-standard Fourier shell correlation (FSC) for the resting state. The red line indicates the 0.143 cutoff criterion which indicates a nominal resolution of 3.5 Å.

(F) Angular distribution of the particles used for the resting state reconstruction

(G) Flow chart showing the image-processing pipeline for the cryo-EM data analysis of the *Ec*MR resting state.

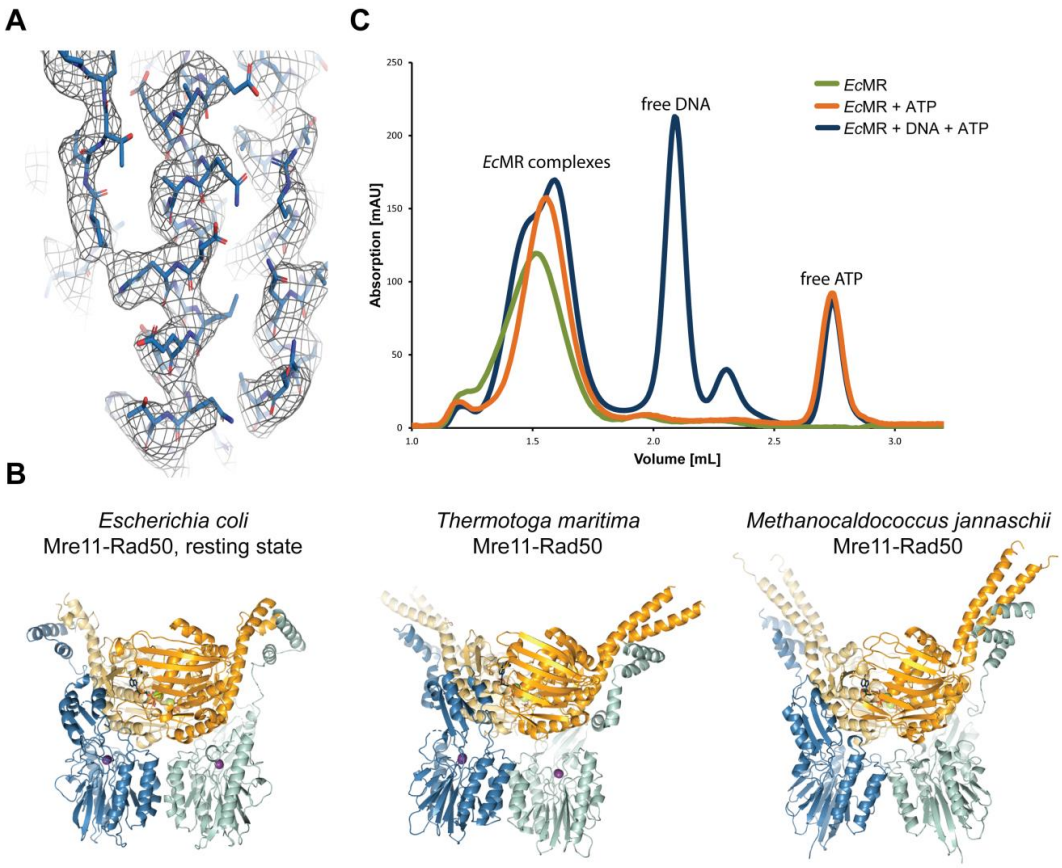

Figure S2 Related to Figure 1| Resting State Analysis

(A) Portion of the electron density superimposed with the 1.8 Å X-ray structure of *Ec*Mre11 (4M0V) shows the quality of the map. This starting model was subsequently adjusted and refined.

(B) Gel filtration retention volumes of *Ec*MR in absence and presence of ATP and/or DNA shows homogeneous species and no formation of stable higher order oligomers as a function of ATP or DNA. ATP/DNA leads to a slight reduction of hydrodynamic radius.

(B) Comparison of the resting state *Ec*MR head with X-ray structures of the MR head from *Thermotoga maritima* (PDB: 3THO) and *Methanocaldococcus jannaschii* (PDB: 3AV0). All three structures show a related fold with slightly different orientations of the coiled coil.

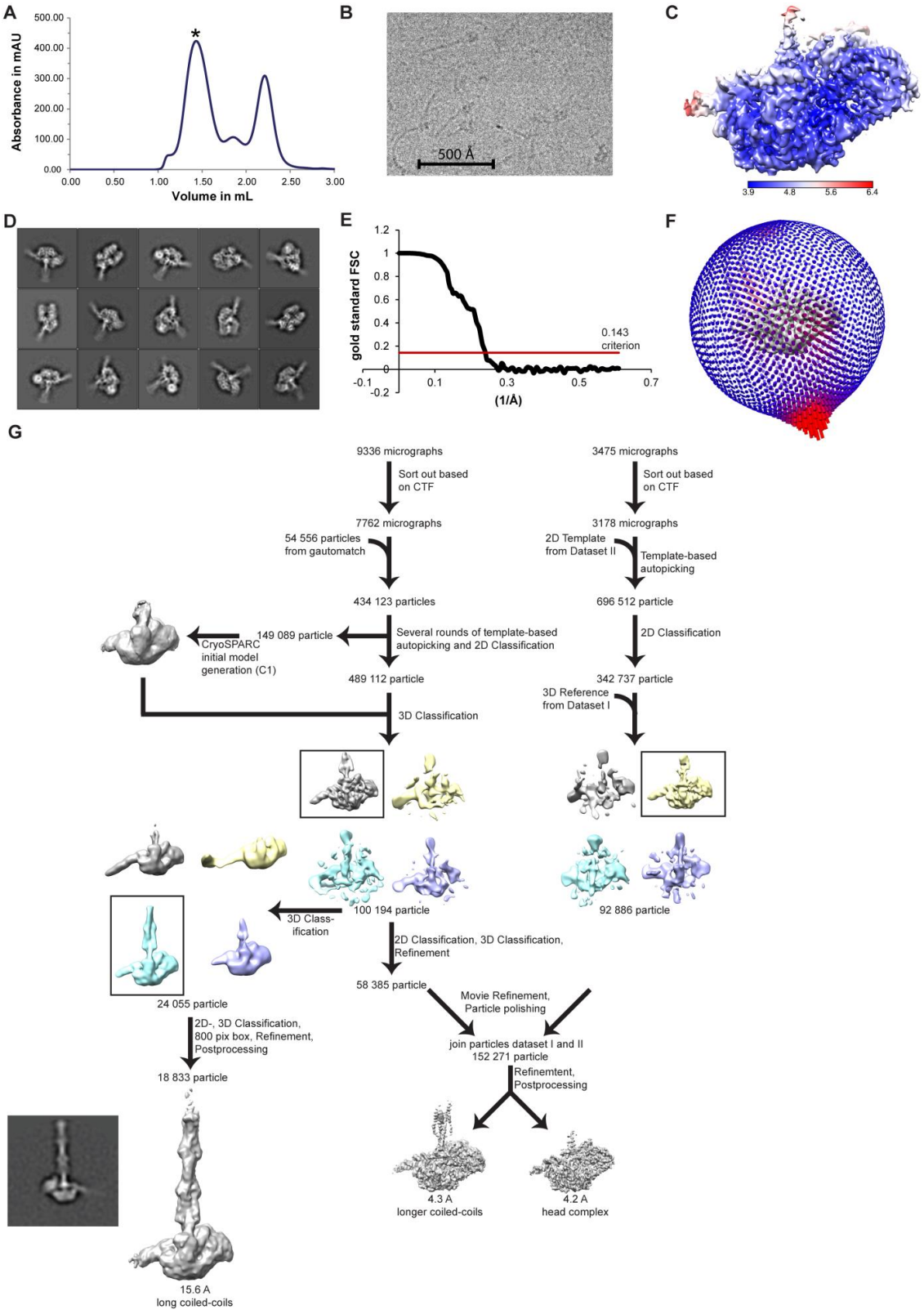
A
Absorbance in mAU
Volume in mL
B
500 Å
C
3.9
4.8
5.6
6.4
D
E
gold standard FSC
0.143
criterion
(1/Å)
F
G
9336 micrographs
Sort out based on CTF
7762 micrographs
54 556 particles from gautomatch
434 123 particles
149 089 particle
CryoSPARC initial model generation (C1)
Several rounds of template-based autopicking and 2D Classification
489 112 particle
3D Classification
100 194 particle
3D Class-ification
24 055 particle
2D-, 3D Classification, 800 pix box, Refinement, Postprocessing
18 833 particle
15.6 A
long coiled-coils
2D Classification, 3D Classification, Refinement
58 385 particle
Movie Refinement, Particle polishing
3475 micrographs
Sort out based on CTF
3178 micrographs
2D Template from Dataset II
Template-based autopicking
696 512 particle
2D Classification
342 737 particle
3D Reference from Dataset I
92 886 particle
join particles dataset I and II
152 271 particle
Refinemtent, Postprocessing
4.3 A
longer coiled-coils
4.2 A
head complex

Figure S3 Related to Figure 1| Cryo-EM processing scheme of the cutting state

(A) Size exclusion profile of full-length EcMR^{H84S}. The peak used for grid preparation is indicated by an asterisk.

(B) Representative micrograph with the cutting state EcMR^{H84S} in complex with ADP and DNA.

(C) The local resolution of the cutting state reconstruction was calculated using ResMap and is shown as a color-coded surface representation.

(D) The fifteen highest populated classes from the 2D classification of the *Ec*MR in the cutting state are shown.

(E) Gold standard Fourier shell correlation (FSC) for the cutting state reconstruction. The red line indicates the 0.143 cutoff criterion which indicates a nominal resolution of 4.2 Å.

(F) Angular distribution of the cutting state reconstruction particles.

(G) Sorting scheme that was used to obtain the 4.2 Å reconstruction of the cutting state.

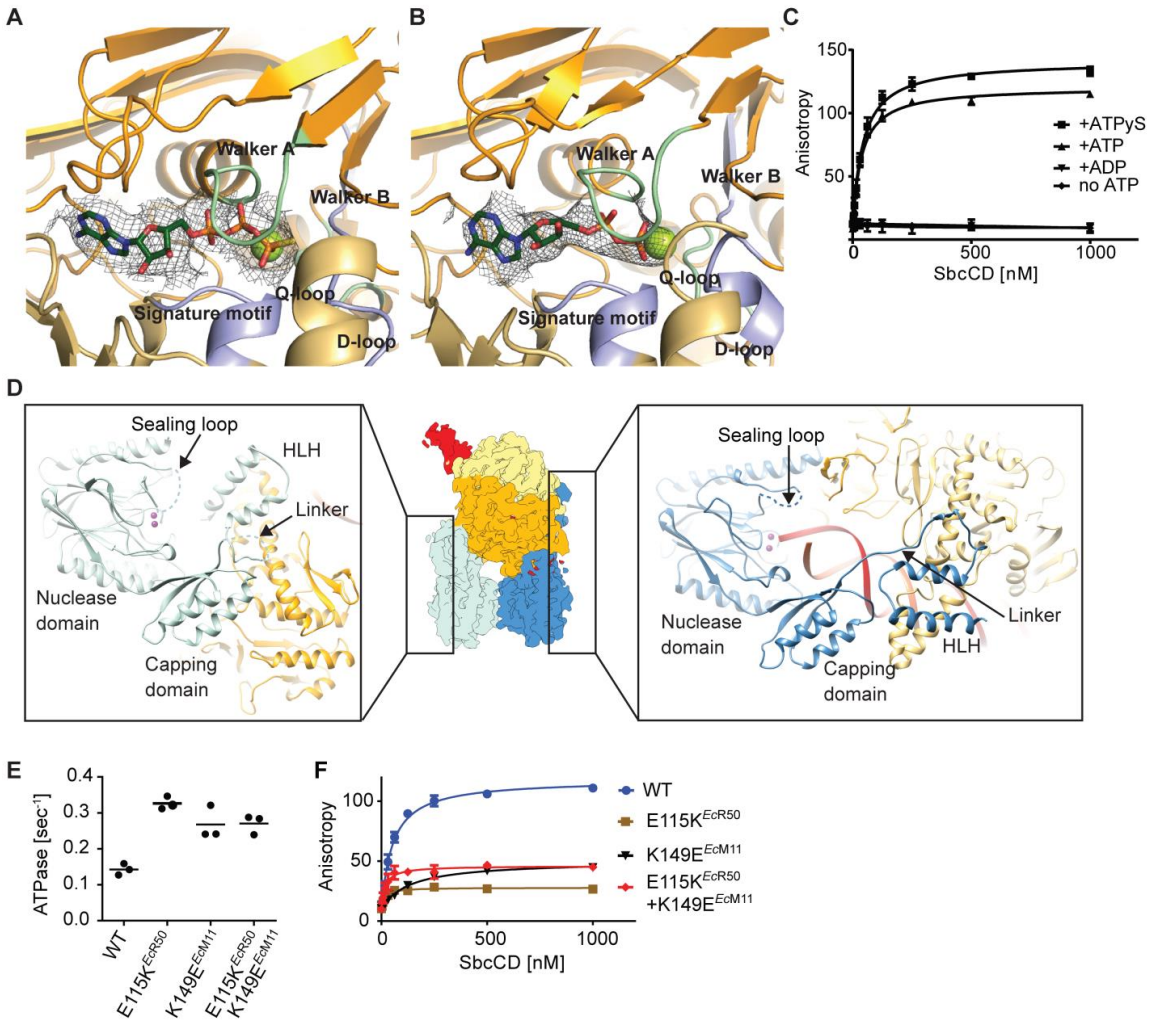

Figure S4 Related to Figure 1 and 2| Structural details of nucleotide and metal binding

(A) ATPγS-Mg^{2+} is visible in the nucleotide binding domain of the resting state reconstruction. The density for the nucleotide is shown and important nucleotide binding motifs are highlighted and color coded.

(B) ADP-Mg^{2+} is visible in the nucleotide binding domain of the cutting state reconstruction.

(C) Interaction of *Ec*MR to fluorescein-labeled 60 bp DNA in the presence of ATP, ADP, ATPγS and no nucleotides monitored by the change in fluorescence anisotropy. DNA binding was detected in the presence of ATP and ATPγS, but not ADP. The data were fit to a 1 to 1 binding equation. Mean and standard deviation are indicated (n = 3, technical replicates).

(D) The linker between the HLH motif and the capping domain of Mre11 adopt different conformations in both monomers. In monomer B (left) no DNA is bound and the linker adopts a

closed conformation while in the DNA binding monomer A (right) an extended conformation is formed.

(E) Steady-state ATPase rates of *Ec*MR charge reverse mutants *Ec*Rad50^{E115K}, *Ec*Mre11^{K149E} and *Ec*Mre11^{K149E}Rad50^{E115K}, stimulated by 60 bp DNA. Mean and individual data point (*n* = 3, technical replicates).

(F) Interaction of *Ec*MR charge reverse mutants with double-stranded DNA monitored by the change in fluorescence anisotropy. The data were fit to a 1 to 1 binding equation. Mean and standard deviation are indicated (*n* = 3, technical replicates). The following K_d values were calculated: *Ec*MR: 51 ± 5 nM; *Ec*MR^{E115K}: 14 ± 4 nM; *Ec*M^{K149E}R: 132 ± 17 nM; *Ec*M^{K149E}R^{E115K}: 17 ± 4 nM.

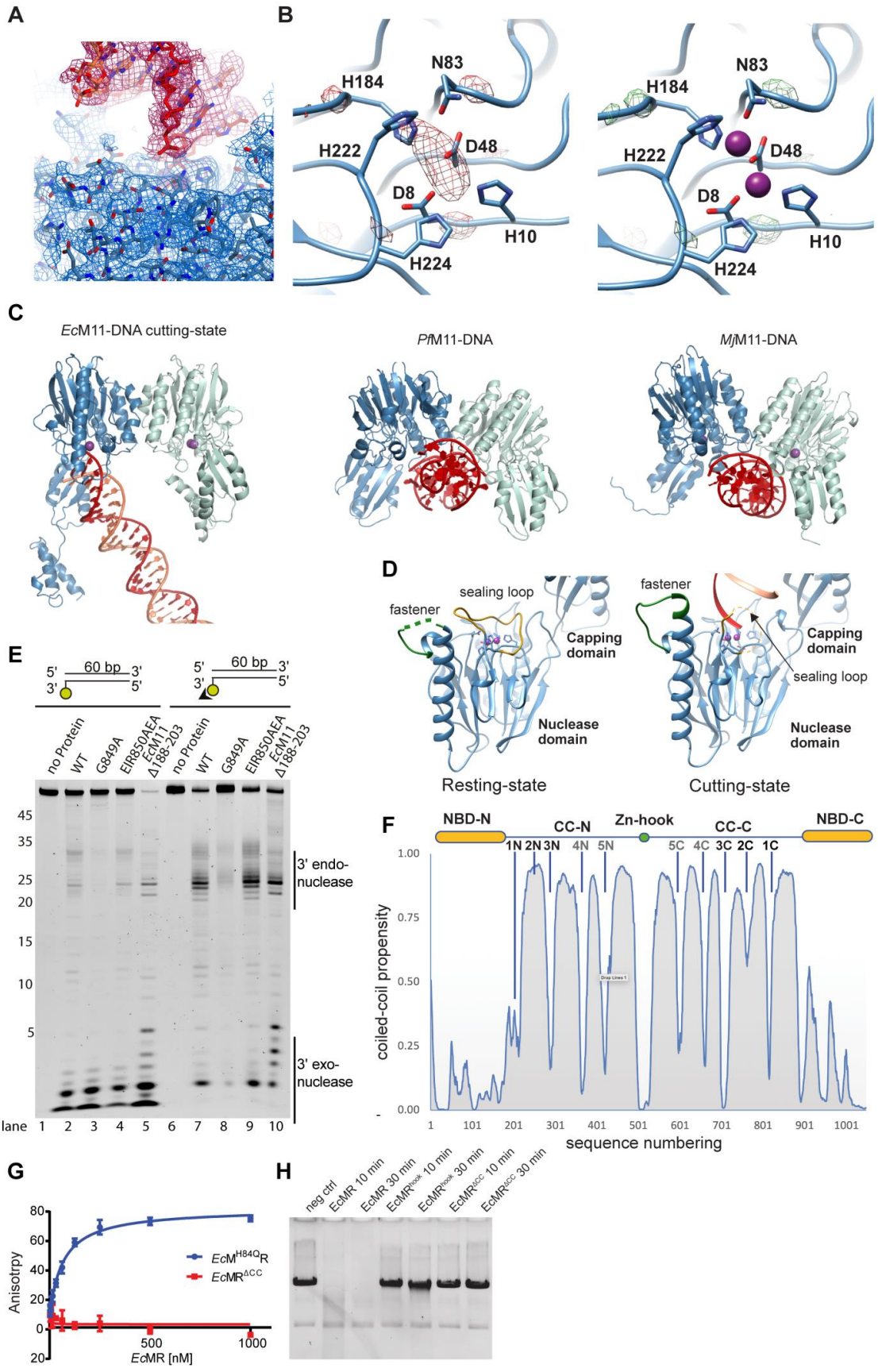
A
B
N83
H184
H222
D48
D8
H10
H224
C
EcM11-DNA cutting-state
PfM11-DNA
MjM11-DNA
D
fastener
sealing loop
Capping domain
Nuclease domain
Resting-state
Cutting-state
E
5' 60 bp 3'
3' 5'
no Protein
WT
G849A
EIR850AEA
EcM11 Δ188-203
3' endo-nuclease
3' exo-nuclease
lane 1 2 3 4 5 6 7 8 9 10
F
NBD-N
CC-N
Zn-hook
CC-C
NBD-C
1N 2N 3N 4N 5N 5C 4C 3C 2C 1C
coiled-coil propensity
sequence numbering
G
Anisotrpy
EcM^H84QR
EcMR^ΔCC
EcMR [nM]
H
neg ctrl
EcMR 10 min
EcMR 30 min
EcMR^hook 10 min
EcMR^hook 30 min
EcMR^ΔCC 10 min
EcMR^ΔCC 30 min

Figure S5 Related to Figure 2 and 3| Mutational analysis of Fastener-NBD interface and coiled-coil

(A) Map at the *Ec*Mre11 active site (blue) bound to DNA (red).

(B) Difference density analysis of *Ec*MR in the cutting shows robust density (left panel) at the di-metal site where crystallographic analysis of *Ec*Mre11 showed two manganese ions (right panel). The difference density was calculated using the command phenix.real_space_diff_map, for pdb maps without (left) and with (right) manganese ions.

(C) Comparison of the Mre11 resting state to Mre11-DNA orientation of the cryo-EM *Ec*MR cutting state and to the X-ray structures of *Pyrococcus furiosus* Mre11-DNA (pdb: 3DSC; bottom, left) and *Methanocaldococcus jannaschii* Mre11-DNA (pdb: 4TUG; bottom, right).

(D) Rearrangement of the *Ec*Mre11 sealing loop (yellow) and *Ec*Mre11 fastener (green) in the resting- and cutting-state respectively.

(E) Nuclease activity of *Ec*MR mutants analyzed with fluorescently labeled 60 bp DNA containing a free DNA end (DNA I) and a DNA end which is blocked by a single-chain fragment against fluorescein (DNA II). To prevent exonucleolytic degradation, the unlabeled 3' DNA end is protected by 10 consecutive phosphothioate linkages. The residues of *Ec*Mre11$^{\text{sealing loop}}$ are deleted in the *Ec*Mre11$^{\Delta 188\text{-}203}$ mutant.

(F) Analysis of coiled-coil propensity along the protein sequence using DeepCoil (Ludwiczak et al., 2019) as implemented in the MPI ToolKit (Zimmermann et al., 2018). NBD's N and C-terminal regions as well as the Zn-hook have low CC propensity as expected. However, the N- and C-terminal parts of the CC domain have another 4 (1N,3N,4N,5N) and 5 (5C,4C,3C,2C,1C) regions of low CC propensity. 2N still has high CC propensity, but in our cryo-EM map pairs with 2C to form the CC break element 2. In total our density shows three CC break elements (1,2,3 in Figure 3D) matching the sequence regions of 1N:1C, 2N:2C, 3N:3C. 4N:4C and 5N:5C might form two additional CC break elements towards the Zn-hook.

(G) Interaction of *Ec*MR$^{\Delta CC}$ with double-stranded DNA monitored by the change in fluorescence anisotropy. The data were fit to a 1 to 1 binding equation. Mean and standard deviation are indicated (n = 3, technical replicates).

(H) Plasmid assay of linearised pBR322 with the coiled-coil mutants *Ec*MR$^{\text{hook}}$ and *Ec*MR$^{\Delta CC}$. Time points were taken after 10 and 30 min.

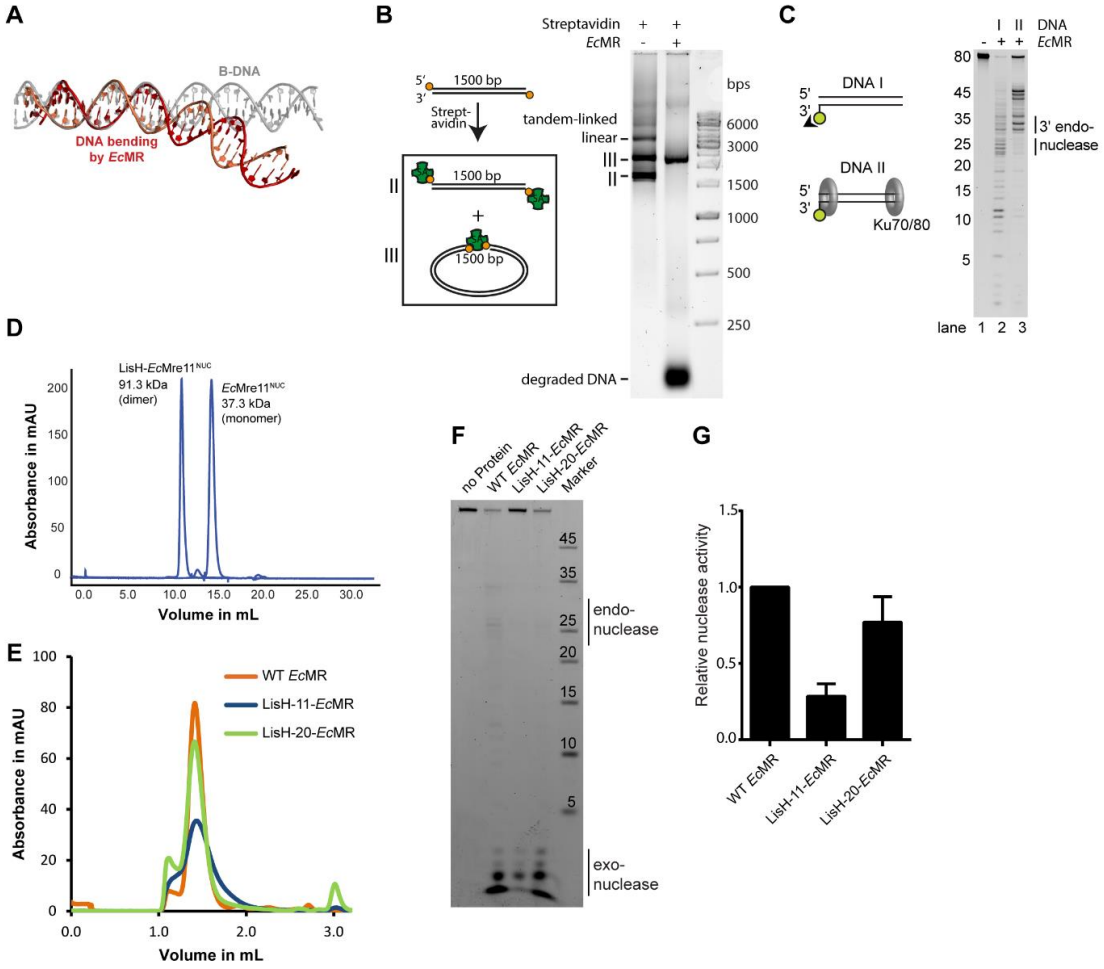

Figure S6 Related to Figure 4 and 5| Characterization of the LisH-*Ec*MR constructs

(A) Comparison of standard B-form -DNA (gray) to the DNA structure in the*Ec*MR cutting-state structure (red).

(B) Nuclease activity assays as in Figure 3A, B but with different DNA/streptavidin ratio leading to a larger fraction of the double-blocked linear species (II) over the circular (III). *Ec*MR selectively degrades linear DNA.

(C) Nuclease activity of *Ec*MR wild type analyzed with 5' fluorescently labeled 80 bp DNA containing a DNA end which is terminally-blocked by a single-chain fragment against fluorescein, scFv (DNA I) and in the presence *Chaetomium thermophilum* Ku70/80 (DNA II). The 3' endonuclease shifts from 25 nucleotides (scFv-bound) to 35 nucleotides (Ku70/80-bound) approximately 10 bp inwards.

(D) Size exclusion profiles of LisH-*Ec*Mre11^{NUC} and *Ec*Mre11^{NUC}.

(E) Size exclusion profiles of LisH-*Ec*MR with 11 and 20 residue linker and *Ec*MR. The runs were done with a S6 5/150 column.
(F) Nuclease activity of LisH-*Ec*MR with 11 and 20 residue linker and *Ec*MR analyzed with fluorescently labeled 60 bp DNA containing a free DNA end. To prevent exonucleolytic degradation, the unlabeled 3' DNA end is protected by 10 consecutive phosphothioate linkages.
(G) Quantification of the exonuclease activity shown in (F), (n=3, technical replicates)

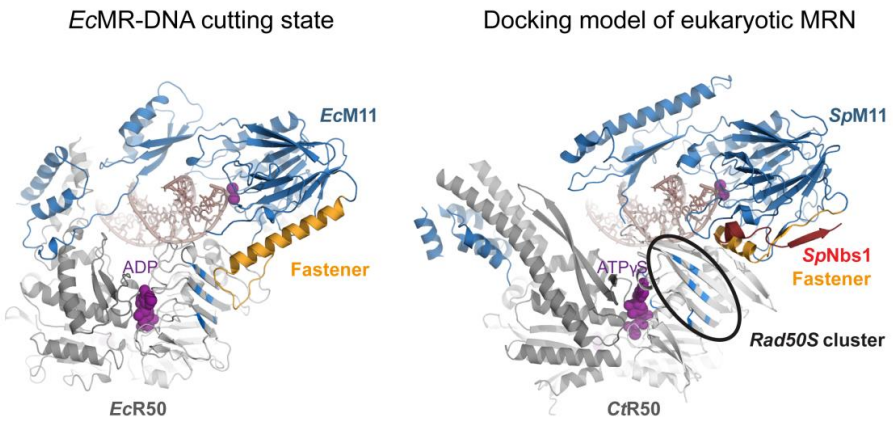

Figure S7 Related to Figure 6| Comparison of EcMR and a model for eukaryotic MRN.

Structural alignment of *Ec*MR cutting-state (left) with a model for eukaryotic MRN (right, obtained by docking the ATPγS bound (*Chaetomium thermophilum*) *Ct*Rad50^{NBD}-Mre11^{HLH} complex (PDB: 5DA9), the CtMre11^{NUC} dimer (PDB: 4YKE), and the Mre11-interacting region of *S. pombe* Nbs1 (PDB: 4FBW) onto the *Ec*MR cutting state model, the relevant *rad50*S residues are shown as blue backbone patches. The *Ec*Mre11^{fastener} helix binds to *Ec*Rad50 at precisely the surface location that harbors the Rad50S cluster of residues. The fastener loop (orange) is much shorter in eukaryotic Mre11 and binds Nbs1 (red). Thus, the bacterial Mre11^{fastener}-Rad50 interaction could be replaced by a Mre11-Nbs1/CtIP-Rad50 interaction, explaining a wide range of biochemical data.

Table S1 Related to Key Resource Table| DNA oligomers used for the assays and the cryo-EM sample

Oligonucleotide	Sequence 5' to 3'
60 bp DNA fwd for nuclease	CGGGTAGTAGATGAGCGCAGGGACACCGAGGTCAA GTACATTACCCTCTC*A*T*A*G*G*A*G*G*T*G
60 bp DNA rev for nuclease	CACCTCCTATGAGAGGGTAATGTACTTGACCTCGGT GTCCCTGCGCTCATCTACTACCCG-6-FAM
60 bp DNA fwd for size exclusion analysis	CGGGTAGTAGATGAGCGCAGG*G*A*C*A*C*C*G*A*G *GTCAAGTACATTACCCTCTCATAGGAGGTG
60 bp DNA rev for size exclusion analysis	CACCTCCTATGAGAGGGTAATGTACTTGACCTCGGT GTCCCTGCGCTCATCTACTACCCG
80 bp DNA fwd for nuclease with Ku70/80	CGGGTAGTAGATGAGCGCAGGGACACCGAGGTCAA GTACATTACCCTCTCATAGGAGGTGCGCTTTATCAG AAGCCAGAC
80 bp DNA rev for nuclease with Ku70/80	GTCTGGCTTCTGATAAAGCGCACCTCCTATGAGAGG GTAATGTACTTGACCTCGGTGTCCCTGCGCTCATCT ACTACCCG-6-FAM
60 bp DNA fwd for ATPase assay	CGCTTTATCAGAAGCCAGACATTAACGCTTCTGGAG AAACTCAACGAGCTGGACGCGGAT
60 bp DNA rev for ATPase assay	ATCCGCGTCCAGCTCGTTGAGTTTCTCCAGAAGCGT TAATGTCTGGCTTCTGATAAAGCG
35 bp DNA fwd for DNA binding assay	CGCTTTATCAGAAGCCAGACATTAACGCTTCTGGA
35 bp DNA rev for DNA binding assay	6-FAM-TCCAGAAGCGTTAATGTCTGGCTTCTGATAAAGCG
60 bp DNA for EM fwd	CGCTTTATCAGAAGCCAGACATTAACGCTTC TGGAGAAACTCAACGAGCTGGACGCGGAT
60 bp DNA for EM rev	ATCCGCGTCCAGCTCGTTGAGTTTCTCCAGAAGCGT TAATGTCTGGCTTCTGATAAAGCG

Movie S1 Related to Figure 1| Depiction of the conformational changes occurring upon DNA binding in *Ec*MR

The first part of the movie explains the structure of *Ec*MR in the resting state and the movement of the Mre11 dimer upon DNA binding. Additionally, it depicts important structural features of the cutting state structure. The second part of the movie explains closing of the CCs using a morph between the resting state and the cutting state of *Ec*MR.

3 Discussion

The MRN complex is a central player in the repair of DSBs. However, despite 20 years of research, several questions remained unanswered especially regarding the binding and processing of dsDNA. The MRN complex has been analysed extensively by X-ray crystallography from different organisms, with and without DNA, however, for these studies the coiled coils always had to be shortened drastically[175,180,187,188]. Since the coiled coils and the zinc hook play an important role for the MR(N) complex, head complexes without the coiled coils cannot fulfil all their functions[192,193].
In the structures of Rad50 with DNA, the DNA binding site is located either only on the NBDs[175,187] or additionally on the coiled coils[188] and this binding site is located opposite of the Mre11 dimer location. In addition, DNA processing is ATP dependent, however, ATP binding by Rad50 also leads to an autoinhibitory state, in which the Mre11 nuclease active site cannot be accessed by the DNA[181]. Structures of Mre11 in complex with DNA showed that the DNA seems to occupy the Rad50 binding site[166,171,176,284].

Thus, two of the most puzzling questions regarding the MRN complex are:
(I) how does the dsDNA enter the active site and
(II) what is the function of the coiled coils.

The recent developments in cryo-EM allowed the use of full-length *Ec*MR for structural and biochemical studies. The *Ec*MR complex is a good model system, since it has similar biochemical and structural properties to its eukaryotic counterpart[116]. This includes the enzymatic activities of 3′ to 5′ exonuclease and endonuclease activity on a blocked dsDNA end, ATPase activity and the high structural conservation[116,265,266,269] (see Section 2.1 and 2.2). However, *Ec*MR is not regulated by posttranslational modifications, has less interacting protein partners and misses the presumably flexible Nbs1[190]. In contrast to many previously used organisms, *E.coli* is a mesophilic organism and allows a more thorough biochemical analysis of the complex. For instance, biochemical assays can be performed at 37°C with *Ec*MR a temperature at which the DNA duplex is more stable than at higher temperatures.

In the course of this work, the head complex of full-length *Ec*MR was solved in complex with ATPγS and denoted the resting state. The *Ec*MR resting state head complex adopts a very similar fold to the head complex structures solved previously with X-ray crystallography from other organisms[171,176,187] (see Section 2.2, Supplementary Figure S2). The nuclease active site is blocked by Rad50 and thus, *Ec*MR adopts an auto-inhibited state (see Figure 16). The similarities between different structures indicates that shortening of the coiled coils does not

have a large impact on the structure of the MR resting state and highlights again the structural conservation observed in the MR core complex.

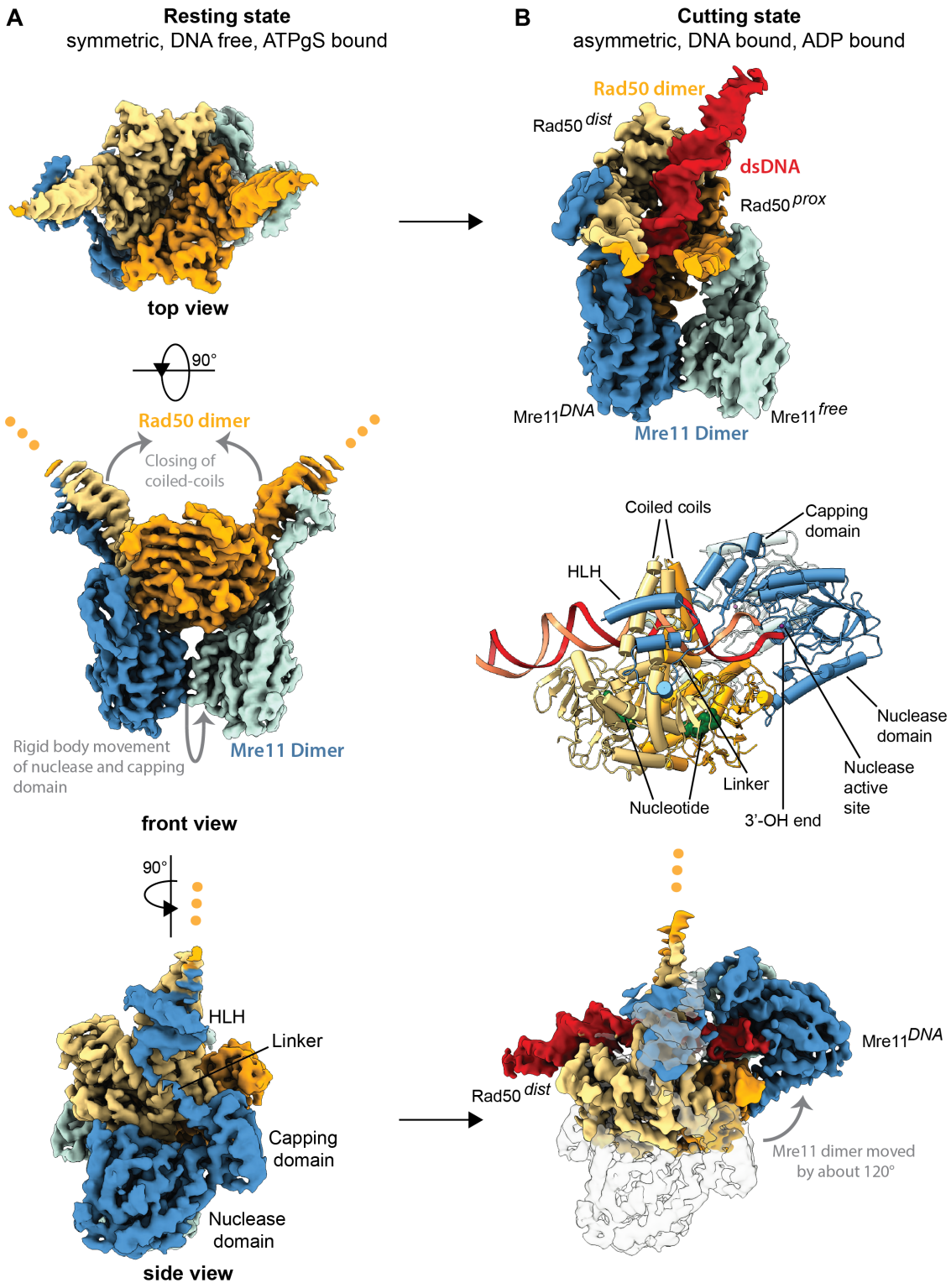

Figure 16: The resting and cutting state structures of *Ec*MR. (A) The resting state of *Ec*MR is shown in three different views. The Rad50 dimer is coloured in orange and the

Figure 16: Mre11 dimer in blue. The two largest conformational changes that occur upon DNA binding - Mre11 dimer movement and closing of the coiled coils - are indicated in the front view of the resting state with arrows. The different domains of Mre11 are labelled in the side view of the resting state. (B) The reconstructed densities of the cutting state in top view (top) and side view (bottom) are shown. Since the complex adopts an asymmetric conformation, the different monomers have assigned names: DNA-binding Mre11 monomer ($Mre11^{DNA}$, blue), DNA-free Mre11 monomer ($Mre11^{free}$, light blue), Rad50 monomer with an additional Mre11 interaction interface ($Rad50^{prox}$, orange), Rad50 monomer without additional Mre11 interaction interface ($Rad50^{dist}$, yellow). In the middle a model of the side view with important structural features is shown. In the side view an overlay with the resting state structure (transparent) illustrates the Mre11 dimer movement.

In the cutting state structure, the head complex is bound to ADP and a 60 bp dsDNA, of which ∼35 bps are visible in the structure. The DNA is bound mainly by residues in the NBD and coiled coils of Rad50 and can access the active site of Mre11. This is possible due to a large movement (∼120°) of the Mre11 nuclease and capping domain to the side of Rad50. This state likely represents the conformation of the exonuclease. The observed *Ec*MR footprint of 22 bp fits very well to the obtained biochemical data, that indicate a minimal requirement of 25-30 bp for DNA binding with high affinity and stimulation of the ATPase (see Section 2.1, Figure 1). Additionally, the cleavage of a blocked end occurs at a distance of 27 bp (from the 3′ end) and 23 bp (from the 5′ end, see Section 2.1, Figure 2 and Section 3.4). The location of Mre11 at the end of the dsDNA explains the observed higher affinity of *Ec*MR to DNA with ends (see Section 2.2, Figure 5). A similar distance between the blocked end and the endonucleolytic incision has also been reported for MR(N) from other organisms[122,177]. Crystal structures of Rad50:DNA complex indicate a footprint of ∼ 20 bps[175,187,188], which is similar to the 22bps observed for *Ec*MR. In accordance with the cutting state structure, single molecule imaging has shown that in human MRN, Mre11 is the subunit responsible for end recognition[285].
ATPγS is present in the Rad50 NBDs in the resting state, while in the cutting state ADP is bound (see Section 2.2, Supplementary Figure S4), despite the use of ATP during grid preparation. This indicates a post-hydrolysis cutting state and is in accordance with the about 26-fold activation of the ATPase activity observed by *Ec*MR in the presence of dsDNA (see Section 2.1). Similar stimulation of the ATPase rate by DNA binding was reported for the human and the yeast MR complex[182,183].

The function of the coiled coils is still enigmatic. In the resting state, only very few turns of the coiled coils could be resolved, due to flexibility and the coiled coils in close proximity to the head complex clearly point outwards. This is in stark contrast to the cutting state structure, in which the coiled coils are far better defined and form a rod, that could be resolved at a low resolution to about 1/3 (∼200 Å) of the entire length of the coiled coils (see Section 2.2, Figure 3). Thus, the coiled coils of two Rad50 monomers interact with each other in the cutting state and point inwards.
DNA binding residues are present in the coiled coils and DNA binding is abolished if these residues are mutated. The ring to rod transition in response to DNA binding has also been

observed for the human MRN complex with AFM[195]. Additionally, the human zinc hook has recently been crystallised in a rod conformation[191] (see Section 1.3.2, Figure 10). Thus, the rod conformation of the coiled coils in response to DNA binding possibly represents a feature that is conserved in pro- and eukaryotes. However, the role of this long coiled coil structure in a cellular context, is not clear. Possibly, the coiled coils serve as protein interaction platform or a domain to transfer signals from the zinc hook to the NBDs[179], however, why they are this long is still mysterious. It was postulated that two DNA strands could be bridged *in trans via* the *P.furiosus* zinc hook (intermolecular model)[189]. Alternatively, an intramolecular model has been proposed in which the zinc hooks of the same molecule engage and form a rod[191,195]. The rod formation of the *Ec*MR coiled coils also seems to indicate that the zinc hook engages rather intramolecular than intermolecular in the cutting state. The observed movement of the coiled coils also has implications for the proposed mechanisms (see Section 3.2).

Interestingly, binding of DNA results in the transition of a symmetric to an asymmetric complex. In the resting state, no asymmetric structural properties were detected. However, in the cutting state clearly an asymmetric complex is present (see Figure 16). This is mainly a result of a flexible linker that connects the HLH of Mre11 with its capping domain. The linker in $Mre11^{DNA}$ is elongated, while it adopts a closed conformation in the $Mre11^{free}$ monomer, which brings the HLH and the nuclease domain in close proximity of each other (see Section 2.2, Supplementary Figure S4). Due to the low resolution of this part of the structure it is not possible to analyse the linker in the $Mre11^{free}$ monomer in further detail, however it might adopt a folded, e.g. α-helical conformation.
The dsDNA binds to the nucleotide bound Rad50 dimer and can access the active site of the $Mre11^{DNA}$ monomer and is thus also bound in an asymmetric manner. The DNA is slightly bend in the *Ec*MR cutting state (see Figure 16 and Section 2.2, Supplementary Figure S6). However, since DNA binding in *Ec*MR is only dependent on ATP binding but not its hydrolysis, DNA binding probably is not the energy consuming step of the mechanism (see Section 2.2, Figure S4).
We used a nuclease dead mutant ($Mre11^{H84S}$) for the cryo-EM studies of the cutting state and the DNA is perfectly located for cleavage in the Mre11 active site, something that has not been observed before[166,175,187,188,284]. The 3′ end is bound close to the active site and cleavage would take place between base 1 and 2 (as seen from the 3′ end bound in the active site) and possibly liberates a nucleoside monophosphate. Thus after cleavage, a 3′ OH group would be present on the residual DNA strand. This is in accordance with biochemical data on *Ec*MR, which showed that after cleavage, the 3′ strand (corresponding to the exiting nucleoside monophosphate) carries a 5′ phosphate, while the 5′ strands (corresponding to the shortened dsDNA) contains a 3′ OH (Section 2.1, Figure 5). MR(N) complexes also cleave hairpins[266,267,286] and *Ec*MR leaves a 5′ phosphate and a 3′ OH attached to the products[267]. Based on the same cleavage chemistry and the space that is present next to the active site in *Ec*MR, free DNA ends and hairpins are likely bound and cleaved in a similar manner.

3.1 Comparison with Other MR Structures

Three crystal structures of Rad50 in complex with DNA have already been solved from the organisms *T. maritima*[188], *M. janaschii*[187] and *C. thermophilum*[175] by X-ray crystallography (see Section 1.3.2, Figure 9). Comparison to all of these structures indicates that the location of the DNA binding residues on the Rad50 surface is similar in all four structures. Most residues in these structures are located on top and close to the β-sheets of the NBD. Despite the variation in amino acid sequence, a similar DNA binding mode is present in all structures.
One residue is involved in DNA binding in all structures and is located on the tip of a helix (denoted DNA binding helix in Figure 17) pointing towards the DNA. In *E. coli* this corresponds to residue K128 (K115 in *T. maritima*, T107 in *M. janaschii*, R132 *C. thermophilum*) and mutation of this residue resulted either in decrease or complete loss of DNA binding[175,187,188].

Additionally, a second binding site is located in the NBD (black circle in Figure 17). While the residues of the NBD binding site are not conserved, the position of this DNA binding site is situated at a similar location in Rad50 of *E. coli*, *M. janaschii* and *C. thermophilum*[175,187]. These DNA binding residues could not be detected for *T. maritima*, however, this might be due to the tilted orientation the DNA adopts in this structure[188]. An additional important DNA binding site is located in the coiled coils of *E. coli* and in the *T. maritima* structure three additional DNA binding residues are located in the coiled coils[188]. The coiled coils are not closed in any of the crystal structures, possibly due to their limited length or the inability to crystallise with closed coiled coils. Additionally, all crystal structures contain either AMP-PNP (*T. maritima*)[188], or ATPγS (*M. janaschii* and *C. thermophilum*)[175,187] as ATP analogues and it is possible that the prevention of ATP hydrolysis keeps the coiled coils in an open state.
DNA binding in *Ec*Rad50 is slightly asymmetric with the Rad50^{dist} monomer engaging in more DNA contacts than the Rad50^{prox} monomer. These three additional residues are located in a loop connecting two β-sheets of the NBD (Figure 17). The Rad50 residues R92 in *M. janaschii* and K94 and R95 in *T. maritima* are located at a similar position[187,188].
Thus, all Rad50 DNA binding sites identified in *Ec*MR are also present in one or more crystal structures, indicating a common DNA binding mode by Rad50 across different species. The differences observed in the structures can likely be attributed to the shortened coiled-coils and the presence of crystal contacts.

Comparing *Ec*MR to other Mre11:DNA structures from *P. furiosus*[166] and *M. janaschii*[284] reveals several differences in the binding mode. In the structure presented here, the DNA accesses the nuclease active site while in the other three structures the DNA is located several Ångstroms away from the active site[166,284] (see Section 1.3.1, Figure 7 and Section 2.2, Figure S5). In *E. coli* only one monomer binds the DNA while in the other structures both monomers are involved[166,284]. Only few DNA binding residues are present in the *E. coli* structure and they are located close to the active site and in the capping domain. In the *P. furiosus* and the *M. janaschii* structures additional binding sites located closer to the Mre11 dimer interface can be found[166,284]. One interesting common feature involves the composition of the residues next to

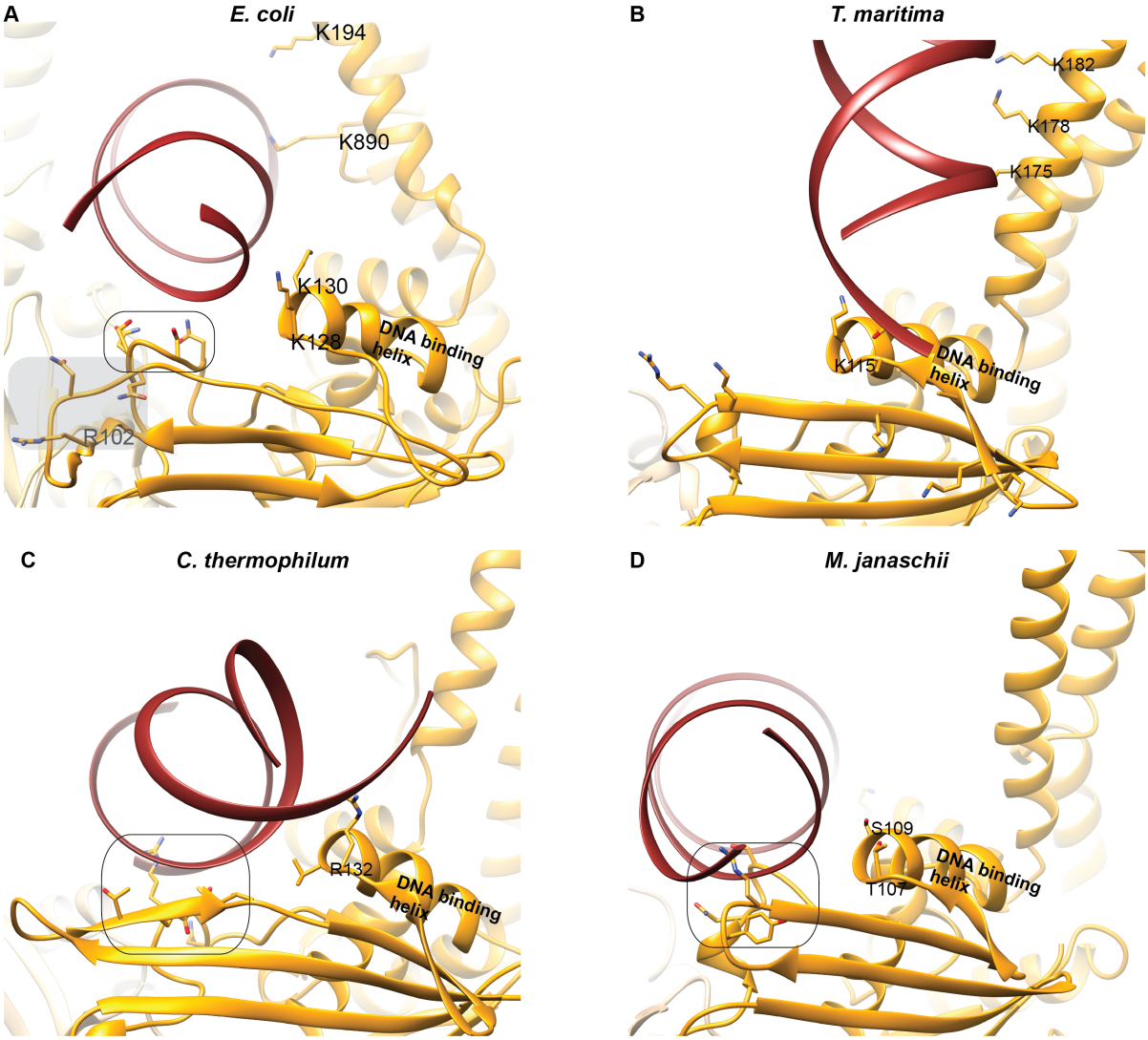

Figure 17: Comparison of DNA binding residues (A) Closeup of the Rad50 DNA binding residues of *E. coli*. Four DNA binding sites are present in *Ec*Rad50: The coiled coils (K194, K890), the tip of the DNA binding helix (K130, K128), the NBD (N63, S65, S67, Q68, black circle) and a loop in the β-sheets (R102, N108, Q110, only in the Rad50^{dist} monomer, grey background). (B) Closeup of the Rad50 DNA binding residues of *T.maritima* (pdb: 4w9m). The DNA binding residues in the coiled coils and the DNA binding helix are labelled. (C) Closeup of the Rad50 DNA binding residues of *C. thermophilum* (pdb: 5da9). The residues in the DNA binding helix are labelled and the residues in the NBD are indicated with a black circle. (D) Closeup of the Rad50 DNA binding residues of *M. janaschii* (pdb: 5dny). The residues in the DNA binding helix are labelled and the residues in the NBD are indicated by a black circle.

the active site. In all three structures aromatic residues are located in this position (*Ec*F15, *Ec*Y16, *Pf*Y13, *Mj*Y13). Possibly these residues are involved in melting of the DNA, especially for the endonuclease reaction (see Section 3.4). The differences in the structures might reflect variations between organisms, point to a different DNA bound state in the endocut or they result from artefacts in the crystallisation, due to the missing Rad50 dimer.

One structure of the *P. furiosus* Mre11 dimer in complex with AMP was solved previously by

crystallography. In this structure the AMP is located close to the active site and is positioned such that the phosphate is located close to the manganese ions[162]. This is similar to the terminal base located in the active site of *Ec*MR, which also points towards the manganese ions with its phosphate. The sugar and base adopt a different conformation in the *P. furiosus* structure, likely due to missing DNA.

3.2 Model for the *Ec*MR Reaction Cycle

The role of the coiled coils for the complex function is not clear, yet. However, the most prominent conformational change takes place in this domain. The coiled coils point outwards from the *Ec*MR head complex in the resting state. In addition they could not be resolved from the cryo-EM data which points to a high degree of flexibility. For the model, it is propose that the coiled coils form an open ring structure in the resting state. AFM studies with human MR showed an open conformation of the coiled coils in the absence of DNA[195]. Additionally, the zinc hook is an import dimerization domain, as shown by crystallographic and biochemical studies[189,191,192]. AFM images with the *Ec*MR complex showed mainly heterodimeric complexes (MR) connected via their zinc hook. However, these experiments were performed in the absence of ATP[283] and the presence of ATP would induce additional dimerization in the Rad50^{NBDs}[181]. Thus, the dimerization of the zinc hook and the Rad50^{NBDs} without simultaneous interaction of the coiled coils results in the proposed ring structure of the coiled coils in the resting state (Figure 18, left).
The coiled coils in the cutting state cryo-EM reconstruction were solved to about 1/3 of the estimated length, due to flexibility. However, the coiled coils in the cutting state are presumably closed completely from the head domain to the zinc hook. This is based on the observation of particles on several micrographs, in which the coiled coils form a rod on the entire length of the coiled coils. Additionally, rod formation of the coiled coils induced by DNA addition has been observed for the *hs*MRN [195] and crystallographic studies of the human zinc hook also indicates a state with closed coiled coils for Rad50[191].

One question that could not be solved to date, is how the MR(N) complex detects a DSB. The DSB recognition protein Ku70/80 is highly abundant in the cell and forms a ring that can slide on free DNA ends with an affinity in the low nanomolar range for DNA ends[7,64,65]. Compared to Ku, MRN is much less abundant in the cell[7]. Furthermore, a DSB detection mechanism similar to Ku would not explain the presence of the coiled coils and some biochemical findings (see below). Thus, the existence of an additional state, denoted the scanning state, is proposed (Figure 18, middle). The scanning state connects the resting and cutting state and suggests an active movement of MR(N) along the DNA to detect DSBs.
This idea is supported by data from human Rad50, Cohesin as well as the bacterial MutS. A recent single-molecule imaging study, reported sliding of MRN on DNA curtains, with Rad50 being the subunit responsible for the sliding activity. Additionally, the authors found, that MRN

can hop over nucleosomes and even Q-dots (with a diameter of 10 nm), which would indicate that an interface, possibly the zinc hook or the nucleotide binding domain opens up and allows dissociation and subsequent association on the DNA [285]. Furthermore, Cohesin from human and yeast has been shown to translocate on DNA [287,288]. MutS is involved in MMR and like Rad50 contains an ABC ATPase [289]. MutS slides along DNA to scan for mismatched bases by one dimensional diffusion. Upon encountering a mismatched base pair the MutS dimer binds and exchanges ADP for ATP, which changes the diffusional behaviour of the MutS dimer on the DNA [290].The relation of Rad50, Cohesin and MutS points to a DNA sliding property, shared by all three proteins.

The scanning model is also supported by biochemical data that shows that *Ec*MR binds a supercoiled and relaxed plasmid with less affinity than a linearized plasmid (see also Section 2.2, Figure 5). Similarly, the ATPase is stimulated maximally only in the presence of a linear and not of a supercoiled plasmid (see Section 2.1). The model predicts that the coiled coils cannot close in the absence of a DSB, due to their inability to close as long as a second DNA strand is trapped between them. In this hypothetical scanning state, the Mre11 dimer is still located in its autoinhibited position and can thus not cleave the DNA. If a break is present in the DNA, the coiled coils are able to close and the Mre11 dimer can move from its autoinhibited position to the side of the complex to form the nuclease proficient cutting state (see Figure 18).

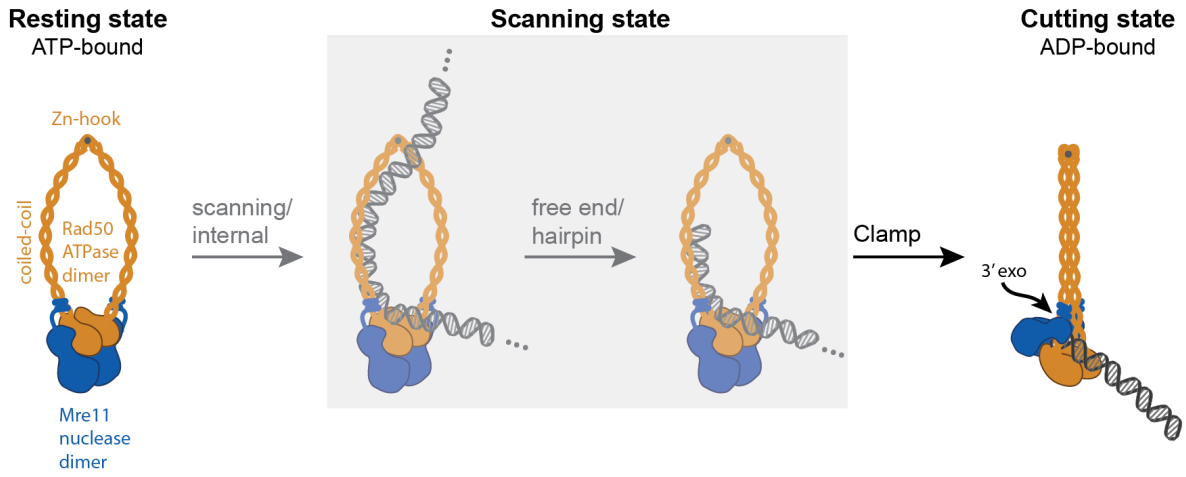

Figure 18: Model for the Mechanism of the exonuclease. The Mre11 dimer is located below Rad50 in an autoinhibitory position in the ATP bound resting state. The hypothetical scanning state is indicated with a grey background. The MR(N) complex moves along the DNA and only if a DSB is encountered are the coiled coils able to close and the Mre11 dimer moves from its autoinhibited position to the nuclease proficient cutting state.

3.3 Implications for the Model from SMC Proteins and ABC ATPases

For the distantly related SMC proteins, different conformations of the coiled coils have been observed. Depending on the organism, rings, rods and V-shaped structures have been found[179]. For instance, rods and V-shaped structures have been observed for the *Bacillus subtilis* SMC protein Smc-ScpAB[291,292], while for Cohesin and Condensin, rings or rods were found, respectively[293]. Thus, the coiled coils seem to be similar for Rad50 and SMC proteins in that they can adopt different conformations.
Structural and biochemical analysis of *B. subtilis* SMC indicated, that in its ATP bound state the coiled coils point outwards, possibly generating a ring structure that has a second point of engagement at the hinge domain. Thereby, ATP binding and simultaneous rod formation of the coiled coils seems to exclude each other and only upon ATP hydrolysis are the coiled coils able to engage, which results in a slight disengagement of the NBDs in the head[292]. Thus, the ATP bound state seems to be similar in *Ec*MR and *Bs*SMC in that the coiled coils are open and presumably form a ring structure. The hinge domain, corresponding to the Rad50 zinc hook, is able to engage DNA and one possible interaction site is located between the coiled coils[184]. This would require the coiled coils to stay in an open state in SMC proteins to be able to bind DNA. Possibly, this corresponds to the scanning state of *Ec*MR. However, in contrast to *Bs*SMC, the ATP hydrolysis does not result in a disengagement of the two Rad50 NBD domains in the cutting state, albeit some conformational changes in the Rad50 monomers occur. Clamping of the DNA between the two Rad50 monomers might prevent disengagement of the NBDs that might otherwise occur more rapidly after ATP hydrolysis. Additionally, it cannot be excluded that a state in which the head slightly disengages exists for *Ec*MR (see below).

The coiled coils of *Ec*MR do not form continuous helices, but contain several breaks and three of these breaks are visible in the structure (see Section 2.2, Figure 3 and Supplementary Figure S5, Figure). Breaks in the coiled coils have also been reported for *hs*MRN[191,197]. SMC proteins contain at least two distinct breaks in the coiled coils. The joint is located in close proximity to the NBDs, while the elbow is located in a more central position in the coiled coils[201,292]. A recent structure of the *Ec*SMC protein MukB showed that the coiled coils fold back onto themselves at the elbow, which brings the hinge and the NBDs in close proximity. For Cohesin from budding yeast a similar conformation could be observed[201]. A conformation with folded coiled coils has not been discovered for the *Ec*MR complex on the micrographs or in any classification up to date. Nevertheless, such a back folded structure could represent a transient state that is adopted during the mechanistic cycle of *Ec*MR and could not be captured by cryo-EM, yet. In the Cohesin proteins, breaks in the coiled coils clearly create flexibility, which allows folding of the coiled coils in half[201]. The breaks in the MR(N) coiled coils probably serve a similar purpose but if they are required to allow the coiled coils to fold back onto themselves has to be determined in the future.

A study in *B. subtilis* SMC found a superstructure in the coiled coils, meaning cells were only viable when the coiled coils were shortened or elongated with a certain periodicity [199]. Attempts to truncate the Rad50 coiled coils resulted in defects in HR, telomere maintenance and meiotic DSB formation [193]. Thus, the Rad50 coiled coils might possess such a periodicity, too, and disturbing this superstructure might be one reason why Rad50 does not tolerate shortening of the coiled coils very well.

Close inspection of the *Ec*MR coiled coils suggests, that the coiled coils wind around each other with a very slow periodicity. In the view shown in Figure 19, the Rad50^{prox} coiled coil is located behind the Rad50^{dist} coiled coil in close proximity to the Rad50^{NBDs}. At their first engagement point, the GEIR motif, the coiled coils are located next to each other. At the point that is located furthest away from the head complex, the Rad50^{dist} coiled coil is located below the Rad50^{prox} coiled coils. This indicates a very low periodicity present in the *Ec*MR coiled coils located in close proximity to the head, with $\sim 1/2$ turn in 150 Å. However, the function of this superstructure is not clear, yet.

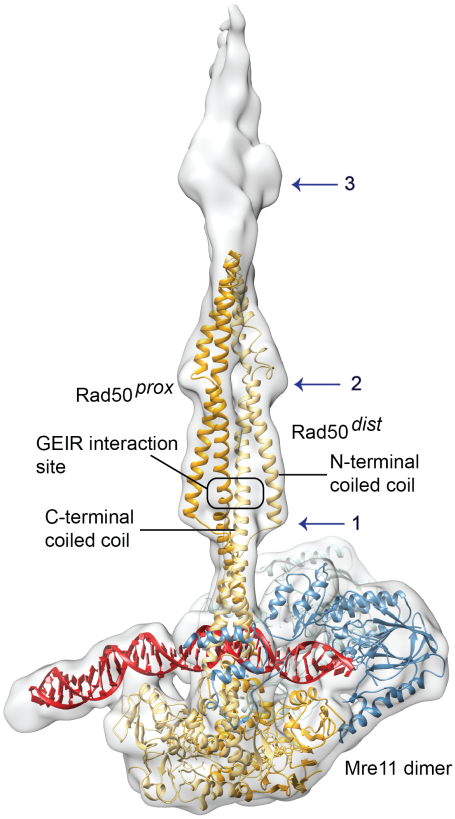

Figure 19: Density and ribbon model of the coiled coils of *Ec*MR. Model of *Ec*MR with long coiled coils fitted in the cryo-EM reconstruction. The N-terminal and C-terminal part of the antiparallel coiled coils are indicated, as well as the first interaction site between the C-terminal portion of the coiled coils (GEIR interaction site). Breaks in the coiled coils are indicated with blue arrow and numbers.

The ATPase cycle of *Ec*MR is still enigmatic and the cutting state poses the question how ATP and ADP exchange might occur. The cutting state represents a post-hydrolysis state, since ADP is present in the structure. ADP seems not to be able to engage the NBDs of *Ec*MR and does not

result in DNA binding or degradation (see Section 2.1, Figure 2 and 2.2, Figure S4). However, the cutting state bound to DNA and ADP seems to be long lived, since it was the major state observed in cryo-EM, despite the presence of ATP. Possibly, the DNA holds the NBDs together after the hydrolysis of ATP. Closer investigation of the *Ec*MR surface reveals that no cavity large enough to channel ADP to the outside is visible in the structure. Thus, exchange of ADP with ATP likely requires opening of the Rad50-Rad50 interface, which has been observed previously for *T. maritima* Rad50[181]. This might indicate that the DNA:MR complex disassembles each time the ADP has to be exchanged for ATP. However, in light of the proposed DNA tethering function of the MR complex[166,189,294] and the stimulation of the ATPase activity of MR(N) complexes from different organisms by DNA[182,183], this seems unlikely. Alternatively, a state with a Rad50 interface that opens only slightly for ADP-ATP exchange or a mechanism in which ATP is hydrolysed in an alternating fashion by the two active sites is possible. Similar mechanisms have been discussed for the related ABC transporters (see below).

ABC transporters are widely distributed in the phylogenetic tree and are an important class of transporters that either import or export their substrate in or out of the cell[295]. In addition to their NBD, ABC transporters contain a transmembrane domain[296]. Transport of substrate molecules across the membrane is coupled to ATP hydrolysis in ABC transporters[296], and two basic models have been proposed.
In the switch model, the transporter exists in a ATP-bound state with engaged NBDs and in an ATP free state with disengaged NBDs during the reaction cycle[297]. This is similar to the situation observed in nucleotide-free and nucleotide-bound *Tm*MR[181]. However, since the ATP concentration in cells is relatively high (e.g. between 1 and 2 mM for *E.coli* cells[298]), most ATP binding proteins, including Rad50 are likely bound to nucleotides most of the time. This might indicate that once the NBDs have released ADP they are instantly bound by ATP. Thus, a small dissociation of the two NBDs is probably enough to exchange ADP with ATP.
Alternatively, the constant contact model is proposed for ABC transporters, in which the two NBDs are always connected by at least one bound ATP and hydrolyse ATP sequentially[299,300]. A similar model for Rad50 would sidestep the question if the DNA can be bound while ADP is exchanged for ATP since such a mechanism probably only requires small conformational changes and would allow continued DNA binding.
For Rad50 it was shown that both active sites are required for ATPase activity. Mutations on one or both active sites drastically decreased the ATPase activity in response to DNA stimulation as well as nuclease activity, DNA binding activity and ATM activation[182].
To decipher the ATP hydrolysis cycle of *Ec*MR a more thorough biochemical characterisation is necessary. The measurement of k_{on} and k_{off} values for the DNA binding might already give a good hint of how rapid DNA is released from the complex. DNA release might also be coupled to the cleavage reaction of the nuclease, which would not have been observed by us in cryo-EM, due to the use of a nuclease dead Mre11 mutant. It should also be noted that the DNA cleavage reaction of *Ec*MR is very inefficient, requiring several hundred ATP molecules per cut (see

Section 2.1).

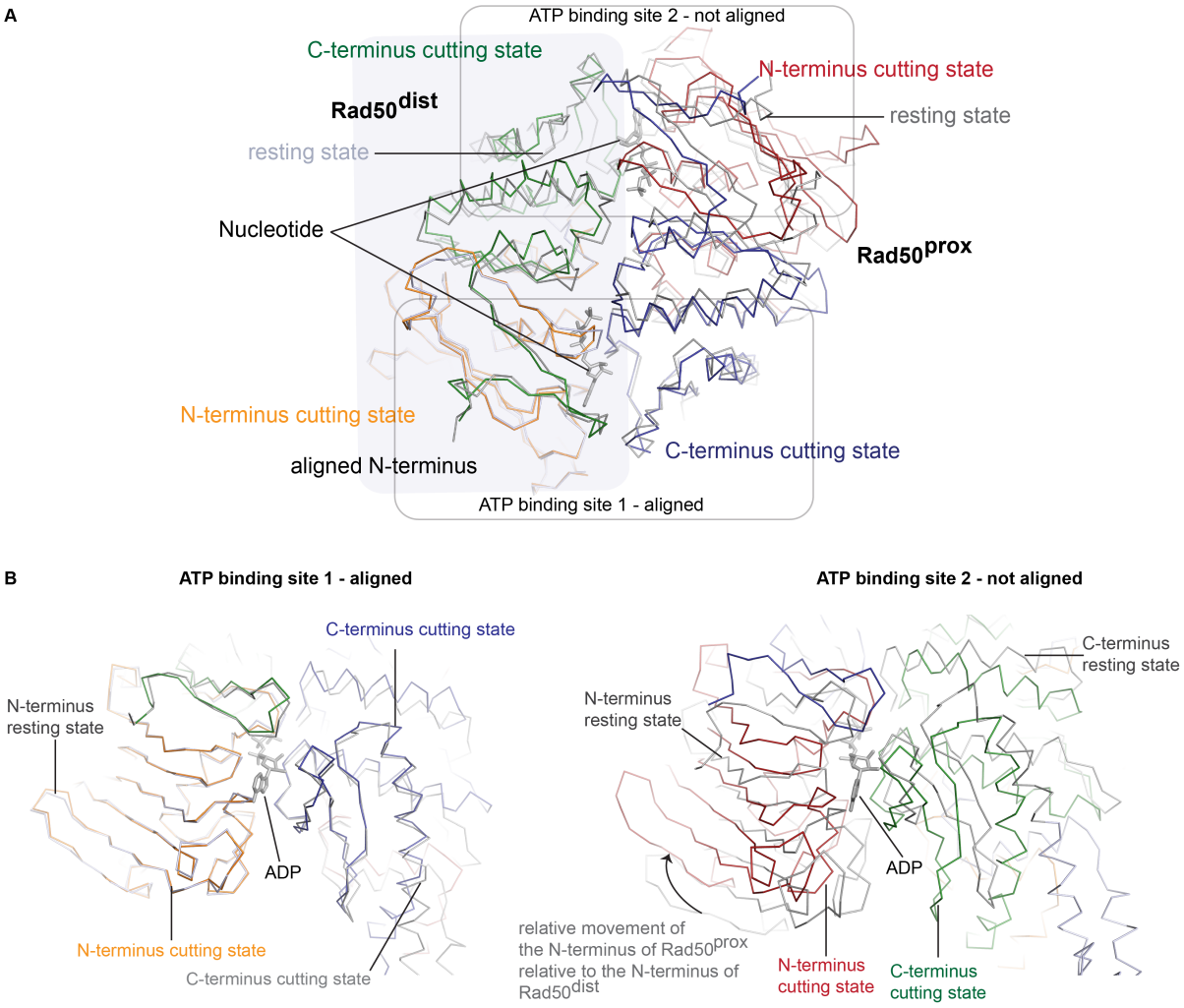

Figure 20: Movement of the Rad50 dimers relative towards each other. (A) The Rad50 dimer is shown from below. The Rad50^{dist} monomer is highlighted by a grey background. The resting state Rad50 is shown as a grey backbone. The cutting state NBDs of Rad50 are coloured in different colours: the N-terminus of Rad50^{dist} (orange), the C-terminus of Rad50^{dist} (green), the N-terminus of Rad50^{prox} (red) and the C-terminus of Rad50^{dist} (blue). The N- terminal domain of the Rad50^{dist} domain was aligned between the cutting and the resting state. ADP is indicated in grey. (B) The ATP binding site containing the aligned N-terminus of Rad50^{dist} (orange) in close up. (C) The ATP binding site of the not aligned N-terminus of Rad50^{prox} (red).

The movement of Rad50 is much more complex than the movement of Mre11 and alignment of *Ec*Rad50 in the cutting and the resting state indicate that conformational changes take place in the Rad50^{NBDs} (see Figure 20). Alignment of the Rad50^{dist} N-terminal residues (aa1-176, forming ATP binding site 1 in Figure 20) shows that this part of the protein aligns very well in resting and cutting state (see Figure 20 A and B). Residues connecting the Q-loop (F157 onwards) and the coiled coils are situated slightly different in the cutting and the resting state structure. The Rad50^{prox} C-terminus that is involved in forming this ATP binding site is well

aligned in proximity to the bound ADP but starts to deviate stronger past the nucleotide binding site (compare the blue and green coloured C-terminus in Figure 20 B and C). This indicates that the two ATP binding sites are shifted in respect to each other. Since the positions of the conserved motifs in the NBDs[180] are very similar in cutting and resting state it is not possible to deduce the reason why ATP hydrolysis is stimulated upon DNA binding. A transition state of *Ec*MR in complex with DNA and an ATP homolog would certainly help to elucidate this mechanism.
The largest deviation from the resting state structure in an alignment of the Rad50^{dist} N-terminus are the β-sheets in theRad50^{prox} N-terminus (see Figure 20 B). To accommodate the DNA an upward movement of this part of Rad50 is necessary, otherwise the protein and DNA would clash. This also means that in the scanning state the NBDs have to move, to allow binding of DNA, without closing of the coiled coils. Alternatively, the DNA might be bound in a different fashion, e.g. not be bend as strong as in the final cutting state.

3.4 Model for the Endonucleolytic Cleavage Based on the Existing Structure of the Exonuclease

The cutting state structure solved in this work shows the *Ec*MR exonuclease activity. Assuming the DNA binding mode is similar for the endo- and the exonuclease activity, biochemical data in combination with the solved structure is used to discuss three possible models of the endonuclease.
In the first and most likely model, the blocked DNA end is located next to Rad50, while the DNA extends through a tunnel close to the active site. This assumption is primarily based on the footprint of *Ec*MR and the observed 23-27 bps that are located between a protein block and the Mre11 cleavage site (see 2.1, Figure 2). The exit tunnel is formed between nuclease, capping and linker domains of Mre11 and the NBD of one Rad50 monomer and has approximate dimensions of 30x13 Å, which could allow the accommodation of a duplex DNA molecule, depending on the binding mode. However, closer inspection of the DNA strand that is located in the active site and addition of one more base to this strand shows that severe kinking of the dsDNA is required to avoid clashes with the Mre11 nuclease domain (see Figure 21 A and B).

Since the nuclease domain has been crystallised from several organisms and only one conformation of the active site was observed in all these structures, it is likely to assume that the nuclease adopts only one conformation[162,171,187]. However, this means that the DNA has to be bend severely to exit the nuclease active site. If no other large conformational changes occur on the protein level, additional melting of the DNA is required to allow accommodation in the exit tunnel. A melting mechanism is supported by higher endonuclease activity observed on AT-rich stretches of dsDNA and the partial rescue of the endonuclease deficient interface mutant Mre11^{V68D} by bubbles in the DNA substrate (see Section 2.1). Additionally, extra density next to the active site is present, that could either stem from the dsDNA or the sealing loop, which

is unordered in the cutting state (see Figure 21 A). It was not possible to build the pairing nucleotide opposite of the nucleotide located in the active site, due to poor density. This could indicate a higher degree of flexibility stemming either from its terminal position in the DNA duplex or melting of the DNA duplex by *Ec*MR. Unwinding of a DNA end by *hs*MRN has been reported previously[286,301].

Another indication that the described exit tunnel might play a role for the endonuclease activity comes from biochemical data of the Mre11 linker between capping domain and HLH motif. Changing the linker length increased the endonuclease activity for the addition of 5 and 8 aa residues but not for 3 and 11 residues. The exonuclease activity was slightly increased in Mre11 linkers containing 5, 8 or 11 extra residues. However, the ATPase activity was similar to the wild type (unpublished data). This might indicate that due to the increased flexibility of this part of Mre11, the DNA can be accommodated better and cleaved more efficiently.

Interestingly, two different cleavage chemistries were found for *Ec*MR and the 3′ exonuclease and the 5′ endonuclease produce chemically equivalent cleavage products (see Section 2.1, Figure 5). Assuming the Mre11 nuclease does not adopt different conformations in these two states, the DNA likely binds in a similar manner for 3′ exonuclease and 5′ endonuclease cleavage. This would allow attacking and cleaving the bond between two nucleotides in a similar manner and supports a model in which the 3′ exonuclease and the 5′ endonuclease bind DNA in the same way relative to the nuclease active site. Indeed, the proposed endonuclease model would result in a 3′ phosphorylated block free DNA end after cleavage (see Section 2.1, Figure 6).

The exit tunnel does not show a distinct charge that directly indicates DNA binding properties. In the beginning of the linker several arginine residues are spaced in close proximity from each other (R339, R340, R342, R345), that could possibly help to guide the DNA through the tunnel. Additionally, R225 of the Mre11 nuclease domain is located in close proximity to the active site and might interact with the exiting DNA. However, since the DNA might be threaded through the tunnel as ssDNA, other interactions, e.g. between the DNA bases and aromatic or hydrophobic amino acid residues are possible.

The proposed structure of the endocut also has implications for the mechanism. For the exonuclease state a simple flipping of the Mre11 dimer can be assumed. However, for the proposed endonuclease state this is not possible, since the Mre11 linker would not be able to move from a position above the DNA in the scanning state to a position below the DNA in the endonuclease state. Since *Ec*MR can cleave off blocks that are much larger than the exit channel, it is very unlikely that the blocked DNA can actually be threaded through this channel. Alternatively, an interface might open up to allow the blocked DNA to pass this channel, which could be either the Rad50^{coiledcoils}:Mre11^{HLH} or the Mre11 dimer interface. Since the Rad50^{coiledcoils}:Mre11^{HLH} interface represents the main interaction site between Mre11 and Rad50 it seems more likely that the Mre11 dimer interface opens up. Linking the Mre11 dimers with a LisH dimerization domain[302] separated by a 8 or 11 aa linker, indeed lowered the endonuclease activity of *Ec*MR slightly (see Section 2.2, Figure 5 and Supplementary Figure S6). However, it should be noted that a functional Mre11 dimer interface

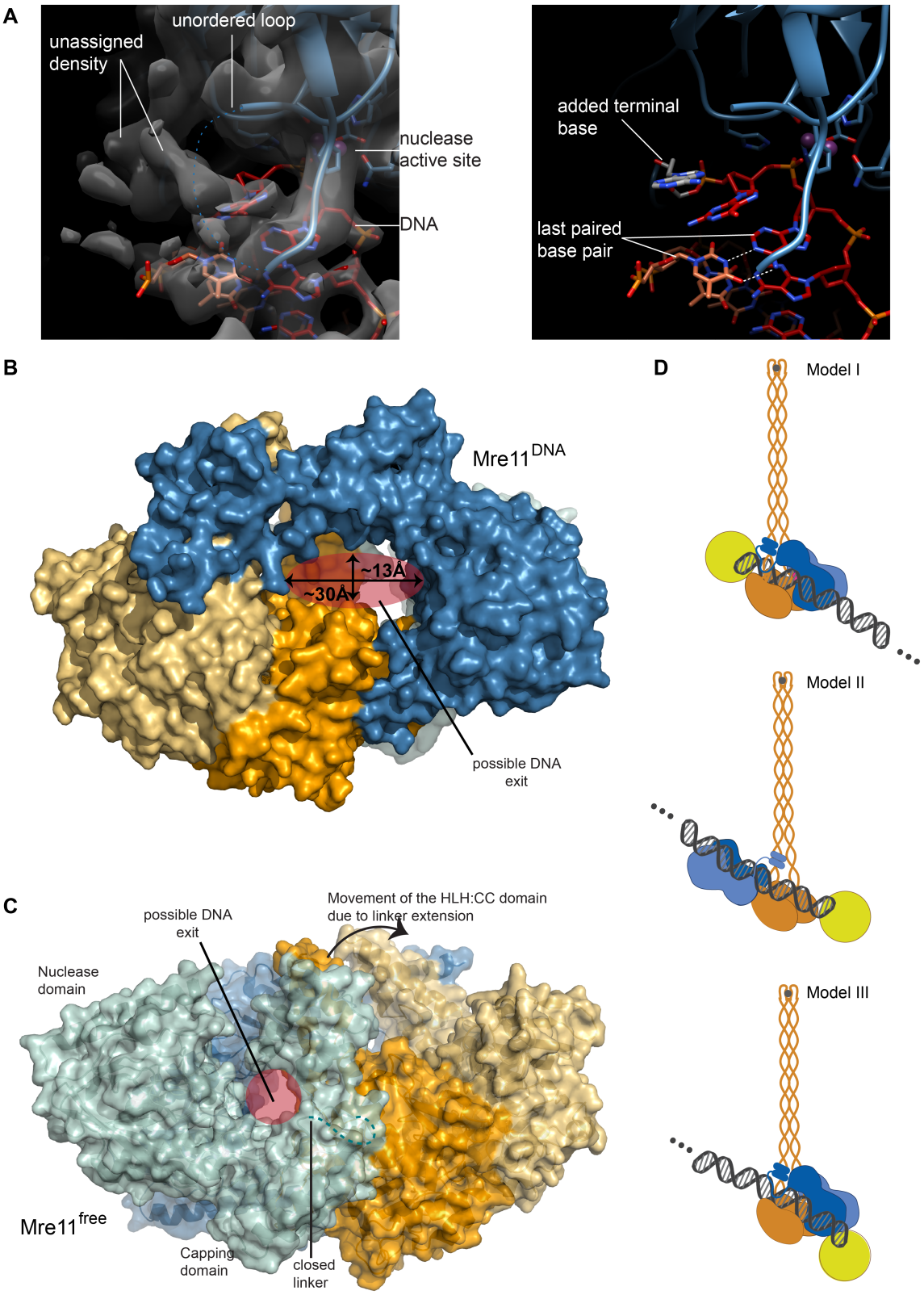

Figure 21: Possible DNA exit site for the endocut. (A) Additional density next to the active site that could be DNA extending from the active site (left). Addition of one more

Figure 21: base shows that a sharp kink is required in the DNA to be accommodate in the exit tunnel. Likely, this sharp kink does not allow proper base pairing in the limited space of the exit tunnel and results in melting of the DNA. The added base is shown in grey (right). (B) The possible DNA exit channel in the Mre11^{DNA} monomer, that would correspond to a 5′ endonuclease that resembles the 3′ exonuclease. (C) The possible DNA exit channel in the Mre11^{free} monomer that is not engaged with the DNA in the current structure. To accommodate the DNA structural rearrangement are necessary, especially in the linker of Mre11. (D) Three possible models for the endonuclease. The protein block would be bound next to the Rad50 dimer and the DNA is engaged either by the Mre11^{DNA} monomer (model I, possibly 5′ endonuclease) or the Mre11^{free} monomer (model II, possibly 3′ endonuclease). These two options are the preferred models. Alternatively, the block might be located next to the Mre11 dimer (model III).

is important for the nuclease function[166] and a mutation in the hydrophobic interface of *Ec*Mre11 (Mre11^{V68D}) abolishes block induced endonuclease activity (see Section 2.1, Figure 4). Additionally, until now all structures of Mre11, either alone or in complex with Rad50 or DNA show a dimer[162,170,174,181,187].

In the second model that shall be discussed here, the DNA blocked end is also located next to Rad50, however, the Mre11^{free} monomer would be involved in DNA binding. The Mre11^{free} monomer is in a conformation, in which the linker is already located on the same side as the capping and nuclease domain. Since the linker adopts a closed conformation in this monomer, only a small opening is formed between the coiled coils and the nuclease domain, that would not be large enough to accommodate a dsDNA duplex (see Figure 21 C). Additionally, in the current conformation the DNA could not reach the active site of this Mre11^{free} monomer. This is due to the coiled coils located close to the Mre11 nuclease domain, which is a result of the closed Mre11^{free} linker.
However, if the linker adopts a similar elongated conformation as the Mre11^{DNA} monomer this would allow the DNA to reach the Mre11 active site without obligate opening of an interface. Presumably, this would also require the linker of the Mre11^{DNA} monomer to adopt a closed conformation. Consequently, a very similar conformation to the one seen now would be adopted, with the exception of Mre11^{free} being involved in DNA binding. An alternative visualisation is to imagine the Mre11 dimer swinging from its resting state position to the other side of the Rad50 dimer while retaining DNA binding to the same Mre11 monomer as in the exonuclease state.
Since 3′ and 5′ endonuclease display a different cleavage chemistry, this might result from DNA binding to the Mre11^{free} monomer. Possibly, this puts DNA and nuclease active site in an alternative orientation towards each other, resulting in a different cleavage chemistry.
The two models described above do not exclude each other necessarily and a complex mechanism in which both Mre11 nuclease active sites are employed sequentially is possible. Such a mechanism would explain the two active sites that are present in the *Ec*MR complex and to my knowledge also in all other known MR(N) complexes, while only one Mre11 monomer is bound to DNA in the cutting state. Furthermore, it is not clear if the endonuclease cleavage of

both strands is performed by the same *Ec*MR molecule or sequentially by different molecules. One important difference between the exo- and the endonuclease activity of *Ec*MR is that the exonuclease only requires binding of ATP while the endonuclease also depends on ATP hydrolysis and was not functional with any of the commonly used ATP analogous in our hands. This shows that in the endonuclease mechanism at least one step requires the energy from the hydrolysis of ATP. Based on the two proposed models, bending and melting of the DNA could be such a step. Since ATP hydrolysis is not necessary during exonucleolytic incision, this clearly indicates a mechanistic difference.

In the third proposed model, the block is located next to Mre11. The active site would be located closer to the blocked DNA end than in the other two models. Thus, smaller DNA fragments should be cleaved off the blocked DNA end. One study reported a 10 bp spacing between the cleavage sites of *Ec*MR. These products were found with dsDNA, hairpins and palindromes, and it was suggested that *Ec*MR proteins serve as block for other *Ec*MR complexes. Thus, the authors propose a model in which several *Ec*MR molecules sit on a DNA end and serve as a molecular ruler[268]. However, the exonuclease structure indicates that the footprint for *Ec*MR is about 22 bp, which would not fit to the proposed 10 bp spacing.
In addition, the observed cleavage chemistry does not seem to fit the third model. The DNA end from which a protein block was cleaved contains a 3′ and 5′ phosphate (see Section 2.1, Figure 6). We assume that in the observed cutting state a nucleotide monophosphate would be cleaved off the 3′ DNA end and leave a 3′ OH group. Since the DNA is bound in the same way in model three and the cutting state, the same cleavage mechanism is expected. Thus, the 3′ end of the cleaved end would contain a 3′ OH and no 3′ phosphate group. This third model is considered to be the most unlikely of the three proposed models.

In addition, a completely different arrangement of the single subunits or a second DNA binding mode is also possible. Crystal structures of Mre11 with DNA shows the DNA bound different to what was found in the cutting state[166,284] (see Section 3.1 and 1.3.1, Figure 7). However, these structures lack the NBDs of Rad50 and thus might not represent the DNA binding conformation in the full-length complex. Since the structures were obtained with X-ray crystallography, crystal contacts might have assisted the formation of the observed Mre11:DNA complexes.

Interestingly, MR(N) does not seem to show a particular preference for a specific block[122,285] and *Ec*MR's endonuclease activity is stimulated by streptavidin, a single chain fragment for fluorescein (FAM-scFv) and *Ct*Ku70/80 (see Section 2.2, Supplementary Figure S6). Of these protein blocks, Ku70/80 is the most relevant, since in contrast to streptavidin and FAM-scFv it sits directly on the DNA[303] and is not attached via a flexible linker. Upon Ku70/80 binding, the endonuclease cut of *Ec*MR shifts from approx. 25 bp from the end to approx. 35 bp from the end (see 2.2, Figure S6). Depending on the orientation of *Ec*MR and Ku70/80 towards each other, the shift of 10 bp fits well with the DNA stretch covered by Ku70/80 in a

crystal structure[303]. Similarly, eukaryotic MR has been shown to cleave Ku70/80 covered DNA ends[285].This indicates, that the recognition of protein blocked DNA ends might be similar in eukaryotic and prokaryotic complexes.
However, this poses several questions: How is the MR(N) complex able to recognise Ku70/80 at a protein end? How is the Ku blocked end distinguished from other proteins on a DNA e.g. Nucleosomes? And does MR(N) also recognise and possibly cleave other structures that resemble protein blocked ends, e.g. RecA/RPA covered stretches of single-stranded DNA at the boundary to dsDNA?
Ku forms a ring around the DNA[303]. Thus it is not very likely that MR(N) is able to melt the DNA covered by Ku. This would mean that MR(N) not only melts DNA far outside its active site but also works against the counterpressure Ku would generate on a melted DNA duplex. Consequently, MR(N) probably does not recognise the DNA end by its increased ability to melt. Since *Ec*MR cuts various protein blocks, there is no requirement for a specific protein bound to the DNA end that might be recognised. Interestingly, *Ec*MR is not able to cut a plasmid that has been circularised by streptavidin, while it is still able to cleave a plasmid with two streptavidin blocked ends (see Section 2.2 Figure 5). Since the protein blocks are chemically exactly the same, this indicates that the DNA topology might be the actual feature that allows *Ec*MR to distinguish a protein located on an end from a protein that is located in a closed DNA ring. In the scanning mode proposed here, the coiled coils would be the domain that enables the complex to recognise DNA ends (see Figure 18). Binding to a circular DNA would prevent complete closing of the coiled coils and thereby the conformational change that allows the nuclease to move from its autocatalytic position to its nuclease active state. This would also provide an elegant mechanism to distinguish a protein blocked end from proteins that are present on the DNA e.g. Nucleosomes, transcription factors or the transcription machinery. Recognition of the DNA topology thus is an essential feature of the proposed scanning mechanism (see Figure 18).
For the *Ec*MR complex it would also be interesting to assess whether it is able to cleave any structures that arise during DNA metabolism, e.g. during HR or replication. Since these structures contain abnormal DNA structures like protein covered ssDNA[8,91], it will be interesting to test if this is recognised by MR(N) and if yes how DNA degradation is prevented in a cellular context.

3.5 The Bacterial *Ec*MR Complex as a Model for the Eukaryotic System

The structures of the Mre11 nuclease and capping domain and the Rad50 NBDs are quite conserved in their structure[116]. To illustrate if the eukaryotic complex could function similar to *Ec*MR, the *S.pombe* Mre11 dimer in complex with Nbs1[170] was aligned onto the *E.coli*

Mre11^{DNA}and the *C.thermophilum* Rad50 dimer[175] was aligned on the *E.coli* Rad50^{prox} (see Figure 22). The aligned monomers fit very well to *Ec*MR, while the not aligned monomer, deviates for both Mre11 and Rad50. For Mre11 this might be a result of the different dimer angle observed for different organisms[116] and for Rad50 the binding of ADP and DNA with closed coiled coils versus binding of Rad50 with bound ATPγS and open coiled coils is the reason[175].

For the *Ec*MR complex an additional interface is formed between Rad50 and Mre11 in the cutting state, denoted the fastener. Mutations in this interface result in a decrease in nuclease activity, especially endonuclease activity and a charge reversal can partially rescue the single mutants. This interface is not formed in the eukaryotic model, since the corresponding loop is not present in *Sp*Mre11 (see Figure A). The Mre11 fastener of *E.coli* interacts with the outer β-sheets of Rad50 for which separation of function mutations have been reported. These Rad50S mutants in *S. cerevisiae* seem to have more severe defects in meiosis than DNA repair[186] and map to the β-sheet that is involved in the new interaction site with the Mre11 fastener.
In the eukaryotic model Rad50 and Mre11 are located more than 6 Å apart from each other at this new interface. Thus they do not seem to be able to interact directly with each other. However, a new interaction platform might be created for other proteins, e.g. CtIP. Interestingly, Nbs1 is also located very close to this site, which could mean, that an additional Nbs1 interaction site is formed upon DNA binding. Alternatively, a protein that binds to this site would be in very close proximity to Nbs1 and thus could interact with all three proteins of the eukaryotic MRN complex at one site.

Inspection of the active site of the eukaryotic model shows that the DNA could be accommodated in a similar manner as in *Ec*MR (see Figure 22 B) with only minor rearrangements. Supposed in the endonuclease state the block is indeed located next to Rad50 and the DNA extends through the opening next to the nuclease actives site as described in model I in Section 3.4 (see Figure 21 D, top), it would also be possible for the eykaryotic complex to adopt this conformation as observed from the model (see Figure 22 B).
The *Ct*Rad50 structure was solved in complex with DNA and binding was observed to the NBD, as in *Ec*MR. Binding to the coiled coils was not observed in this crystal structure[175], probably a result of the shortened coiled coils. Due to the poor sequence conservation in the coiled coils, it is not possible to identify the DNA binding residues corresponding to the ones identified in the *E.coli* coiled coils based on the amino acid sequence. However, especially in the beginning of the N-terminal coiled coil of *C. thermophilum* are several basic residues, that could be involved in forming a DNA binding interface (K184, K187, R193, K196). These residues are conserved in human, mouse and yeast in regard of their basicity and are either a lysine or arginine residue (see Figure 22). In the C-terminal part of the coiled coils no such conserved residues could be found, however, close to the coiled coils is a β-sheet insertion that possibly has to move together with the coiled coils. In these β-sheets additional four Arginines are located (R1171, R1186, R1185, R1191) that are quite conserved and might move towards the DNA in the cutting state. Studies with the human complex have indicated that rod formation of the coiled coils can be observed with crystallography[191] and with AFM in response to DNA binding[195]. Future studies

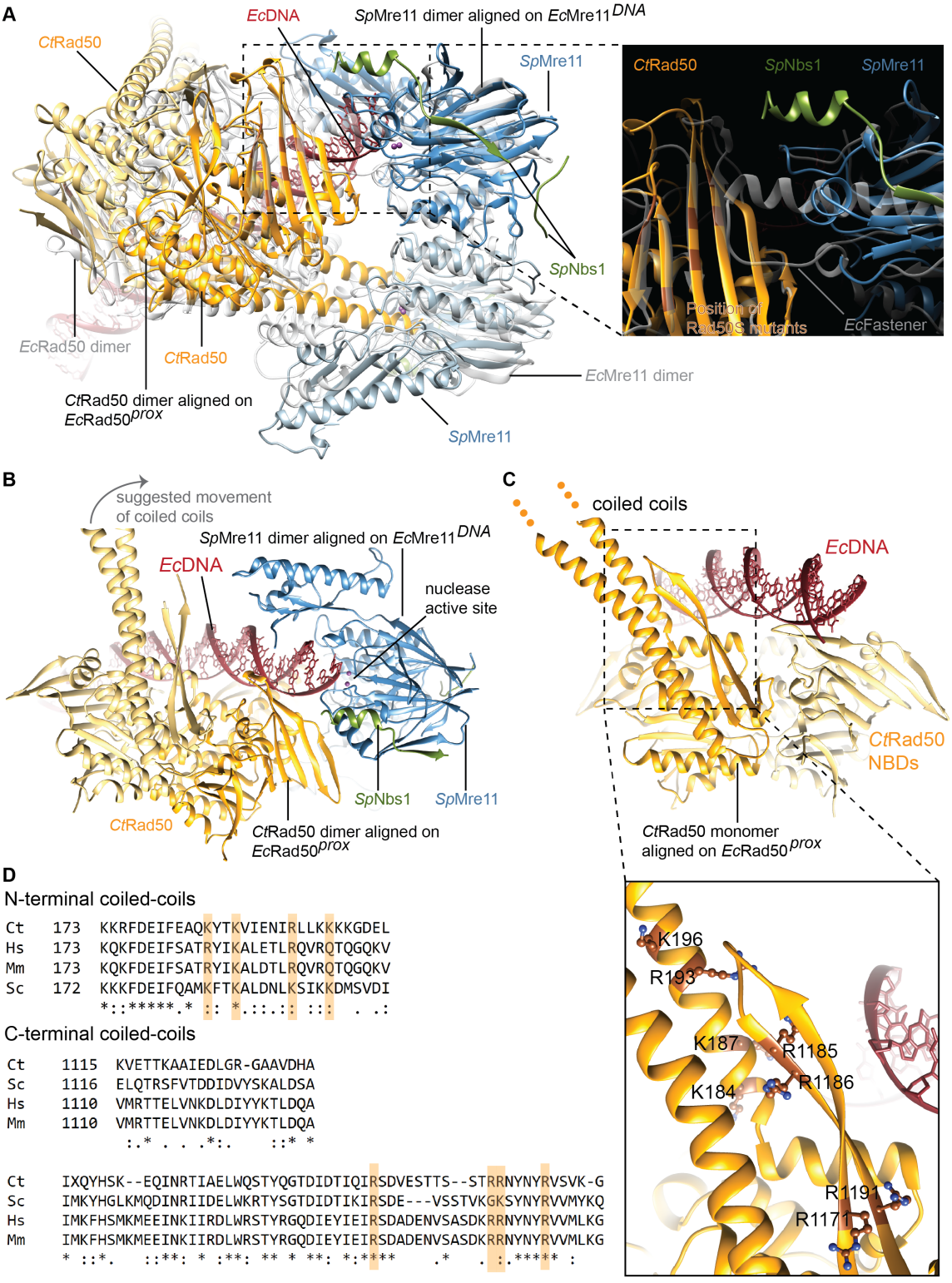

Figure 22: Alignment of eukaryotic structures on the *Ec*MR cutting state. (A) The *C. termophilum* Rad50 dimer (pdb: 5da9) and the *S.pombe* Mre11:Nbs1 complex

Figure 22: (pdb: 4fbq) were aligned on Mre11^{DNA}and *Ec*Rad50^{prox}, respectively. *Ec*MR is shown in grey and the eukaryotic complexes are coloured in blue (Mre11), orange (Rad50) and green (Nbs1). Positions of Rad50S mutants are shown in brown. A close up of the *Ec*MR fastener interface and the corresponding interface in the eukaryotic complex is shown on the right hand side. (B) The possible active site of a eukaryotic complex. (C) Possible DNA binding by the *Ct*Rad50 coiled coils. (D) Sequence alignment of the N- and C-terminal part of the coiled coil domain of *C. termophilum*, *S. cerevisiae*, human and mouse. Conserved basic residues are highlighted.

with the eukaryotic complex are necessary to elucidate the exact binding mode of MRN to DNA.

Taken together the result generated during this thesis provide first insight into the mechanism of the full-length *Ec*MR complex that can possibly also be extrapolated to the eukaryotic MRN complex to large extends. The structural and biochemical data give a more comprehensive view of the exonuclease and endonuclease activity and future studies will hopefully be able to depict the mechanism in more detail.

4 Bibliography

[1] Bruce Alberts, Alexander Johnson, Julian Lewis, David Morgan, Martin Raff, Keith Roberts, and Peter Walter. *Molecular Biology of the Cell*. Garland Science, 6th edition, 2015.

[2] Nimrat Chatterjee and Graham C. Walker. Mechanisms of DNA damage, repair, and mutagenesis. *Environmental and Molecular Mutagenesis*, 58(5):235–263, 2017.

[3] Richard Fishel. Mismatch repair. *Journal of Biological Chemistry*, 290(44):26395–26403, 2015.

[4] Yun-Jeong Kim and David M. Wilson III. Overview of Base Excision Repair Biochemistry. *Current Molecular Pharmacology*, 5(1):3–13, 2012.

[5] Graciela Spivak. Nucleotide excision repair in humans. *DNA Repair (Amst).*, 36:13–18, 2015.

[6] Keith W. Caldecott. Single-strand break repair and genetic disease. *Nature Reviews Genetics*, 9 (8):619–631, 2008.

[7] Howard H.Y. Chang, Nicholas R. Pannunzio, Noritaka Adachi, and Michael R. Lieber. Non-homologous DNA end joining and alternative pathways to double-strand break repair. *Nature Reviews Molecular Cell Biology*, 18(8):495–506, 2017.

[8] William Douglass Wright, Shanaya Shital Shah, and Wolf Dietrich Heyer. Homologous recombination and the repair of DNA double-strand breaks. *Journal of Biological Chemistry*, 293(27): 10524–10535, 2018.

[9] Helen Walden and Andrew J. Deans. The Fanconi Anemia DNA Repair Pathway: Structural and Functional Insights into a Complex Disorder. *Annual Review of Biophysics*, 43:257–278, 2014.

[10] Chengqi Yi and Chuan He. DNA repair by reversal of DNA damage. *Cold Spring Harbor Perspectives in Biology*, 5(1):a012575, 2013.

[11] Stephen Jackson and Jiri Bartek. The DNA-damage response in human biology and disease. *Nature*, 461(7267):1071–1078, 2009.

[12] Wynand P. Roos, Adam D. Thomas, and Bernd Kaina. DNA damage and the balance between survival and death in cancer biology. *Nature Reviews Cancer*, 16(1):20–33, 2016.

[13] Rebecca L. Siegel, Kimberly D. Miller, and Ahmedin Jemal. Cancer statistics, 2018. *CA: A Cancer Journal for Clinicians*, 68(1):7–30, 2018.

[14] visited on 2019/11/29. URL `https://ec.europa.eu/eurostat/statistics-explained/index.php?title=Causes_of_death_statistics#Main_findings`.

[15] Kahlin Cheung-Ong, Guri Giaever, and Corey Nislow. DNA-damaging agents in cancer chemotherapy: Serendipity and chemical biology. *Chemistry and Biology*, 20(5):648–659, 2013.

[16] Christopher J. Lord and Alan Ashworth. The DNA damage response and cancer therapy. *Nature*, 481(7381):287–294, 2012.

[17] D. Bell and et al. Integrated genomic analyses of ovarian carcinoma. *Nature*, 474(7353):609–615, 2011.

[18] Hannah Farmer, Huala McCabe, Christopher J. Lord, Andrew H.J. Tutt, Damian A. Johnson, Tobias B. Richardson, Manuela Santarosa, Krystyna J. Dillon, Ian Hickson, Charlotte Knights, Niall M.B. Martin, Stephen P. Jackson, Graeme C.M. Smith, and Alan Ashworth. Targeting the DNA repair defect in BRCA mutant cells as a therapeutic strategy. *Nature*, 434(7035):917–921, 2005.

[19] Christopher J. Lord and Alan Ashworth. PARP inhibitors: Synthetic lethality in the clinic. *Science*, 355(6330):1152–1158, 2017.

[20] Gabriella Fabbrocini, Maria Triassi, Maria Chiara Mauriello, Guglielma Torre, Maria Carmela Annunziata, Valerio de Vita, Francesco Pastore, Vincenza D'Arco, and Giuseppe Monfrecola. Epidemiology of skin cancer: Role of some environmental factors. *Cancers (Basel).*, 2(4):1980–1989, 2010.

[21] Errol C Friedberg, Graham C Walker, Wolfram Siede, Richard D Wood, Roger A Schultz, and Tom Ellenberger. *DNA Repair and Mutagenesis*. ASM Press, 2nd edition, 2006.

[22] Dragony Fu, Jennifer A. Calvo, and Leona D. Samson. Balancing repair and tolerance of DNA damage caused by alkylating agents. *Nature Reviews Cancer*, 12(2):104–120, 2012.

[23] J. W. Bennett and M. Klich. Mycotoxins. *Clinical microbiology reviews*, 16(3):497–516, 2003.

[24] Rinne De Bont and Nik van Larebeke. Endogenous DNA damage in humans: A review of quantitative data. *Mutagenesis*, 19(3):169–185, 2004.

[25] Lawrence A Loeb and Raymond J Monnat. DNA polymerases and human disease. *Nature Reviews Genetics*, 9(8):594–604, 2008.

[26] Thomas A. Kunkel and Dorothy A. Erie. Eukaryotic Mismatch Repair in Relation to DNA Replication. *Annual Review of Genetics*, 49:291–313, 2015.

[27] Brown T. A. *Genomes*. Wiley-Liss, 2nd edition, 2002.

[28] Robert J. Buckland, Danielle L. Watt, Balasubramanyam Chittoor, Anna Karin Nilsson, Thomas A. Kunkel, and Andrei Chabes. Increased and Imbalanced dNTP Pools Symmetrically Promote Both Leading and Lagging Strand Replication Infidelity. *PLoS Genetics*, 10(12):e1004846, 2014.

[29] Benjamin D. Bax, Garib Murshudov, Anthony Maxwell, and Thomas Germe. DNA Topoisomerase Inhibitors: Trapping a DNA-Cleaving Machine in Motion. *Journal of Molecular Biology*, 431(18): 3427–3449, 2019.

[30] Lance Stewart, Matthew R. Redinbo, Xiayang Qiu, Wim G. J. Hol, and James J. Champoux. A model for the mechanism of human topoisomerase I. *Science*, 279(5356):1534–1541, 1998.

[31] Yves Pommier, Glenda Kohlhagen, Philippe Pourquier, Jane M Sayer, Heiko Kroth, and Donald M Jerina. Benzo[a]pyrene diol epoxide adducts in DNA are potent suppressors of a normal topoisomerase I cleavage site and powerful inducers of other topoisomerase I cleavages. *Proceedings of the National Academy of Sciences of the United States of America*, 97(5):2040–2045, 2000.

[32] Philippe Pourquier, André A. Pilon, Glenda Kohlhagen, Abhijit Mazumder, Aditi Sharma, and Yves Pommier. Trapping of mammalian topoisomerase I and recombinations induced by damaged DNA containing nicks or gaps. Importance of DNA end phosphorylation and camptothecin effects. *Journal of Biological Chemistry*, 272(42):26441–26447, 1997.

[33] Matthew R. Redinbo, Lance Stewart, Peter Kuhn, James J Champoux, and Wim G.J. Hol. Crystal structures of human topoisomerase I in covalent and noncovalent complexes with DNA. *Science*, 279(5356):1504–1513, 1998.

[34] Tomas Lindahl. Instability and decay of the primary structure of DNA. *Nature*, 362(6422):709–715, 1993.

[35] Chongyuan Luo, Petra Hajkova, and Joseph R Ecker. Dynamic DNA methylation: In the right place at the right time. *Science*, 361(6409):1336–1340, 2018.

[36] E. S. Henle and S. Linn. Formation, prevention, and repair of DNA damage by iron/hydrogen peroxide. *Journal of Biological Chemistry*, 272(31):19095–19098, 1997.

[37] J. A. Imlay and I. Fridovich. Assay of metabolic superoxide production in Escherichia coli. *Journal of Biological Chemistry*, 266(11):6957–6965, 1991.

[38] Anthony W. Segal. How neutrophils kill microbes. *Annual Review of Immunology*, 23:197–223, 2005.

[39] Fabrice Collin. Chemical basis of reactive oxygen species reactivity and involvement in neurodegenerative diseases. *International Journal of Molecular Sciences*, 20(10):2407, 2019.

[40] Svein Bjelland and Erling Seeberg. Mutagenicity, toxicity and repair of DNA base damage induced by oxidation. *Mutation Research - Fundamental and Molecular Mechanisms of Mutagenesis*, 531 (1-2):37–80, 2003.

[41] Ted P. Szatrowski and Carl F. Nathan. Production of Large Amounts of Hydrogen Peroxide by Human Tumor Cells. *Cancer Research*, 51(3):794–798, 1991.

[42] Michael M Vilenchik and Alfred G Knudson. Endogenous DNA double-strand breaks: Production, fidelity of repair, and induction of cancer. *Proceedings of the National Academy of Sciences of the United States of America*, 100(22):12871–12876, 2003.

[43] Lamarche B J., N I Orazio, and Weitzman M D. The MRN complex in Double-Strand Break Repair and Telomere Maintenance. *FEBS Lett*, 584:3682–3695, 2010.

[44] Anuja Mehta and James E. Haber. Sources of DNA double-strand breaks and models of recombinational DNA repair. *Cold Spring Harbor Perspectives in Biology*, 6(9):a016428, 2014.

[45] Giuseppina D'Allesandro and d'Adda di Fagagna. Transcription and dna damage: Holding hands or crossing swords? *Journal of Molecular Biology*, 429:3215–3229, 2017.

[46] Michelle K. Zeman and Karlene A. Cimprich. Causes and consequences of replication stress. *Nature Cell Biology*, 16(1):2–9, 2014.

[47] Janeway Jr., Charles A. and Travers, Paul and Walport Mark and Capra, J. Donald. *The Immune System in Health and Disease*. Garland, 4th edition, 1999.

[48] Craig H Bassing, Wojciech Swat, and Frederick W Alt. The mechanism and regulation of chromosomal V(D)J recombination. *Cell*, 109:S45–S55, 2002.

[49] Rahul Arya and Craig H. Bassing. V(D)J Recombination Exploits DNA Damage Responses to Promote Immunity. *Trends in Genetics*, 33(7):479–489, 2017.

[50] Heng Ru, Melissa G Chambers, Tian-Min Fu, Alexander B Tong, Maofu Liao, and Hao Wu. Molecular Mechanism of V(D)J Recombination from Synaptic RAG1-RAG2 Complex Structures. *Cell*, 163(5):1138–1152, 2015.

[51] Luigi D Notarangelo, Min Sung Kim, Jolan E Walter, and Yu Nee Lee. Human RAG mutations: Biochemistry and clinical implications. *Nature Reviews Immunology*, 16(4):234–246, 2016.

[52] Zhenming Xu, Hong Zan, Egest J Pone, Thach Mai, and Paolo Casali. Immunoglobulin class-switch DNA recombination: induction, targeting and beyond. *Nature Reviews Immunology*, 12(7):517–31, 2012.

[53] Janet Stavnezer and Carol E. Schrader. IgH Chain Class Switch Recombination: Mechanism and Regulation. *The Journal of Immunology*, 193(11):5370–5378, 2014.

[54] Robert W Maul, Huseyin Saribasak, Stella A Martomo, Rhonda L McClure, William Yang, Alexandra Vaisman, Hillary S Gramlich, David G Schatz, Roger Woodgate, David M Wilson, and Patricia J Gearhart. Uracil residues dependent on the deaminase AID in immunoglobulin gene variable and switch regions. *Nature Immunology*, 12(1):70–76, 2011.

[55] Isabel Lam and Scott Keeney. Mechanism and Regulation of Meiotic Recombination Initiation. *Cold Spring Harbor Perspectives in Biology*, 7(1):a016634, 2014.

[56] Scott Keeney, Craig N Giroux, and Nancy Kleckner. Meiosis-specific DNA double-strand breaks are catalyzed by Spo11, a member of a widely conserved protein family. *Cell*, 88(3):375–384, 1997.

[57] Agnès Bergerat, Bernard De Massy, Danielle Gadelle, Paul Christophe Varoutas, Alain Nicolas, and Patrick Forterre. An atypical topoisomerase II from archaea with implications for meiotic recombination. *Nature*, 386(6623):414–417, 1997.

[58] Scott Keeney. Spo11 and the formation of DNA double-strand breaks in meiosis. *Genome Dynamics and Stability*, 2:81–123, 2008.

[59] Geoffrey P. Margison and Mauro F. Santibáñez-Koref. O6-alkylguanine-DNA alkyltransferase: Role in carcinogenesis and chemotherapy. *BioEssays*, 24(3):255–266, 2002.

[60] T A Kunkel. Evolving views of DNA replication (in)fidelity. *Cold Spring Harbor Symposia on Quantitative Biology*, 74:91–101, 2009.

[61] Josef Jiricny. Postreplicative mismatch repair. *Cold Spring Harbor Perspectives in Biology*, 5(4): a012633, 2013.

[62] Raphael Ceccaldi, Prabha Sarangi, and Alan D. D'Andrea. The Fanconi anaemia pathway: New players and new functions. *Nature Reviews Molecular Cell Biology*, 17(6):337–349, 2016.

[63] Kishore K. Chiruvella, Zhuobin Liang, and Thomas E. Wilson. Repair of double-strand breaks by end joining. *Cold Spring Harbor Perspectives in Biology*, 5(5):a012757, 2013.

[64] P. R. Blier, A. J. Griffith, J. Craft, and J. A. Hardin. Binding of Ku protein to DNA. Measurement of affinity for ends and demonstration of binding to nicks. *Journal of Biological Chemistry*, 268 (10):7594–7601, 1993.

[65] T. Mimori and J. A. Hardin. Mechanism of interaction between Ku protein and DNA. *Journal of Biological Chemistry*, 261(22):10375–10379, 1986.

[66] Xiaotong Yin, Mengjie Liu, Yuan Tian, Jiawei Wang, and Yanhui Xu. Cryo-EM structure of human DNA-PK holoenzyme. *Cell Research*, 27(11):1341–1350, 2017.

[67] Humayun Sharif, Yang Li, Yuanchen Dong, Liyi Dong, Wei Li Wang, Youdong Mao, and Hao Wu. Cryo-EM structure of the DNA-PK holoenzyme. *Proceedings of the National Academy of Sciences of the United States of America*, 114(28):7367–7372, 2017.

[68] Howard H.Y. Chang, Go Watanabe, Christina A Gerodimos, Takashi Ochi, Tom L Blundell, Stephen P Jackson, and Michael R Lieber. Different DNA end configurations dictate which NHEJ components are most important for joining efficiency. *Journal of Biological Chemistry*, 291(47): 24377–24389, 2016.

[69] Stephanie A. Nick McElhinny, Carey M. Snowden, Joseph McCarville, and Dale A. Ramsden. Ku Recruits the XRCC4-Ligase IV Complex to DNA Ends. *Molecular and Cellular Biology*, 20(9): 2996–3003, 2000.

[70] Yunmei Ma, Ulrich Pannicke, Klaus Schwarz, and Michael R. Lieber. Hairpin opening and overhang processing by an Artemis/DNA-dependent protein kinase complex in nonhomologous end joining and V(D)J recombination. *Cell*, 108(6):781–794, 2002.

[71] Kristijan Ramadan, Igor V Shevelev, Giovanni Maga, and Ulrich Hübscher. De Novo DNA synthesis by human DNA polymerase λ, DNA polymerase μ and terminal deoxyribonucleotidyl transferase. *Journal of Molecular Biology*, 339(2):395–404, 2004.

[72] Kristijan Ramadan, Giovanni Maga, Igor V. Shevelev, Giuseppe Villani, Luis Blanco, and Ulrich Hübscher. Human DNA polymerase λ possesses terminal deoxyribonucleotidyl transferase activity and can elongate RNA primers: Implications for novel functions. *Journal of Molecular Biology*, 328 (1):63–72, 2003.

[73] Jiafeng Gu, Haihui Lu, Brigette Tippin, Noriko Shimazaki, Myron F Goodman, and Michael R Lieber. XRCC4:DNA ligase IV can ligate incompatible DNA ends and can ligate across gaps. *EMBO Journal*, 26(4):1010–1023, 2007.

[74] John M Pryor, Crystal A Waters, Ana Aza, Kenjiro Asagoshi, Christina Strom, Piotr A Mieczkowski, Luis Blanco, and Dale A Ramsden. Essential role for polymerase specialization in cellular nonhomologous end joining. *Proceedings of the National Academy of Sciences of the United States of America*, 112(33):E4537–E4545, 2015.

[75] Haley D.M. Wyatt and Stephen C. West. Holliday junction resolvases. *Cold Spring Harbor Perspectives in Biology*, 6(9):a023192, 2014.

[76] Huichen Wang, Bustanur Rosidi, Ronel Perrault, Minli Wang, Lihua Zhang, Frank Windhofer, and George Iliakis. DNA ligase III as a candidate component of backup pathways of nonhomologous end joining. *Cancer Research*, 65(10):4020–4030, 2005.

[77] Emilie Rass, Anastazja Grabarz, Isabelle Plo, Jean Gautier, Pascale Bertrand, and Bernard S. Lopez. Role of Mre11 in chromosomal nonhomologous end joining in mammalian cells. *Nature Structural and Molecular Biology*, 16(8):819–824, 2009.

[78] Anyong Xie, Amy Kwok, and Ralph Scully. Role of mammalian Mre11 in classical and alternative nonhomologous end joining. *Nature Structural and Molecular Biology*, 16(8):814–818, 2009.

[79] Yibin Deng, Xiaolan Guo, David O. Ferguson, and Sandy Chang. Multiple roles for MRE11 at uncapped telomeres. *Nature*, 460(7257):914–918, 2009.

[80] Mieun Lee-Theilen, Allysia J Matthews, Dierdre Kelly, Simin Zheng, and Jayanta Chaudhuri. CtIP promotes microhomology-mediated alternative end joining during class-switch recombination. *Nature Structural and Molecular Biology*, 18(1):75–80, 2011.

[81] Isabelle Robert, Françoise Dantzer, and Bernardo Reina-San-Martin. Parp1 facilitates alternative NHEJ, whereas Parp2 suppresses IgH/c-myc translocations during immunoglobulin class switch recombination. *Journal of Experimental Medicine*, 206(5):1047–1056, 2009.

[82] Marc Audebert, Bernard Salles, and Patrick Calsou. Involvement of poly(ADP-ribose) polymerase-1 and XRCC1/DNA ligase III in an alternative route for DNA double-strand breaks rejoining. *Journal of Biological Chemistry*, 279(53):55117–55126, 2004.

[83] David W Wyatt, Wanjuan Feng, Michael P Conlin, Matthew J Yousefzadeh, Steven A Roberts, Piotr Mieczkowski, Richard D Wood, Gaorav P Gupta, and Dale A Ramsden. Essential Roles for Polymerase θ-Mediated End Joining in the Repair of Chromosome Breaks. *Molecular Cell*, 63(4): 662–673, 2016.

[84] Deniz Simsek, Erika Brunet, Sunnie Yan-Wai Wong, Sachin Katyal, Yankun Gao, Peter J McKinnon, Jacqueline Lou, Lei Zhang, James Li, Edward J Rebar, Philip D Gregory, Michael C Holmes, and Maria Jasin. DNA ligase III promotes alternative nonhomologous end-joining during chromosomal translocation formation. *PLoS Genetics*, 7(6):e1002080, 2011.

[85] Minli Wang, Weizhong Wu, Wenqi Wu, Bustanur Rosidi, Lihua Zhang, Huichen Wang, and George Iliakis. PARP-1 and Ku compete for repair of DNA double strand breaks by distinct NHEJ pathways. *Nucleic Acids Research*, 34(21):6170–6182, 2006.

[86] Jingxin Sun, Kyung Jong Lee, Anthony J. Davis, and David J. Chen. Human Ku70/80 protein blocks exonuclease 1-mediated DNA resection in the presence of human Mre11 or Mre11/Rad50 protein complex. *Journal of Biological Chemistry*, 287(7):4936–4945, 2012.

[87] Lan N Truong, Yongjiang Li, Linda Z Shi, Patty Yi Hwa Hwang, Jing He, Hailong Wang, Niema Razavian, Michael W Berns, and Xiaohua Wu. Microhomology-mediated End Joining and Homologous Recombination share the initial end resection step to repair DNA double-strand breaks in mammalian cells. *Proceedings of the National Academy of Sciences of the United States of America*, 110(19):7720–7725, 2013.

[88] Claire Bertrand, Annabelle Thibessard, Claude Bruand, François Lecointe, and Pierre Leblond. Bacterial NHEJ: a never ending story. *Molecular Microbiology*, 111(5):1139–1151, 2019.

[89] Stephen McGovern, Sonia Baconnais, Pierre Roblin, Pierre Nicolas, Pascal Drevet, Heloise Simonson, Olivier Pietrement, Jean Baptiste Charbonnier, Eric Le Cam, Philippe Noirot, and Francois Lecointe. C-terminal region of bacterial Ku controls DNA bridging, DNA threading and recruitment of DNA ligase D for double strand breaks repair. *Nucleic Acids Research*, 44(10):4785–4806, 2016.

[90] Nicole Hustedt and Daniel Durocher. The control of DNA repair by the cell cycle. *Nature Cell Biology*, 19(1):1–9, 2016.

[91] Stephen C. Kowalczykowski. An Overview of the Molecular Mechanisms of Recombinational DNA Repair. *Cold Spring Harbor Perspectives in Biology*, 7(11):a016410, 2015.

[92] P E Boehmer and P T Emmerson. The RecB subunit of the Escherichia coli RecBCD enzyme couples ATP hydrolysis to DNA unwinding. *The Journal of Biological Chemistry*, 267(7):4981–7, 1992.

[93] Jian Zhong Sun, Douglas A. Julin, and Jin Shan Hu. The nuclease domain of the Escherichia coli RecBCD enzyme catalyzes degradation of linear and circular single-stranded and double-stranded DNA. *Biochemistry*, 45(1):131–140, 2006.

[94] Jingdi Wang, Ruiwu Chen, and Douglas A Julin. A single nuclease active site of the Escherichia coli RecBCD enzyme catalyzes single-stranded DNA degradation in both directions. *Journal of Biological Chemistry*, 275(1):507–513, 2000.

[95] Naofumi Handa, Seishi Ohashi, Kohji Kusano, and Ichizo Kobayashi. χ^*, a χ-related 11-mer sequence partially active in an E coli recC* strain. *Genes to Cells*, 2(8):525–536, 1997.

[96] Mark S. Dillingham, Maria Spies, and Stephen C. Kowalczykowski. RecBCD enzyme is a bipolar DNA helicase. *Nature*, 423(6942):893–897, 2003.

[97] I D Hickson, C N Robson, K E Atkinson, L Hutton, and P T Emmerson. Reconstitution of RecBC DNase activity from purified Escherichia coli RecB and RecC proteins. *The Journal of Biological Chemistry*, 260(2):1224–9, 1985.

[98] Hua Wei Chen, Biao Ruan, Misook Yu, Jing Di Wang, and Douglas A. Julin. The RecD subunit of the RecBCD enzyme from Escherichia coli is a single- stranded DNA-dependent ATPase. *Journal of Biological Chemistry*, 272(15):10072–10079, 1997.

[99] Dan A. Dixon and Stephen C. Kowalczykowski. The recombination hotspot χ is a regulatory sequence that acts by attenuating the nuclease activity of the E. coli RecBCD enzyme. *Cell*, 73(1): 87–96, 1993.

[100] Piero R Bianco and Stephen C Kowalczykowski. The recombination hotspot Chi is recognized by the translocating RecBCD enzyme as the single strand of DNA containing the sequence 5'-GCTGGTGG-3'. *Proceedings of the National Academy of Sciences of the United States of America*, 94(13):6706–6711, 1997.

[101] Kazuharu Arakawa, Reina Uno, Yoichi Nakayama, and Masaru Tomita. Validating the significance of genomic properties of Chi sites from the distribution of all octamers in Escherichia coli. *Gene*, 392(1-2):239–246, 2007.

[102] Daniel G Anderson and Stephen C Kowalczykowski. The recombination hot spot χ is a regulatory element that switches the polarity of DNA degradation by the RecBCD enzyme. *Genes and Development*, 11(5):571–581, 1997.

[103] Daniel G. Anderson and Stephen C. Kowalczykowski. The translocating RecBCD enzyme stimulates recombination by directing RecA protein onto ssDNA in a χ-regulated manner. *Cell*, 90(1):77–86, 1997.

[104] Stephan Uphoff and David J Sherratt. Single-Molecule Analysis of Bacterial DNA Repair and Mutagenesis. *Annual Review of Biophysics*, 46:411–432, 2017.

[105] Anthony L. Forget and Stephen C. Kowalczykowski. Single-molecule imaging of DNA pairing by RecA reveals a three-dimensional homology search. *Nature*, 482(7385):423–427, 2012.

[106] Scott W Morrical. DNA-pairing and annealing processes in homologous recombination and homology-directed repair. *Cold Spring Harbor Perspectives in Biology*, 7(2):a016444, 2015.

[107] Silvia Ayora, Begoña Carrasco, Paula P Cárdenas, Carolina E César, Cristina Cañas, Tribhuwan Yadav, Chiara Marchisone, and Juan C Alonso. Double-strand break repair in bacteria: A view from Bacillus subtilis. *FEMS Microbiology Reviews*, 35(6):1055–1081, 2011.

[108] Kevin Hiom and Stephen C West. Branch migration during homologous recombination: assembly of a RuvAB-holliday junction complex in vitro. *Cell*, 80(5):787–793, 1995.

[109] Andrzej Stasiak, Irina R. Tsaneva, Stephen C. West, Catherine J.B. Benson, Xiong Yu, and Edward H. Egelman. The Escherichia coli RuvB branch migration protein forms double hexameric rings around DNA. *Proceedings of the National Academy of Sciences of the United States of America*, 91(16):7618–7622, 1994.

[110] John B Rafferty, Svetlana E Sedelnikova, David Hargreaves, Peter J Artymiuk, Patrick J Baker, Gary J Sharples, Akeel A Mahdi, Robert G Lloyd, and David W Rice. Crystal structure of DNA recombination protein RuvA and a model for its binding to the Holliday junction. *Science*, 274 (5286):415–421, 1996.

[111] Martin R. Singleton, Sarah Scaife, and Dale B. Wigley. Structural Analysis of DNA Replication Fork Reversal by RecG. *Cell*, 107(1):79–89, 2001.

[112] P. McGlynn and R. G. Lloyd. Rescue of stalled replication forks by RecG: Simultaneous translocation on the leading and lagging strand templates supports an active DNA unwinding model of fork reversal and holliday junction formation. *Proceedings of the National Academy of Sciences of the United States of America*, 98(15):8227–8234, 2001.

[113] Matthew C Whitby, Lizanne Ryder, and Robert G Lloyd. Reverse branch migration of holliday junctions by RecG protein: A new mechanism for resolution of intermediates in recombination and DNA repair. *Cell*, 75(2):341–350, 1993.

[114] Richard J Bennett, Hazel J Dunderdale, and Stephen C West. Resolution of holliday junctions by RuvC resolvase: Cleavage specificity and DNA distortion. *Cell*, 74(6):1021–1031, 1993.

[115] Frank G Harmon, Russell J DiGate, and Stephen C Kowalczykowski. RecQ helicase and topoisomerase III comprise a novel DNA strand passage function: A conserved mechanism for control of DNA recombination. *Molecular Cell*, 3(5):611–620, 1999.

[116] Christian Bernd Schiller, Florian Ulrich Seifert, Christian Linke-Winnebeck, and K.-P. Hopfner. Structural Studies of DNA End Detection and Resection in Homologous Recombination. *Cold Spring Harbor Perspectives in Biology*, 6(10):a017962, 2014.

[117] Tanya T Paull and Martin Gellert. The 3' to 5' exonuclease activity of Mre11 facilitates repair of DNA double-strand breaks. *Molecular Cell*, 1(7):969–979, 1998.

[118] Kelly M. Trujillo, Shyng Shiou F. Yuan, Eva Y.H.P. Lee, and Patrick Sung. Nuclease activities in a complex of human recombination and DNA repair factors Rad50, Mre11, and p95. *Journal of Biological Chemistry*, 273(34):21447–21450, 1998.

[119] Atsushi Shibata, Davide Moiani, Andrew S. Arvai, Jefferson Perry, Shane M. Harding, Marie Michelle Genois, Ranjan Maity, Sari van Rossum-Fikkert, Aryandi Kertokalio, Filippo Romoli, Amani Ismail, Ermal Ismalaj, Elena Petricci, Matthew J. Neale, Robert G. Bristow, Jean Yves Masson, Claire Wyman, Penny A. Jeggo, and John A. Tainer. DNA Double-Strand Break Repair Pathway Choice Is Directed by Distinct MRE11 Nuclease Activities. *Molecular Cell*, 53(1):7–18, 2014.

[120] Valerie Garcia, Sarah E. L. Phelps, Stephen Gray, and Matthew J. Neale. Bidirectional resection of DNA double-strand breaks by Mre11 and Exo1. *Nature*, 479(7372):241–244, 2011.

[121] Weibin Wang, James M Daley, Youngho Kwon, Xiaoyu Xue, Danielle S Krasner, Adam S Miller, Kevin A Nguyen, Elizabeth A Williamson, Eun Yong Shim, Sang Eun Lee, Robert Hromas, and Patrick Sung. A DNA nick at Ku-blocked double-strand break ends serves as an entry site for exonuclease 1 (Exo1) or Sgs1–Dna2 in long-range DNA end resection. *Journal of Biological Chemistry*, 293(44):17061–17069, 2018.

[122] Elda Cannavo and Petr Cejka. Sae2 promotes dsDNA endonuclease activity within Mre11-Rad50-Xrs2 to resect DNA breaks. *Nature*, 514(7520):122–125, 2014.

[123] P Szankasi and G R Smith. A DNA exonuclease induced during meiosis of Schizosaccharomyces pombe. *The Journal of Biological Chemistry*, 267(5):3014–23, 1992.

[124] Jochen Genschel, Laura R. Bazemore, and Paul Modrich. Human exonuclease I is required for 5' and 3' mismatch repair. *Journal of Biological Chemistry*, 277(15):13302–13311, 2002.

[125] Zhu Zhu, Woo Hyun Chung, Eun Yong Shim, Sang Eun Lee, and Grzegorz Ira. Sgs1 Helicase and Two Nucleases Dna2 and Exo1 Resect DNA Double-Strand Break Ends. *Cell*, 134(6):981–994, 2008.

[126] Lorraine S Symington. Mechanism and regulation of DNA end resection in eukaryotes. *Critical Reviews in Biochemistry and Molecular Biology*, 51(3):195–212, 2016.

[127] Thomas Costelloe, Raphaël Louge, Nozomi Tomimatsu, Bipasha Mukherjee, Emmanuelle Martini, Basheer Khadaroo, Kenny Dubois, Wouter W. Wiegant, Agnès Thierry, Sandeep Burma, Haico Van Attikum, and Bertrand Llorente. The yeast Fun30 and human SMARCAD1 chromatin remodellers promote DNA end resection. *Nature*, 489(7417):581–584, 2012.

[128] Tomohiko Sugiyama and Stephen C Kowalczykowski. Rad52 protein associates with replication protein A (RPA)-single-stranded DNA to accelerate Rad51-mediated displacement of RPA and presynaptic complex formation. *Journal of Biological Chemistry*, 277(35):31663–31672, 2002.

[129] Bin Wei Song and Patrick Sung. Functional interactions among yeast Rad51 recombinase, Rad52 mediator, and replication protein A in DNA strand exchange. *Journal of Biological Chemistry*, 275 (21):15895–15904, 2000.

[130] Ryan B. Jensen, Aura Carreira, and Stephen C. Kowalczykowski. Purified human BRCA2 stimulates RAD51-mediated recombination. *Nature*, 467(7316):678–683, 2010.

[131] Alexander V Mazin, Andrei A Alexeev, and Stephen C Kowalczykowski. A novel function of Rad54 protein: Stabilization of the Rad51 nucleoprotein filament. *Journal of Biological Chemistry*, 278 (16):14029–14036, 2003.

[132] Zhi Qi, Sy Redding, Ja Yil Lee, Bryan Gibb, YoungHo Kwon, Hengyao Niu, William A Gaines, Patrick Sung, and Eric C Greene. DNA sequence alignment by microhomology sampling during homologous recombination. *Cell*, 160(5):856–869, 2015.

[133] Eliana Moreira Tavares, William Douglass Wright, Wolf Dietrich Heyer, Eric Le Cam, and Pauline Dupaigne. In vitro role of Rad54 in Rad51-ssDNA filament-dependent homology search and synaptic complexes formation. *Nature Communications*, 10(1):4058, 2019.

[134] William Douglass Wright and Wolf-Dietrich Heyer. Rad54 functions as a heteroduplex DNA pump modulated by its DNA substrates and Rad51 during D loop formation. *Molecular Cell*, 53(3): 420–32, 2014.

[135] Grzegorz Ira, Anna Malkova, Giordano Liberi, Marco Foiani, and James E Haber. Srs2 and Sgs1-Top3 Suppress Crossovers during Double-Strand Break Repair in Yeast. *Cell*, 115(4):401–411, 2003.

[136] Stephanie A Hagstrom and Thaddeus P Dryja. Mitotic recombination map of 13cen-13q14 derived from an investigation of loss of heterozygosity in retinoblastomas. *Proceedings of the National Academy of Sciences of the United States of America*, 96(6):2952–2957, 1999.

[137] Mary Ellen Moynahan and Maria Jasin. Mitotic homologous recombination maintains genomic stability and suppresses tumorigenesis. *Nature Reviews Molecular Cell Biology*, 11(3):196–207, 2010.

[138] Xuan Li, Carrie M Stith, Peter M Burgers, and Wolf Dietrich Heyer. PCNA Is Required for Initiation of Recombination-Associated DNA Synthesis by DNA Polymerase delta. *Molecular Cell*, 36(4):704–713, 2009.

[139] Jessica L. Sneeden, Sara M. Grossi, Inger Tappin, Jerard Hurwitz, and Wolf Dietrich Heyer. Reconstitution of recombination-associated DNA synthesis with human proteins. *Nucleic Acids Research*, 41(9):4913–4925, 2013.

[140] A. V. Nimonkar, R. A. Sica, and S. C. Kowalczykowski. Rad52 promotes second-end DNA capture in double-stranded break repair to form complement-stabilized joint molecules. *Proceedings of the National Academy of Sciences*, 106(9):3077–3082, 2009.

[141] Kelly A Manthei and James L Keck. The BLM dissolvasome in DNA replication and repair. *Cellular and Molecular Life Sciences*, 70(21):4067–4084, 2013.

[142] Stephen C.Y. Ip, Ulrich Rass, Miguel G. Blanco, Helen R. Flynn, J. Mark Skehel, and Stephen C. West. Identification of Holliday junction resolvases from humans and yeast. *Nature*, 456(7220): 357–361, 2008.

[143] Xiao Bo Chen, Roberta Melchionna, Cecile Marie Denis, Pierre Henri L. Gaillard, Alessandra Blasina, Inez Van de Weyer, Michael N. Boddy, Paul Russell, Jorge Vialard, and Clare H. McGowan. Human Mus81-associated endonuclease cleaves Holliday junctions in vitro. *Molecular Cell*, 8(5): 1117–1127, 2001.

[144] Samira Fekairi, Sarah Scaglione, Charly Chahwan, Ewan R Taylor, Agnès Tissier, Stéphane Coulon, Meng Qiu Dong, Cristian Ruse, John R Yates, Paul Russell, Robert P Fuchs, Clare H McGowan, and Pierre Henri L. Gaillard. Human SLX4 Is a Holliday Junction Resolvase Subunit that Binds Multiple DNA Repair/Recombination Endonucleases. *Cell*, 138(1):78–89, 2009.

[145] Ragini Bhargava, David O. Onyango, and Jeremy M. Stark. Regulation of Single-Strand Annealing and its Role in Genome Maintenance. *Trends in Genetics*, 32(9):566–575, 2016.

[146] Eli Rothenberg, Jill M Grimme, Maria Spies, and Taekjip Ha. Human Rad52-mediated homology search and annealing occurs by continuous interactions between overlapping nucleoprotein complexes. *Proceedings of the National Academy of Sciences of the United States of America*, 105(51): 20274–20279, 2008.

[147] Neal Sugawara, Frédéric Pâques, Mónica Colaiácovo, and James E Haber. Role of Saccharomyces cerevisiae Msh2 and Msh3 repair proteins in double-strand break-induced recombination. *Proceedings of the National Academy of Sciences of the United States of America*, 94(17):9214–9219, 1997.

[148] Teresa A Motycka, Tadayoshi Bessho, Sean M Post, Patrick Sung, and Alan E Tomkinson. Physical and Functional Interaction between the XPF/ERCC1 Endonuclease and hRad52. *Journal of Biological Chemistry*, 279(14):13634–13639, 2004.

[149] Moreshwar B Vaze, Achille Pellicioli, Sang Eun Lee, Grzegorz Ira, Giordano Liberi, Ayelet Arbel-Eden, Marco Foiani, and James E Haber. Recovery from checkpoint-mediated arrest after repair of a double-strand break requires Srs2 helicase. *Molecular Cell*, 10(2):373–385, 2002.

[150] Beth Elliott, Christine Richardson, and Maria Jasin. Chromosomal translocation mechanisms at intronic Alu elements in mammalian cells. *Molecular Cell*, 17(6):885–894, 2005.

[151] C L Rieder and R W Cole. Entry into mitosis in vertebrate somatic cells is guarded by a chromosome damage checkpoint that reverses the cell cycle when triggered during early but not late prophase. *Journal of Cell Biology*, 142(4):1013–22, 1998.

[152] Simona Giunta, Rimma Belotserkovskaya, and Stephen P Jackson. DNA damage signaling in response to double-strand breaks during mitosis. *Journal of Cell Biology*, 190(2):197–207, 2010.

[153] Lorraine S. Symington and Jean Gautier. Double-Strand Break End Resection and Repair Pathway Choice. *Annual Review of Genetics*, 45:247–271, 2011.

[154] Nozomi Tomimatsu, Bipasha Mukherjee, Molly Catherine Hardebeck, Mariya Ilcheva, Cristel Vanessa Camacho, Janelle Louise Harris, Matthew Porteus, Bertrand Llorente, Kum Kum Khanna, and Sandeep Burma. Phosphorylation of EXO1 by CDKs 1 and 2 regulates DNA end resection and repair pathway choice. *Nature communications*, 5:3561, 2014.

[155] Jacob Falck, Josep V Forment, Julia Coates, Martin Mistrik, Jiri Lukas, Jiri Bartek, and Stephen P Jackson. CDK targeting of NBS1 promotes DNA-end resection, replication restart and homologous recombination. *EMBO Reports*, 13(6):561–568, 2012.

[156] Pablo Huertas and Stephen P. Jackason. Human CtIP mediates cell cycle control of DNA end resection and double strand break repair. *Journal of Biological Chemistry*, 284(14):9558–9565, 2009.

[157] Aleem Syed and John A. Tainer. The MRE11–RAD50–NBS1 Complex Conducts the Orchestration of Damage Signaling and Outcomes to Stress in DNA Replication and Repair. *Annual Review of Biochemistry*, 87(1):263–294, 2018.

[158] Gary J. Sharples and David R F Leach. Structural and functional similarities between the SbcCD proteins of Escherichia coli and the RAD50 and MRE11 (RAD32) recombination and repair proteins of yeast. *Molecular Microbiology*, 17(6):1215–1217, 1995.

[159] S. Matsuoka, B. A. Ballif, A. Smogorzewska, E. R. McDonald, K. E. Hurov, J. Luo, C. E. Bakalarski, Z. Zhao, N. Solimini, Y. Lerenthal, Y. Shiloh, S. P. Gygi, and S. J. Elledge. ATM and ATR Substrate Analysis Reveals Extensive Protein Networks Responsive to DNA Damage. *Science*, 316 (5828):1160–1166, 2007.

[160] Martin Lavin, Sergei Kozlov, Magtouf Gatei, and Amanda Kijas. ATM-Dependent Phosphorylation of All Three Members of the MRN Complex: From Sensor to Adaptor. *Biomolecules*, 5(4):2877–2902, 2015.

[161] M Ajimura, S H Leem, and H Ogawa. Identification of new genes required for meiotic recombination in Saccharomyces cerevisiae. *Genetics*, 133(1):51–66, 1993.

[162] Karl Peter Hopfner, Annette Karcher, Lisa Craig, Tammy T. Woo, James P. Carney, and John A. Tainer. Structural biochemistry and interaction architecture of the DNA double-strand break repair Mre11 nuclease and Rad50-ATPase. *Cell*, 105(4):473–485, 2001.

[163] Gareth J. Williams, R. Scott Williams, Jessica S Williams, Gabriel Moncalian, Andrew S Arvai, Oliver Limbo, Grant Guenther, Soumita Sildas, Michal Hammel, Paul Russell, and John A Tainer. ABC ATPase signature helices in Rad50 link nucleotide state to Mre11 interface for DNA repair. *Nature Structural and Molecular Biology*, 18(4):423–432, 2011.

[164] Munenori Furuse, Yuko Nagase, Hideo Tsubouchi, Kimiko Murakami-Murofushi, Takehiko Shibata, and Kunihiro Ohta. Distinct roles of two separable in vitro activities of yeast Mre11 in mitotic and meiotic recombination. *EMBO Journal*, 17(21):6412–6425, 1998.

[165] U. Dery, Y. Coulombe, A. Rodrigue, A. Stasiak, S. Richard, and J.-Y. Masson. A Glycine-Arginine Domain in Control of the Human MRE11 DNA Repair Protein. *Molecular and Cellular Biology*, 28(9):3058–3069, 2008.

[166] R. Scott Williams, Gabriel Moncalian, Jessica S. Williams, Yoshiki Yamada, Oliver Limbo, David S. Shin, Lynda M. Groocock, Dana Cahill, Chiharu Hitomi, Grant Guenther, Davide Moiani, James P. Carney, Paul Russell, and John A. Tainer. Mre11 Dimers Coordinate DNA End Bridging and Nuclease Processing in Double-Strand-Break Repair. *Cell*, 135(1):97–109, 2008.

[167] Rajashree A. Deshpande, Ji Hoon Lee, Sucheta Arora, and Tanya T. Paull. Nbs1 Converts the Human Mre11/Rad50 Nuclease Complex into an Endo/Exonuclease Machine Specific for Protein-DNA Adducts. *Molecular Cell*, 64(3):593–606, 2016.

[168] Federica Marini, Chetan C. Rawal, Giordano Liberi, and Achille Pellicioli. Regulation of DNA Double Strand Breaks Processing: Focus on Barriers. *Frontiers in Molecular Biosciences*, 6:55, 2019.

[169] Edgar Hartsuiker, Kenichi Mizuno, Monika Molnar, Juerg Kohli, Kunihiro Ohta, and Antony M Carr. Ctp1CtIP and Rad32Mre11 Nuclease Activity Are Required for Rec12Spo11 Removal, but Rec12Spo11 Removal Is Dispensable for Other MRN-Dependent Meiotic Functions. *Molecular and Cellular Biology*, 29(7):1671–1681, 2009.

[170] Christian B. Schiller, Katja Lammens, Ilaria Guerini, Britta Coordes, Heidi Feldman, Florian Schlauderer, Carolin Möckel, Alexandra Schele, Katja Strässer, Stephen P. Jackson, and Karl-Peter Hopfner. Structural biology of the Mre11:Nbs1 complex structure yields insights into ataxia–telangiectasia–like disease mutations and DNA damage signaling. *Nature structural & molecular biology*, 19(7):693–700, 2012.

[171] Carolin Möckel, Katja Lammens, Alexandra Schele, and Karl Peter Hopfner. ATP driven structural changes of the bacterial Mre11:Rad50 catalytic head complex. *Nucleic Acids Research*, 40(2):914–927, 2012.

[172] Florian Ulrich Seifert, Katja Lammens, and Karl Peter Hopfner. Structure of the catalytic domain of Mre11 from Chaetomium thermophilum. *Acta Crystallographica Section F:Structural Biology Communications*, 71(6):752–757, 2015.

[173] Young Bong Park, Jina Chae, Young Chang Kim, and Yunje Cho. Crystal Structure of Human Mre11: Understanding Tumorigenic Mutations. *Structure*, 19(11):1591–1602, 2011.

[174] Shun Liu, Li-fei Tian, Yan-ping Liu, Xiao-min An, Qun Tang, Xiao-xue Yan, and Dong-cai Liang. Structural basis for DNA recognition and nuclease processing by the Mre11 homologue SbcD in double-strand breaks repair. *Acta crystallographica. Section D, Biological crystallography*, 70(Pt 2):299–309, 2014.

[175] Florian Ulrich Seifert, Katja Lammens, Gabriele Stoehr, Brigitte Kessler, and Karl-Peter Hopfner. Structural mechanism of ATP-dependent DNA binding and DNA end bridging by eukaryotic Rad50. *The EMBO journal*, 35(7):759–72, 2016.

[176] Hye Seong Lim, Jin Seok Kim, Young Bong Park, Gwang Hyeon Gwon, and Yunje Cho. Crystal structure of the Mre11-Rad50-ATPγS complex: Understanding the interplay between Mre11 and Rad50. *Genes and Development*, 25(10):1091–1104, 2011.

[177] Roopesh Anand, Lepakshi Ranjha, Elda Cannavo, and Petr Cejka. Phosphorylated CtIP Functions as a Co-factor of the MRE11-RAD50-NBS1 Endonuclease in DNA End Resection. *Molecular Cell*, 64(5):940–950, 2016.

[178] Jeffrey Buis, Yipin Wu, Yibin Deng, Jennifer Leddon, Gerwin Westfield, Mark Eckersdorff, JoAnn M. Sekiguchi, Sandy Chang, and David O. Ferguson. Mre11 Nuclease Activity Has Essential Roles in DNA Repair and Genomic Stability Distinct from ATM Activation. *Cell*, 135(1): 85–96, 2008.

[179] Linda Truebestein and Thomas A Leonard. Coiled-coils: The long and short of it. *BioEssays*, 38 (9):903–916, 2016.

[180] K P Hopfner, A Karcher, D S Shin, L Craig, L M Arthur, J P Carney, and J A Tainer. Structural biology of Rad50 ATPase: ATP-driven conformational control in DNA double-strand break repair and the ABC-ATPase superfamily. *Cell*, 101(7):789–800, 2000.

[181] Katja Lammens, Derk J. Bemeleit, Carolin Möckel, Emanuel Clausing, Alexandra Schele, Sophia Hartung, Christian B. Schiller, Maria Lucas, Christof Angermüller, Johannes Söding, Katja Sträßer, and Karl Peter Hopfner. The Mre11:Rad50 structure shows an ATP-dependent molecular clamp in DNA double-strand break repair. *Cell*, 145(1):54–66, 2011.

[182] Rajashree A Deshpande, Ji Hoon Lee, and Tanya T Paull. Rad50 ATPase activity is regulated by DNA ends and requires coordination of both active sites. *Nucleic Acids Research*, 45(9):5255–5268, 2017.

[183] Kelly M Trujillo, Dong Hyun Roh, Ling Chen, Stephen Van Komen, Alan Tomkinson, and Patrick Sung. Yeast xrs2 binds DNA and helps target rad50 and mre11 to DNA ends. *Journal of Biological Chemistry*, 278(49):48957–48964, 2003.

[184] Markus Hassler, Indra A. Shaltiel, and Christian H. Haering. Towards a Unified Model of SMC Complex Function. *Current Biology*, 28(21):R1266–R1281, 2018.

[185] Linda J Roman and Stephen C Kowalczykowski. Characterization of the Adenosinetriphosphatase Activity of the Escherichia coli RecBCD Enzyme: Relationship of ATP Hydrolysis to the Unwinding of Duplex DNA. *Biochemistry*, 28(7):2873–2881, 1989.

[186] Eric Alani, Ruth Padmore, and Nancy Kleckner. Analysis of wild-type and rad50 mutants of yeast suggests an intimate relationship between meiotic chromosome synapsis and recombination. *Cell*, 61(3):419–436, 1990.

[187] Yaqi Liu, Sihyun Sung, Youngran Kim, Fuyang Li, Gwanghyun Gwon, Aera Jo, Ae-Kyoung Kim, Taeyoon Kim, Ok-kyu Song, Sang Eun Lee, and Yunje Cho. ATP -dependent DNA binding, unwinding, and resection by the Mre11/Rad50 complex. *The EMBO Journal*, 35(7):743–758, 2016.

[188] Anna Rojowska, Katja Lammens, Florian Seifert, Carolin Direnberger, Heidi Feldmann, and Karl-Peter Hopfner. Structure of the Rad50 DNA double-strand break repair protein in complex with DNA. *The EMBO Journal*, 33(23):e201488889, 2014.

[189] Karl Peter Hopfner, Lisa Craig, Gabriel Moncalian, Robert A. Zinkel, Takehiko Usui, Barbara A.L. Owen, Annette Karcher, Brendan Henderson, Jean Luc Bodmer, Cynthia T. McMurray, James P. Carney, John H.J. Petrini, and John A. Tainer. The Rad50 zinc-hook is a structure joining Mre11 complexes in DNA recombination and repair. *Nature*, 418(6897):562–566, 2002.

[190] Travis H. Stracker and John H J Petrini. The MRE11 complex: Starting from the ends. *Nature Reviews Molecular Cell Biology*, 12(2):90–103, 2011.

[191] Young Bong Park, Marcel Hohl, Michał Padjasek, Eunyoung Jeong, Kyeong Sik Jin, Artur Kręzel, John H.J. Petrini, and Yunje Cho. Eukaryotic Rad50 functions as a rod-shaped dimer. *Nature Structural and Molecular Biology*, 24(3):248–257, 2017.

[192] Jed J.W. Wiltzius, Marcel Hohl, James C. Fleming, and John H.J. Petrini. The Rad50 hook domain is a critical determinant of Mre11 complex functions. *Nature Structural and Molecular Biology*, 12 (5):403–407, 2005.

[193] Marcel Hohl, Youngho Kwon, Sandra Muñoz Galván, Xiaoyu Xue, Cristina Tous, Andrés Aguilera, Patrick Sung, and John H J Petrini. The Rad50 coiled-coil domain is indispensable for Mre11 complex functions. *Nature Structural and Molecular Biology*, 18(10):1124–1131, 2010.

[194] Marcel Hohl, Tomasz Kochańczyk, Cristina Tous, Andrés Aguilera, Artur KrEzel, and John H.J. Petrini. Interdependence of the Rad50 Hook and Globular domain functions. *Molecular Cell*, 57 (3):479–491, 2015.

[195] Fernando Moreno-Herrero, Martijn De Jager, Nynke H. Dekker, Roland Kanaar, Claire Wyman, and Cees Dekker. Mesoscale conformational changes in the DNA-repair complex Rad50/Mre11/Nbs1 upon binding DNA. *Nature*, 437(7057):440–443, 2005.

[196] Ji Hoon Lee, Michael R. Mand, Rajashree A. Deshpande, Eri Kinoshita, Soo Hyun Yang, Claire Wyman, and Tanya T. Paull. Ataxia Telangiectasia-Mutated (ATM) kinase activity is regulated by ATP-driven conformational changes in the Mre11/Rad50/Nbs1 (MRN) complex. *Journal of Biological Chemistry*, 288(18):12840–12851, 2013.

[197] John van Noort, Thijn van Der Heijden, Martijn de Jager, Claire Wyman, Roland Kanaar, and Cees Dekker. The coiled-coil of the human Rad50 DNA repair protein contains specific segments of increased flexibility. *Proceedings of the National Academy of Sciences of the United States of America*, 100(13):7581–7586, 2003.

[198] Neville Cobbe and Margarete M.S. Heck. The evolution of ATPase activity in SMC proteins. *Proteins: Structure, Function and Genetics*, 63(3):685–696, 2006.

[199] Frank Bürmann, Alrun Basfeld, Roberto Vazquez Nunez, Marie Laure Diebold-Durand, Larissa Wilhelm, and Stephan Gruber. Tuned SMC Arms Drive Chromosomal Loading of Prokaryotic Condensin. *Molecular Cell*, 65(5):861–872.e9, 2017.

[200] Mariana Diaz and Ales Pecinka. Scaffolding for repair: Understanding molecular functions of the SMC5/6 complex. *Genes*, 9(1):36, 2018.

[201] Frank Bürmann, Byung Gil Lee, Thane Than, Ludwig Sinn, Francis J. O'Reilly, Stanislau Yatskevich, Juri Rappsilber, Bin Hu, Kim Nasmyth, and Jan Löwe. A folded conformation of MukBEF and cohesin. *Nature Structural and Molecular Biology*, 26(3):227–236, 2019.

[202] R. Scott Williams, Gerald E Dodson, Oliver Limbo, Yoshiki Yamada, Jessica S Williams, Grant Guenther, Scott Classen, J. N.Mark Glover, Hiroshi Iwasaki, Paul Russell, and John A Tainer. Nbs1 Flexibly Tethers Ctp1 and Mre11-Rad50 to Coordinate DNA Double-Strand Break Processing and Repair. *Cell*, 139(1):87–99, 2009.

[203] Daniel Durocher and Stephen P. Jackson. The FHA domain. *FEBS Letters*, 513(1):58–66, 2002.

[204] Dietlind L. Gerloff, Nicholas T. Woods, April A. Farago, and Alvaro N.A. Monteiro. BRCT domains: A little more than kin, and less than kind. *FEBS Letters*, 586(17):2711–2716, 2012.

[205] J Ross Chapman and Stephen P Jackson. Phospho-dependent interactions between NBS1 and MDC1 mediate chromatin retention of the MRN complex at sites of DNA damage. *EMBO Reports*, 9(8):795–801, 2008.

[206] Fredrik Melander, Simon Bekker-Jensen, Jacob Falck, Jiri Bartek, Niels Mailand, and Jiri Lukas. Phosphorylation of SDT repeats in the MDC1 N terminus triggers retention of NBS1 at the DNA damage-modified chromatin. *Journal of Cell Biology*, 181(2):213–226, 2008.

[207] Christoph Spycher, Edward S. Miller, Kelly Townsend, Lucijana Pavic, Nicholas A. Morrice, Pavel Janscak, Grant S. Stewart, and Manuel Stucki. Constitutive phosphorylation of MDC1 physically links the MRE11-RAD50-NBS1 complex to damaged chromatin. *Journal of Cell Biology*, 181(2): 227–240, 2008.

[208] Zhongsheng You, Charly Chahwan, Julie Bailis, Tony Hunter, and Paul Russell. ATM Activation and Its Recruitment to Damaged DNA Require Binding to the C Terminus of Nbs1. *Molecular and Cellular Biology*, 25(13):5363–5379, 2005.

[209] Jacob Falck, Julia Coates, and Stephen P. Jackson. Conserved modes of recruitment of ATM, ATR and DNA-PKcs to sites of DNA damage. *Nature*, 434(7033):605–611, 2005.

[210] Christine S Vissinga, Tiong C Yeo, Sarah Warren, James V Brawley, Jennifer Phillips, Karen Cerosaletti, and Patrick Concannon. Nuclear Export of NBN Is Required for Normal Cellular Responses to Radiation. *Molecular and Cellular Biology*, 29(4):1000–1006, 2009.

[211] James P Carney, Richard S Maser, Heidi Olivares, Elizabeth M Davis, Michelle Le Beau, John R Yates, Lara Hays, William F Morgan, and John H.J. Petrini. The hMre11/hRad50 protein complex and Nijmegen breakage syndrome: Linkage of double-strand break repair to the cellular DNA damage response. *Cell*, 93(3):477–486, 1998.

[212] Nodar Makharashvili and Tanya T. Paull. CtIP: A DNA damage response protein at the intersection of DNA metabolism. *DNA Repair*, 32:75–81, 2015.

[213] Owen R Davies, Josep V Forment, Meidai Sun, Rimma Belotserkovskaya, Julia Coates, Yaron Galanty, Mukerrem Demir, Christopher R Morton, Neil J Rzechorzek, Stephen P Jackson, and Luca Pellegrini. CtIP tetramer assembly is required for DNA-end resection and repair. *Nature Structural and Molecular Biology*, 22(2):150–157, 2015.

[214] Sara N Andres, C Denise Appel, James W Westmoreland, Jessica Scott Williams, Yvonne Nguyen, Patrick D Robertson, Michael A Resnick, and R Scott Williams. Tetrameric Ctp1 coordinates DNA binding and DNA bridging in DNA double-strand-break repair. *Nature Structural and Molecular Biology*, 22(2):158–166, 2015.

[215] Sara N. Andres and R. Scott Williams. CtIP/Ctp1/Sae2, molecular form fit for function. *DNA Repair*, 56:109–117, 2017.

[216] Xin Yu, Leeju C Wu, Anne M Bowcock, Ami Aronheim, and Richard Baer. The C-terminal (BRCT) domains of BRCA1 interact in vive with CtIP, a protein implicated in the CtBP pathway of transcriptional repression. *Journal of Biological Chemistry*, 273(39):25388–25392, 1998.

[217] Ashok K. Varma, Raymond S. Brown, Gabriel Birrane, and John A.A. Ladias. Structural basis for cell cycle checkpoint control by the BRCA1-CtIP complex. *Biochemistry*, 44(33):10941–10946, 2005.

[218] Bettina M Lengsfeld, Alison J Rattray, Venugopal Bhaskara, Rodolfo Ghirlando, and Tanya T Paull. Sae2 Is an Endonuclease that Processes Hairpin DNA Cooperatively with the Mre11/Rad50/Xrs2 Complex. *Molecular Cell*, 28(4):638–651, 2007.

[219] Nodar Makharashvili, Anthony T Tubbs, Soo Hyun Yang, Hailong Wang, Olivia Barton, Yi Zhou, Rajashree A Deshpande, Ji Hoon Lee, Markus Lobrich, Barry P Sleckman, Xiaohua Wu, and Tanya T Paull. Catalytic and Noncatalytic Roles of the CtIP Endonuclease in Double-Strand Break End Resection. *Molecular Cell*, 54(6):1022–1033, 2014.

[220] Sara N Andres, Zimeng M Li, Dorothy A Erie, and R Scott Williams. Ctp1 protein–DNA filaments promote DNA bridging and DNA double-strand break repair. *Journal of Biological Chemistry*, 294 (9):3312–3320, 2019.

[221] Alessandro A. Sartori, Claudia Lukas, Julia Coates, Martin Mistrik, Shuang Fu, Jiri Bartek, Richard Baer, Jiri Lukas, and Stephen P. Jackson. Human CtIP promotes DNA end resection. *Nature*, 450 (7169):509–514, 2007.

[222] Oliver Limbo, Charly Chahwan, Yoshiki Yamada, Robertus A.M. de Bruin, Curt Wittenberg, and Paul Russell. Ctp1 Is a Cell-Cycle-Regulated Protein that Functions with Mre11 Complex to Control Double-Strand Break Repair by Homologous Recombination. *Molecular Cell*, 28(1):134–146, 2007.

[223] Pablo Huertas, Felipe Cortés-Ledesma, Alessandro A. Sartori, Andrés Aguilera, and Stephen P. Jackson. CDK targets Sae2 to control DNA-end resection and homologous recombination. *Nature*, 455(7213):689–692, 2008.

[224] Andrew N. Blackford and Stephen P. Jackson. ATM, ATR, and DNA-PK: The Trinity at the Heart of the DNA Damage Response. *Molecular Cell*, 66(6):801–817, 2017.

[225] Tanya T. Paull. Mechanisms of ATM Activation. *Annual Review of Biochemistry*, 84(1):711–738, 2015.

[226] Tanya M Gottlieb and Stephen P Jackson. The DNA-dependent protein kinase: Requirement for DNA ends and association with Ku antigen. *Cell*, 72(1):131–142, 1993.

[227] Lee Zou and Stephen J Elledge. Sensing DNA damage through ATRIP recognition of RPA-ssDNA complexes. *Science*, 300(5625):1542–1548, 2003.

[228] Christian T. Carson, Rachel A. Schwartz, Travis H. Stracker, Caroline E. Lilley, Darwin V. Lee, and Matthew D. Weitzman. The Mre11 complex is required for ATM activation and the G2/M checkpoint. *EMBO Journal*, 22(24):6610–6620, 2003.

[229] Ji Hoon Lee and Tanya T Paull. Direct Activation of the ATM Protein Kinase by the Mre11/Rad50/Nbs1 Complex. *Science*, 304(5667):93–96, 2004.

[230] Ji Hoon Lee and Tanya T Paull. ATM activation by DNA double-strand breaks through the Mre11-Rad50-Nbs1 complex. *Science*, 308(5721):551–554, 2005.

[231] Tamar Uziel, Yaniv Lerenthal, Lilach Moyal, Yair Andegeko, Leonid Mittelman, and Yosef Shiloh. Requirement of the MRN complex for ATM activation by DNA damage. *EMBO Journal*, 22(20): 5612–5621, 2003.

[232] Song Zhao, Yi Chinn Wong, Shyng Shlou F. Yuan, Yi Tzu Lin, Hao Chi Hsu, Suh Chin J. Lin, Elvira Gerbino, Mel Hua Song, Malgorzata Z. Zdzlenlcka, Richard A. Gatti, Jerry W. Shay, Yael Ziv, Yosef Shilch, and Eva Y.H.P. Lee. Functional link between ataxia-telangiectasia and Nijmegen breakage syndrome gene products. *Nature*, 405(6785):473–477, 2000.

[233] Magtouf Gatei, Burkhard Jakob, Philip Chen, Amanda W Kijas, Olivier J Becherel, Nuri Gueven, Geoff Birrell, Ji Hoon Lee, Tanya T Paull, Yaniv Lerenthal, Shazrul Fazry, Gisela Taucher-Scholz, Reinhard Kalb, Detlev Schindler, Regina Waltes, Thilo Dörk, and Martin F Lavin. ATM protein-dependent phosphorylation of Rad50 protein Regulates DNA repair and cell cycle control. *Journal of Biological Chemistry*, 286(36):31542–31556, 2011.

[234] Amanda W. Kijas, Yi Chieh Lim, Emma Bolderson, Karen Cerosaletti, Magtouf Gatei, Burkhard Jakob, Frank Tobias, Gisela Taucher-Scholz, Nuri Gueven, Greg Oakley, Patrick Concannon, Ernst Wolvetang, Kum Kum Khanna, Lisa Wiesmüller, and Martin F. Lavin. ATM-dependent phosphorylation of MRE11 controls extent of resection during homology directed repair by signalling through Exonuclease 1. *Nucleic Acids Research*, 43(17):8352–8367, 2015.

[235] Dae Sik Lim, Seong Tae Kim, Bo Xu, Richard S. Maser, Junyu Lin, John H.J. Petrini, and Michael B. Kastan. ATM phosphorylates p95/nbs1 in an S-phase checkpoint pathway. *Nature*, 404 (6778):613–617, 2000.

[236] Maria Pia Longhese. DNA damage response at functional and dysfunctional telomeres. *Genes and Development*, 22(2):125–140, 2008.

[237] Mahmood Chamankhah and Wei Xiao. Formation of the yeast Mre11-Rad50-Xrs2 complex is correlated with DNA repair and telomere maintenance. *Nucleic Acids Research*, 27(10):2072–2079, 1999.

[238] Simon J. Boulton and Stephen P. Jackson. Components of the Ku-dependent non-homologous end-joining pathway are involved in telomeric length maintenance and telomeric silencing. *EMBO Journal*, 17(6):1819–1828, 1998.

[239] Hideki Takata, Yayoi Tanaka, and Akira Matsuura. Late S phase-specific recruitment of Mre11 complex triggers hierarchical assembly of telomere replication proteins in Saccharomyces cerevisiae. *Molecular Cell*, 17(4):573–583, 2005.

[240] David B Lombard and Leonard Guarente. Nijmegen breakage syndrome disease protein and MRE11 at PML nuclear bodies and meiotic telomeres. *Cancer Research*, 60(9):2331–2334, 2000.

[241] Xu-Dong Zhu, Bernhard Küster, Matthias Mann, John H.J. Petrini, and Titia de Lange. Cell-cycle-regulated association of RAD50/MRE11/NBS1 with TRF2 and human telomeres. *Nature Genetics*, 25(3):347–352, 2000.

[242] Rekha Rai, Chunyi Hu, Cayla Broton, Yong Chen, Ming Lei, and Sandy Chang. NBS1 Phosphorylation Status Dictates Repair Choice of Dysfunctional Telomeres. *Molecular Cell*, 65(5):801–817.e4, 2017.

[243] Fabrizio D'Adda Di Fagagna, Philip M. Reaper, Lorena Clay-Farrace, Heike Fiegler, Philippa Carr, Thomas Von Zglinicki, Gabriele Saretzki, Nigel P. Carter, and Stephen P. Jackson. A DNA damage checkpoint response in telomere-initiated senescence. *Nature*, 426(6963):194–198, 2003.

[244] Caroline E. Lilley, Rachel A. Schwartz, and Matthew D. Weitzman. Using or abusing: viruses and the cellular DNA damage response. *Trends in Microbiology*, 15(3):119–126, 2007.

[245] Travis H. Stracker, Christian T. Carson, and Matthew D. Weilzman. Adenovirus oncoproteins inactivate the Mre11-Rad50-NBs1 DNA repair complex. *Nature*, 418(6895):348–352, 2002.

[246] Govind A Shah and Clodagh C O'Shea. Viral and Cellular Genomes Activate Distinct DNA Damage Responses. *Cell*, 162(5):987–1002, 2015.

[247] Giuseppe Mariggiò, Sandra Koch, Guigen Zhang, Magdalena Weidner-Glunde, Jessica Rückert, Semra Kati, Susann Santag, and Thomas F. Schulz. Kaposi Sarcoma Herpesvirus (KSHV) Latency-Associated Nuclear Antigen (LANA) recruits components of the MRN (Mre11-Rad50-NBS1) repair complex to modulate an innate immune signaling pathway and viral latency. *PLoS Pathogens*, 13 (4):e1006335, 2017.

[248] Karen Campos-León, Kalpanee Wijendra, Abida Siddiqa, Ieisha Pentland, Katherine M Feeney, Alison Knapman, Rachel Davies, Elliot J Androphy, and Joanna L Parish. Association of Human Papillomavirus 16 E2 with Rad50-Interacting Protein 1 Enhances Viral DNA Replication. *Journal of virology*, 91(5):e02305–02316, 2017.

[249] Yoshiyuki Matsumoto, Tatsuo Miyamoto, Hiromi Sakamoto, Hideki Izumi, Yuka Nakazawa, Tomoo Ogi, Hidetoshi Tahara, Shozo Oku, Azuma Hiramoto, Toshihide Shiiki, Yoshiki Fujisawa, Hirofumi Ohashi, Yoshihiro Sakemi, and Shinya Matsuura. Two unrelated patients with MRE11A mutations and Nijmegen breakage syndrome-like severe microcephaly. *DNA repair*, 10(3):314–21, 2011.

[250] Naoki Uchisaka, Naomi Takahashi, Masaki Sato, Akira Kikuchi, Shinji Mochizuki, Kohsuke Imai, Shigeaki Nonoyama, Osamu Ohara, Fumiaki Watanabe, Shuki Mizutani, Ryoji Hanada, and Tomohiro Morio. Two Brothers with Ataxia-Telangiectasia-like Disorder with Lung Adenocarcinoma. *The Journal of Pediatrics*, 155(3):435–438, 2009.

[251] Maryam Sedghi, Mehri Salari, Ali Reza Moslemi, Ariana Kariminejad, Mark Davis, Hayley Goullée, Björn Olsson, Nigel Laing, and Homa Tajsharghi. Ataxia-telangiectasia-like disorder in a family deficient for MRE11A, caused by a MRE11 variant. *Neurology: Genetics*, 4(6):e295, 2018.

[252] Grant S Stewart, Richard S Maser, Tanja Stankovic, Debra A Bressan, Mark I Kaplan, Nikolaas G.J. Jaspers, Anja Raams, Philip J Byrd, John H.J. Petrini, and A. Malcolm R. Taylor. The DNA double-strand break repair gene hMRE11 is mutated in individuals with an ataxia-telangiectasia-like disorder. *Cell*, 99(6):577–587, 1999.

[253] Marie Fernet, Moez Gribaa, Mustafa A.M. Salih, Mohamed Zein Seidahmed, Janet Hall, and Michel Koenig. Identification and functional consequences of a novel MRE11 mutation affecting 10 Saudi Arabian patients with the ataxia telangiectasia-like disorder. *Human Molecular Genetics*, 14(2): 307–318, 2005.

[254] Oliver Limbo, Davide Moiani, Aryandi Kertokalio, Claire Wyman, John A. Tainer, and Paul Russell. Mre11 ATLD17/18 mutation retains Tel1/ATM activity but blocks DNA double-strand break repair. *Nucleic Acids Research*, 40(22):11435–11449, 2012.

[255] Ryosuke Miyamoto, Hiroyuki Morino, Akio Yoshizawa, Yoshimichi Miyazaki, Hirofumi Maruyama, Nagahisa Murakami, Kei Fukada, Yuishin Izumi, Shinya Matsuura, Ryuji Kaji, and Hideshi Kawakami. Exome sequencing reveals a novel MRE11 mutation in a patient with progressive myoclonic ataxia. *Journal of the Neurological Sciences*, 337(1-2):219–223, 2014.

[256] Regina Waltes, Reinhard Kalb, Magtouf Gatei, Amanda W. Kijas, Markus Stumm, Alexandra Sobeck, Britta Wieland, Raymonda Varon, Yaniv Lerenthal, Martin F. Lavin, Detlev Schindler, and Thilo Dörk. Human RAD50 Deficiency in a Nijmegen Breakage Syndrome-like Disorder. *American Journal of Human Genetics*, 84(5):605–616, 2009.

[257] Krystyna H Chrzanowska, Hanna Gregorek, Bożenna Dembowska-Bagińska, Maria A Kalina, and Martin Digweed. Nijmegen breakage syndrome (NBS). *Orphanet Journal of Rare Diseases*, 7(1): 13, 2012.

[258] E. Seemanová, K. Sperling, H. Neitzel, R. Varon, J. Hadac, O. Butova, E. Schröck, P. Seeman, and M. Digweed. Nijmegen breakage syndrome (NBS) with neurological abnormalities and without chromosomal instability. *Journal of Medical Genetics*, 43(3):218–224, 2006.

[259] Lei Bian, Yiling Meng, Meichao Zhang, and Dong Li. MRE11-RAD50-NBS1 complex alterations and DNA damage response: implications for cancer treatment. *Molecular cancer*, 18(1):169, 2019.

[260] Zdenek Kleibl and Vessela N. Kristensen. Women at high risk of breast cancer: Molecular characteristics, clinical presentation and management. 28:136–144, 2016.

[261] Giorgia Simonetti, Antonella Padella, Italo Farìa do Valle, Maria Chiara Fontana, Eugenio Fonzi, Samantha Bruno, Carmen Baldazzi, Viviana Guadagnuolo, Marco Manfrini, Anna Ferrari, Stefania Paolini, Cristina Papayannidis, Giovanni Marconi, Eugenia Franchini, Elisa Zuffa, Maria Antonella Laginestra, Federica Zanotti, Annalisa Astolfi, Ilaria Iacobucci, Simona Bernardi, Marco Sazzini, Elisa Ficarra, Jesus Maria Hernandez, Peter Vandenberghe, Jan Cools, Lars Bullinger, Emanuela Ottaviani, Nicoletta Testoni, Michele Cavo, Torsten Haferlach, Gastone Castellani, Daniel Remondini, and Giovanni Martinelli. Aneuploid acute myeloid leukemia exhibits a signature of genomic alterations in the cell cycle and protein degradation machinery. *Cancer*, 125(5):712–725, 2019.

[262] Cezary Cybulski, B. Górski, T. Debníak, B. Gliniewicz, M. Mierzejewski, B. Masojć, A. Jakubowska, J. Matyjasik, E. Złowocka, A. Sikorski, S. A. Narod, and J. Lubiński. NBS1 Is a Prostate Cancer Susceptibility Gene. *Cancer Research*, 64(4):1215–1219, 2004.

[263] Nancy Berte, Andrea Piée-Staffa, Nadine Piecha, Mengwan Wang, Kerstin Borgmann, Bernd Kaina, and Teodora Nikolova. Targeting homologous recombination by pharmacological inhibitors enhances the killing response of glioblastoma cells treated with alkylating drugs. *Molecular Cancer Therapeutics*, 15(11):2665–2678, 2016.

[264] Sandra Aedo and Yuk Ching Tse-Dinh. SbcCD-mediated processing of covalent gyrase-DNA complex in Escherichia coli. *Antimicrobial Agents and Chemotherapy*, 57(10):5116–5119, 2013.

[265] John C. Connelly and David R F Leach. The sbcC and sbcD genes of Escherichia coli encode a nuclease involved in palindrome inviability and genetic recombination. *Genes to Cells*, 1(3): 285–291, 1996.

[266] J. Connelly, E S de Leau, and D R Leach. DNA cleavage and degradation by the SbcCD protein complex from Escherichia coli. *Nucleic Acids Research*, 27(4):1039–1046, 1999.

[267] J C Connelly, L A Kirkham, and D R Leach. The SbcCD nuclease of Escherichia coli is a structural maintenance of chromosomes (SMC) family protein that cleaves hairpin DNA. *Proceedings of the National Academy of Sciences of the United States of America*, 95(14):7969–74, 1998.

[268] Chew Theng Lim, Pey Jiun Lai, David R.F. Leach, Hisaji Maki, and Asako Furukohri. A novel mode of nuclease action is revealed by the bacterial Mre11/Rad50 complex. *Nucleic Acids Research*, 43(20):9804–9816, 2015.

[269] John C. Connelly, Erica S. De Leau, and David R.F. Leach. Nucleolytic processing of a protein-bound DNA end by the E. coli SbcCD (MR) complex. *DNA Repair*, 2(7):795–807, 2003.

[270] Gareth A. Cromie and D. R F Leach. Recombinational repair of chromosomal DNA double-strand breaks generated by a restriction endonuclease. *Molecular Microbiology*, 41(4):873–883, 2001.

[271] Judita Mascarenhas, Humberto Sanchez, Serkalem Tadesse, Dawit Kidane, Mahalakshmi Krisnamurthy, Juan C Alonso, and Peter L Graumann. Bacillus subtilis SbcC protein plays an important role in DNA inter-strand cross-link repair. *BMC Molecular Biology*, 7(1):20, 2006.

[272] Vidya A. Kamble and Hari S. Misra. The SbcCD complex of Deinococcus radiodurans contributes to radioresistance and DNA strand break repair in vivo and exhibits Mre11-Rad50 type activity in vitro. *DNA Repair*, 9(5):488–494, 2010.

[273] Elise Darmon, Manuel A. Lopez-Vernaza, Anne C. Helness, Amanda Borking, Emily Wilson, Zubin Thacker, Laura Wardrope, and David R F Leach. SbcCD regulation and localization in Escherichia coli. *Journal of Bacteriology*, 189(18):6686–6694, 2007.

[274] Aurelia Battesti, Nadim Majdalani, and Susan Gottesman. The RpoS-mediated general stress response in Escherichia coli. *Annual Review of Microbiology*, 65:189–213, 2011.

[275] S K Kulkarni and F W Stahl. Interaction between the sbcC gene of Escherichia coli and the gam gene of phage lambda. *Genetics*, 123(2):249–53, 1989.

[276] John K. Eykelenboom, John K. Blackwood, Ewa Okely, and D. R F Leach. SbcCD Causes a Double-Strand Break at a DNA Palindrome in the Escherichia coli Chromosome. *Molecular Cell*, 29(5):644–651, 2008.

[277] Susanna M. Lewis and Atina G. Coté. Palindromes and genomic stress fractures: Bracing and repairing the damage. *DNA Repair*, 5(9-10):1146–1160, 2006.

[278] Elise Darmon, John K. Eykelenboom, Frédéric Lincker, Lucy H. Jones, Martin White, Ewa Okely, John K. Blackwood, and David R. Leach. E. coli SbcCD and RecA Control Chromosomal Rearrangement Induced by an Interrupted Palindrome. *Molecular Cell*, 39(1):59–70, 2010.

[279] Robert D. Wells. Molecular basis of genetic instability of triplet repeats, 1996.

[280] P S Sarkar, H C Chang, F B Boudi, and S Reddy. CTG repeats show bimodal amplification in E. coli. *Cell*, 95(4):531–40, 1998.

[281] X Pan and D R Leach. The roles of mutS, sbcCD and recA in the propagation of TGG repeats in Escherichia coli. *Nucleic Acids Research*, 28(16):3178–84, 2000.

[282] Brian M. Wendel, Jessica M. Cole, Charmain T. Courcelle, and Justin Courcelle. SbcC-SbcD and ExoI process convergent forks to complete chromosome replication. *Proceedings of the National Academy of Sciences*, 115(2):349–354, 2018.

[283] Martijn De Jager, Kelly M. Trujillo, Patrick Sung, Karl Peter Hopfner, James P. Carney, John A. Tainer, John C. Connelly, David R.F. Leach, Roland Kanaar, and Claire Wyman. Differential arrangements of conserved building blocks among homologs of the Rad50/Mre11 DNA repair protein complex. *Journal of Molecular Biology*, 339(4):937–949, 2004.

[284] S. Sung, F. Li, Y. B. Park, J. S. Kim, A.-K. Kim, O.-k. Song, J. Kim, J. Che, S. E. Lee, and Y. Cho. DNA end recognition by the Mre11 nuclease dimer: insights into resection and repair of damaged DNA. *The EMBO Journal*, 33(20):2422–2435, 2014.

[285] Logan R. Myler, Ignacio F. Gallardo, Michael M. Soniat, Rajashree A. Deshpande, Xenia B. Gonzalez, Yoori Kim, Tanya T. Paull, and Ilya J. Finkelstein. Single-Molecule Imaging Reveals How Mre11-Rad50-Nbs1 Initiates DNA Break Repair. *Molecular Cell*, 67(5):891–898.e4, 2017.

[286] Tanya T. Paull and Martin Gellert. Nbs1 potentiates ATP-driven DNA unwinding and endonuclease cleavage by the Mre11/Rad50 complex. *Genes and Development*, 1999.

[287] Iain F Davidson, Daniela Goetz, Maciej P Zaczek, Maxim I Molodtsov, Pim J Huis in 't Veld, Florian Weissmann, Gabriele Litos, David A Cisneros, Maria Ocampo-Hafalla, Rene Ladurner, Frank Uhlmann, Alipasha Vaziri, and Jan-Michael Peters. Rapid movement and transcriptional re-localization of human cohesin on DNA. *The EMBO Journal*, 35(24):2671–2685, 2016.

[288] Tsuyoshi Terakawa, Shveta Bisht, Jorine M. Eeftens, Cees Dekker, Christian H. Haering, and Eric C. Greene. The condensin complex is a mechanochemical motor that translocates along DNA. *Science*, 358(6363):672–676, 2017.

[289] Alexander E. Gorbalenya and Eugene V. Koonin. Superfamily of UvrA-related NTP-binding proteins. Implications for rational classification of recombination/repair systems. *Journal of Molecular Biology*, 213(4):583–591, 1990.

[290] Won Ki Cho, Cherlhyun Jeong, Daehyung Kim, Minhyeok Chang, Kyung Mi Song, Jeungphill Hanne, Changill Ban, Richard Fishel, and Jong Bong Lee. ATP alters the diffusion mechanics of MutS on mismatched DNA. *Structure*, 20(7):1264–1274, 2012.

[291] Young Min Soh, Frank Bürmann, Ho Chul Shin, Takashi Oda, Kyeong Sik Jin, Christopher P. Toseland, Cheolhee Kim, Hansol Lee, Soo Jin Kim, Min Seok Kong, Marie Laure Durand-Diebold, Yeon Gil Kim, Ho Min Kim, Nam Ki Lee, Mamoru Sato, Byung Ha Oh, and Stephan Gruber. Molecular basis for SMC rod formation and its dissolution upon DNA binding. *Molecular Cell*, 57 (2):290–303, 2015.

[292] Marie Laure Diebold-Durand, Hansol Lee, Laura B. Ruiz Avila, Haemin Noh, Ho Chul Shin, Haeri Im, Florian P. Bock, Frank Bürmann, Alexandre Durand, Alrun Basfeld, Sihyun Ham, Jérôme Basquin, Byung Ha Oh, and Stephan Gruber. Structure of Full-Length SMC and Rearrangements Required for Chromosome Organization. *Molecular Cell*, 67(2):334–347.e5, 2017.

[293] David E. Anderson, Ana Losada, Harold P. Erickson, and Tatsuya Hirano. Condensin and cohesin display different arm conformations with characteristic hinge angles. *Journal of Cell Biology*, 156 (3):419–424, 2002.

[294] Martijn De Jager, John Van Noort, Dik C. Van Gent, Cees Dekker, Roland Kanaar, and Claire Wyman. Human Rad50/Mre11 is a flexible complex that can tether DNA ends. *Molecular Cell*, 8 (5):1129–1135, 2001.

[295] Douglas C. Rees, Eric Johnson, and Oded Lewinson. ABC transporters: The power to change. *Nature Reviews Molecular Cell Biology*, 10(3):218–227, 2009.

[296] Dániel Szöllősi, Dania Rose-Sperling, Ute A Hellmich, and Thomas Stockner. Comparison of mechanistic transport cycle models of ABC exporters. *Biochimica et Biophysica Acta - Biomembranes*, 1860(4):818–832, 2018.

[297] Christopher F. Higgins and Kenneth J. Linton. The ATP switch model for ABC transporters. *Nature Structural and Molecular Biology*, 11(10):918–926, 2004.

[298] Hideyuki Yaginuma, Shinnosuke Kawai, Kazuhito V. Tabata, Keisuke Tomiyama, Akira Kakizuka, Tamiki Komatsuzaki, Hiroyuki Noji, and Hiromi Imamura. Diversity in ATP concentrations in a single bacterial cell population revealed by quantitative single-cell imaging. *Scientific Reports*, 4: 6522, 2014.

[299] Alan E. Senior, Marwan K. Al-Shawi, and Ina L. Urbatsch. The catalytic cycle of P-glycoprotein. *FEBS Letters*, 377(3):285–289, 1995.

[300] Stephan Wilkens. Structure and mechanism of ABC transporters. *F1000Prime Reports*, 7, 2015.

[301] Brian Cannon, Jeffrey Kuhnlein, Soo Hyun Yang, Anita Cheng, Detlev Schindler, Jeremy M. Stark, Rick Russell, and Tanya T. Paull. Visualization of local DNA unwinding by Mre11/Rad50/ Nbs1 using single-molecule FRET. *Proceedings of the National Academy of Sciences of the United States of America*, 110(47):18868–18873, 2013.

[302] Carolyn F. Delto, Frank F. Heisler, Jochen Kuper, Bodo Sander, Matthias Kneussel, and Hermann Schindelin. The LisH motif of muskelin is crucial for oligomerization and governs intracellular localization. *Structure*, 23(2):364–373, 2015.

[303] John R. Walker, Richard A. Corpina, and Jonathan Goldberg. Structure of the Ku heterodimer bound to dna and its implications for double-strand break repair. *Nature*, 412(6847):607–614, 2001.

List of Abbreviations

53BP1	p53-binding protein 1
Å	Ångstrom
aa	amino acid
ABC	ATP-binding cassette
ADP	adenosine diphosphate
AFM	atomic force microscopy
ALT	alternative lengthening of telomeres
alt-NHEJ	alternative non-homologous end joining
AT	ataxia-telangiectasia
ATLD	ataxia-telangiectasia like disease
ATM	ataxia-telangiectasia mutated
ATP	adenosine triphosphate
ATPγS	adenosine 5′-(γ-thio)triphoshpate
ATR	Ataxia telangiectasia and Rad3 related
ATRIP	ATR Interacting Protein
BER	Base Excision Repair
BIR	Break-induced replication
BLM	Bloom syndrome protein
bp	base pair
BRCA1/2	breast cancer 1/2
BRCT	breast cancer carboxy terminus
CDK	cyclin-dependent kinase
c-NHEJ	classical non-homologous end joining
cryo-EM	cryo-electron microscopy
C-terminus	carboxy terminus
CTBP	C-terminal-binding protein
CtIP	CtBP-interacting protein
CO	crossover
DDR	DNA damage response
dHJ	double Holliday junction
D-loop	displacement loop
DNA	deoxyribonucleic acid
DNA2	DNA replication ATP-dependent helicase/nuclease 2
DNA-PKcs	DNA-dependent protein kinase catalytic subunit
DSB	DNA double strand break
DSBR	DNA double strand break repair
dsDNA	double stranded DNA
EXO1	exonuclease 1
FHA	forkhead associated

GAR	glycine-arginine-rich
G phase	gap phase
HEAT	Huntingtin, elongation factor 3 (EF3), protein phosphatase 2A (PP2A), and the yeast kinase TOR1
HLH	helix-loop-helix
HR	homologous recombination
HJ	Holliday junction
ICL	interstrand crosslink
Ig	immunoglobulin
IR	ionizing radiation
K_D	dissociation constant
kDA	kilo dalton
LOH	loss of heterozygosity
MDC1	Mediator of DNA damage checkpoint 1
Mec1	mitosis entry checkpoint 1
MMEJ	micro-homology mediated end joining
MMR	mismatch repair
MMS	methyl methanesulfate
M phase	mitotic phase
Mre11	meiotic recombination 11
MR	Mre11-Rad50
MRN	Mre11-Rad50-Nbs1
MRX	Mre11-Rad50-Xrs2
NBD	nucleotide binding domain
Nbs1	Nijmegen breakage syndrome 1
NBS	Nijmegen breakage syndrome
NBSLD	NBS-like disorder
NCO	non crossover
NER	nucleotide excision repair
NHEJ	non-homologous end joining
N-terminus	amino terminus
PAH	Polycyclic aromatic hydrocarbons
PARP	Poly(ADP-ribose)-Polymerase
PAXX	Paralogue of XRCC4 and XLF
PCNA	Proliferating cell nuclear antigen
PDB	Protein Databank
PI-3 kinase	phosphatidylinositol-3
PIKK	PI-3 kinase-like kinase
PTM	post-translation modification

PTO 1	protection of telomeres 1
Pol	Polymerase
Rad50	radiation sensitive 50
Rag-1/2	Recombination-activating gene-1 and -2
Rap1	repressor and activator protein 1
RFC	Replication factor C
RMI 1/2	RecQ-mediated genome instability protein 1/2
ROS	reactive oxygen species
RPA	replication protein A
RpoS	RNA polymerase sigma factor
SFM	Scanning force microscopy
SMARCAD1	SWI/SNF-related matrix-associated actin-dependent regulator of chromatin subfamily A containing DEAD/H box 1
SMC	structural maintenance of chromosomes
SSA	Single-strand annealing
SSB	single strand break
SSB	single-stranded DNA-binding protein
SSBR	single strand break repair
S phase	synthesis phase
Spo11	Sporulation 11
ssDNA	single stranded DNA
SDSA	Synthesis-dependent strand annealing
TIN 2	TRF1-interacting nuclear protein 2
T-loop	telomere loops
TLS	translesion synthesis
Top III	Topoisomerase III
TPP1	TIN2- and POT1-interacting protein
TRF1/2	Telomeric repeat-binding Factors 1 and 2
TRFH	TRF homology
UV	ultraviolet
V(D)J	variable, diversity, joining
wt	wild type
XLF	XRCC4-like factor
XPF	Xeroderma pigmentosum group F-complementing protein
XRCC4	X-ray repair cross-complementing protein 4
Xrs2	X-ray sensitive 2
Zn	zinc

Acknowledgements

First, I would like to thank my supervisor Prof. Dr. Karl-Peter Hopfner for his support during my work in his lab. I am very grateful for the project I could work on and the help and advice I received. For me it was a great experience to be given so much freedom to explore my own scientific ideas.

I also want to thank Jan-Hinnerk Saathoff, who introduced me to the bacterial Mre11-Rad50 project. We worked very well together as a team and I am thankful for the successful cooperation we established. It was a great time with many nice discussions, productive days and funny moments.

In addition, I want to thank Katja Lammens who introduced me to cryo-EM and supported me during the whole project. We shared some good and bad days at the microscope and I am very thankful that I could always ask questions about all structural and biochemical topics.

Furthermore, I want to thank Fabian Gut, who joined just at the right time for the revisions of our paper. It was great to have this support during the revisions and I am glad that we can continue to work together on this project.

I also want to thank all members of the MRN subgroup, especially, the members who worked in the lab during my time: Aaron Alt, Robert Byrne, Brigitte Kessler, Marijke Jansma, Kristina Stakyte, Matthias Rotheneder and Joe Bartho. We are a great subgroup.

My thanks also go to the whole Hopfner lab. It is a really nice working atmosphere and I had a good time with all of you. I also want to thank you for all the help, input and support I received.

Special thanks go to Gregor Witte for answering all my questions; Mike Strauss and the cryo-EM facility at the MPI for the support during data collection and screening; Dirk Kostrewa for help with data processing and Sandra Schuller for her help with grid preparation.

The IMPRS-LS graduate school provided me with great workshops, events and support and I am very happy to be a member of this school.

Most importantly I want to thank several people who supported me on the way. My boyfriend Martin was always there to encourage me as well as my parents, my sister and several good friends. I am very lucky to have you in my life.